International
Progress Report

IPR-05-38

Äspö Hard Rock Laboratory

TRUE Block Scale continuation project

BS2B experiment: Discrete fracture and channel network modeling of solute transport modeling in fault and non-fault structures

Aaron Fox, Golder Associates Inc.
William Dershowitz, Golder Associates Inc.
Matthaeus Ziegler, Golder Associates GMbH
Masahiro Uchida, JNC Tokai
Shinji Takeuchi, JNC Mizunami

November 2005

Svensk Kärnbränslehantering AB
Swedish Nuclear Fuel
and Waste Management Co
Box 5864
SE-102 40 Stockholm Sweden
Tel 08-459 84 00
+46 8 459 84 00
Fax 08-661 57 19
+46 8 661 57 19

Äspö Hard Rock
Laboratory

Report no.
IPR-05-38
No.
F56K
Author
Aaron Fox
William Dershowitz
Matthaeus Ziegler
Masahiro Uchida
Shinji Takeuchi
Date
November 2005
Checked by
Anders Winberg
Date
October 2006
Approved
Anders Sjöland
Date
2006-11-29

Äspö Hard Rock Laboratory

TRUE Block Scale continuation project

BS2B experiment: Discrete fracture and channel network modeling of solute transport modeling in fault and non-fault structures

Aaron Fox, Golder Associates Inc.
William Dershowitz, Golder Associates Inc.
Matthaeus Ziegler, Golder Associates GMbH
Masahiro Uchida, JNC Tokai
Shinji Takeuchi, JNC Mizunami

November 2005

Keywords: Channel, Discrete, Fault, Fracture, Prediction, Retention, Sorbing, Tracer

Abstract

This report describes the JNC/Golder team's flow and transport analysis and modeling in support of Task BS2B of the TRUE Block Scale Continuation project. BS2B focuses on a series of hypotheses concerning conservative and reactive transport in pathways defined within a rock block of scale approximately 100 m.

Simulations and analyses were carried out to improve our understanding of the behavior of the BS2B fracture network. This evaluation was carried out within the framework of two of the hypotheses defined for the TRUE-BSC project:

- Hypothesis Ia) Microstructural (i.e. detailed geological, mineralogical and geochemical) information can provide significant support for predicting transport of sorbing solutes at experimental time scales, and

- Hypothesis Ib) Transport at experimental time scales is significantly different for faults (a high degree of alteration, brecciation and the presence of fault gouge) and joints (with or without alteration), due to the indicated differences in microstructure and properties

The JNC/Golder modeling was carried out in a 500 m scale discrete fracture network (DFN) flow and transport model for the TRUE-BSC rock block, with steady state flow solved by the finite element method, and transport flow solved by the Laplace Transform Galerkin (LTG) method.

The intention of the JNC/Golder team was to utilize forward modeling, sensitivity studies to support hypothesis testing, based solely on the hydrostructural and microstructural models as developed by the project. Therefore, calibration was limited to the extent possible, and the project hydrostructural and microstructural models were utilized as much as possible. In addition, Monte Carlo simulation was used to understand the sensitivity of simulations to variability within the hydrostructural model.

Model calibration was carried out to identify head boundary conditions for assignment to the edges of the 500 m scale rock block to match the head measurements within the block

In addition, because the hydrostructural model did not contain information about channel geometry, and because of the potential role of alternative realizations of background fractures, sensitivity studies were carried out to compare alternative BS2B predictive models against the non-sorbing pre-test CPT-4c. These alternative predictive models varied the path width and aperture, the algorithm used to generate the channel network within the fracture planes, and the geometry of the DFN for stochastic background fractures. The basic hydrostructural and micro-structural models were kept unchanged.

As part of the evaluation phase considering the BS2B tracer transport results, an additional series of simulations was carried out to consider the role of alternative realization and channel geometry. From these simulations, it appears that channel width may be the key parameter necessary to better model BS2B sorbing tracer transport.

The predictive and analysis simulations reported here indicate the value of hydrostructural and microstructural analysis and modeling to understand the differences between both advective transport and solute retention on the Structure 19 pathway (Path I) and the Structure BG1 pathways (Path II). The two pathways have similar Cartesian lengths, but their lengths through the fracture network, and the retention properties of the different types of fractures on those pathways explain the difference in solute transport breakthrough curves.

Sammanfattning

Denna rapport beskriver JNC/Golder-teamets flödes- och transportanalys och modellering till stöd för fas BS2B av projektet TRUE Block Scale Continuation. BS2B analyserar en serie av hypoteser rörande icke-reaktiv och reaktiv transport i flödesvägar inom en bergvolym med en längdskala om c. 100 m.

Modellsimuleringar och analyser genomfördes för att öka förståelsen av hur det undersökta spricknätverket fungerar. Den aktuella utvärderingen genomfördes inom ramen för följande två hypoteser som definierats för TRUE Block Scale Continuation-projektet:

- Hypotes Ia) Mikrostrukturell (dvs detaljerad geologisk, mineralogisk och geokemisk) information kan ge viktigt stöd för prediktering av transport av sorberande spårämnen på en experimentell tidskala, och

- Hypotes Ib) Transport på experimentell tidskala skiljer väsentligt mellan förskastningsstrukturer (”faults”, som karakteriseras av en omfattande omvandling, brecciering och förekomst av sprickfyllnader (”fault gouge”)) och bakgrundssprickor (med eller utan omvandling), på grund av noterade skillnader i mikrostruktur och egenskaper.

Modelleringen av JNC/Golder genomfördes i en diskret nätverksmodell för flöde och transport (500 m skala) fokuserad på TRUE Block Scale volymen, där flöde för stationära förhållanden löstes med hjälp av Laplace Transform Galerkin (LTG) metoden.

JNC/Golder-teamets avsikt var att använda prediktiv modellering och känslighetsanalyser som stöd för hypotestestning, baserad enbart på de mikrostrukturella och hydrostrukturella modeller som utvecklats av projektet. Därför har kalibrering begränsats så långt som möjligt med en emfas på utnyttjande av de mikrostrukturella och hydrostrukturella modellerna som sådana. Därutöver har Monte Carlo-simulering använts för att förstå känsligheten hos simuleringarna beroende på variationer i den hydrostrukturella modellen.

Kalibrering av modellerna för genomfördes för att identifiera tryckrandvillkor att ansättas på ränderna av ett 500 m block som möjliggör att mätta tryck i blocket kan reproduceras.

Dessutom, och beroende på att den hydrostrukturella modellen inte innehåller information om kanalgeometri, och på grund av den möjliga roll som bakgrundssprickor kan ha, genomfördes känslighetsanalyser för att jämföra alternativa prediktiva BS2B-modeller med resultat från det icke-sorberande för-försöket CPT-4c. I dessa alternativa prediktiva modeller varierades vidden på flödesvägar, dess aperturer, algoritmen för generering av kanalnätverk över sprickplanen, liksom geometrin hos DFN-modellen för stokastiska bakgrundssprickor. De underliggande hydrostrukturella och mikrostrukturella modellerna behölls dock oförändrade.

Som en del av utvärderingen av BS2B-försöken genomfördes också ytterligare en serie beräkningar för att analysera rollen av alternativa realiseringar och kanalgeometri. Från dessa simuleringar framgår det att kanalvidden är en nyckelparameter för att bättre modellera BS2B-försöken med sorberande spårämnen.

De prediktiva och utvärderande modellberäkningarna visar på betydelesen av kombinationen av den hydrostrukturella och mikrostrukturella analysen och modelleringen för att förstå skillnaderna mellan både advektiv transport och retention av sorberande spårämnen i struktur #19 (flödesväg I) och BG-1 flödesvägen (flödesväg II). De två flödesvägarna har jämförbara kartesiska längder, men deras längder i spricknätverket, och skillnader i retentioinsegenskaper hos olika typer av sprickor längs de två flödesvägarna förklarar noterade skillnader i genombrottskurvorna.

Contents

List of Figures

List of Tables

1 Introduction

1.1 Background

Solute transport in fractured rock is a key aspect of repository safety. As a result, detailed approaches have been developed for the analysis and simulation of solute transport within a discrete-fracture network (DFN) for both performance assessment (PA) and repository site characterization (SC). Geosphere barriers in the JNC repository program focus particularly on the 50 to 100 m scale rock block between the repository and a near-by fault zone. The TRUE-BS Continuation experiment is therefore of significant value, since it focuses directly on this scale of rock block.

Specifically, this report describes tracer test simulations in support of TRUE Block Scale Continuation (TRUE-BSC) Phase BS2B, which includes in-situ testing, evaluation of experimental results, analysis and updating of geologic and chemical models of transport within the TRUE Block Scale rock volume. This BS2B experiments studied conservative and sorbing tracer transport in a single reactivated mylonite fault, referred to as "Structure 19", and a background fracture referred to as "Structure BG1".

The JNC/Golder team built a 500 m scale discrete fracture network flow and transport model for the TRUE-BSC rock block, and used this model to predict tracer transport in the BS2B experiment. This was a "blind" prediction; the purpose of the prediction was not to test the software and modeling methodology but to improve our understanding of solute transport in fractured rocks.

Prediction results were compared to in-situ observations to determine areas in which our understanding of the behavior of the BS2B fracture system was limited. This comparative evaluation was carried out within the framework of two of the hypotheses defined for the TRUE-BSC project:

- Hypothesis Ia) Microstructural (i.e. detailed geological, mineralogical and geochemical) information can provide significant support for predicting transport of sorbing solutes at experimental time scales, and
- Hypothesis Ib) Transport at experimental time scales is significantly different for faults (a high degree of alteration, brecciation and the presence of fault gouge) and joints (with or without alteration), due to the indicated differences in microstructure and properties

Hypothesis Ia was addressed through the evaluation of the performance of the JNC/Golder team's channel-network (CN) model in a blind prediction of the BS2B tracer experiment. This evaluation, as well as changes made to the base hydrostructural model (as described in the Task 6C report /Dershowitz et al., 2003/) is addressed in "Step 1" of the evaluation process.

Hypothesis Ib is addressed through a comparison of the tracer breakthroughs for the two pathways tested in BS2B. This comparison was made based both in terms of the BS2B experimental results for the two different (Path I and II) pathways and on the basis of a comparison of the JNC/Golder CN model implementation for the two pathways. These issues are addressed in "Step 2" of the model evaluation.

1.2 Objectives

This report describes the JNC/Golder team's efforts for the reactive tracer portion (BS2B) of the TRUE Block Scale Continuation project, which studies solute transport at site characterization (SC) experimental time scales. Project experiments and numerical models are constrained to a 500 m scale block of rock in which faults and background fractures have been defined deterministically from Dershowitz et al. (2002). Studies were carried out using the following codes:

- Hydraulic Modeling: FracWorks XP, MAFIC/PC
- Pathway Identification and Transport: PAWorks/PC, LTG
- Data Analysis and Visualization: Microsoft Excel, MATLAB R13/R14

This report presents forward modeling simulations based on two alternative conceptual models:

A. Transport occurs through a network of major structural features and background fractures (including Structure BG1) connecting the injection sections either directly to the sink boreholes or to Structure 19 (Path I). Two separate realizations were performed.

B. Transport occurs through a single, isolated, hydraulically-homogenous background fracture that may or may not be connected to Structure 19 (Path II). A single set of realizations were performed.

Since there was no characterization of the properties of the background fractures connecting Structure BG1 to Structure 19, these properties needed to be obtained through a calibration. This calibration was used only to define properties for these specific background fractures. This calibration was carried out a) directly based on the CPT-4c tracer test /Andersson et al., 2004/, and b) assuming that the CPT-4c tracer test was an anomalous result, due to some kind of testing error, and should really have been shifted significantly earlier in time. This is because the CPT-4c result shows little dispersion considering the very slow travel (one quarter the speed of the flow which was exclusively on Structure 19).

Specific objectives for this study were to:

1. Develop boundary conditions appropriate for the 500 m region of the TRUE-BS rock block;
2. Utilize the results of past tracer test modeling (specifically, CPT-4c) carried out on the target BS2B tracer pathways to suggest hydraulic parameters for the targeted test structures;
3. Predict the results of the BS2B tracer experiment through forward modeling;
4. Calculate the specified performance measures, including breakthrough curves, anticipated recovery, and pathway statistics for each conceptual model to aid in the comparison of modeling results between teams;
5. Compare the JNC/Golder team's blind predictions to BS2B tracer in-situ observations to evaluate areas where the hydrostructural conceptual models do not match reality;
6. Evaluate the need for changes to the hydrostructural model, the microstructural model, or to tracer chemical parameters, based on the evaluation of the forward model results with respect to the observed experimental results.

1.3 Outline of Report

- Chapter 2 discusses the model requirements, spatial and temporal scales, geologic and structural conceptual models, boundary conditions, and tracer chemistry data specified for modeling teams working on Phase BS2B.

- Chapter 3 describes the simulation study carried out to develop a suitable head field for the 500 m scale model

- Chapter 4 describes the JNC/Golder team's modeling strategy and the specific implementation of the Task 6C discrete fracture network (DFN) as a one-dimensional channel network (CN)

- Chapter 5 presents forward model prediction results for each of the different conceptual models (Models 20 and 9; full source term and a hypothetical Dirac pulse).

- Chapter 6 describes our evaluation of the results of the BS2B tracer experiment with respect to the JNC/Golder predictive model. Iterative changes to various components of the model are discussed in an attempt to reconcile the differences between the JNC / Golder model and the observed BS2B tracer test results

- Chapter 7 describes our conclusions regarding our forward modeling, the results of our test evaluations, and recommendations for changes and additional work in future work phases.

2 TRUE-BSC Discrete Fracture Network Model

This section provides a summary of the modeling parameters specified for Phase BS2B transport simulations within the TRUE Block. The JNC/Golder implementation of the Task 6C hydrostructural model is also discussed. Unless otherwise indicated, all simulations utilized geological, geochemical, and structural parameters specified by SKB (2004), Poteri (2004), and Byegård and Tullborg (2004) for the Phase BS2B of the TRUE Block Scale Continuation Project.

2.1 Temporal and Spatial Scales

The Phase BS2B models of the TRUE-BS Continuation Project were designed to be carried out at site characterization spatial and temporal scales. The simulation time scale is specified as 0 to 5000 hours relative to tracer injection. JNC/Golder models generally are carried out to 10,000 hours; however performance measures were calculated for test durations of 5000 hours.

The spatial scale for TRUE-BSC can be defined by (a) the scale of the model, which was a 500 m block, (b) the Euclidian distance between injection and withdrawal sections (19 – 22 m), and (c) the estimated fracture network path length between the injection and withdrawal sections (25 to 75 m, depending on the fractures involved). For DFN simulations, there are several potential transport pathways through the fracture network, with lengths varying from 50 m to more than 100 m, as described below in the pathways (PAWorks) analysis.

2.2 JNC/Golder BS2B Hydrostructural DFN Model

The JNC / Golder Associates DFN-CN model (Figure 2-1) was based on the "semi-synthetic" hydrostructural model developed within Task 6C /Dershowitz et al, 2003/. The model combines:

- Deterministic structures (Figure 2-2) directly identified in the TRUE Block Scale experimental volume. The deterministic network consists of Structures 5, 6, 7, 8, 10, 13, 19, 20, 21, 22, 23, 24, the new Structure 19 splay, Structure BG1, and Structure Z.

- Stochastic background fractures (Figure 2-3) generated using FracMan software, based on analysis of data from the TRUE Block Scale rock volume and other portions of the laboratory. Both background fractures described in the Task 6C hydrostructural model and in POSIVA flow logging results were used.

- Additional stochastic background fractures (Figure 2-4) were generated inside the 500 meter TRUE Block Scale rock volume and outside the smaller-scale 200 m interior rock block – the so-called BS2B experimental volume. These fractures were necessary to provide adequate connectivity between the specified constant head boundaries on the 500-meter cube and the modeling region. These fractures were generated as part of the Task 6C modeling effort (the fractures were taken from the northwest-trending 200 m lognormal-sized fracture set). Fracture apertures and transmissivities were set to small values so as not to disrupt the final flow solution; the fractures merely provide sufficient connectivity for a stable steady-state head field to develop.

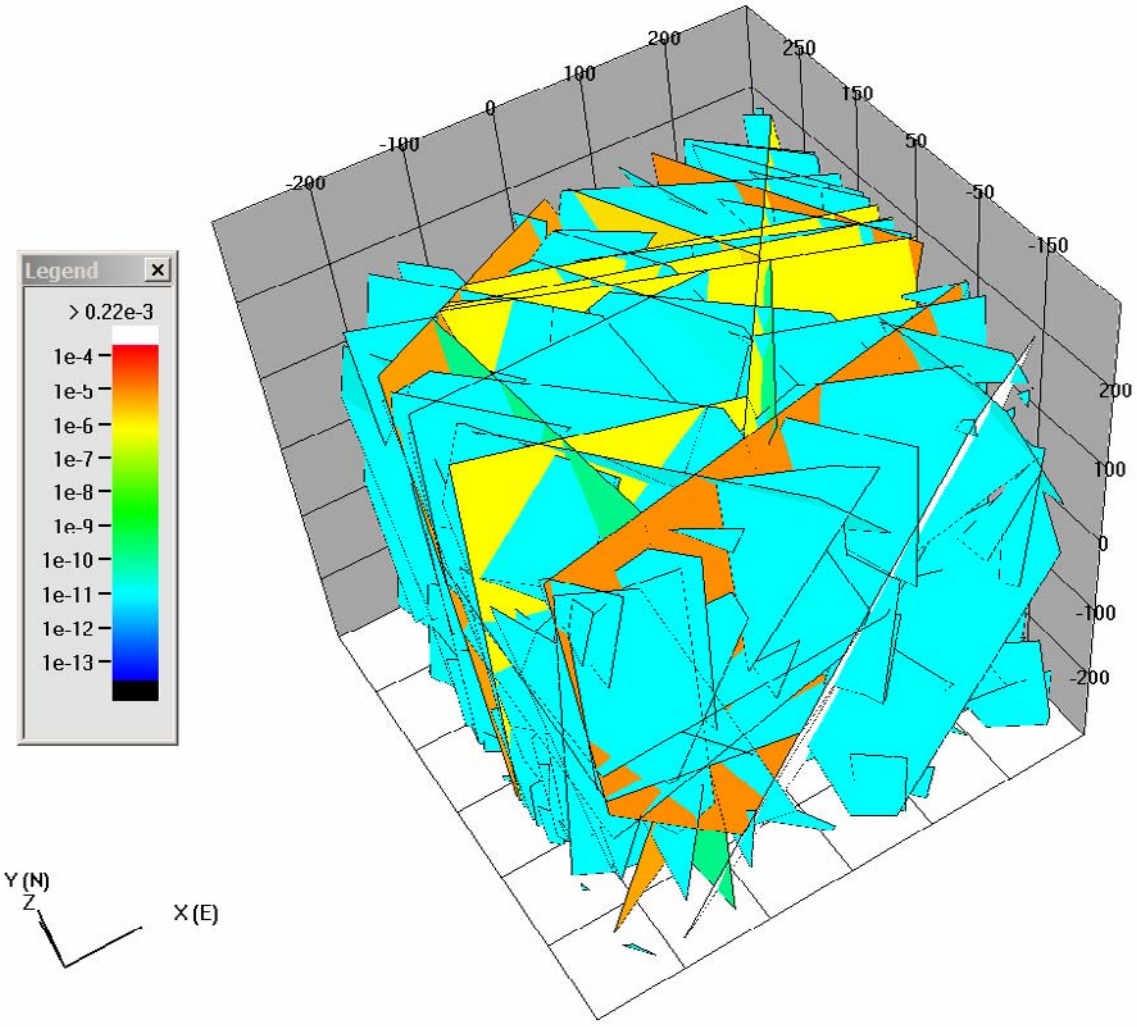

Figure 2-1: *Base discrete fracture network (DFN) used for JNC/Golder BS2B simulations. Fractures are colored by the base-10 logarithm of their transmissivity. View is looking northeast towards the HRL tunnel.*

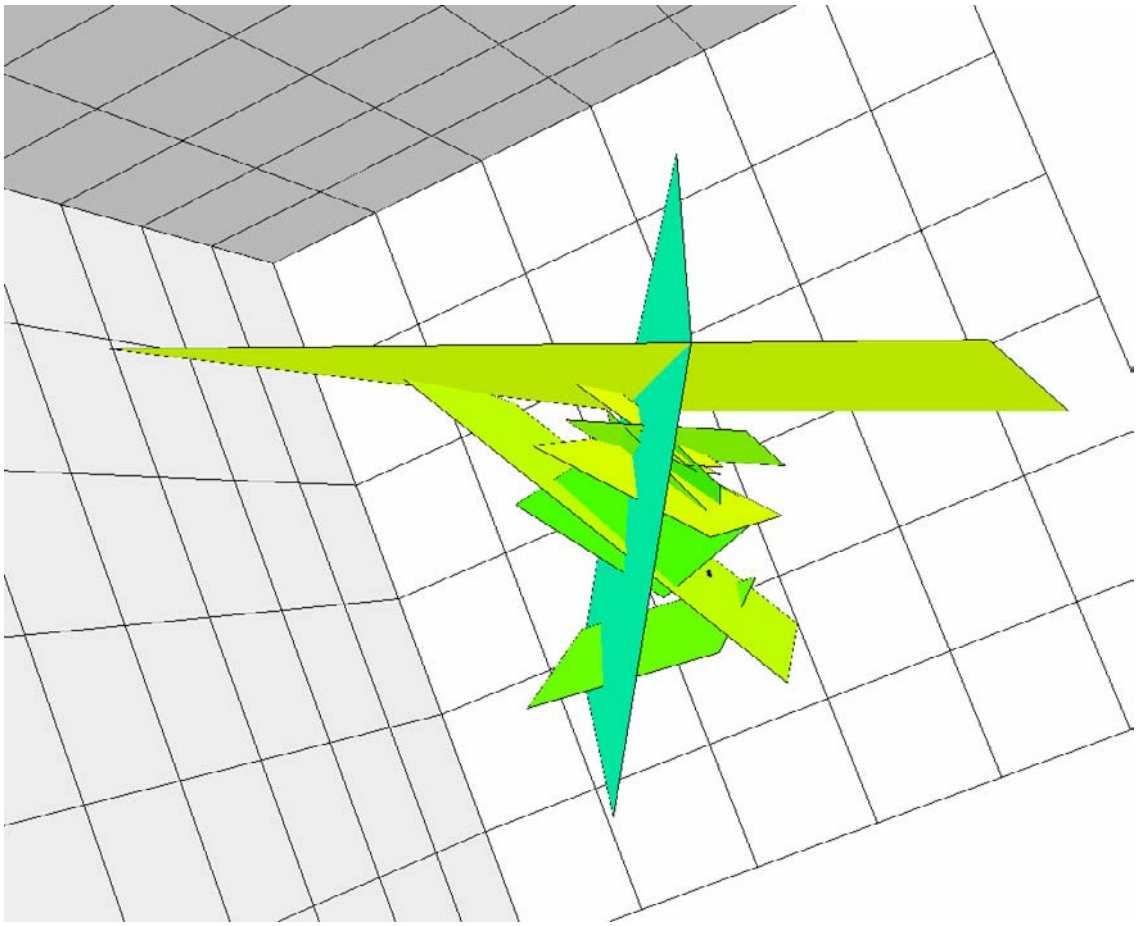

Figure 2-2: *Deterministic structures as implemented in the JNC/Golder BS2B prediction simulations. Fractures are colored by the base-10 logarithm of their transmissivity. The view is looking down on the BS2B volume; the HRL tunnel is to the upper-right (NE) of the target volume.*

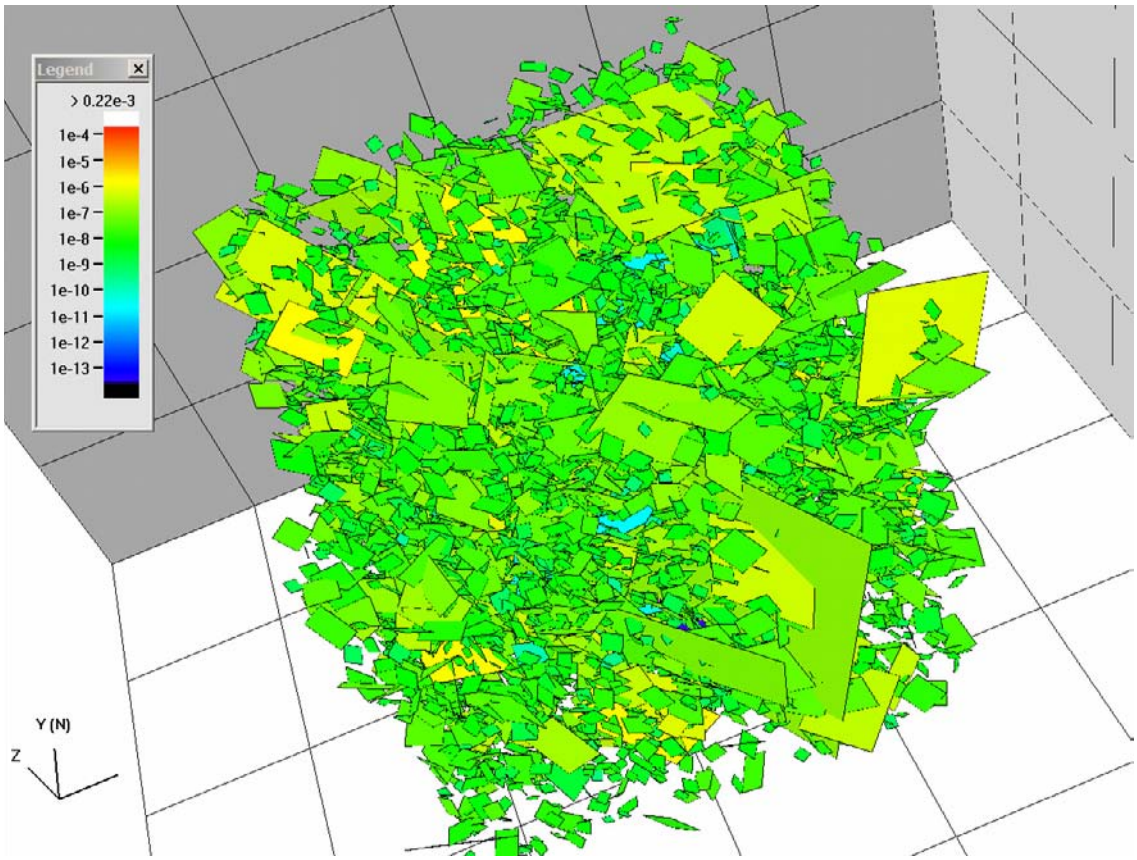

Figure 2-3: *Background fracture model as implemented in the JNC/Golder BS2B prediction simulations. Fractures were taken from the Task 6C hydrostructural model /Dershowitz et al., 2002/, and are colored by log_{10} of their transmissivity. View is looking directly north, from the south and from a position above the target volume. The HRL tunnel is to the upper-right of the volume.*

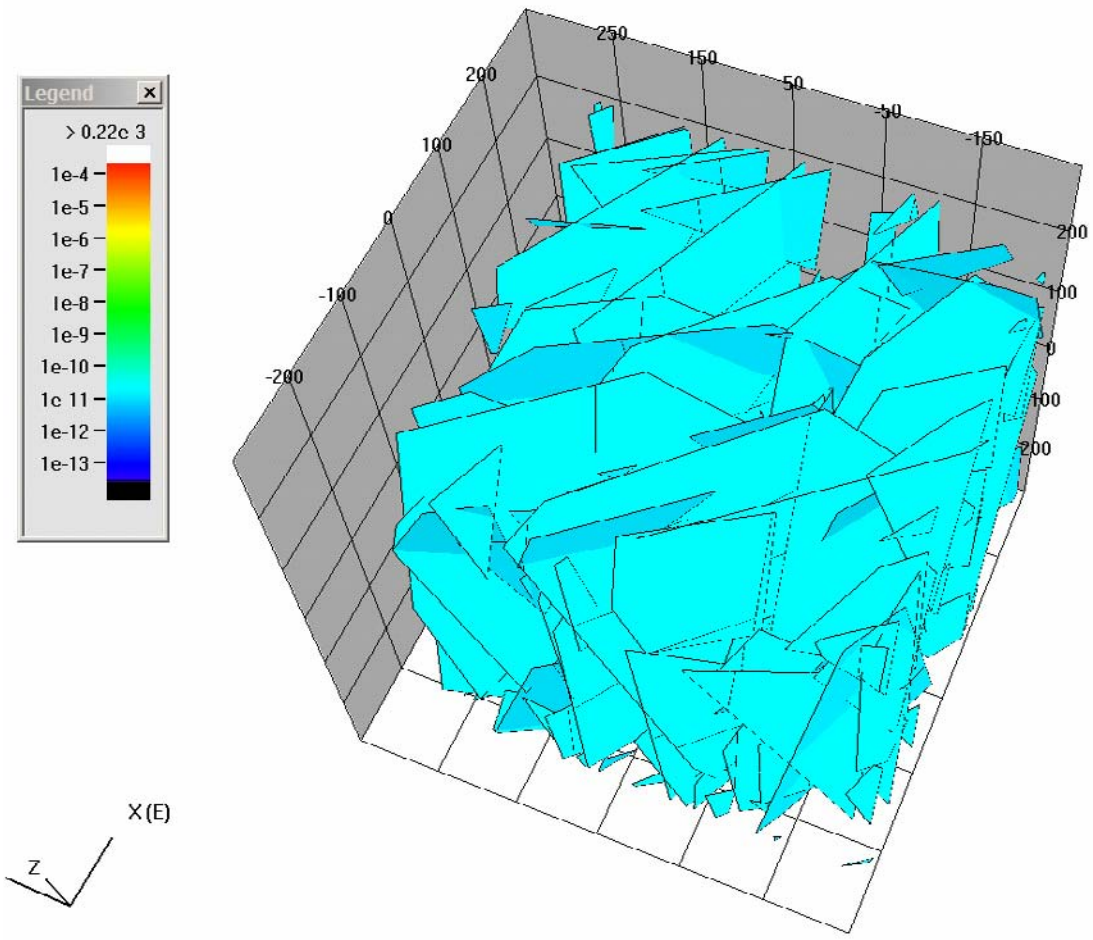

Figure 2-4: *Additional 500 meter scale fractures taken from the 2000 m NNW lognormal set presented in the Task 6C modeling report /Dershowitz et al., 2003/. Fractures are colored by the natural log of their transmissivity. View is to the ENE from above; the HRL tunnel would be in the upper left corner of the figure.*

Figure 2-5 illustrates the relationship between the source (KI0025F02) and sink (KI0025F03) boreholes, background fracture Structure BG1 (in the base model), and the interpreted Structure 19 splay present in borehole KA2563A. In addition, the geometry and size of this feature was not precisely known at the time of model development, so there was considerable uncertainty in transport solutions for pathways that utilized Structure BG1.

Structure BG1 was implemented as a single square discrete fracture with a 15 m equivalent radius, a strike and dip of N30W / 76N, and an intersection point 3 m from the top of the packer in KI0025F02 Section 2 /Tullborg and Hermanson, 2004/. Orientation and size parameters of Structure BG1 were constant throughout the prediction; a single realization of the background fractures was used for all simulations. Note that Structure BG1 does not directly intersect Structure 19 (Figure 2-5). Previous hydraulic testing has suggested that Structure BG1 and 19 may not be directly connected; the hydraulic response of Structure BG1 to activity in boreholes intersecting Structure 19 is significantly delayed /Andersson et al. 2004/. The JNC/Golder modeling hypothesis is that the Structure 19 – Structure BG1 response occurs through a network of background fractures.

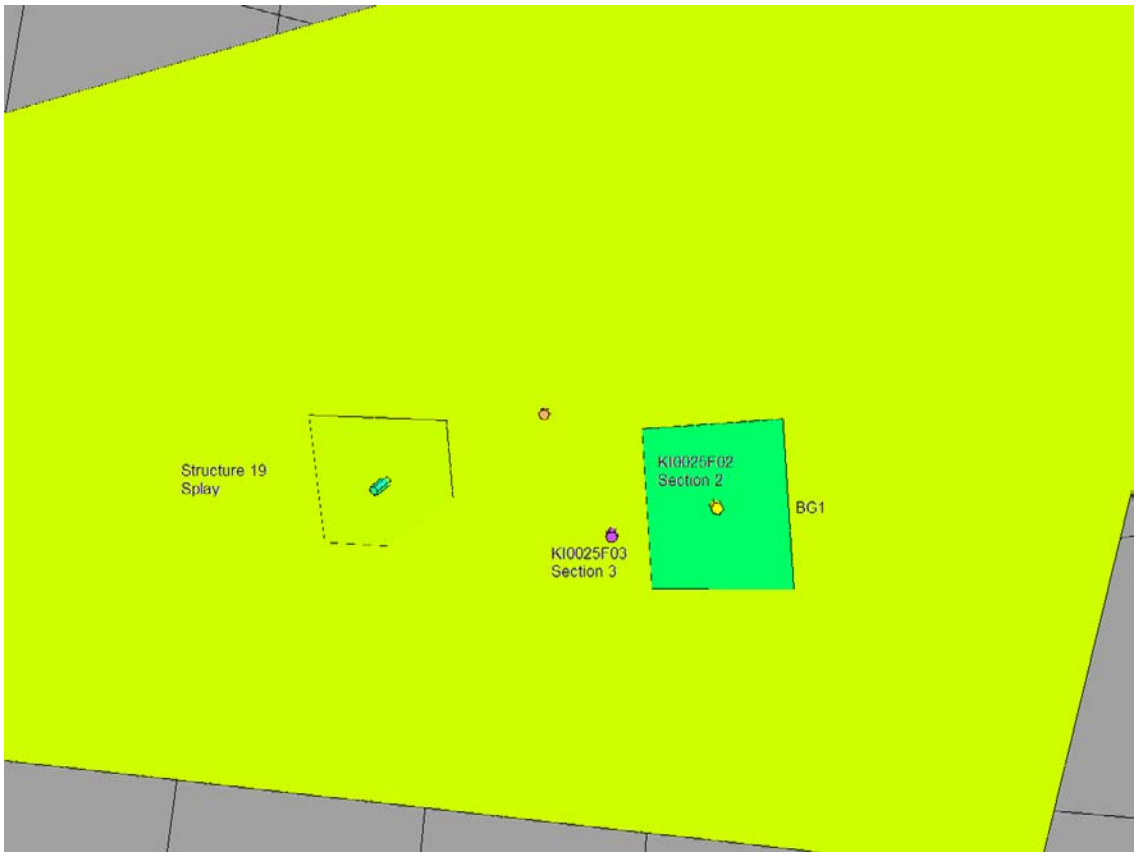

Figure 2-5: *Structures 19, 19 Splay, and Structure BG1 as implemented in the base JNC/Golder BS2B model. View is looking to the north at Structure 19 (yellow).*

2.3 Structure Properties

The Task 6C semi-synthetic hydrostructural model also included a specification of a microstructural model for faults (Figure 2-6) and joints (Figure 2-7), and a specification of structural complexity (Table 2-1). The geometry and structural characteristics of the microstructural models were implemented in the JNC/Golder CN model as immobile zones, which provided for solute retention. The availability of this information made it possible to model the solute transport in fractures in a more deterministic fashion, as the immobile zones were no longer a purely calibrated parameter.

Every natural fracture contains a different mixture of immobile zones and a variation in geologic modes. Thus, the division into two "archetypal" structure types constitutes a significant simplification. However, this conceptual model represented a significant advance in the degree of characterization of the retention properties of transport pathways, and could be very valuable for future transport modeling.

Similarly, both the specification of "complexity factors" to describe the number of individual fractures that make up a hydraulically significant structure and the microstructural model, which describes variations in geology and morphology within a complex fault structure, are also significant simplifications. However, these changes also represented a significant advance in modeling solute transport, as they illustrated how much more reactive surface area is potentially available than just the two sides of a single "parallel plate" fracture.

Structural type and complexity was used in the channel network model to simulate solute retention; however, the JNC/Golder modeling approach implements these characteristics only in the transport model; the basic flow model consists solely of discrete features with no additional information besides their flow (transmissivity, aperture, and storativity) parameters.

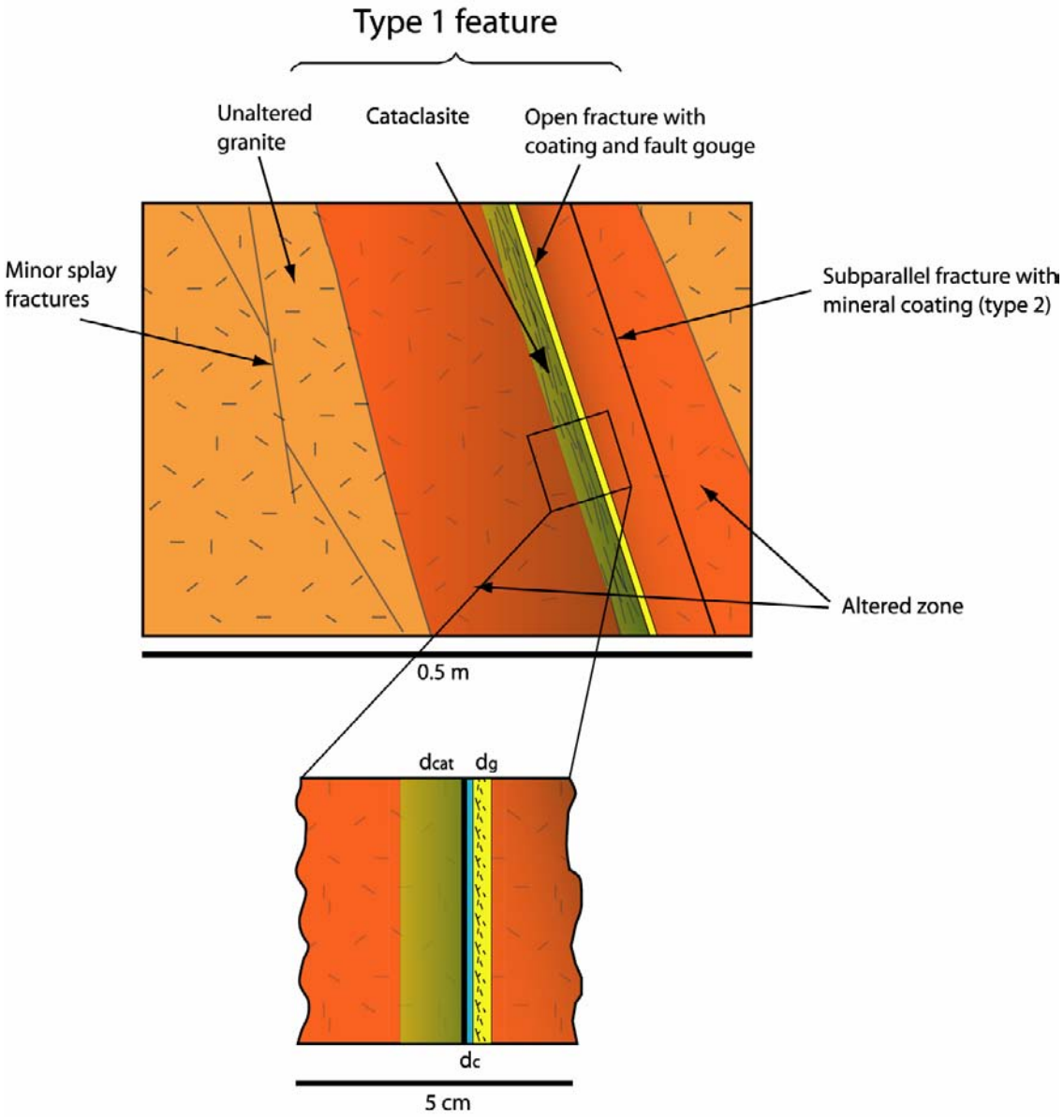

Figure 2-6: *Illustration of a typical Type I (Fault) geological structure. The figure is taken from the Task 6C final report (Dershowitz et al., 2003).*

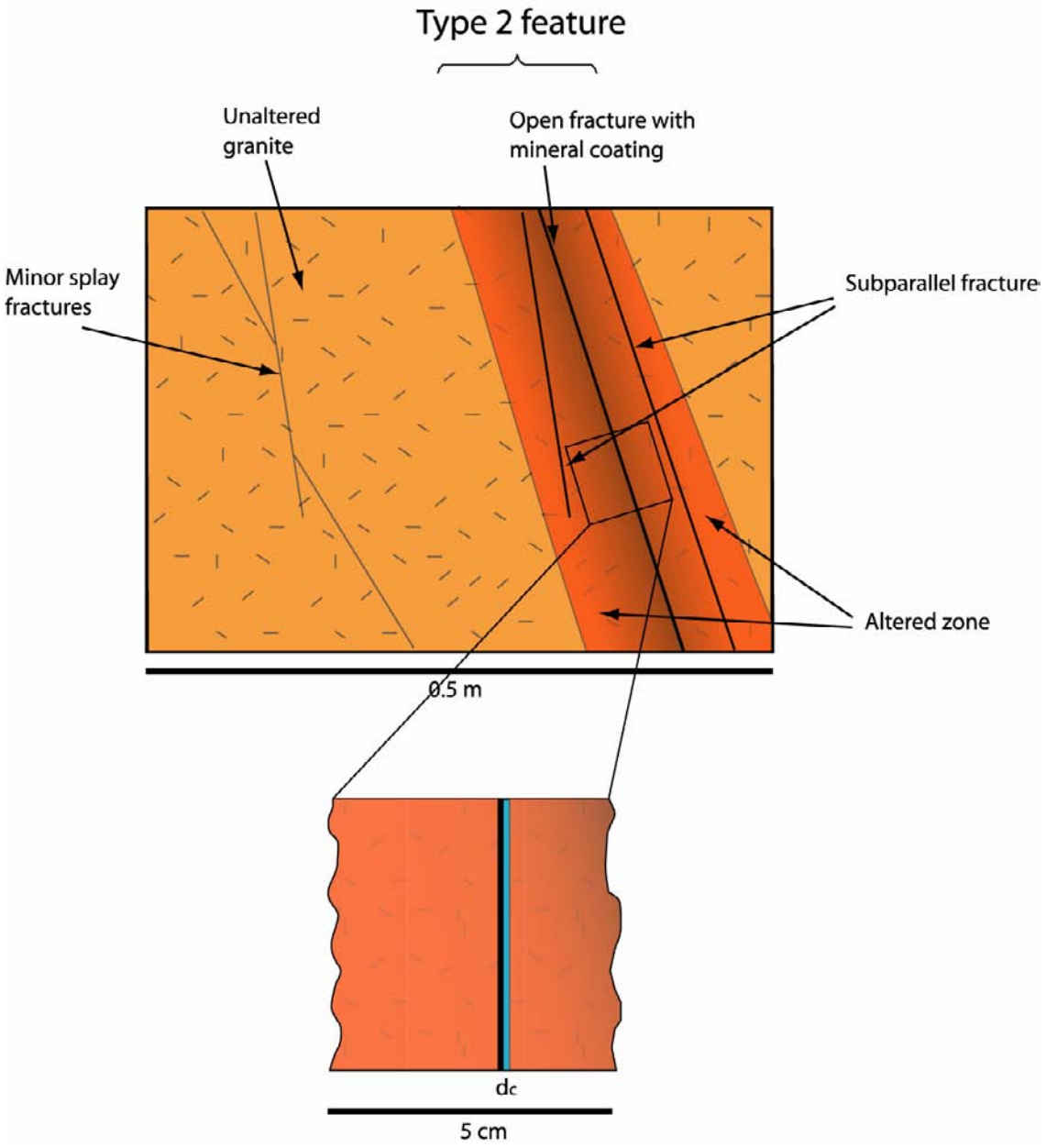

Figure 2-7: *Illustration of a Type II (Joint / Simple Fracture) geological structure. The figure is taken from the Task 6C final report (Dershowitz et al., 2003).*

Table 2-1: Definition of fracture 'Complexity Factor' (from the Task 6C report)

Complexity Factor	Number of subparallel conductive fractures per structure	% of primary or combination of geological structural types (by area)
1	1	90 – 100%
2	1 to 2	70 – 100%
3	1 to 3	50 – 90%
4	3 to 10	50 – 90%
5	10+	50 – 90%

2.4 Boundary Conditions

2.4.1 Hydraulic Boundary Conditions

Hydraulic boundary conditions were calculated for the edges of the 500m scale TRUE Block Scale cube. Heads were calibrated against in-situ measurements by minimizing the difference between measured and simulated heads in the test region in the center of the 200m scale BS2B experimental volume . Heads elsewhere in the TRUE Block may or may not match observed values. The calibration process is described in Section 3.

Figure 2-8 through Figure 2-10 illustrate modeled heads in the JNC/Golder CN model used for the JNC/Golder blind predictions of the BS2B sorbing tracer tests, given a steady-state flow field with no actively pumped wells. These heads were used as the 'base state' of the TRUE Block Scale rock volume before the beginning of any new tracer tests; we assumed the test region was allowed time to equilibrate. Since the BS2B sorbing experiments were conducted as radially-converging tracer tests with a dipole-like geometry, it was not necessary to model the transient flow field.

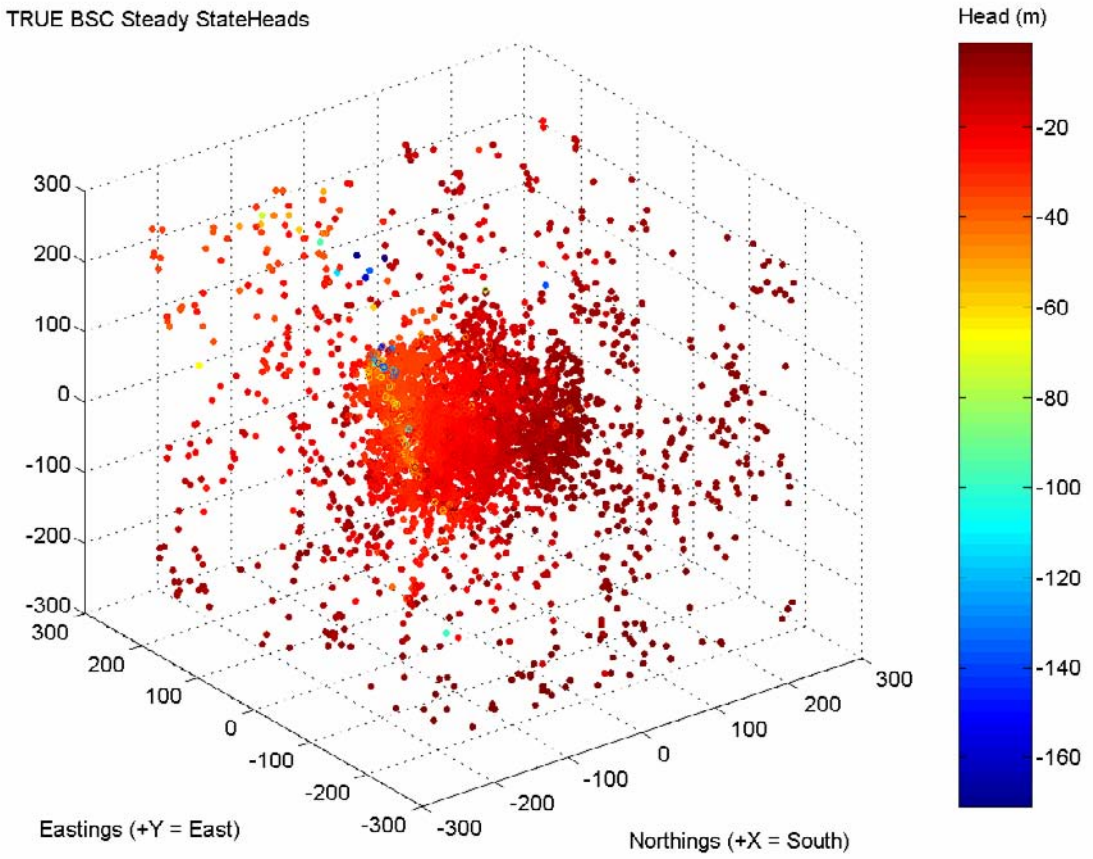

Figure 2-8: *Calculated heads at channel network (CN) model nodes. Nodes represent the intersection of two fractures, and are the endpoints for sets of pipes. Nodes are colored by head, relative to the center of the 500 m TRUE Block Scale rock volume. View is looking southeast from the Äspö HRL tunnel.*

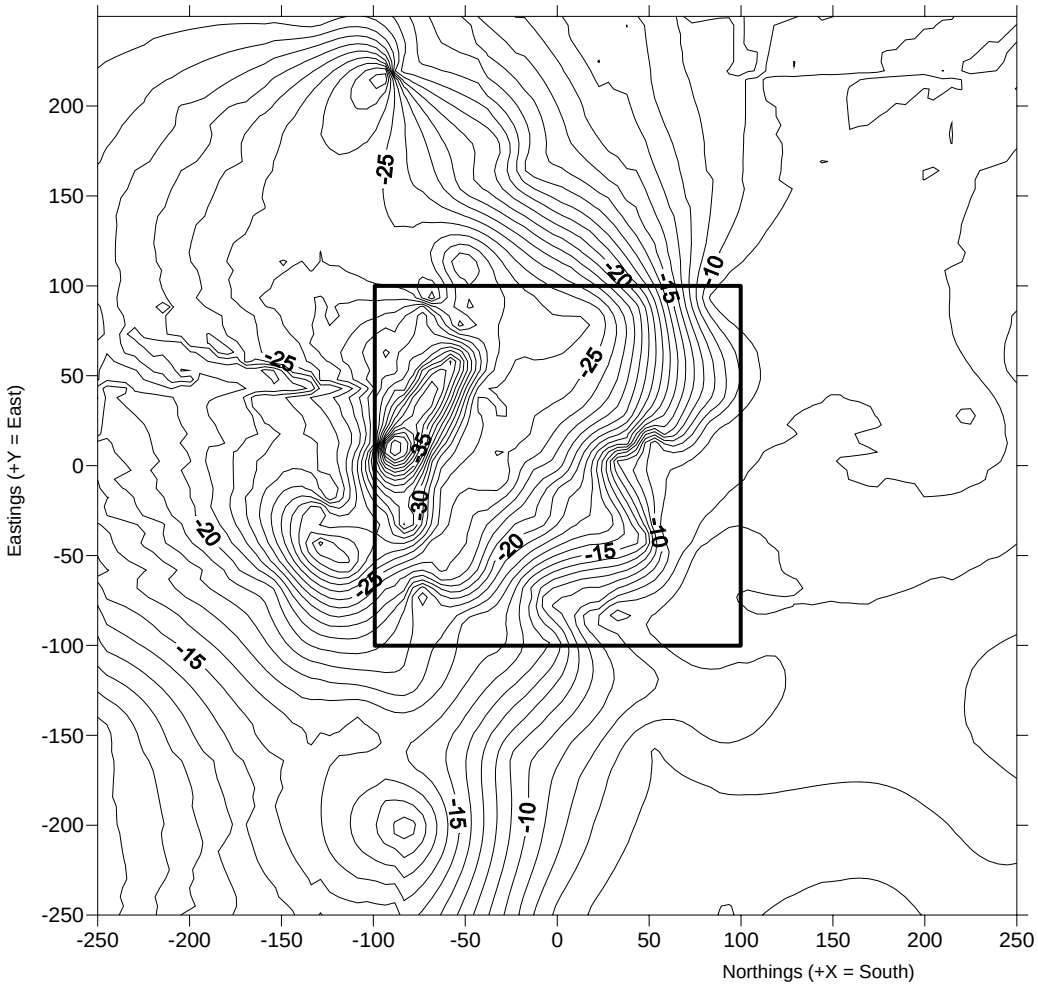

Figure 2-9: *One-meter head contours through the CN model used for the BS2B sorbing tracer predictions. Contour map is a slice in the X-Y plane through the center of the 500 m TRUE Block Scale rock volume. The black box indicates the boundary of the 200 m model region. The Äspö HRL tunnel would be in the upper left corner of this diagram. Coordinate system is FracMan local (+X = South).*

In general, the steady-state head field compared favorably with in-situ measurements. There was a small (0.028 m/m) gradient towards the HRL tunnel, with a head drop of approximately 20 meters across the TRUE Block Scale rock volume from southwest to northeast. Hydraulic head within the area of influence of the BS2B tracer tests were within +/- 5 meters of observed values. However, significant deflections were noted along the northern edge of the 200m cube, with a low of approximately -40m at (90, 0). The cause of these low head values is unknown.

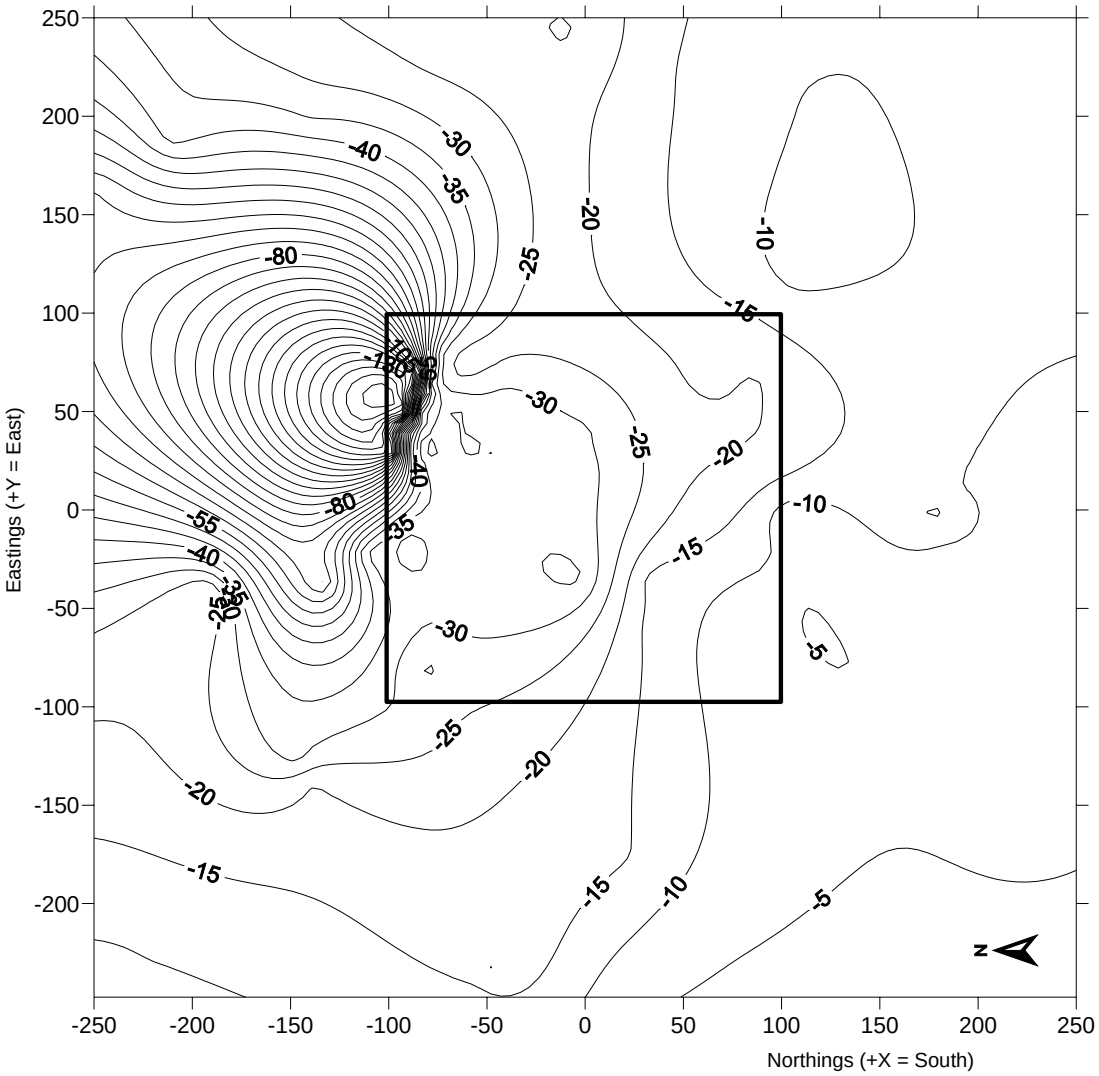

Figure 2-10: *Five-meter groundwater head contours through the CN model used for the BS2B sorbing tracer predictions. Contour map is a slice in the X-Y plane through the center of the 500 m TRUE Block Scale rock volume. The black box indicates the boundary of the 200 m model region. The Äspö HRL tunnel would be in the upper left corner of this diagram. Coordinate system is FracMan local (+X = South).*

2.4.2 Tracer Test Boundary Conditions

Tracer injection boundary conditions were provided in an internal project memorandum, and are summarized below in Table 2-2. The injection flow rate was assumed to be the water pulse injection rate (designed to prevent excessively long recovery curve tailing), and was continued for the duration of the test (as the model assumes a steady-state head field). The sink section was assumed to be pumped at a constant rate to maintain a radially-converging flow field; in reality, some fluctuation of the sink pump flow rate did occur during the actual in-situ tests.

Table 2-2: Data for source and sink sections used in tracer test

Parameter	Source section KI0025F02:R2 (BG1)	Source Section KI0025F02:R3 (#19)	Sink section KI0025F03:R3 (#19)
Eastings (m)	1910.705	1912.801	1903.657
Northings (m)	7120.08	7126.153	7143.081
Elevation (m)	-505.562	-502.782	-508.187
Injection rate	8.33×10^{-8} m^3/s (5 ml/min)	3.33×10^{-8} m^3/s (2 ml/min)	N/A
Pumping rate	N/A	N/A	4.12×10^{-5} m^3/s (2.47 l/min)
Tracers Used	HTO, $^{155}EuDTPA^{2-}$ $^{22}Na^{+}$, $^{133}Ba^{2+}$, $^{54}Mn^{2+}$	$^{131}I^{-}$, $^{160}TbDTPA^{2-}$, $^{85}Sr^{2+}$, $^{86}Rb^{2+}$, $^{137}Cs^{+}$	
Cartesian distance (to sink)	24.2 m	6.99 m	0 m
DFN Path Length* (to sink)	43 – 340 m	29.5 – 122.8	0 m
Structures involved	19, 19 Splay, BG1, Background Fracture Network		

* Note that, in the CN model, there are a number of different paths between the sources and sinks. The DFN path lengths presented here are averages for all the paths found during a graph-theory path search.

During the development of this model, differences in borehole geometries and structural intercepts were noted between the sampling structure files (.SAB) and the published structure intercepts. Borehole intercepts were off by ± 5-10 meters, which resulted in some test sections not intersecting their target structures (Structure 19, Structure BG1, and the Structure 19 Splay). Some adjustments of the borehole network were required; this resulted in a shorter Euclidian distance between test sections KI0025F02_R3 and KI0025F03_R3 than that indicated in SKB model parameter documentation /Anderson, 2004a/.

The JNC/Golder BS2B blind prediction simulations utilized either a Dirac pulse input (full injection mass added to the model in one minute) or the provided full source term measured pulse injection functions to introduce tracers into the flow system. Injection concentrations were specified in an internal project memorandum. Table 2-3 summarizes the injected activities, while Figure 2-11 and Figure 2-12 illustrate the details of each injection. Concentrations are presented in terms of injected activity per solution mass unit injected.

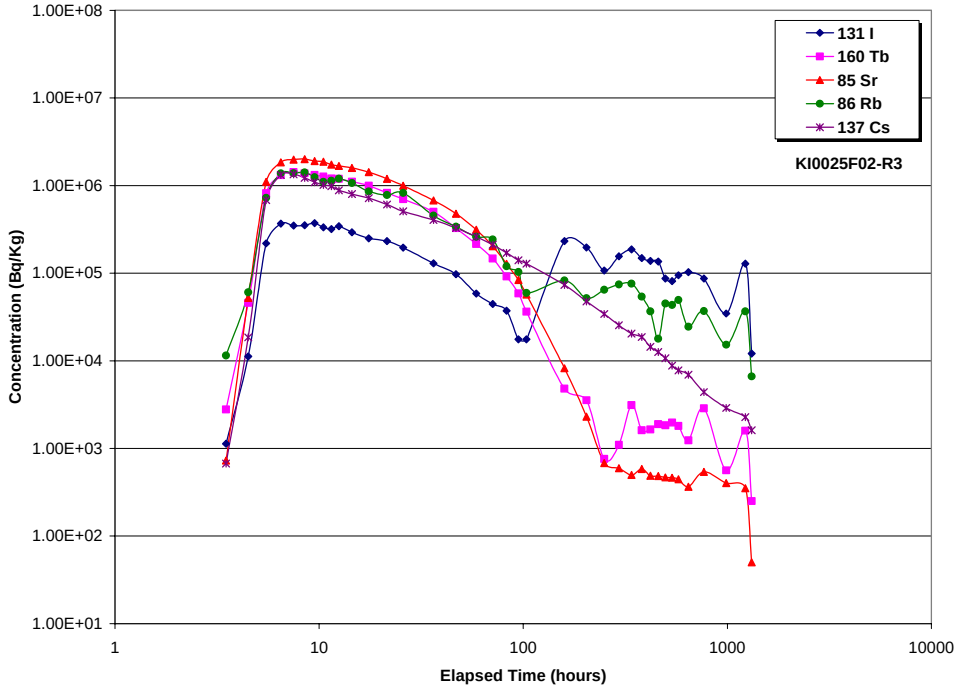

Figure 2-11: *Tracer injection concentrations in borehole KI0025F02, Section R3 (Structure 19, Path I).*

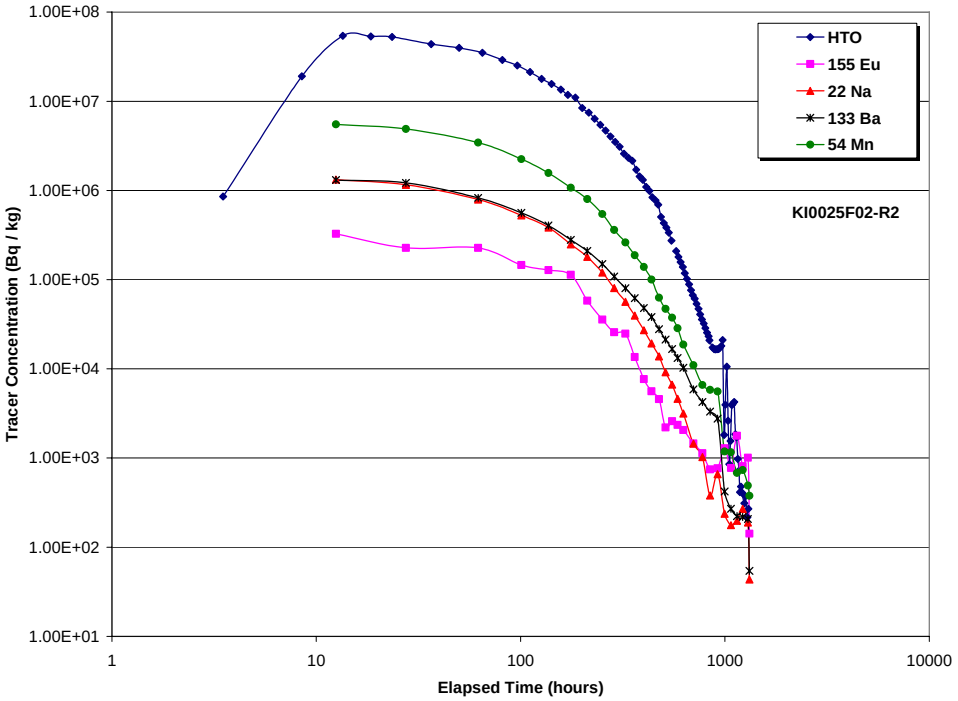

Figure 2-12: *Tracer injection concentrations in borehole KI0025F02, Section R2 (Structure BG1, Path II).*

Table 2-3: Injected tracer activities during BS2B tracer test.

Tracer	Borehole	Injected Activity (Bq)
$^{131}I^{-}$	KI0025F02_R3	3.994×10^{6}
$^{160}Tb^{2-}$	KI0025F02_R3	1.568×10^{7}
$^{85}Sr^{2+}$	KI0025F02_R3	2.228×10^{7}
$^{86}Rb^{2+}$	KI0025F02_R3	1.521×10^{7}
$^{137}Cs^{+}$	KI0025F02_R3	2.176×10^{7}
HTO	KI0025F02_R2	7.202×10^{8}
$^{155}Eu^{2-}$	KI0025F02_R2	5.217×10^{6}
$^{22}Na^{+}$	KI0025F02_R2	1.520×10^{7}
$^{133}Ba^{2+}$	KI0025F02_R2	1.756×10^{7}
$^{54}Mn^{2+}$	KI0025F02_R2	6.695×10^{7}

2.5 Solute Transport Properties

The solute retention material properties for the "Type 1" and "Type 2" structures were provided in Byegård and Tullborg /2004/. The values used in simulations are based on these specifications. No calibration was carried out.

Immobile zone properties were specified based on a specific combination of immobile zones for "Type 1" and "Type 2" structures. Immobile zones were assigned on a set-by-set basis; as such, fracture sets were grouped in the geologic model by geologic structure type (I or II). The thickness, formation factor F, and porosity *n* are specified by immobile zone as given in Table 2-4 through Table 2-6. These properties were based on those previously reported in the Task 6C hydrostructural model /Dershowitz et al., 2003/, with site-specific modifications for the BS2B experiment /Tullborg and Hermanson, 2004, and Byegärd and Tullborg, 2004/.

Table 2-7 and Table 2-8 present effective diffusivities (D_e) and volumetric sorption coefficients (K_d) for the specified tracers in contact with the different geological material types present in Type I and Type II features. K_d values were those provided for TRUE Block Scale groundwater in the Task 6D modeling specifications /Elert and Selroos, 2002/. Effective diffusivity (D_e) was based on the product of the formation factor F and the free-water diffusivity (D_w).

Table 2-4: Immobile Zone Properties for Type 1 (Fault) Structures

Rock Type	Extent (cm)	Porosity (%)	Formation Factor (-)
Intact wall rock	100	0.3	7.3×10^{-5}
Altered zone	15	0.6	2.2×10^{-4}
Cataclasite d_{cat}	1	1	4.9×10^{-4}
Fault gouge d_g	0.3	20	5.6×10^{-2}
Fracture coating	0.05	5	6.2×10^{-3}

Table 2-5: Immobile Zone Properties for Structure Z (modified Fault)

Rock Type	Extent (cm)	Porosity (%)	Formation Factor (-)
Intact wall rock	100	0.3	7.3×10^{-5}
Altered zone	25	0.6	2.2×10^{-4}
Cataclasite d_{cat}	2	1	4.9×10^{-4}
Fault gouge d_g	0.5	20	5.6×10^{-2}
Fracture coating	0.05	5	6.2×10^{-3}

Table 2-6: Immobile Zone Properties for Type 2 (Joint) Structures

Rock Type	Extent (cm)	Porosity (%)	Formation Factor (-)
Intact wall rock	100	0.3	7.3×10^{-5}
Altered zone	5	0.6	2.2×10^{-4}
Fracture coating	0.05	5	6.2×10^{-3}

Table 2-7: Effective Diffusivity D_e

		Fracture Coating	Fault gouge	Cataclasite	Altered Zone	Unaltered wall rock
	Porosity (%)	5	20	1	0.6	0.3
	Formation factor, F	6.20E-03	5.60E-02	4.90E-04	2.20E-04	7.30E-05
	D_w (m^2/s)[A)]	D_e (m^2/s)	D_e (m^2/s)	D_e (m^2/s)	D_e (m^2/s)	D_e (m^2/s)
HTO	2.13E-09	1.30E-11	1.20E-10	1.00E-12	4.70E-13	1.60E-13
I^-	2.00E-09	1.20E-11	1.10E-10	9.80E-13	4.40E-13	1.50E-13
Na^+	1.33E-09	8.30E-12	7.40E-11	6.50E-13	2.90E-13	9.70E-14
Mg^{2+}	7.05E-10	4.40E-12	3.90E-11	3.50E-13	1.50E-13	5.20E-14
K^+	1.96E-09	1.20E-11	1.10E-10	9.60E-13	4.30E-13	1.40E-13
Ca^{2+}	7.93E-10	5.00E-12	4.40E-11	3.90E-13	1.70E-13	5.80E-14
Rb^+	2.06E-09	1.30E-11	1.20E-10	1.00E-12	4.50E-13	1.50E-13
Sr^{2+}	7.94E-10	5.00E-12	4.40E-11	3.90E-13	1.70E-13	5.80E-14
Cs^+	2.07E-09	1.30E-11	1.20E-10	1.00E-12	4.50E-13	1.50E-13
Ba^{2+}	8.48E-10	5.30E-12	4.70E-11	4.20E-13	1.90E-13	6.20E-14
Ra^{2+}	8.89E-10	5.60E-12	5.00E-11	4.40E-13	1.90E-13	6.50E-14
Am(III)	5.95E-10	3.70E-12	3.30E-11	2.90E-13	1.30E-13	4.40E-14
Tc(IV)	5.00E-10	3.10E-12	2.80E-11	2.50E-13	1.10E-13	3.70E-14

Table 2-8: Volumetric Sorption Coefficient K_d

	Fracture Coating K_d (m^3/kg)	Fault Gouge K_d (m^3/kg)	Cataclasite K_d (m^3/kg)	Altered Zone K_d (m^3/kg)	Intact wall rock K_d (m^3/kg)
I^-	0	0	0	0	0
Ca^{2+}	2.30E-04	7.10E-04	6.70E-05	8.80E-05	4.40E-05
Cs^+	5.20E-02	1.60E-01	1.50E-02	2.00E-02	1.00E-02
Ra2+	4.60E-02	1.40E-01	1.30E-02	1.80E-02	8.80E-03
Tc(IV)	2.00E-01	2.00E-01	2.00E-01	2.00E-01	2.00E-01
Am(III)	5.00E-01	5.00E-01	5.00E-01	5.00E-01	5.00E-01
Ba^{2+}	4.60E-03	1.40E-02	1.30E-03	1.80E-03	8.80E-04

Free water diffusivity (D_w) for the rhenium oxide tracer (ReO^{4-}) was assumed to be the same as that of iodide and pertechnetate, as recommended in the Task 6D specification /Elert and Selroos, 2002/.

Surface sorption distribution coefficients (K_a) were calculated from the K_d values according to the following formula:

$$K_a = (K_d * \rho + n) * d$$

where *d* is the thickness of the fracture coating in meters, *n* is the porosity of the material within the immobile zone, and ρ is the bulk density of the material in kilograms per cubic meter (see Table 2-9). K_a values were calculated within PAWorks as an immobile zone property, and, as such, vary between fracture sets. Geologic material densities were calculated using mineralogical breakdowns specified in the Task 6C hydrostructural report /Dershowitz et al., 2002/ and average chemical compositions of typical mineral end-members /Deer et al., 1966 and Kline & Hurlbut, 1993/.

Table 2-9: Geologic material densities calculated using mineralogical breakdowns specified in the Task 6C hydrostructural report.

Mineral	Specific Gravity (-)	Bulk Density (kg/m^3)	Fracture Coating		Fault Gouge	
			%	Fracture Volume	%	Fracture Volume
Smectite (assumed montmorillonite)	2.5	2500	-	-	0.04	100
Illite	2.6	2600	0.03	65	0.12	312
Mixed-layer clay	2.59	2590	0.03	64.75	0.08	207.2
Chlorite	2.95	2950	0.35	1032.5	0.25	737.5
Mica (50% musc. / 50% biotite)	2.84	2840	-	-	0.07	198.8
Epidote	3.4	3400	0.05	170	0.01	34
Plagioclase	2.69	2690	-	-	0.12	322.8
Potassium Feldspar (orthoclase)	2.57	2570	0.1	257	0.06	154.2
Sulphides (est.average)	4.75	4750	-	-	0.01	47.5
Calcite	2.71	2710	0.35	948.5	0.08	216.8
Quartz	2.65	2650	0.08	212	0.16	424
Hematite	5.26	5260	0.02	78.9	-	-
Pyrite	5.02	5020	0.01	25.1	-	-
Bulk Density (kg/m^3)				**2853.75**		**2754.8**
Bulk Density (adjusted for porosity)			95%	**2761.1**	80%	**2403.8**

Mineral	Specific Gravity	Bulk Density (kg/m^3)	Cataclasite		Altered Zone	
			%	Frac. Vol.	%	Frac. Vol.
Chlorite	2.95	2950	0.06	177	0.17	491.67
Epidote	3.4	3400	0.2	680	0.17	566.67
Plagioclase	2.69	2690	0.1	269	-	-
Potassium Feldspar (orthoclase)	2.57	2570	-	-	-	-
Calcite	2.71	2710	-	-	-	-
Quartz	2.65	2650	0.14	371	0.17	441.67
Biotite	3	3000	0.03	90	-	-
Albite	2.62	2620	0.4	1048	0.42	1106.22
Sericite	2.82	2820	0.04	112.8	0.02	62.67
Magnetite	5.18	5180	0.0125	64.75	0.02	86.33
Hematite	5.26	5260	0.005	26.3	0.01	29.22
Titanite	3.48	3480	0.0125	43.5	0.02	58.0
Apatite	3.175	3175	0.01	31.75	0.02	52.92
Pyrite	5.02	5020	-	-	-	-
Bulk Density (kg/m^3)				**2914.1**		**2895.4**
Bulk Density adjusted for porosity			99	**2895.0**	99.4	**2878.0**

2.6 Assumptions and Constraints

This section accounts for the assumptions and constraints included in modeling.

1. Radioactive decay was not considered in the modeling, such that all concentrations reported are values which would be measured if there were no radioactive decay. This is equally true for tracer injection time histories and breakthrough curves.

2. Simulations were carried out up to a time of 10,000 hours; however, performance measures were calculated at the 5,000 hour mark, as per the BS2B modeling specifications.

3. The immobile zone conceptual model assumed a combination of immobile zones arranged in parallel (fault gouge, fracture coating, cataclasite, altered wall rock, and intact wall rock). The PAWorks / LTG toolchain is limited to modeling immobile-zone retardations in parallel; see Chapter 4 for further details. Up to five immobile zones (as a combination of matrix and non-flowing pore space zones) can be assigned to a single fracture set.

4. Steady-state flow. Time-varying fluxes (injection and sink wells) were converted to average flow rates for the duration of the test.

5. Water flow and radionuclide transport occur within the fracture network. Transport within the rock matrix (outside of diffusion losses) was not modeled.

6. Only a limited calibration to tracer pre-test CPT-4c was performed. The only parameters changed were the size, extent, and hydraulic properties of Structure BG1; the remainder of the DFN model was not modified during calibration.

3 Developing the 500-m scale boundary conditions

The goal of this task was to develop a reasonable initial head field for the 500 m TRUE Block Scale rock volume that was constrained to head values observed in relevant boreholes. Previously-used head boundaries were either case-specific (Task 6D, 6E), or utilized a head field sliced from a larger regional-scale model. Neither option was truly desirable for producing accurate predictions of in-situ conditions; a model that represented actual site heads was required.

3.1 Head Calibration Model Description

The hydraulic head calibration model consists of two fundamental components; a set of interconnected discrete pipes ('channel network') representing the fracture network within the TRUE Block volume, and a set of initial boundary conditions for the external (500 m) boundaries of the BS2B simulation volume.

3.1.1 Model elements and boundary conditions

The BS2B calibration model was based primarily on the Task 6C TRUE Block Scale hydrostructural model /Andersson et al., 2002a; Dershowitz et al., 2003/. The model represents a 0.125 km^3 volume, centered at (1900 m, 7170 m, -450 m) in the Äspö local coordinate system. A summary sketch of the model extents is presented as Figure 3-1. To perform the calibrations, head data from 50 measurement intervals spread throughout an array of six boreholes (KA2511A, KA2563A, KI0023B, KI0025F, KI0025F02, and KI0025F03) within the 200 m BS2B volume was used. The borehole array is illustrated below in Figure 3-2.

The DFN implementation consisted of three separate fracture populations from the Task 6C hydrostructural model:

1. 500 m scale features. These features provide connectivity between the model boundaries, the interior (200 m region) fracture network, and the boreholes. Figure 3-3 illustrates these features.
2. 200 m scale features. These features represent deterministic structures identified as hydraulically significant during Task 6C. This set also includes Structure #19, which is the focus of the BS2B experiment. Figure 3-4 illustrates these features.
3. Background fractures: These features represent a set of small (1 – 20 m size) background fractures identified during POSIVA borehole flow logging as possessing hydraulically significant inflows. These features are shown in Figure 3-5.

The complete background fracture network was not simulated; only fractures with borehole intersections that were identified as conductive during POSIVA flow logging or in BIPS image logs were utilized. The DFN implemented for head calibration efforts was slightly different compared with that used to model tracer transport; the same level of detail at the 200 m scale (BS2B experimental volume) was not needed.

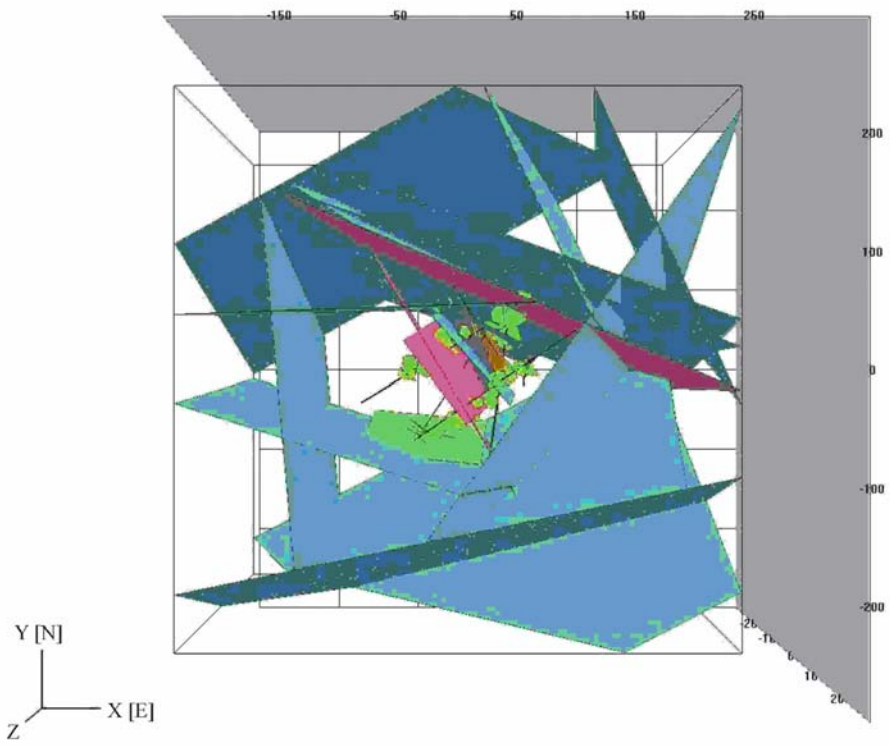

Figure 3-1: *Fractures and model extents used for 500 m TRUE Block Scale rock volume head field calibration.*

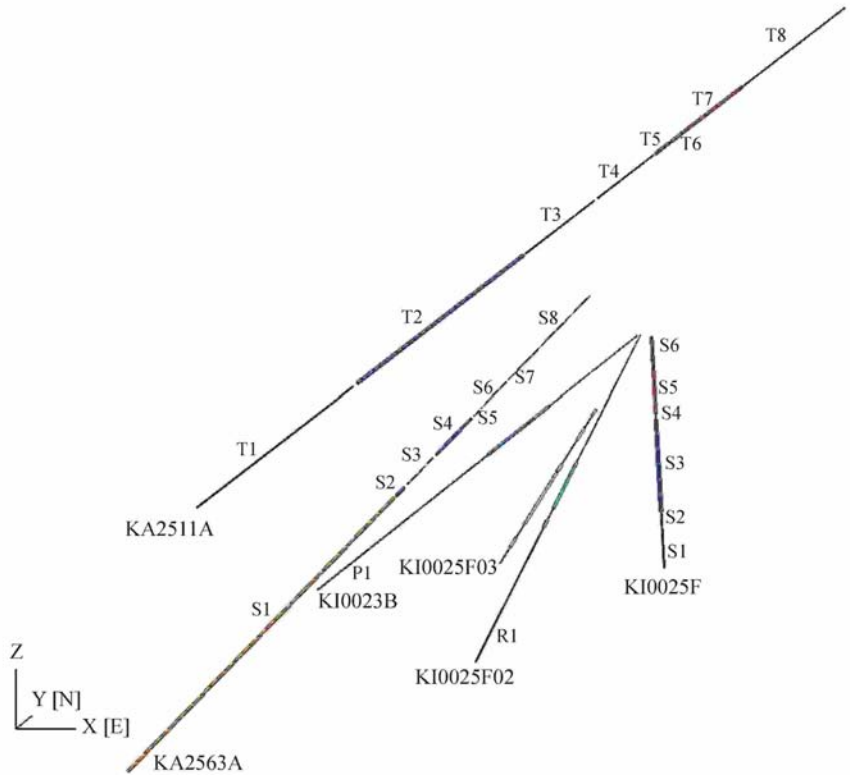

Figure 3-2: *Boreholes and numbered packer intervals used for 500 m TRUE Block Scale rock volume head field calibration. View is looking northwest at a slight up angle.*

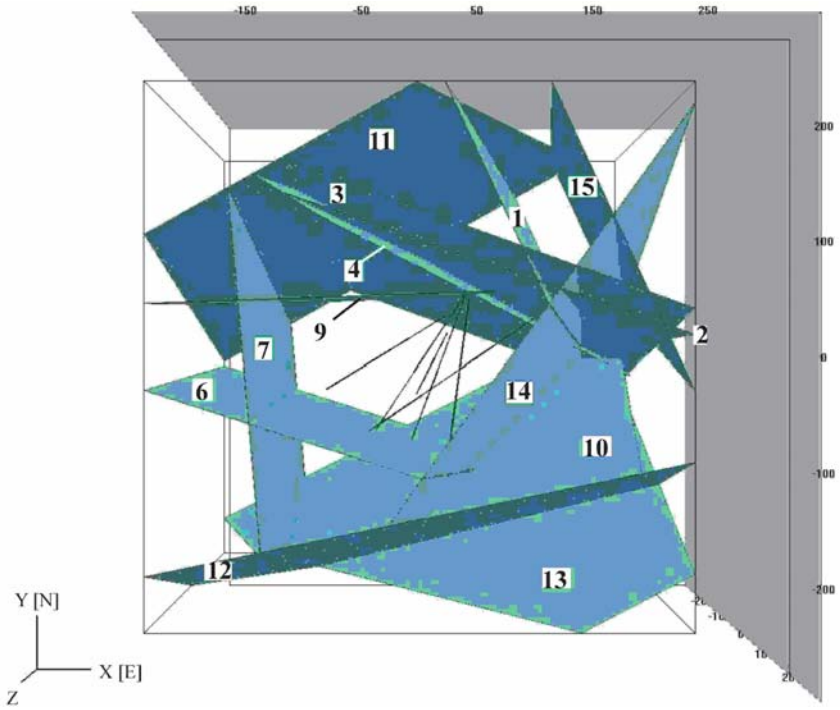

Figure 3-3: *Intercepts of 500 m scale fractures with the borehole array used in the head field calibration. Numbering of structures is in accord with that introduced in the Task 6C model /Dershowitz et al., 2003/.*

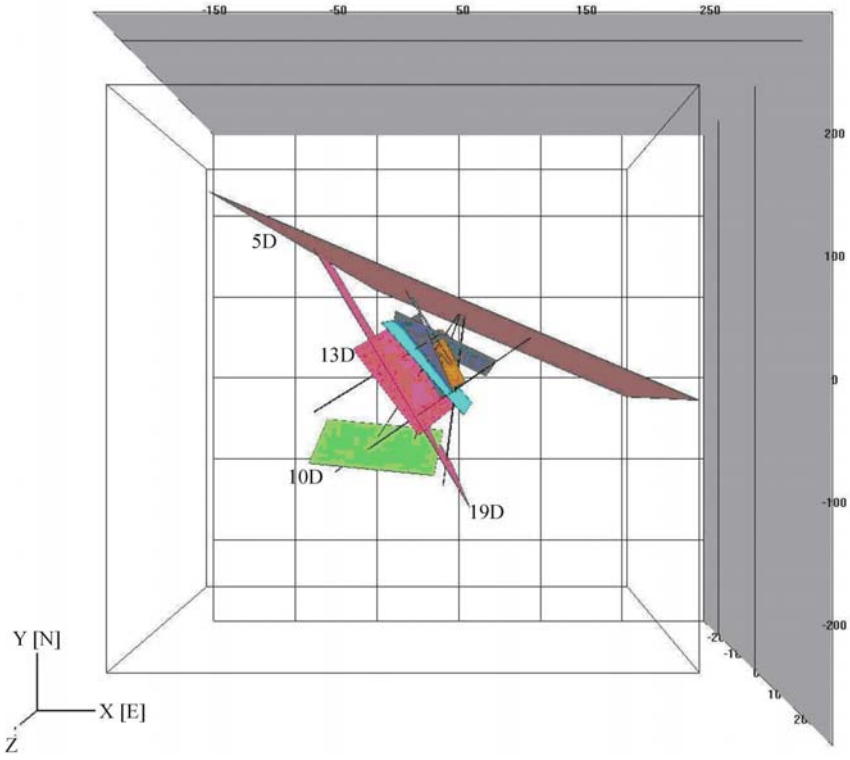

Figure 3-4: *Intercepts of 200 m-scale BS2B experimental volume structures with the borehole array used in the head field calibration. Numbering of structures is in accord with the BS2B hydrostructural model.*

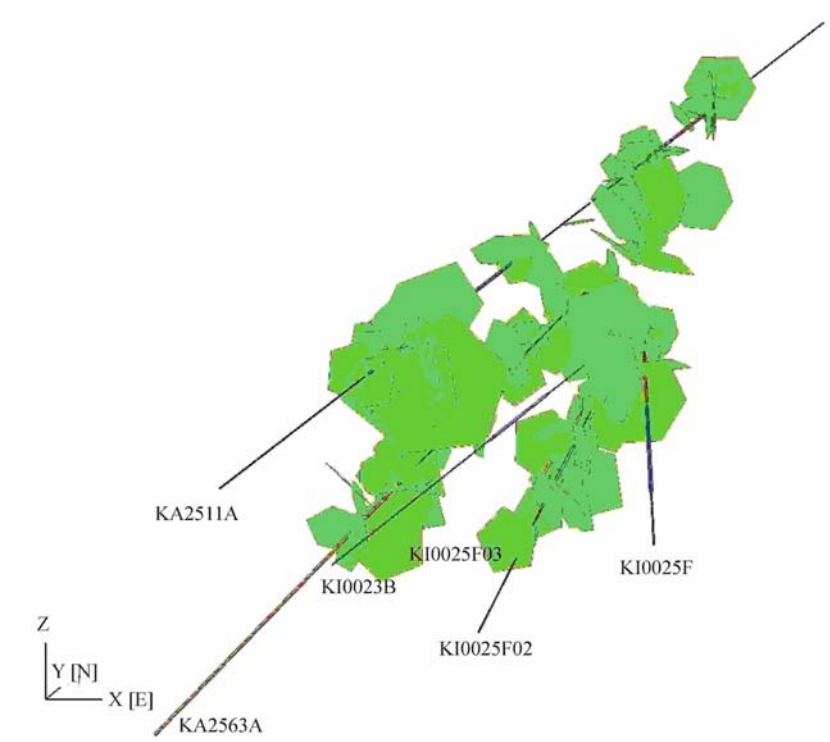

Figure 3-5: *Conditioned background fractures derived from BIPS imagery or Posiva flow logging within the 200 m BS2B experimental volume.*

Table 3-1 and Table 3-2 illustrate the relationships between the large-scale (500 m) and small-scale (200 m) features. These intersections are critical as they provide connections to the block boundaries, which allows for the head solution to propagate to the interior of the block.

Table 3-1: Relationships between 500 m scale and 200 m scale features. The 'X' indicates an intersection between features at different scales.

500 m	200 m scale fracture					500 m scale fractures											
scale	5D	6D	7D	10D	19D	1	2	3	4	6	7	9	10	11	12	13	14
2					X	X											
3	X				X	X	X										
4	X					X	X	X									
5																	
6				X	X												
7										X							
9	X	X	X		X						X						
10	X				X	X	X	X	X	X	X						
11	X					X	X	X	X		X	X					
12											X		X				
13	X							X		X	X						
14	X				X	X	X	X	X	X			X		X	X	
15	X						X	X		X				X			X

All fractures within the 500 m scale (14 structures total) were assigned default a default transmissivity and aperture value of 1.00×10^{-6} (m^2/s and m, respectively). The 200 m scale features were assigned properties according to the Task 6C hydrostructural model; a summary of the relevant properties is presented below in Table 3-3.

Table 3-2: Intersections between significant Task 6C deterministic structures and 200 m / 500 m scale features.

Deterministic Fracture	200 m Scale Feature Intersections	500 m Scale Feature Intersections
5D	6D,19D	3,4,9,10,11,12,13,14
6D	5D,7D,22D	3,9
7D	6D,13D,20D,21D,22D	9
10D	19D	6
13D	7D,19D,20D,21D,22D	-
19D	5D,10D,13D	2,3,9,10,11,14
20D	7D, 13D, 21D, 22D	-
21D	7D,13D,20D	9
22D	6D,7D,13D,20D,23D	-
23D	22D	-

Table 3-3: Hydraulic properties of significant deterministic structures used in BS2B head calibration.

Deterministic Feature	Transmissivity m^2/s	Aperture m
5D	4.020×10^{-7}	2.917×10^{-4}
6D	1.910×10^{-7}	2.010×10^{-4}
7D	9.760×10^{-8}	1.437×10^{-4}
10D	2.980×10^{-8}	7.941×10^{-5}
13D	1.380×10^{-8}	5.404×10^{-5}
19D	1.020×10^{-7}	1.469×10^{-4}
20D	1.430×10^{-7}	1.740×10^{-4}
21D	6.020×10^{-8}	1.129×10^{-4}
22D	2.190×10^{-8}	6.807×10^{-5}
23D	1.660×10^{-7}	1.874×10^{-4}
24D	8.510×10^{-8}	1.342×10^{-4}

3.1.2 Simplified Channel Network (CN) Model

The three-dimensional calibration DFN was transformed to a series of one-dimensional nodes and interconnected pipes ('channel network') using the PAWorks software package /Dershowitz et al., 2000/. The details of the channel network discretization process are presented in Section 4. Figure 3-6 through Figure 3-9 illustrate the nodes (pipe endpoints) connected to the target 500 m boundaries.

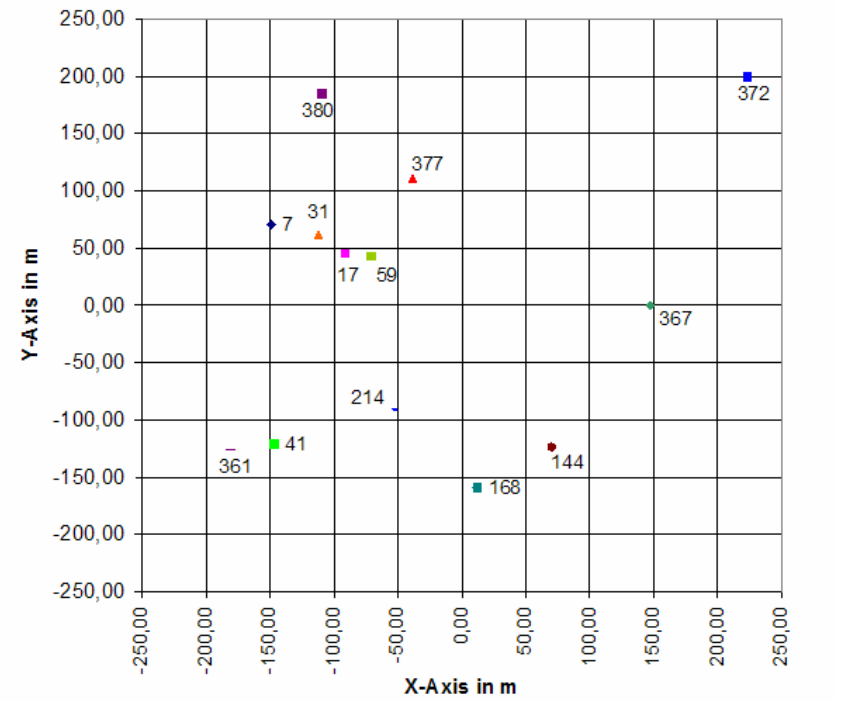

Figure 3-6: *CN node intersections with upper boundary (Z = -200 m above mean sea level (masl)) of 500 m TRUE Block Scale rock volume.*

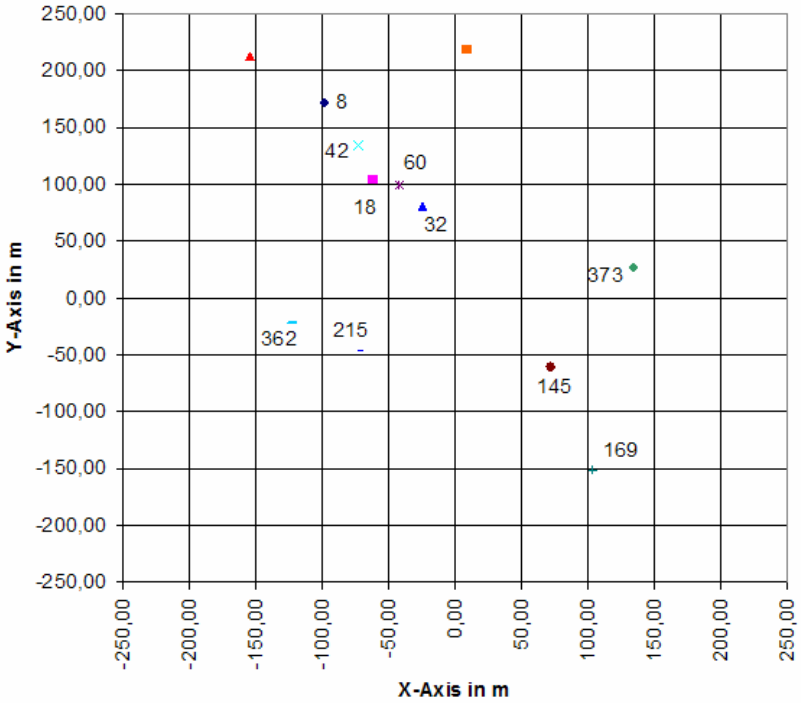

Figure 3-7: *CN node intersections with lower boundary (Z = -700m above mean sea level (masl)) of 500 m TRUE Block Scale rock volume.*

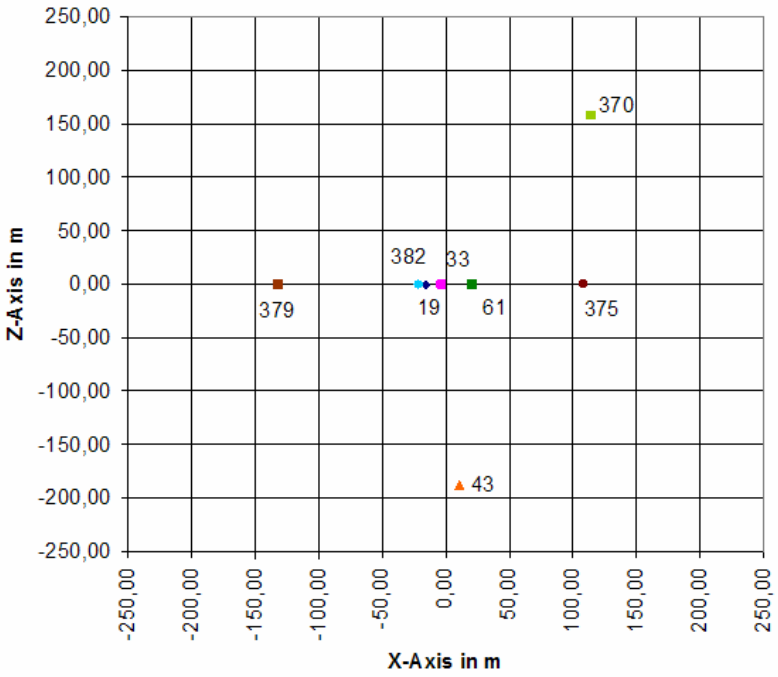

Figure 3-8: *CN node intersections with east face of 500 m TRUE Block Scale rock volume.*

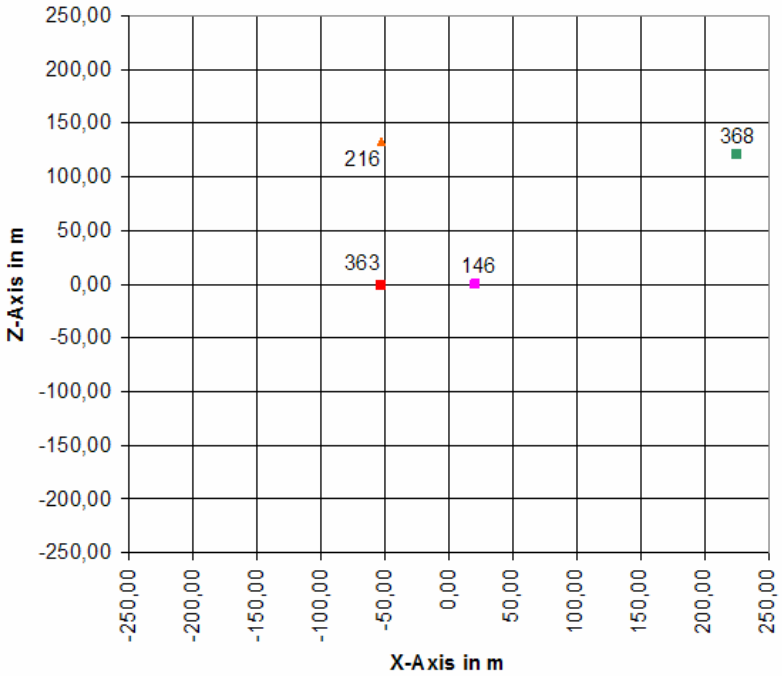

Figure 3-9: *CN node intersections with west face of 500 m TRUE Block Scale rock volume.*

3.2 Model Calibration of Hydraulic Head

3.2.1 Input Data

The initial head field was obtained from the site-scale interpolation of available hydraulic head data /Anderson et al., 2002a/. These pressure conditions were interpolated to a regular array of 20-m spaced points over a 500-m cube. This head field was not conditioned to the measured heads provided for this study. It served as a first approximation for the task and was changed accordingly as required throughout the calibration. The head field was in fact the only parameter where changes were made throughout the calibration.

Figure 3-10 through Figure 3-13 illustrate the initial head field conditions prior to model calibration. Heads generally decrease from south to north, and show some gradient towards the Äspö HRL tunnel.

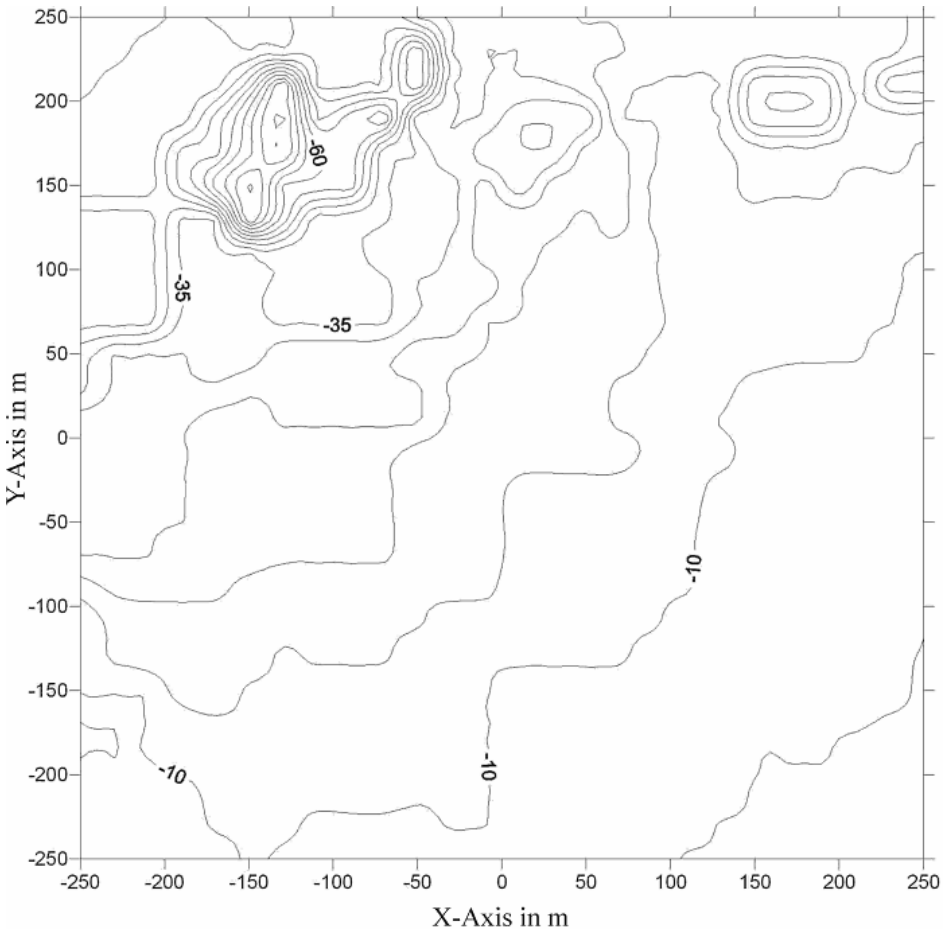

Figure 3-10: *Initial head field contours in the XY plane, Z = -200 m above mean sea level (masl) (top of model).*

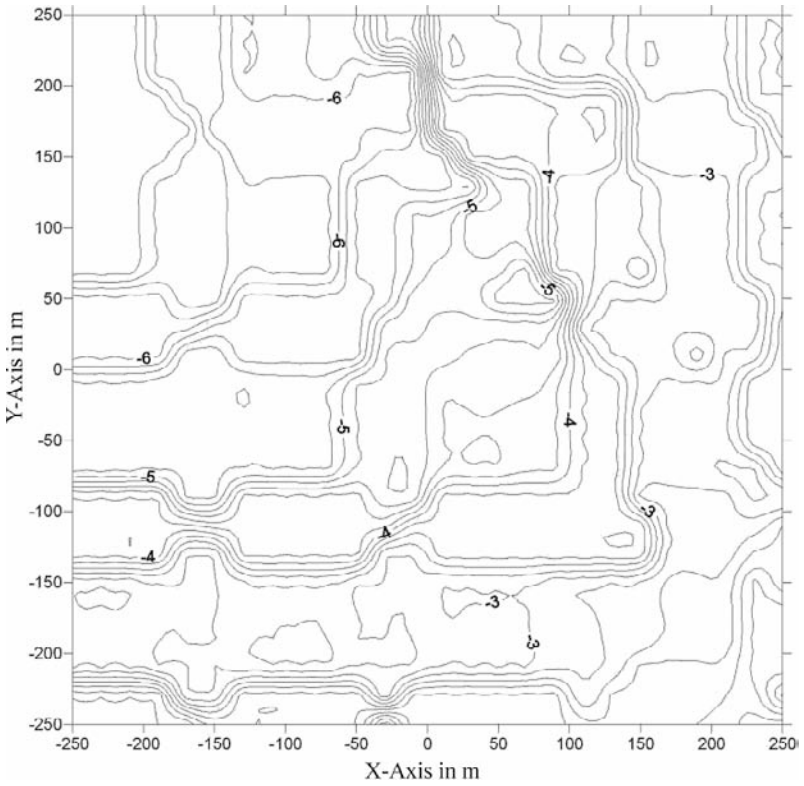

Figure 3-11: *Initial head field contours in the XY plane, Z = -700 m above mean sea level (masl)(bottom of model).*

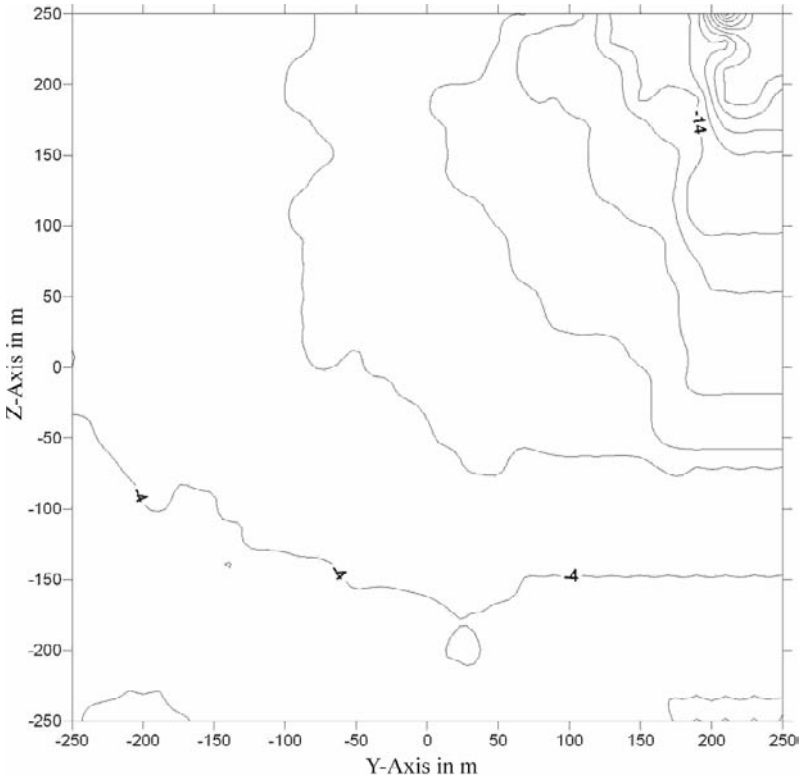

Figure 3-12: *Initial head field contours in the YZ plane, X = 6920 m (south face of 500 m cube).*

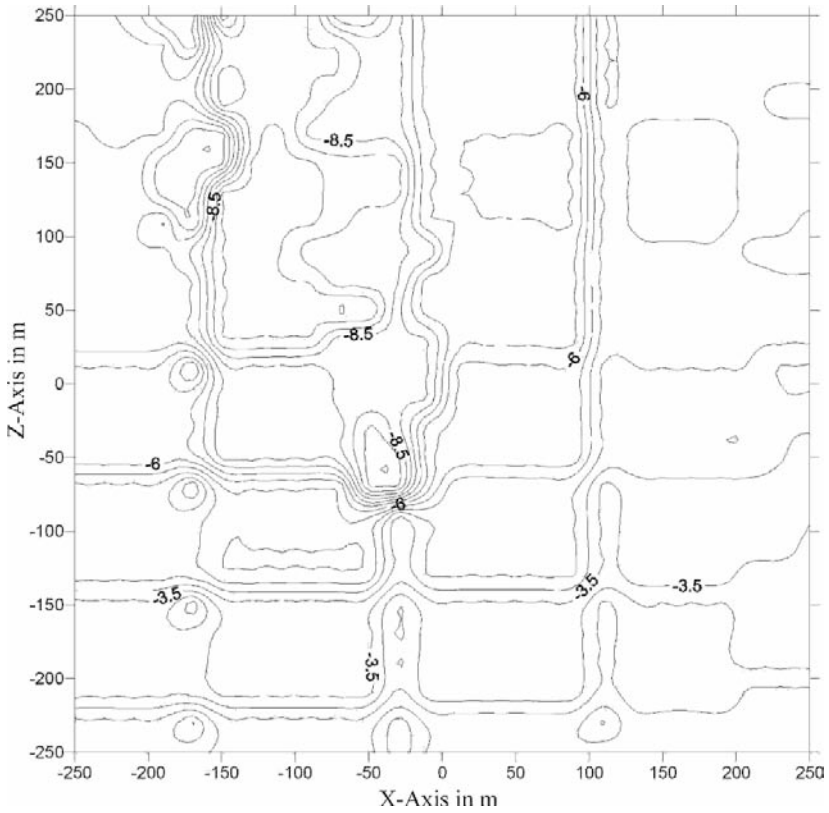

Figure 3-13: *Initial head field contours in the XZ plane, Y = 1650 m (west face of 500 m cube).*

Once the discretization of the channel network was complete, the initial head field was applied as a boundary condition, and a steady-state flow solution completed using MAFIC (Miller et al., 2001). This resulting model formed the basis for the BS2B head calibration efforts. Calibration was achieved by adjusting head values at nodes on the 500 m boundaries to match head values observed within specific sections of the TRUE Block Scale borehole array (see Section 3.1).

3.2.2 Head Calibration Criteria and Workflow

Three specific criteria, consisting of limits for interval head differences, were chosen to determine the 'goodness of fit' for a specific calibration run. Calibration consisted of a stepped iterative process of minimizing global errors while keeping head values in the test sections within criteria limitations. The goal for each step was to maximize the number of test sections meeting the step criteria. The criteria were:

- Difference between simulated and measured head: $\Delta H < 1$ m
- Difference between simulated and measured head: 1 m $< \Delta H <$ 5 m
- Difference between simulated and measured head: 5 m $< \Delta H <$ 6 m

The model was calibrated to match heads recorded in the borehole array on 11 September, 2003, at 0800 local time. Data from this date was assumed to represent natural gradient conditions (i.e. there were no active wells or significant pressure disturbances during the measurement period).

Nine test intervals recorded no fracture intersections given the DFN implemented and these sections were discarded from the calibration process. In-situ pressure readings were not available for three additional borehole sections; these sections were retained in the modeling process.

3.2.3 Calibration Stages

As discussed in Section 3.2.2, the first calibration stage consisted of applying the existing 500 m cube head field to the channel network and comparing heads in selected sections of the borehole array to in-situ observations. The difference between measured and simulated head was quite large; an absolute error of 33.08 m, with a standard deviation of 13.24 m, was recorded. Formal results for all test sections are presented in Table 3-4.

Table 3-4: Comparison of simulated head (first calibration stage) derived from a steady-state 1D flow solution using the initial 500 m block head values (Section 3.2.1) versus observed head from the TRUE Block Scale borehole array.

Borehole Interval	Node Group	Intersecting Structures	Measured Head (masl)	Simulated Head (masl)	Abs. Error (m) ΔH (m)
KA2511A_T1	2	10D	-23.37	-14.62	8.75
KA2511A_T2	3	10D, 73	-27.85	-18.88	8.97
KA2511A_T3	4	13D, 19D	-35.26	-23.06	12.2
KA2511A_T4	5	20D	-35.93	-23.01	12.92
KA2511A_T8	9	5D	-49.11	-34.91	14.2
KA2563A_S1	10	19D, 84	-41.11	-28.74	12.37
KA2563A_S2	11	19D, 84, 148	-41.55	-29.18	12.37
KA2563A_S3	12	19D	-42.57	-30.19	12.38
KA2563A_S4	13	13D, 92, 128	-43.83	-31.44	12.39
KA2563A_S5	14	13D	-47.24	-34.85	12.39
KA2563A_S6	15	13D, 135	No Data		
KA2563A_S7	16	20D	No Data		
KA2563A_S8	17	6D, 7D, 21D	No Data		
KI0025F_S1	18	6, 10	-63.32	-52.58	10.74
KI0025F_S2	19	19D	-41.68	-30.13	11.55
KI0025F_S4	21	20D	-44.01	-31.09	12.92
KI0025F_S5	22	7D, 20D, 22D, 23D	-49.5	-36.58	12.92
KI0025F_S6	23	5D, 24D	-52.81	-39.74	13.07
KI0023B_P1	24	10D	-24.57	-15.9	8.67
KI0023B_P2	25	19D	-41.28	-29.15	12.13
KI0023B_P4	27	13D	-42.42	-29.7	12.72
KI0023B_P6	29	21D	-43.75	-30.85	12.9
KI0023B_P7	30	6D, 20D, 22D	-44.07	-31.15	12.92
KI0023B_P8	31	7D	-49.13	-36.19	12.94

Borehole Interval	Node Group	Intersecting Structures	Measured Head (masl)	Simulated Head (masl)	Abs. Error (m) ΔH (m)
KI0023B_P9	32	5D	-71.64	-58.65	12.99
KI0025F02_R1	33	10D	-25.98	-16.95	9.03
KI0025F02_R2	34	54	-45.77		
KI0025F02_R3	35	19D, 31	-42.42	-30.56	11.86
KI0025F02_R5	37	13D, 21D	-42.83	-29.98	12.85
KI0025F02_R6	38	13D, 21D, 43	-107.79	-94.93	12.86
KI0025F02_R7	39	20D	-44.67	-31.75	12.92
KI0025F02_R8	40	22D	-44.22	-31.3	12.92
KI0025F02_R9	41	23D	-52.95	-40.02	12.93
KI0025F02_R10	42	5D, 6D, 7D, 24D	-52.01	-39.03	12.98
KI0025F03_R2	44	19D, 119	-42.47	-30.48	11.99
KI0025F03_R3	45	19D	-42.54	-30.58	11.96
KI0025F03_R4	46	21D, 129	-42.31	-29.45	12.86
KI0025F03_R5	47	21D	-43.14	-30.28	12.86
KI0025F03_R6	48	13D	-44.67	-31.82	12.85
KI0025F03_R7	49	20D	-44.89	-31.98	12.91
KI0025F03_R8	50	22D	-43.92	-30.99	12.93
KI0025F03_R9	51	23D	-49.27	-36.34	12.93

The second calibration stage, which consisted of 49 different flow model iterations, focused on changes to the head field applied to the top and bottom of the model region. Hydraulic Head along the east and west faces of the model were not changed from their 'best-fit' values determined in the first calibration stage.

The third (and final) calibration stage, consisted of 53 different model iterations, and used calibration step 12zh (the 'best-fit' model calculated during the second calibration stage) as a starting point. During these simulations, only the heads atop the model volume (Z = -200 masl) were changed iteratively.

3.3 Calibration Results

The stepped iterative calibration approach was able to significantly reduce the level of error, relative to current TRUE Block Scale head measurements, in a steady-state, natural gradient flow solution. The overall standard deviation of the absolute error (Figure 3-14) between measured and observed heads was reduced from 13.23 to 12.50, and the average absolute error for the summed borehole segments (Figure 3-15) was reduced from approximately 35 meters to slightly less than 6 meters. For most of the calibration borehole sections, head values were brought to within 5 meters of their recorded in-situ values.

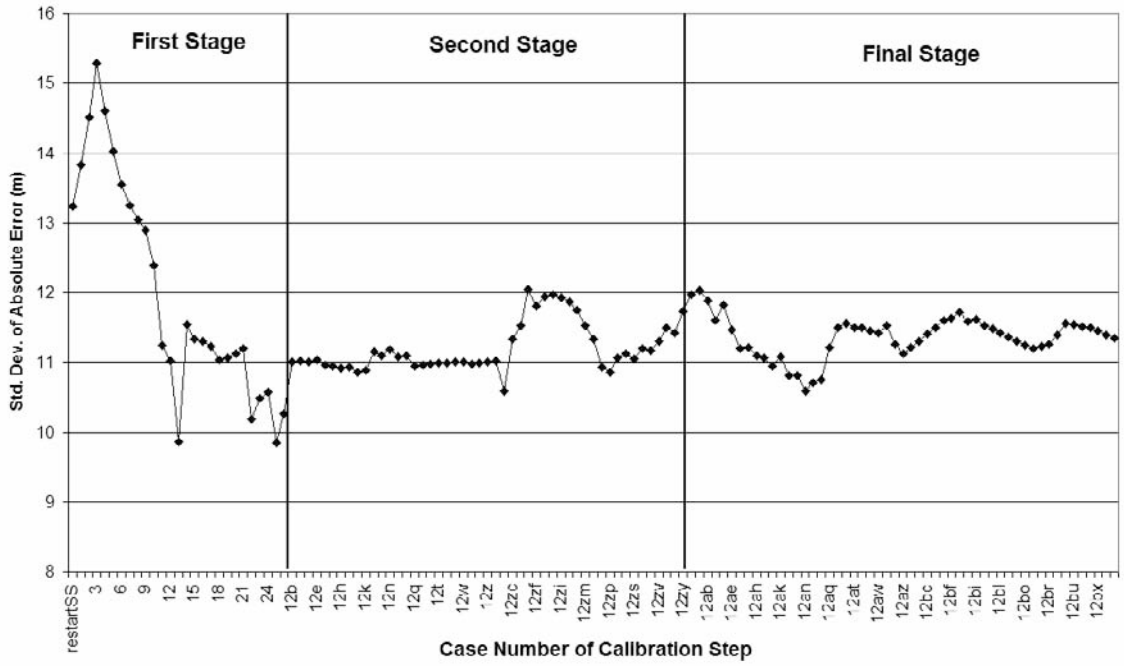

Figure 3-14: *Standard deviation of absolute error measurements during BS2B calibration runs. This represents a measure of the total error throughout the system, and not of the fit of individual borehole segments.*

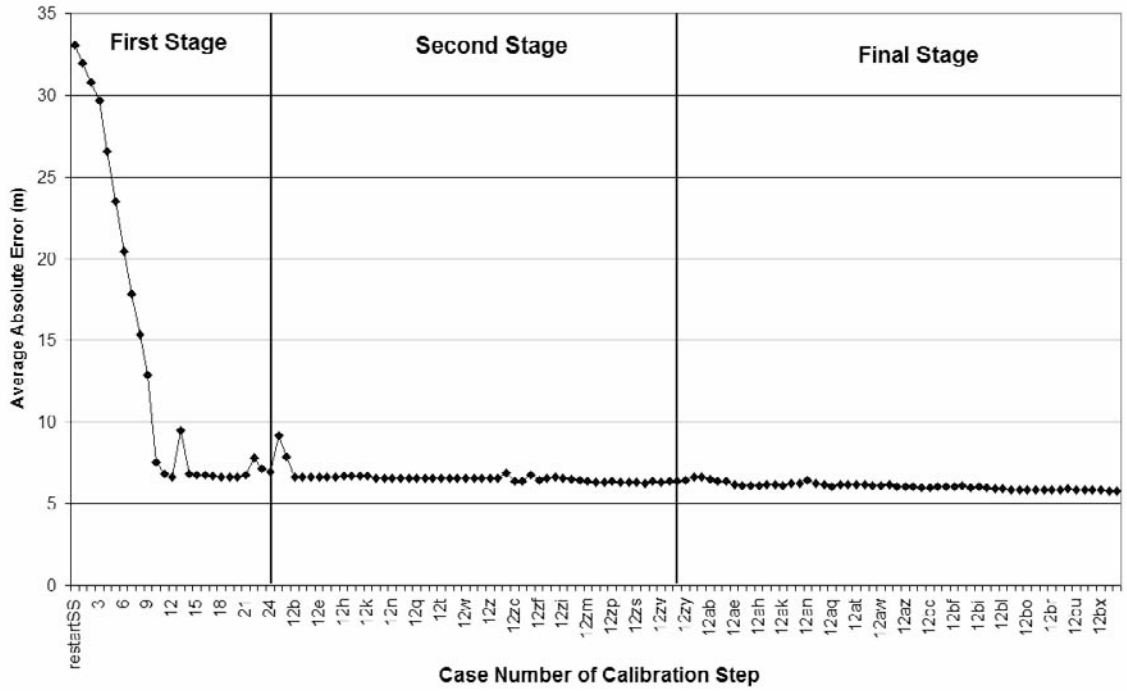

Figure 3-15: *Average of absolute error measurement population during BS2B calibration runs. This parameter represents a measure of the average error throughout the system, and not of individual borehole segments.*

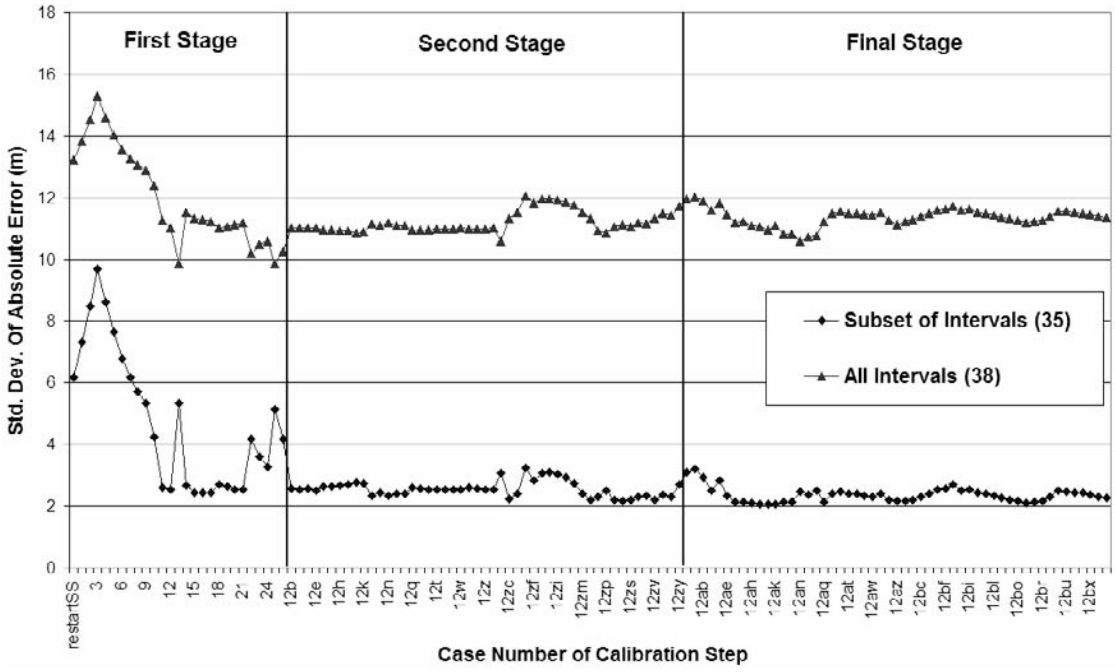

Figure 3-16: *Average of absolute error measurement population during BS2B calibration runs. Three borehole sections with inadequate connectivity have been removed from the calibration statistics; the boreholes are still present within the CN model.*

The calibration fit (Figure 3-16) was improved even more with the removal of three abnormal borehole sections (KI0025F Section 1, KI0023B Section 9, and KI0025F02 Section 6) from the calibration. These anomalies were most likely due to limited connectivity between the deterministic structures in those intervals and the external head boundaries. The limited connectivity is probably due to the exclusion of the full background fracture network in the calibration DFN. The exclusion of these segments reduces the final standard deviation of absolute error by more than 75% and the final average of absolute error by more than 50%. Table 3-5 presents the results of the calibration; head values for observation sections at significant steps and iterations are presented. The three columns (12, 12zh, and 12bz) represent three different 'best-fit' head solution cases; the 12zh solution was chosen as the target initial head distribution for the BS2B model simulations.

Table 3-5: BS2B Head Field calibration performance

Borehole Interval	Measured Head (m)	Simulated Heads During Calibration (masl)			
		Initial	12	12zh	12bz
KA2511A_T1	-23.37	-8.752	-28.198	-27.72	-26.791
KA2511A_T2	-27.847	-8.964	-28.238	-27.763	-27.332
KA2511A_T3	-35.255	-12.191	-38.818	-37.1	-40.1
KA2511A_T4	-35.927	-12.915	-48.768	-44.235	-45.683
KA2511A_T8	-49.11	-14.203	-46.368	-44.71	-48.595
KA2563A_S1	-41.111	-12.372	-41.497	-39.43	-41.493
KA2563A_S2	-41.549	-12.372	-41.5	-39.45	-41.495
KA2563A_S3	-42.567	-12.373	-41.511	-39.53	-41.501
KA2563A_S4	-43.832	-12.387	-41.705	-39.19	-41.613
KA2563A_S5	-47.241	-12.395	-41.816	-39.268	-41.676
KI0025F_S2	-41.684	-11.558	-33.393	-32.584	-36.294
KI0025F_S4	-44.6	-12.914	-48.754	-44.225	-45.675
KI0025F_S5	-49.501	-12.925	-48.813	-44.291	-45.737
KI0025F_S6	-52.814	-13.75	-47.53	-43.662	-45.592
KI0023B_P1	-24.569	-8.667	-27.26	-26.61	-25.989
KI0023B_P2	-41.278	-12.127	-38.431	-36.764	-39.668
KI0023B_P4	-42.42	-12.716	-46.182	-42.356	-44.176
KI0023B_P6	-43.75	-12.9	-48.642	-44.133	-45.593
KI0023B_P7	-44.74	-12.92	-48.919	-44.342	-45.76
KI0023B_P8	-49.132	-12.94	-48.841	-44.296	-45.761
KI0025F02_R1	-25.984	-9.3	-26.995	-26.682	-26.967
KI0025F02_R3	-42.424	-11.859	-36.856	-35.414	-38.379
KI0025F02_R5	-42.835	-12.859	-48.134	-43.76	-45.292
KI0025F02_R7	-44.675	-12.92	-48.784	-44.26	-45.708
KI0025F02_R8	-44.224	-12.92	-48.785	-44.262	-45.71
KI0025F02_R9	-52.954	-12.929	-48.815	-44.3	-45.75
KI0025F02_R10	-52.11	-12.982	-48.466	-44.127	-45.733
KI0025F03_R2	-42.471	-11.988	-37.569	-36.36	-38.98
KI0025F03_R3	-42.543	-11.967	-37.319	-35.858	-38.821
KI0025F03_R4	-42.314	-12.86	-48.14	-43.765	-45.295
KI0025F03_R5	-43.136	-12.86	-48.137	-43.763	-45.294
KI0025F03_R6	-44.673	-12.857	-48.103	-43.738	-45.275
KI0025F03_R7	-44.89	-12.914	-48.766	-44.235	-45.682
KI0025F03_R8	-43.919	-12.93	-48.813	-44.299	-45.75
KI0025F03_R9	-49.269	-12.93	-48.815	-44.301	-45.751

4 Theoretical basis and functional implementation of the DFN-CN model

The goal of the JNC/Golder modeling team during the BS2B prediction effort was to apply the knowledge gained from past tracer tests (TRUE Block Scale C1 to C4, Task 6D, Task 6E, and the BS2B pre-tests CPT 1-4) to an updated version of the Task 6C hydrostructural model to produce a block-scale transport model able of adequately predicting the results of the BS2B sorbing tracer tests. This modeling effort focused on understanding solute retention processes in the geologically complex zones at the interface between flowing fractures and the rock matrix.

4.1 Implementation of the BS2B channel network (CN) model

All of the background fractures and deterministic structures of the Task 6C (Dershowitz et al., 2002) semi-synthetic hydrostructural model were used to construct the BS2B base DFN. The inclusion of additional larger-scale fractures generated during Task 6C but not included in the final 500 m scale model, was necessary to provide adequate connections to external head boundaries to produce a stable steady-state flow solution, cf. Chapter 3.

4.1.1 Geometrical description of the discrete fracture network

The JNC/Golder BS2B blind prediction DFN model was largely based on the Task 6C DFN. However, due to file formats requirements imposed by the PAWorks software package, it was necessary to transform the model from Äspö local coordinates (positive x points east) into FracMan local coordinates (positive x points south). Each fracture was represented by a polygon, whose extent and orientations are specified by nodal coordinates at the vertices and by a normal vector to the fracture plane. The details of the JNC/Golder implementation of the Task 6C DFN are presented in Section 2.2.

The discrete fracture network was reduced to a three-dimensional network of one-dimensional, rectangular cross-section pipe elements (a ‘channel network’) utilizing the PAWorks software suite. The discretization process is described in detail in Section 4.2. Samples of the resulting network are illustrated in Figure 4-1 and Figure 4-2.

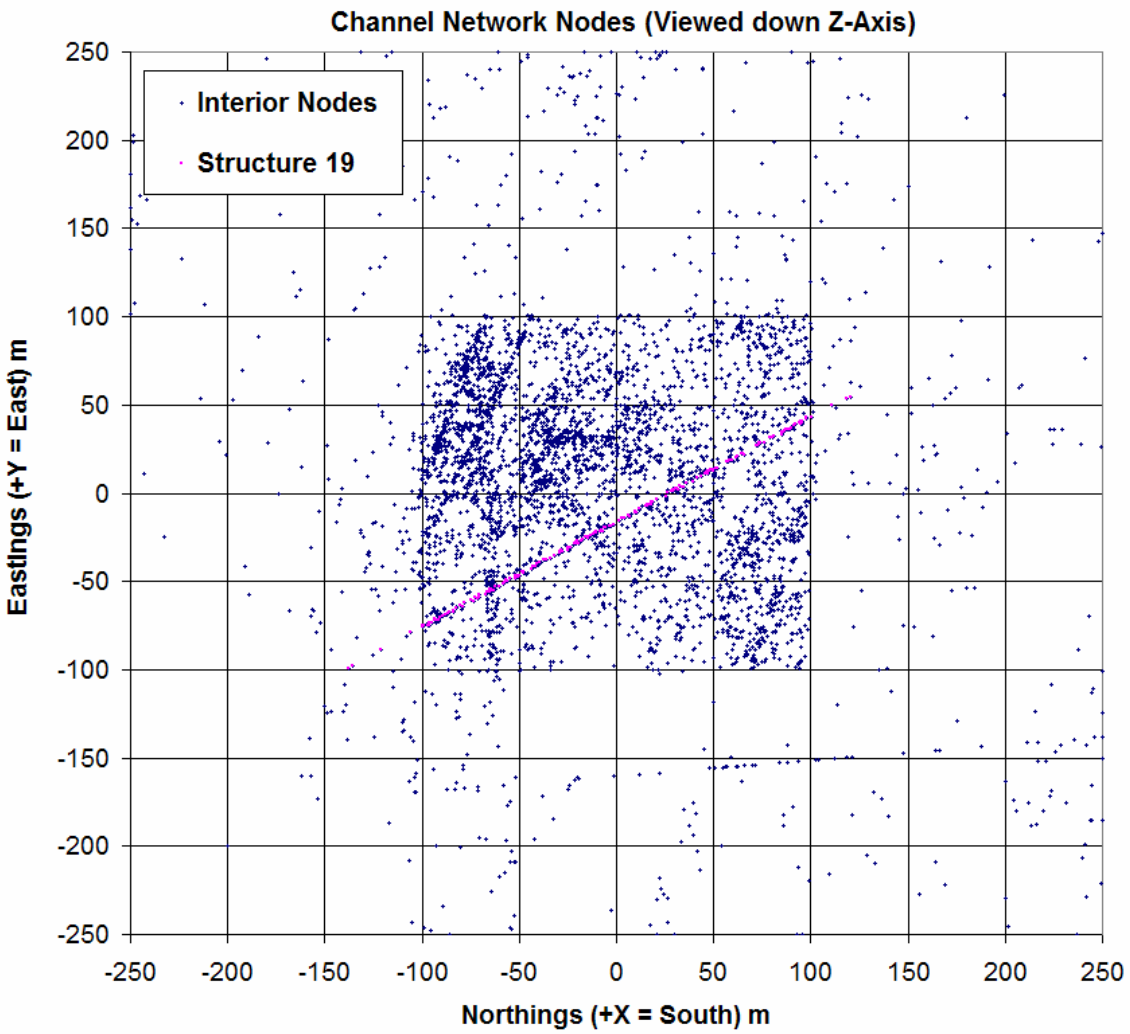

Figure 4-1: *TRUE Block Scale BS2B channel network model. Blue dots are nodes representing pipe endpoint connections in the model; the pink dots are nodes representing pipes along Structure #19. The model is expressed in FracMan coordinates; the Äspö HRL tunnel is in the upper left corner of the map.*

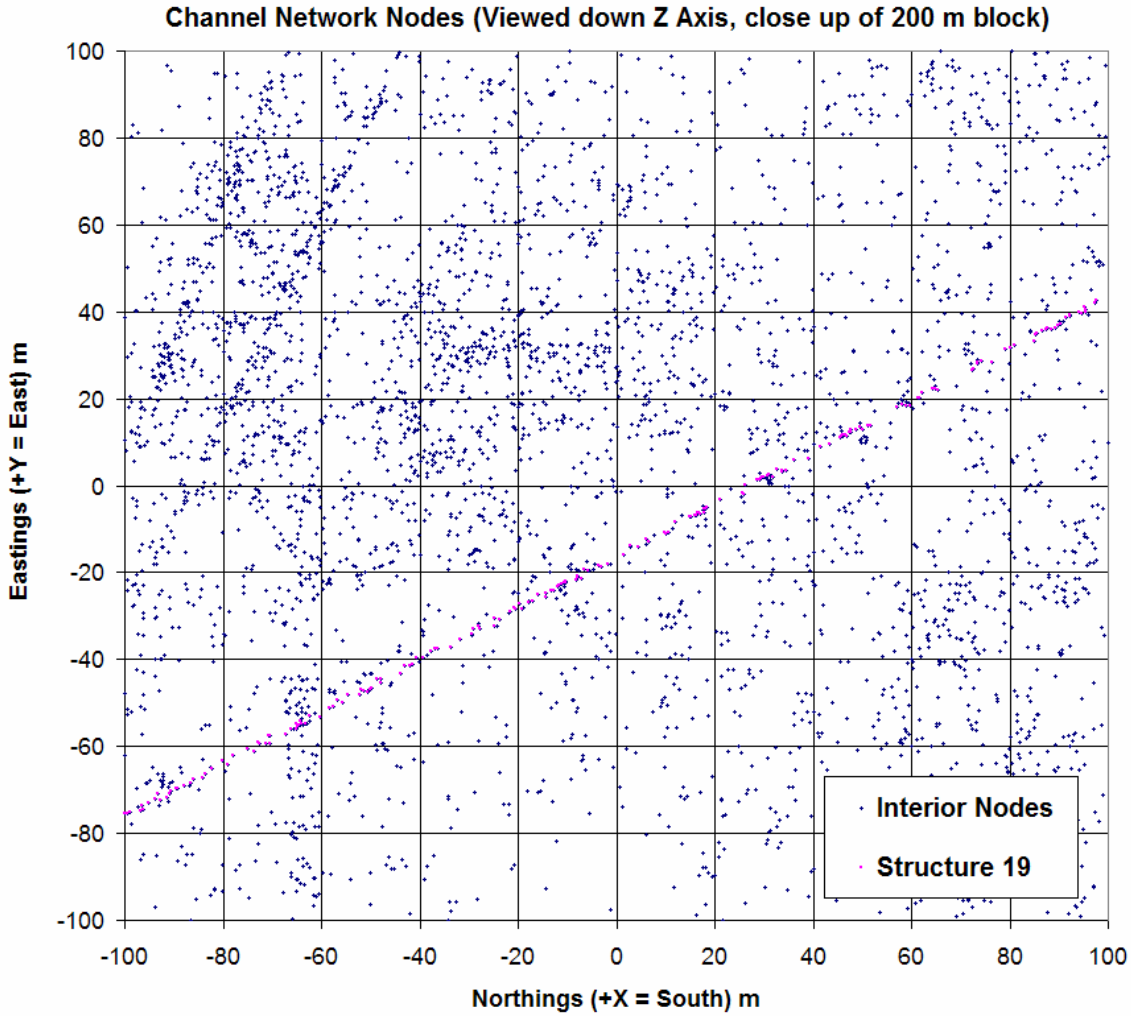

Figure 4-2: *500-m TRUE Block channel network model, zoomed in on the 200-m BS2B experimental volume. Blue dots are nodes representing pipe endpoint connections in the model; the pink dots are nodes representing pipes along Structure #19. The model is expressed in FracMan coordinates; the Äspö HRL tunnel is in the upper left corner of the map.*

4.1.2 Geometrical description of pore space

The pore space models used for "Type 1" and "Type 2" structures are illustrated in Figure 2-6 and Figure 2-7. Pore spaces representing fault gouge, cataclasite / mylonite, fracture mineral coatings, altered wall rock, and fresh wall rock (Äspö diorite) were implemented as PAWorks/LTG immobile zones /Dershowitz et al., 2000/. In PAWorks/LTG, immobile zones simulate mechanical and chemical transport processes by applying retardation factors to solute transport based on the zone properties. Fundamentally, mass is not 'lost' from a model to immobile zones; it is merely slowed down to a point where it does not reach the specified sinks during the time frame of the simulation. The basic conceptual model behind the PAWorks / LTG implementation of immobile zones is illustrated in Figure 4-3.

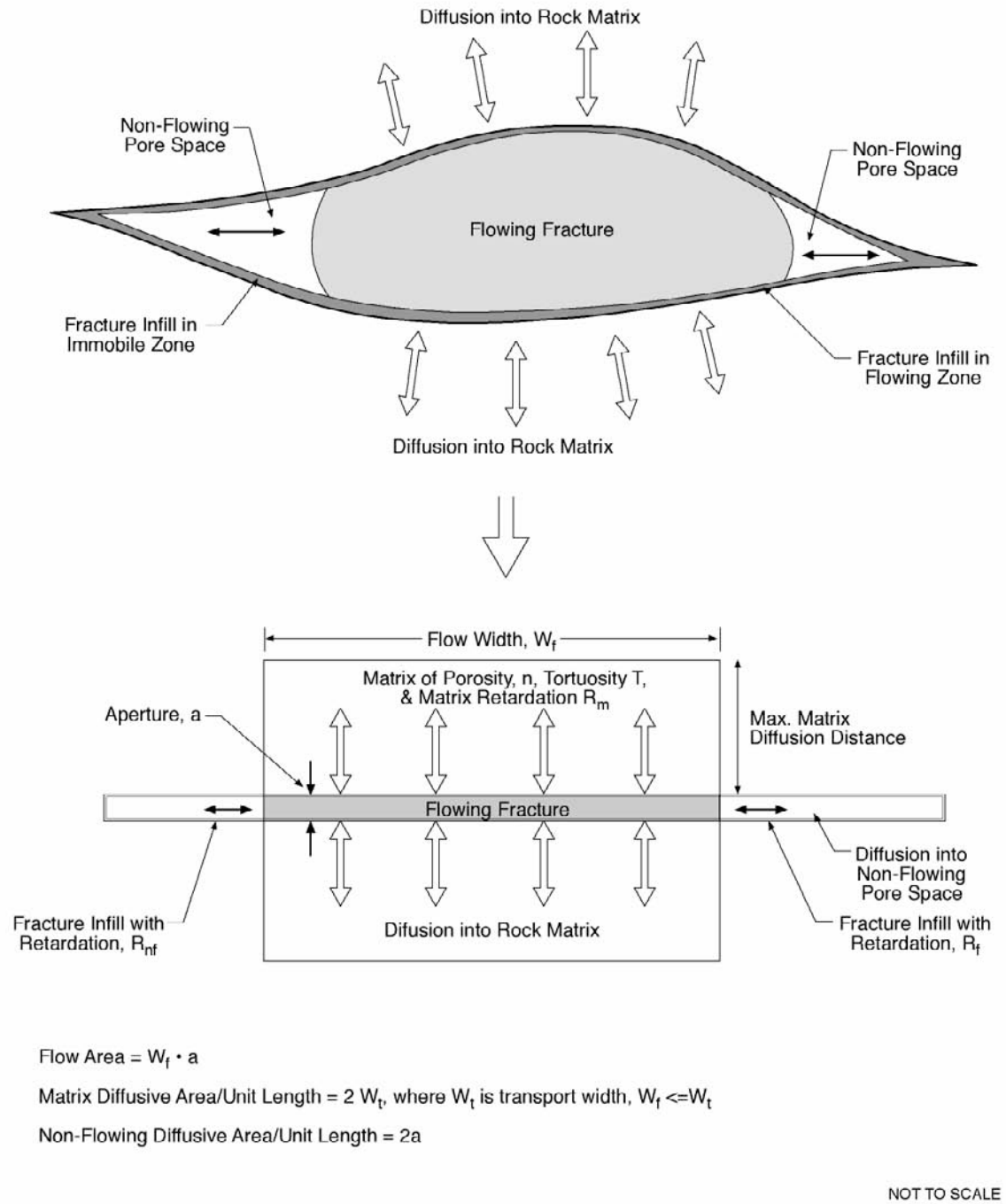

Figure 4-3: *Implementation of pore space as parallel immobile zones in PAWorks and LTG channel-network modeling. This figure was taken from the PAWorks / LTG users manual, version 1.62 /Dershowitz et al., 2000/.*

4.2 Flow Model

Flow was modeled using the FracMan/MAFIC code. The MAFIC flow model is described in Miller et al. (2001). In the MAFIC conceptual model, each of the fracture intersections are considered to be line segments ("traces"). These segments, along with the edges of the polygonal fractures, are then used to discretize the fractures to either 1D or 2D finite elements. When discretizing a DFN to 2D elements, the fractures are transformed into triangular finite elements conditioned to match the edges of the fracture and the intersection traces. When discretizing a DFN to 1D (pipe) elements, the pipes are defined to provide connections between the intersection traces, maintaining the same flow area between the fracture traces (Figure 4-4). The discretization process is described in detail by Dershowitz et al. /2000/.

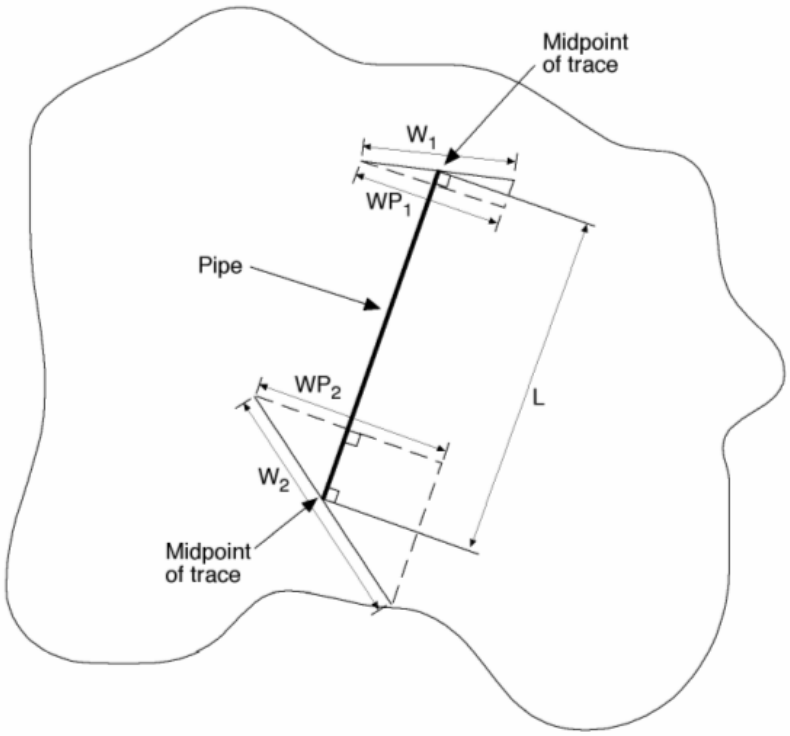

Figure 4-4: *Implementation of rectangular pipe elements between fracture intersection traces.*

4.2.1 Processes considered

The flow model considered only advective flow, modeled as Darcy flow through rectangular cross-section pipes or triangular finite elements.

4.2.2 Mathematical description

The mathematical description of flow modeling in MAFIC is taken from Miller et al, /2001/. Using continuum principles of mass balance, the diffusivity equation that describes flow can be written as (Bear, 1972):

$$\frac{\partial}{\partial x_i}[\frac{\rho}{\mu}k_{ij}(\frac{\partial P}{\partial x_i}+\rho g\frac{\partial z}{\partial x_j})] = \rho(\alpha+\phi\beta)\frac{\partial P}{\partial t} - q$$

Equation 4-1

where:

x_i	=	coordinate directions (L)
ρ	=	fluid density (M/L^3)
μ	=	fluid viscosity (M/LT)
k_{ij}	=	permeability (absolute) (L^2)
P	=	fluid pressure (M/LT^2)
g	=	gravitational acceleration (L/T^2)
z	=	vertical direction (upward) (L)
α	=	pore compressibility (LT^2/M)
Φ	=	porosity
β	=	fluid compressibility (LT^2/M)
q	=	source term (M/T)
t	=	time (T)

For nearly incompressible fluid (e.g., water), and for flow in two dimensions (e.g., in a fracture), the mass-conservation of equation (4-1) can be simplified to a volume-conservation equation:

$$S\frac{\partial h}{\partial t} - K\overline{\nabla}^2 h = q$$

Equation 4-2

where:

S	=	Fracture Storativity (dimensionless)
h	=	Hydraulic head (L)
T	=	Fracture Transmissivity (L^2 /T)
q	=	Source/Sink Term (L/T)
t	=	Time (T)
$\overline{\nabla}^2$	=	Two-dimensional Laplace Operator

4.2.3 Numerical Implementation

MAFIC uses a Galerkin finite element solution scheme to approximate the solution for Equation 4-1. The finite element approximation to the diffusivity equation in two dimensions is given by:

$$\sum_{m=1}^{N}\left[\int_R (T_{nm}\,\overline{\Delta}\,\xi_n \bullet \overline{\Delta}\,\xi_m\, dR)h_m\right] + \sum_{m=1}^{N}\left[\int_R (S_{nm}\,\xi_n\,\xi_m\, dR)\frac{dh_m}{dt}\right] = \int_R q\,\xi_n\, dR \quad n = 1,2,\ldots N \qquad \textbf{Equation 4-3}$$

where:

T	=	fracture transmissivity (L^2 /T)
S	=	fracture storativity (dimensionless)
q	=	source flux, volume per unit area (L/T)
ξ	=	linear or quadratic basis function
R	=	element area (L^2)
h	=	nodal hydraulic head (L)
t	=	time (T)
N	=	number of nodes

For the present study, flow modeling was carried out using a three-dimensional network of rectangular cross-section pipe elements generated from the base discrete-fracture network model.

4.2.4 Flow Model Parameters

Flow modeling was carried out assuming steady-state conditions, with the injection and pumping rates specified in Table 2-2, and the head boundary conditions as calibrated for the 500 m TRUE Block Scale volume (see Chapter 3).

For steady state flow modeling, the only important parameters are fracture transmissivity (m^2/s) and aperture. These values were specified for each fracture as provided in the Task 6C report /Dershowitz et al., 2003/, except for Structure BG1, where transmissivity was altered to attempt to match previous (CPT-4C) tracer test results. The distributions of values for fracture transport aperture and transmissivity are described in Chapter 5.

4.3 Transport Model

Solute transport was simulated using the Laplace Transform Galerkin method, as implemented in PAWorks / LTG /Dershowitz et al., 2000/. Radionuclide transport occur within a three-dimensional channel network composed of one-dimensional pipe elements, with multiple immobile zones working in parallel to simulate rock and structural interactions.

4.3.1 Processes Considered

Solute transport modeling with the PAWorks and LTG packages considers the following processes:

- advection
- dispersion (longitudinal only)
- diffusion (to immobile zones)
- sorption (in immobile zones)
- surface sorption (onto fracture mineral coatings)

For these simulations, radionuclide decay, and non-equilibrium chemical processes were not considered.

4.3.2 Mathematical Description

This section describes the mathematical basis of the FracMan/PAWorks Laplace Transform Galerkin (LTG) solute transport model. This section of text was taken from the PAWorks/LTG manual /Dershowitz et al., 2000/. The model topology is illustrated in Figure 4-5.

The LTG transport solution is carried out assuming steady-state flow. A second-order approach is used to describe the diffusive mass transfer of a solute between the groundwater in a pipe and the multiple immobile porosity zones attached to it. The advective-dispersive transport of solute species (index *n*) in a pipe network is given by:

$$A\left[R_n(\ell)\frac{\partial C_n}{\partial t} + q(\ell)\frac{\partial C_n}{\partial \ell} - \frac{\partial}{\partial \ell} D_{l_n}(\ell)\frac{\partial C_n}{\partial \ell} + R_n(\ell)\lambda_n C_n - R_{n-1}(\ell)\lambda_{n-1} C_{n-1} \right]$$

$$\pm \sum_{\ell'} \dot{M}\,\delta(\ell - \ell') + \sum_{\ell^*} Q(C_n - C_n^*)\delta(\ell - \ell^*) + \sum_{im=1}^{IM} P_{im}\theta_{im} D_{im} \frac{\partial C_n^{im}}{\partial w}\Big|_{w=0} = 0 \qquad \textbf{\textit{Equation 4-4}}$$

where:

n = nuclide index [-]

$_{im}$ = immobile zone class number (note: if desired $_{im}$ can equal 0) [-]

IM(ℓ) = total number of immobile zones attached to pipe ℓ [-]

A(ℓ) = pipe cross-sectional area [L^2]

Rn(ℓ) = retardation factor [-]

$q\ (\ell)$ = specific discharge (≡ Pipe velocity v) [L/T]

$D_{\ell_n}(\ell)$ = dispersion coefficient = $\alpha v + D_n^o$ [L^2/T]

α = pipe longitudinal dispersivity [L],

D_n^o = free-solution diffusion coefficient [L^2/T]

λ_n = decay constant [1/T]

$\dot{M}$ (t) = internal solute mass source/sink [M/T]

Q = external fluid source/sink [L^3/T]

$\delta(\ell - \ell')$ = Dirac delta [1/L]

$\delta(\ell - \ell^*)$ = Dirac delta [1/L]

P_{im} = block surface area per unit length of matrix (equivalent to the effective perimeter of immobile zone $_{im}$) [L]

D_{im} = matrix effective diffusion coefficient [L^2/T]

θ_{im} = immobile zone porosity for immobile zone $_{im}$

Cn = pipe concentration [M/L^3]

C_n^* = concentration of injectate in external fluid source [M/L^3]

C_n^{im} = immobile zone concentration [M/L^3]

ℓ = distance along interconnected pipe network [L]

ℓ' = location of solute mass source/sink [L]

ℓ^* = location of external fluid source/sink [L]

w = distance perpendicular to plane of fracture [L]

t = time [T]

It should be noted that if there is no flow along a particular pipe within the network (i.e. *q(l) = 0)*, then the model allows for diffusive transport along the length of this pipe. It should also be pointed out that if fluid is withdrawn at a resident concentration, $C_n^* = C_n$, then the term involving Q in (1) vanishes. If the injectate concentration $C_n^* = 0.0$, then this term accounts for the dilution effect of the injection of solute-free water.

The initial concentrations of all species within the domain are assumed to be zero. Boundary conditions may be either of the Dirichlet-type where the input concentration history of each species is a specified function of time, or of the Cauchy-type where the advective input mass flux can be prescribed as a function of time at the origin of a pipe on the boundary of the domain. Mathematically, these boundary conditions are described by:

Dirichlet: $Cn = C_n^o(t)$ on Γ ***Equation 4-5***

Cauchy: $A(\ell)q(\ell)C_n^o(t) = A(\ell)\left[q(\ell)C_n(\ell,t) - D_{\ell_n}(\ell)\frac{\partial C_n}{\partial \ell}\right]$ on Γ ***Equation 4-6***

where C_n^o is the specified concentration for species n. LTG also allows the concentration or flux rate (e.g. mol/yr) to be specified at an interior point.

4.3.2.1 *Immobile Zone*

In order to represent the diffusive exchange of solute mass between the pipes and any on the immobile zones (index *im*) attached to them, LTG uses a second-order approach described by:

$$\theta_{im}(im,\ell)R_n^{im}(im.\ell)\frac{\partial C_n^{im}}{\partial t} - \frac{\partial}{\partial w}\theta_{im}(im,\ell)D_{im}\frac{\partial C_n^{im}}{\partial w} + \theta_{im}(im,\ell)R_n^{im}(im,\ell)\lambda_n C_n^{im} - \theta_{im}(im,\ell)R_{n-1}^{im}(im,\ell)\lambda_{n-1}C_{n-1}^{im} = 0 \qquad \textbf{Equation 4-7}$$

where:

$\theta_{im}(_{im}, \ell)$ = immobile zone porosity for immobile zone "*im*" attached to pipe "ℓ" [-]

R_n^{im} $(^{im}, \ell)$ = immobile zone retardation factor for immobile zone "*im*" attached to pipe "ℓ" [-]

C_n^{im} = concentration in matrix [M/L^3]

D_{im} = matrix effective diffusion coefficient [L^2/T]

= D_n^0 τ

D_n^o = free-solution diffusion coefficient [L^2/T]

τ = tortuosity [-]

If a particular immobile zone is fluid-filled, such as within an immobile water zone attached to a pipe within a fracture plane, then the immobile zone porosity, θ_{im}, would equal 1.0.

4.3.3 Numerical Implementation

The LTG method /Sudicky, 1989; Sudicky, 1990; Sudicky and McLaren, 1992/ is a numerical solution procedure where the Laplace transform is first applied to the governing equation, and the transformed equation is then solved numerically using the Galerkin finite element procedure (or alternatively any other discretization method such as finite differences). Finally, upon a solution for the nodal Laplace-space solution, the time-domain solution is recovered by a numerical inversion of the Laplace transformed nodal solution.

Let the Laplace transform of a function *f(t)* be defined according to:

$$\bar{f}(p) = \int_0^\infty f(t)e^{-pt}\,dt \qquad \textbf{Equation 4-8}$$

where *p* is the Laplace-transform parameter. Applying this to Equation 4-7 for the im^{th} immobile zone and following algebraic manipulations, one obtains:

$$g_n\overline{C}_n = -qA\frac{\partial\overline{C}_n}{\partial\ell} + A\frac{\partial}{\partial\ell}D_{\ell_n}\frac{\partial\overline{C}_n}{\partial\ell} + AR_{n-1}\lambda_{n-1}\overline{C}_{n-1} + \sum_{im=1}^{IM}\sum_{k=1}^{n-1}G_{nk}^{im}\overline{C}_n \qquad \textbf{Equation 4-9}$$

The *k* summation in Equation 4-9 is summing the nuclide's predecessors, where nuclide *1* is the first species in the chain, and nuclide *n-1* is the direct parent.

In Equation 4-9:

VSA = volume per surface area [L]

p = Laplace transform parameter

$$g_n = \left[AR_n(p+\lambda_n) + \sum_{im=1}^{IM} V_{im}\theta_{im}D_{im}\frac{Z_n^{im^2}}{VSA_{im}}B_n^{im}(Z_n^{im}) \right] \qquad \textbf{Equation 4-10}$$

$$G_{n,k}^{im} = -V_{im}\theta_{im}D_{im}\sum_{\ell=k}^{n} E_{n,k}^{\ell,im}\frac{Z_\ell^{im^2}}{VSA_{im}}B_\ell^{im}(Z_\ell^{im}) \qquad \textbf{Equation 4-11}$$

$$E_{n,k}^{\ell,im} = \frac{\prod_{p=k}^{n-1}(\lambda_p R_p^{im})}{\prod_{\substack{p=k \\ p\neq\ell}}^{n}\left[R_p^{im}(p+\lambda_p) - R_\ell^{im}(p+\lambda_\ell)\right]} \qquad \textbf{Equation 4-12}$$

$$\phi_n^{im} = \sqrt{\frac{(p+\lambda_n)R_n^{im}}{D_{im}}} \qquad \textbf{Equation 4-13}$$

$$Z_n^{im} = \phi_n^{im} VSA_{im} \qquad \textbf{Equation 4-14}$$

For a "slab" geometry for a matrix block $B_n^{im}(Z_n^{im})$ and VSA are defined by:

$$B_n^{im}(Z_n^{im}) = \frac{\tanh(Z_n^{im})}{Z_n^{im}} \qquad \textbf{Equation 4-15}$$

VSA, the volume to surface area ratio is equal to half the total slab width, 2dmax.

VSA = d_{max}.

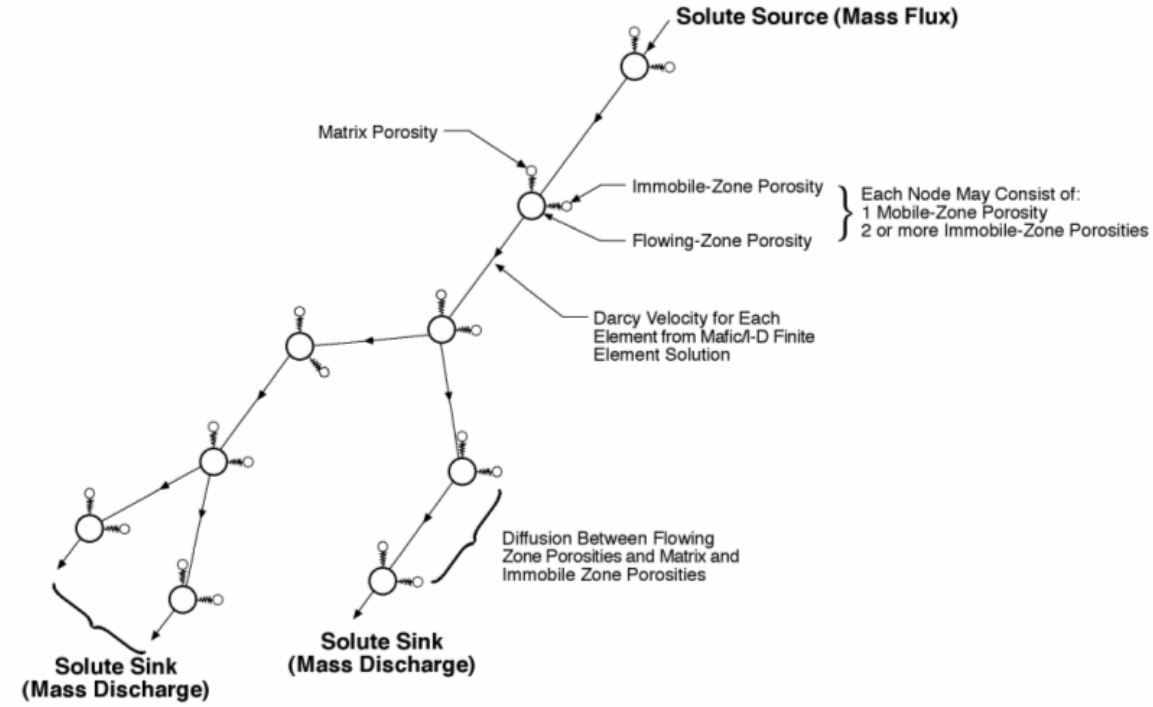

Figure 4-5: *Topology of LTG transport solution.*

4.3.4 Parameters

The parameters for the LTG transport solution are as follows:

- Geometric parameters for flow channel area (for each rectangular cross-section pipe): length *L*, width *W*, transport aperture *e*, and pipe velocity *v*
- Immobile zone material parameters (for each immobile zones): porosity *n*, material bulk density ρ, and maximum diffusion distance (*d*).
- Immobile Zone geometric parameters (for each immobile zone, for each rectangular cross-section pipe) immobile zone material thickness *t*, diffusion perimeter *p*, transport aperture *e*, and tortuosity / formation factor (*F*).
- Solute chemical parameters (for each species): Volumetric sorption coefficient $K_{d,}$ free-water diffusivity, and decay constant (λ) where applicable. Note that species decay during the BS2B experiment is corrected for and is not explicitly included in the analysis/modelling.

4.4 TRUE-BSC modeling strategy and implementation

The goal of the JNC/Golder team in TRUE-BSC was not to determine the single "correct" set of transport pathway properties for the fracture network, but rather, to study the relative significance of each of the transport assumptions provided in the rock block characterization. This is fundamentally a forward modeling approach, rather than a calibration approach. Consequently, all the models carried out as forward models to the extent possible.

4.4.1 Strategy

The strategy used for TRUE-BSC BS2B was one of forward modeling. In this strategy, a modified Task 6C rock block was implemented in FracMan, incorporating the specified flow geometry, boundary conditions, and material properties. The modifications consisted of the addition of low-transmissivity northeast-trending stochastic fractures to provide connections between the 500 m block and the 200 m simulation volume, and the addition of Structure BG1. A limited calibration to previously-completed tracer tests (CPT-4C) following a similar geometry was performed to determine if the implementation of the modified Task 6C hydrostructural model /Dershowitz, et al., 2002/ would produce reasonable simulation results. As the BS2B model requirements demand a blind prediction utilizing the current 'model state', no formal calibration was performed.

4.4.2 Model Implementation

The procedure for DFN model implementation was as follows.

1. Construct the Task 6C hydrostructural model as a three-dimensional discrete feature network (DFN) model using the FracWorks XP software package. This model included all deterministic, semi-synthetic, and background structures.

2. Convert the DFN into a one-dimensional pipe network model, using PAWorks/Genpipe. This pipe network was conditioned to match the connectivity of the DFN model, with pipe properties set to match the apertures and transmissivities of their host fractures. Pipes that did not connect to a head or flow boundary were removed from the system for computational efficiency

3. Apply the specified steady state flow boundary conditions through the MAFIC software package to obtain a nodal head and flux field. The resulting flow solution assigns an advective transport velocity to all pipes.

4. Convert the full channel network into a smaller mesh of just the "downstream" network of pipes between the defined tracer injection sources and sink. The new mesh is then exported this from PAWorks to the LTG solver. Immobile zone parameters are assigned to pipes based on set membership of their host fractures. Solute transport boundary conditions are also assigned at this stage.

5. Derive advective flow performance metrics (beta-factor and water residence time distributions) from transport pathways identified in PAWorks through a graph-theory traversal of the channel network.

6. Calculate τ and β values /Poteri et al., 2002/ for the flow pathway that each particle took by dividing the travel time t_w in each pipe by the pipe aperture e, and summing the result over the length of the pipe.

7. Simulate fracture complexity by altering the perimeters of pipes on a set-by-set basis in the LTG input files (IMMDATA.IN, GRID.IN). Pipes belonging to fractures of complexity 2 had their pipe perimeter available to transport processes doubled, while pipes belonging to fractures of complexity 3 had their perimeters tripled. Flow perimeters, and therefore pipe velocities, were left unchanged.

8. Simulate solute transport using FracMan/LTG in the pipe network. This program reports fluxes, concentrations, and cumulative releases at user-specified trace planes and at specified head / flux boundaries (the western edge of the 200-m BS2B experimental volume).

9. Calculate additional performance measure statistics (breakthrough curves, t_5, t_{50}, t_{95}).

4.4.3 Immobile Zones

Twenty-five separate immobile zones were necessary to characterize the geological complexity in the current BS2B transport model within the 200 m scale BS2B experimental volume. Immobile zones are assigned on a set by set basis. Therefore, it was necessary to reclassify DFN fractures into geologically similar fracture sets. A breakdown of the immobile zones includes:

- One immobile zone representing intact Äspo granite / diorite, in contact with all fractures in the model. This immobile zone generally represents transport through background fractures, whose contribution to retention is likely relatively small. As such, the perimeters for pipes in this zone were not adjusted for complexity.

- Seven zones representing fracture mineral coatings. This immobile zone is present in every fracture set in the model.

- Seven zones representing altered wall rock. The zones are subdivided based on the geological complexity factor of the structure (1, 2, 3) and the structure type (I, II). In addition, separate alteration immobile zones for Structures 19 and Z were created to allow for explicit parameter differences detailed in the modeling specifications.

- Five zones representing fault gouge. The zones are subdivided between Type I structures by complexity factor (1, 2, or 3), and are also present along Structures Z and Structure 19/ Structure 19 Splay.

- Five zones representing mylonitic and/or cataclastic rocks surrounding Type I faults, Structure 19, and Structure Z.

4.4.4 Implementing Fracture Complexity

Geologic and structural complexity is implemented in the JNC/Golder channel network model through a post-processing modification of the immobile zone surface area in the 'downstream' network of pipes between sources and sink. These modifications take place after the flow solution and pathway identification has been made; retention effects are simulated solely within the transport code.

In the JNC/Golder BS2B prediction and evaluation models, retention was modeled by increasing the effective surface area (and corresponding pore volume) available to diffusion and surface sorption. This was accomplished by multiplying the (diffusion) perimeter of the material-specific immobile zones by the complexity factor [(pipe width *2 + aperture *2) * complexity factor]. For example, fractures of Complexity 2 had a diffusion perimeter of twice that of Complexity 1 fractures.

Within the DFN (prior to CN discretization), fracture complexity was accommodated by subdividing fractures into different sets based on their theoretical complexity and geologic type. All structure numbers are equivalent to the numbering of determinisistic structures presented in the Task 6C report. The set breakdown within the DFN is as follows:

- Set 1: Deterministic Features, Geologic Type 1, Complexity 2. This set consists of numbered structures 6, 13, and 22
- Set 2: Deterministic Features, Geologic Type 1, Complexity 3. This set consists of numbered structures 7, 8, and 20.
- Set 3: Deterministic Features, Geologic Type 2, Complexity 1. This set consists of numbered structures 23 and 24.
- Set 4: Deterministic Features, Geologic Type 1, Complexity 2. This set consists of numbered structures 5, 10, and 21.
- Set 5: Structure 19, Geologic Type 1, Complexity 2.
- Set 6: Regional Structure Z, Geologic Type 1, Complexity 3.
- Set 7: Deterministic large-scale Features, Geologic Type 2, Complexity 1. This set consists of numbered structures 1, 2, 3, 4, 9, 11, 12, 14, 15, 16, 17, 18, 26, 27, 28, 29, and 30.
- Set 8: Semi-stochastic Background Fractures, Geologic Type 1, Complexity 1.
- Set 9: Semi-stochastic Background Fractures, Geologic Type 1, Complexity 2.
- Set 10: Semi-stochastic Background Fractures, Geologic Type 2, Complexity 1.
- Set 11: Semi-stochastic Background Fractures, Geologic Type 2, Complexity 2.
- Set 12: Deterministic Background Fractures (from POSIVA flow logs) that intersect KI0025F02, KI0025F, KI0025F03, and KA2563. These fractures were modeled as Geologic Type 2, Complexity 1 features.
- Set 13: Deterministic Structure 19 Splay (seen as intersection in KA2563A). This feature is modeled as a 4-sided fracture with an equivalent radius of 15 m, with a pole trend and plunge of 215/36, and transmissivity / aperture values equivalent to that of Structure 19. The 19 Splay was implemented as a Geologic Type 1, Complexity 2 feature.
- Set 14: Deterministic Structure #25 / BG1, This feature was modeled as a 4-sided fracture with an equivalent radius of 15 m, a strike and dip of N30W/76NE, and an intersection with KI0025F02_R2 approximately 3 m from the top of the packer. BG1 was implemented as a Geologic Type 1, Complexity 2 feature.
- Set 15: 2000 m scale lognormal fractures. These features were included to provide connectivity between the 100 m scale TRUE Block volume and the 500 m scale head calibration volume. The fractures were clipped so as to lie outside (but slightly penetrating at the edge) of the 100 m TRUE Block volume. These fractures were modeled as Geologic Type 1, Complexity 1 features.

5 BS2B Forward Models – Results and Performance Measures

5.1 Model Cases

The limited attempt to calibrate the BS2B channel-network model to the CPT-4c tracer pre-test suggested that no single set of network parameters was adequate to correctly simulate transport properties along the Structure BG1/Structure 19 system. Pathways primarily along Structure 19 behaved well; calibrated tracer breakthrough curves were quite similar to those observed during the CPT-4c experiment. Pathways utilizing Structure BG1 did not behave quite as well; significant differences from in-situ observations were noted. As such, the JNC/Golder team elected to run two different prediction models (Model Case 9 and Model Case 20).

5.1.1 CPT-4c Test Parameters

TRUE Block Scale conservative tracer pre-test 4c (CPT-4c) consisted of a radially-converging pump test, with borehole KI0025F03, Section 3, as the sink well. The sink well was pumped at a time-varying flow rate averaging 2.7 liters per minute (this average value was used in the calibration, as the BS2B predictions are all run assuming steady-state flow). Tracer was injected into three wells: KI0025F02 Section 3 (Structure 19 – Path I), KI0023B Section 2 (Structure 19), and KI0025F02 Section 2 (Structure BG1 – Path II). The test was designed to test the transport of conservative tracers (fluorescent dyes) along both direct pathways in Structure 19 and through a network of background fractures.

5.1.2 Model Case 20

Model 20 represented a set of channel properties that produced the best fit for initial conservative tracer breakthrough (t_5) in the limited CPT-4c calibrations. The accuracy of the overall breakthrough curve was good for transport within Structure 19, but only the initial breakthrough was truly accurate for transport within Structure BG1 (Path I). Figure 5-1 and Figure 5-2 show sample breakthrough curves for this model case. This model utilizes the modified Task 6C DFN as discussed in Chapters 1 and 4, with the following changes:

- BG1 was assigned an aperture of 4.0×10^{-3} m, and a transmissivity of 1.0×10^{-9} m^2/s
- The geometry (equivalent radius) of Structure BG1 was increased to 35 m, so that it connected to the background fracture network (and, by extension, Structure 19) through the conductive features identified in POSIVA flow logs.

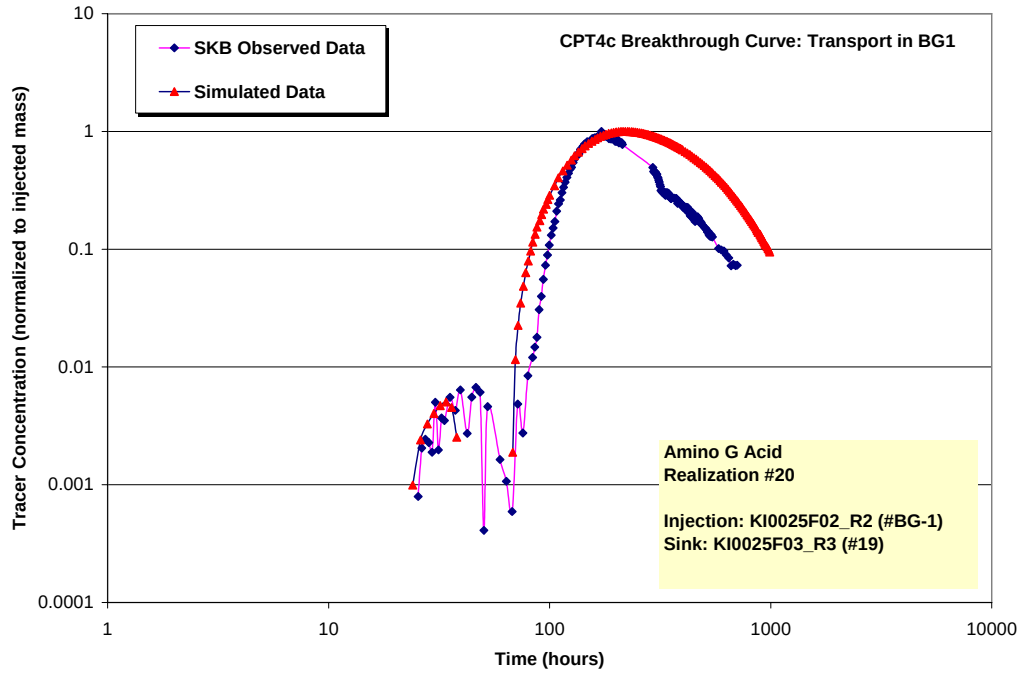

Figure 5-1: *Breakthrough curve for BS2B calibration to CPT4c for Model 20 for the Structure 19/BG1 combination pathways (Path II). Note the good agreement for initial tracer breakthrough, but the relatively poor tail.*

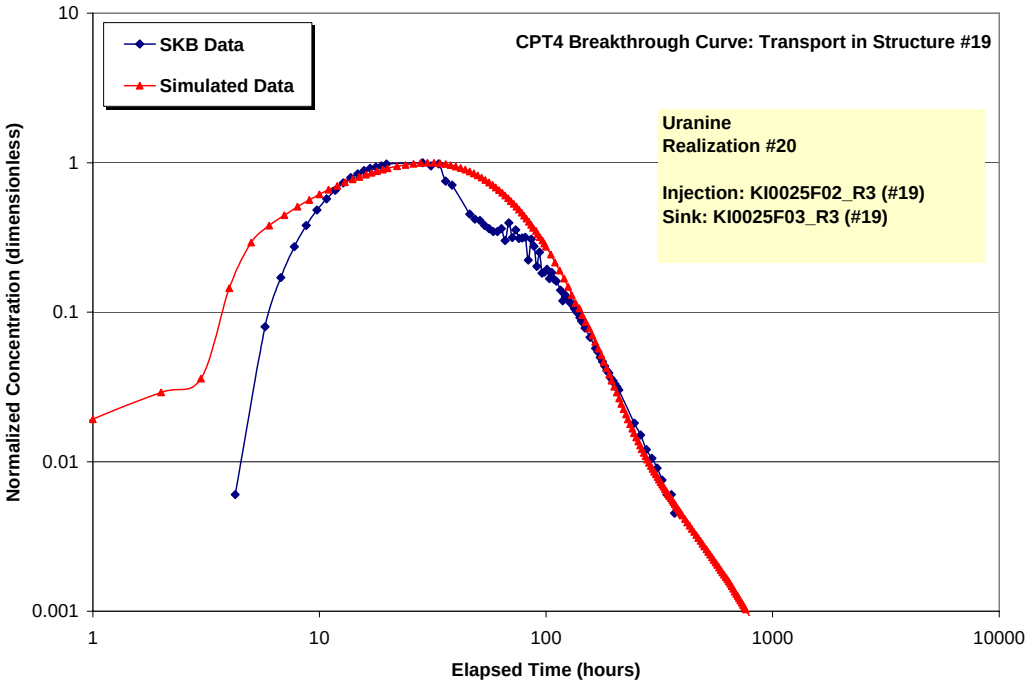

Figure 5-2: *Breakthrough curve for BS2B calibration to CPT4c for Model 20 for the direct Structure 19 pathways (Path I). Note the generally good agreement between simulated and actual tracer breakthroughs.*

5.1.3 Model Case 9

Model 9 consisted of a set of channel properties that represented the best fit to the overall breakthrough curve, with an emphasis on accurately predicting the tracer tails. Specifically, the channel network model was changed as follows:

- Apertures of the conductive fractures identified through POSIVA flow logging were increased by one order of magnitude. This had the effect of reducing flow velocities and delaying the tracer breakthrough, as well as producing a longer tracer tail.

- Transmissivities of several background features between Structure 19 and Structure BG1 were increased by one order of magnitude. This helped to reduce the tracer tail without significantly reducing the initial breakthrough time.

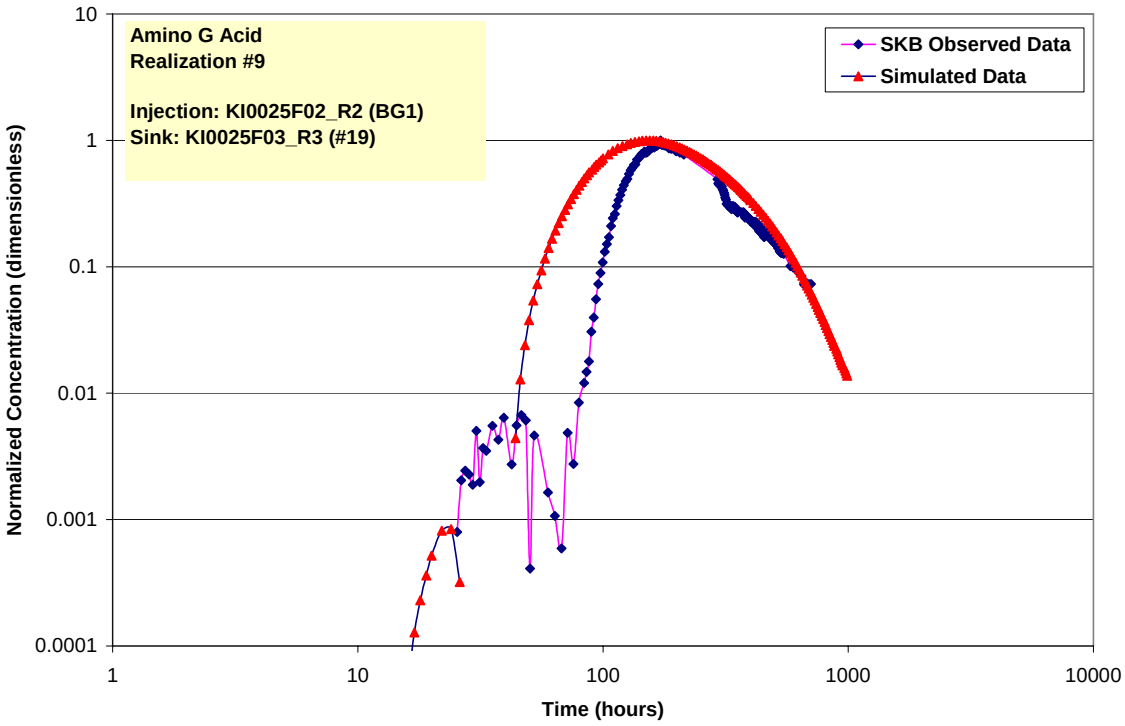

Figure 5-3: *Breakthrough curve for BS2B calibration to CPT4c for Model 9 for the Structure 19/BG1 combination pathway (Path II). Note the good agreement for the tracer tails, but the poor agreement for initial tracer breakthrough.*

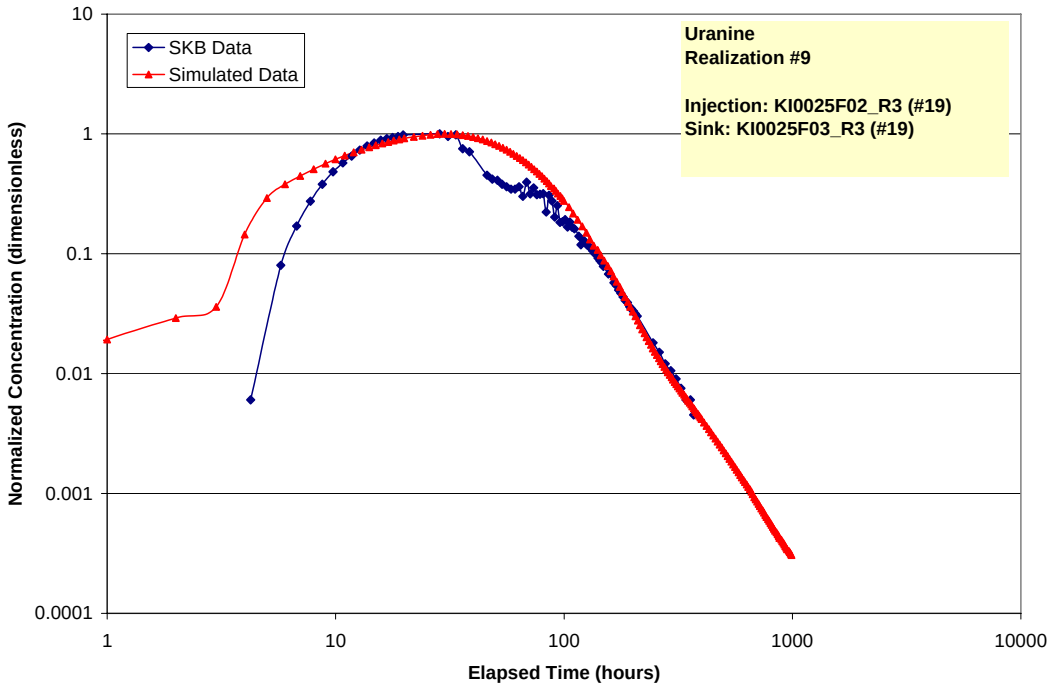

Figure 5-4: *Breakthrough curve for BS2B calibration to CPT4c for Model 9 for the direct Structure 19 pathway (Path I). Note the generally good agreement between simulated and actual tracer breakthroughs.*

5.2 BS2B Forward Modeling - Model Case 20

5.2.1 Water Residence Time

The water residence time distribution was predicted by running the BS2B channel network model through the formal tracer test protocol, while only allowing for advective transport (diffusion, longitudinal dispersion and surface sorption switched off), and assuming a Dirac pulse injection condition (all tracer injected in one hour). Figure 5-5 summarizes the water residence time calculations.

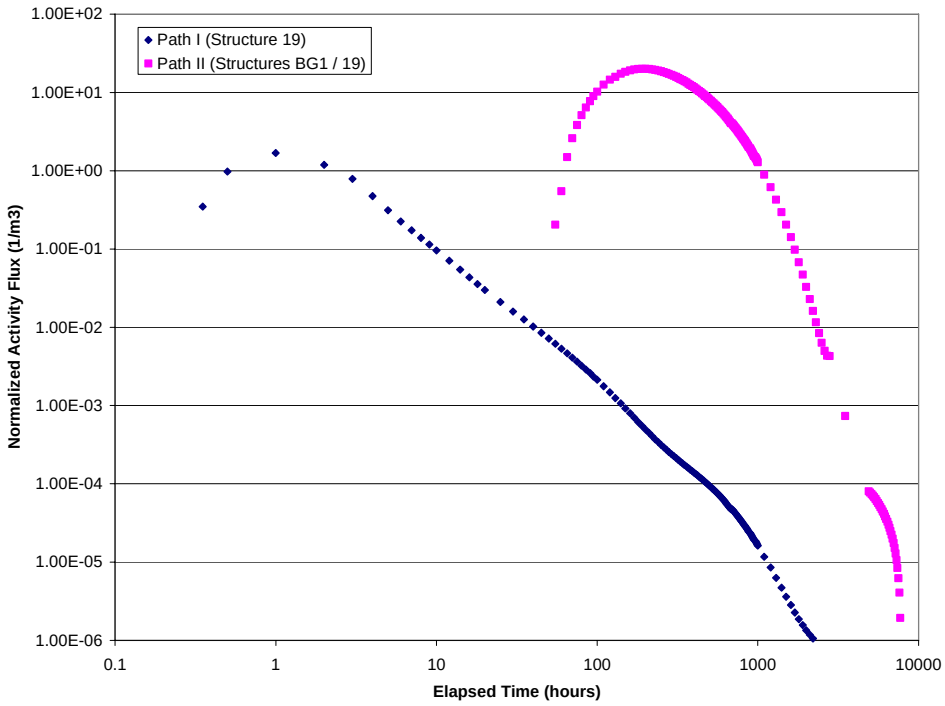

Figure 5-5: *Simulated water residence time distribution (advection-only breakthrough curve) for flow paths I and II, assuming a Dirac pulse injection (elapsed injection time of one hour).*

5.2.2 Pore space implementation and specification of flow paths

Pore spaces in the model were implemented as described in Chapters 2 and 4, and as summarized below in Table 5-1 and Table 5-2.

Table 5-1: Pore space implementation for Type I structures in the JNC/Golder BS2B model.

Type I Features (faults)					
Immobile Zone	**Thickness (m)**	**Porosity (%)**	**Formation Factor**	**Density (kg/m^3)**	**Perimeter Factor**
Gouge	0.003	20	5.6×10^{-2}	2755	1x, 2x, or 3x times the pipe perimeter (2 * pipe width + 2 * pipe aperture), according to assigned structure complexity
Cataclasite	0.01	1	4.9×10^{-4}	2914	
Coating	0.0005	5	6.2×10^{-3}	2853	
Altered Walls	0.15	0.6	2.2×10^{-4}	2895	
Fresh Rock	1	0.3	7.3×10^{-5}	2839	

Table 5-2: Pore space implementation for Type II structures in the JNC/Golder BS2B model.

Type II Features (fractures)					
Immobile Zone	**Thickness (m)**	**Porosity (%)**	**Formation Factor**	**Density (kg/m^3)**	**Perimeter Factor**
Coating	0.0005	5	6.2×10^{-3}	2853	1x or 2x based on complexity
Altered Walls	0.05	0.6	2.2×10^{-4}	2895	1x or 2x based on complexity
Fresh Rock	1	0.3	7.3×10^{-5}	2839	1x or 2x based on complexity

Actual node / pipe transport pathways were identified in the BS2B prediction model using both a particle-tracking algorithm and the weighted graph theory traversal within PAWorks. One thousand particles were released into the advection-only flow solution network used to produce the water residence time distribution from each tracer release site.

One limitation to the particle tracking approach within the PAWorks software package is that particles can only move along pathways previously identified through the graph theory search; i.e. though the means of the particle travel times are well-constrained, the outliers are sensitive to the number of transport pathways found. For the BS2B simulations, the number of pathways was hard-coded to be 50. In practice, this had little effect on the simulations; for most geometries, there were only 5-6 hydraulically significant pathways. The major difference between pathways was in the selection of in-plane fracture nodes, rather than the selection of alternate fractures.

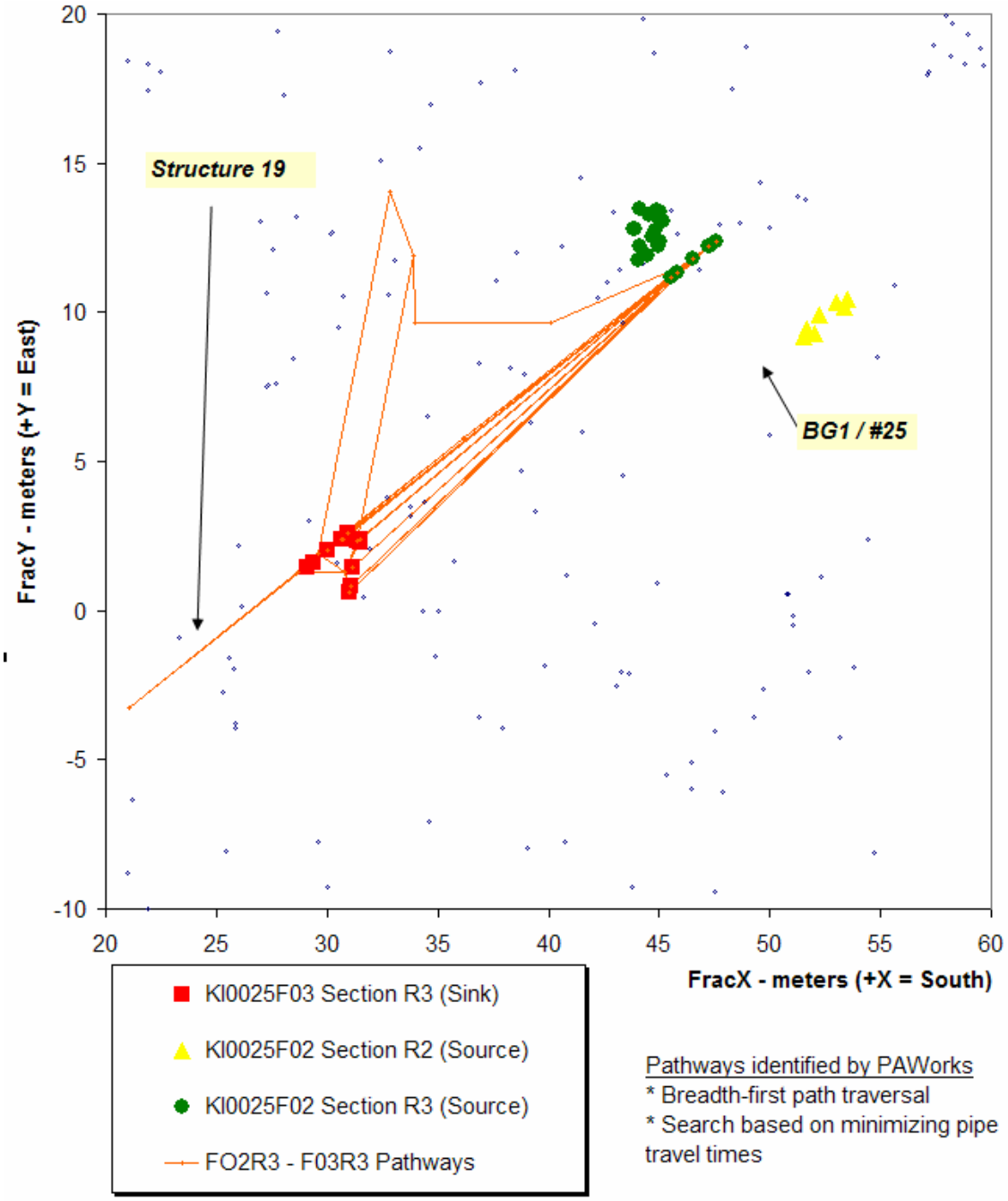

Figure 5-6: *Transport pathways between KI0025F02 Section 3 and KI0025F03 Section 3 (Path I) in the JNC/Golder BS2B channel network model. Transport occurs largely in the plane of Structure 19, with the exception of a lone off-plane slow pathway.*

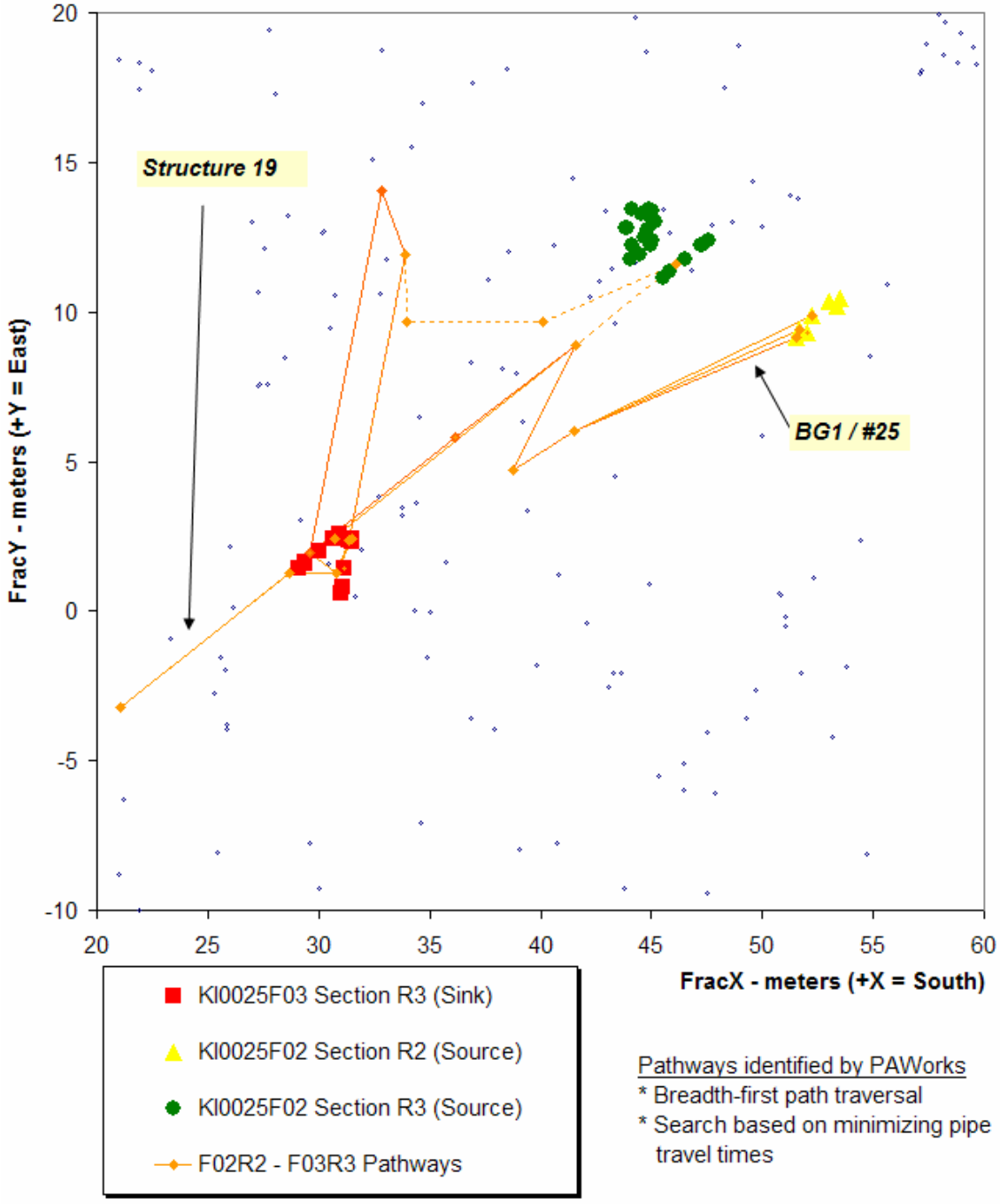

Figure 5-7: *Transport pathways model between KI0025F02 Section 2 and KI0025F03 Section 3 (Path II) in the JNC/Golder channel network model. Principle retardation appears to occur along Structure BG1 and the background fractures that connect it to Structure 19.*

5.2.3 Hydrologic control of retention

The β-factor is a parameter group that is a combined measure of the area available in a transport model to surface and matrix interactions, along with the time constant necessary for those interactions to occur /Elert and Selroos, 2004/. In the BS2B simulations, the β-factor was calculated by using flow pathways defined through

PAWorks graph-theory searches. The β-factor for each identified pathway was calculated by dividing the average channel cross-sectional area by the channel flux rate. Computation of the β-factor and the τ-β relationship is made after the flow simulation is completed, but before the transport calculations are executed. Predicted travel time and β-factor distributions for the Model 20 BS2B simulations are presented below.

Table 5-3: β-factor distribution for Model 20, JNC/Golder BS2B sorbing tracer predictions

19 (Path I) F02R3 to F03R3	**Travel Time τ (hrs)**	**Beta Factor β (hrs /m)**
Mean	5	1.30×10^{5}
Std. Deviation	5	1.72×10^{5}
5%	0.20	1.36×10^{3}
50%	1.48	1.01×10^{4}
90%	10.94	3.90×10^{5}
BG1 (Path II) - F02R2 to F03R3		
Mean	502	2.86×10^{5}
Std. Deviation	18	1.75×10^{5}
5%	480.86	1.44×10^{5}
50%	499.73	1.59×10^{5}
90%	542.89	5.25×10^{5}

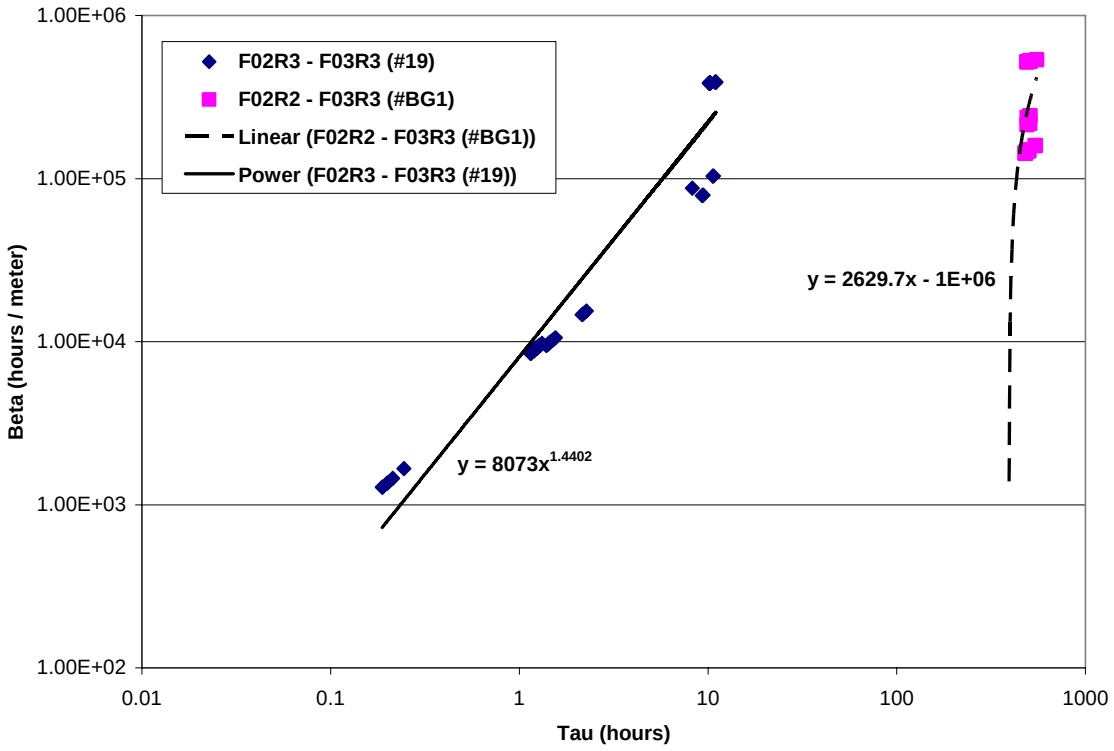

Figure 5-8: *JNC/Golder Model 20 τ-β distribution; Path I pathways generally lie within the plane of Structure 19, while Path II pathways utilize a combination of background fractures, Structure BG1, and Structure 19.*

Note that in both Table 5-3 and Figure 5-8, pathways that utilize Structure 19 show significant spread. This indicates the presence of multiple connections to (and through) Structure 19, and suggests that Structure 19 is relatively well-connected to the rest of the BS2B flow system. In contrast, the Structure BG1 flow system shows very little variation; in this model, it exists as a highly isolated set of discrete pathways with few hydraulic connections to the rest of the flow simulation. This is in line with existing pump test data for intervals intersecting Structure BG1 /Dershowitz, personal communication/.

5.2.4 Tracer breakthrough and recovery

Figure 5-9 through Figure 5-12 present tracer breakthrough and cumulative recovery curves for Model 20, while Table 5-4 and Table 5-5 contain details of activity recovery at specified recovery times (t_5, t_{50}, and t_{95}).

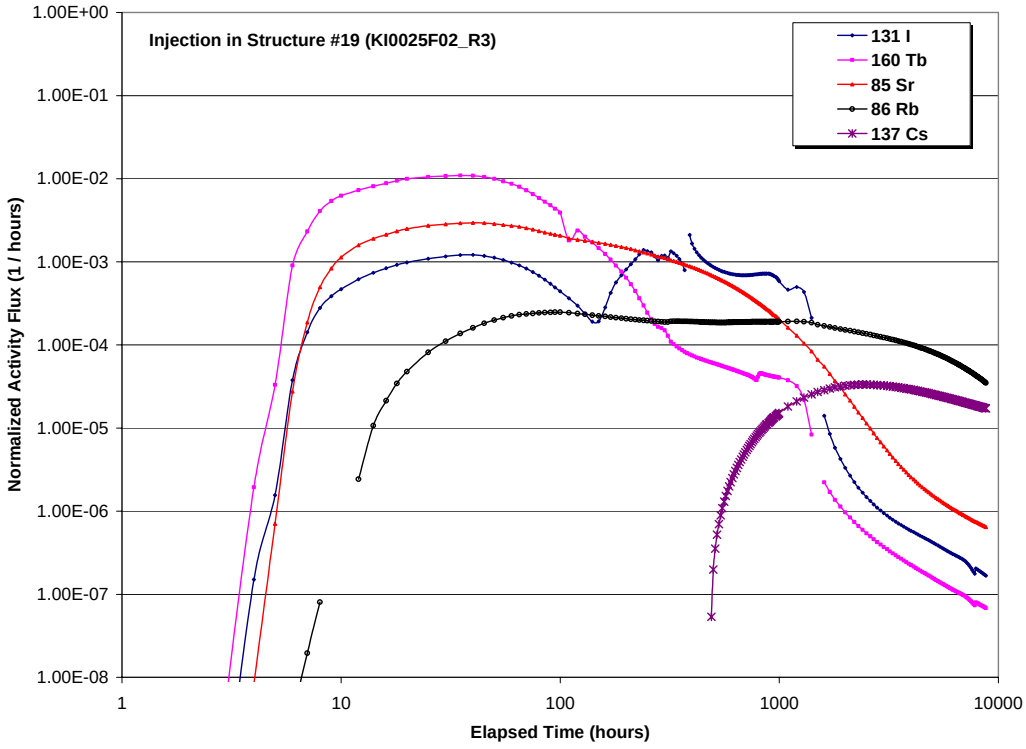

Figure 5-9: *Breakthrough curves for tracers injected for full source term in borehole KI0025F02 Section 3 (Path I).*

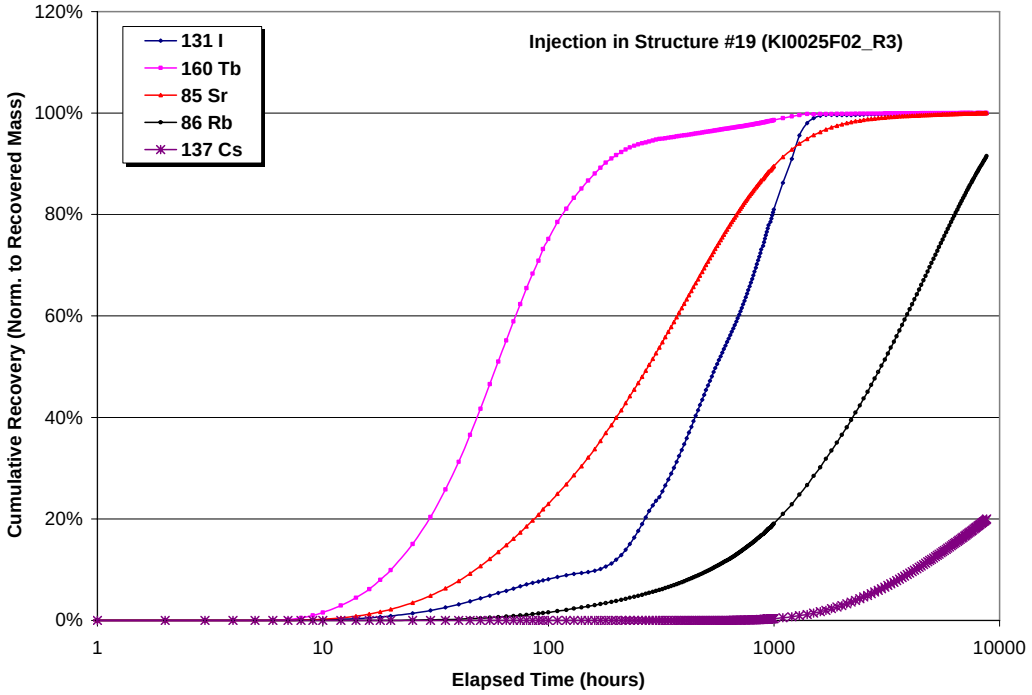

Figure 5-10: *Cumulative recovery curves for tracers injected for full source term in borehole KI0025F02 Section 3 (Path I).*

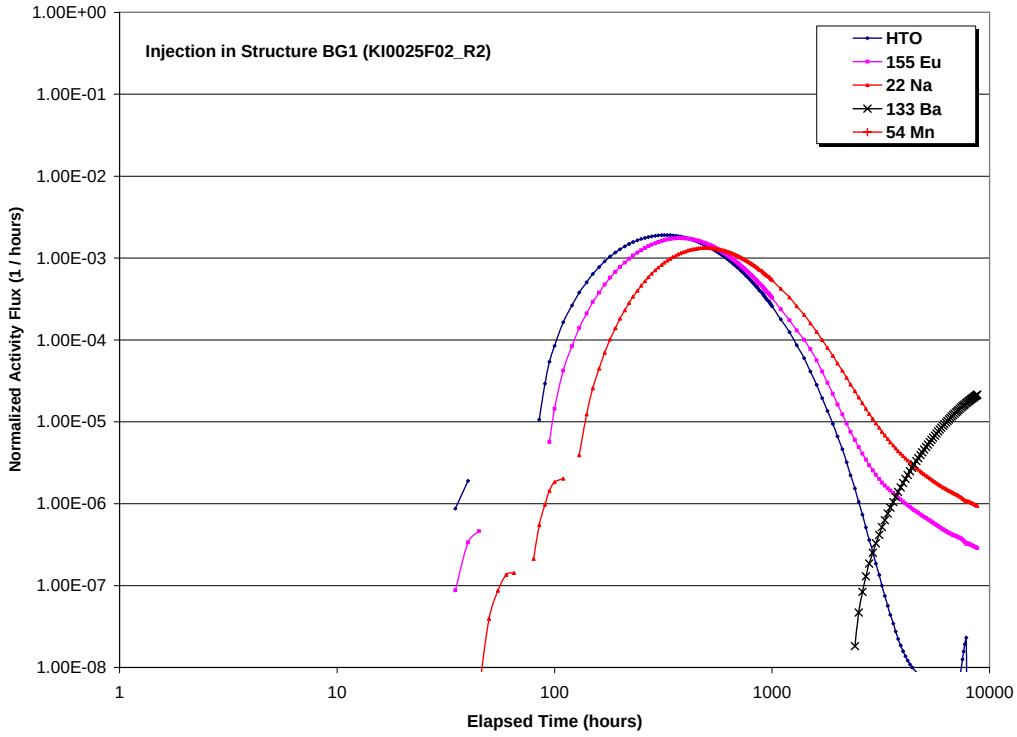

Figure 5-11: *Breakthrough curves for tracers injected for full source term in borehole KI0025F02 Section 2 (Path II).*

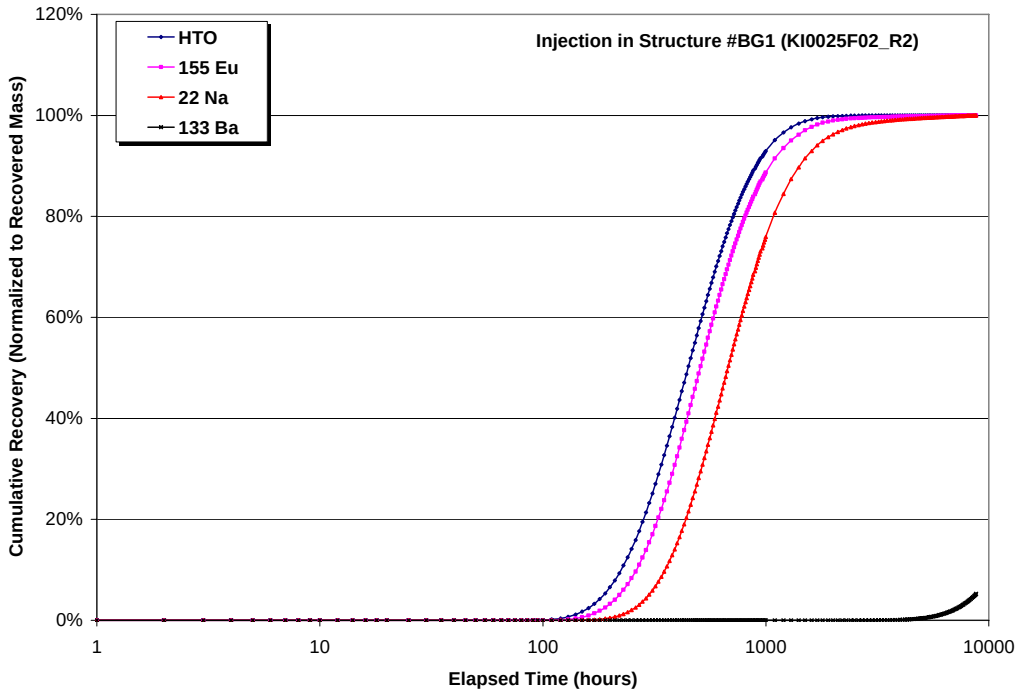

Figure 5-12: *Cumulative recovery curves for tracers injected for full source term in borehole KI0025F02 Section 2 (Path II).*

To assess the effect of the source injection term on the tracer breakthrough curves, simulations using Dirac pulse injections were also run for the BS2B experiment. The Dirac pulse injections tend to show enhanced tails. However, due to the very high tracer concentrations at relatively low flow rates present at the beginning of the test, the initial time steps for the Dirac simulations exhibit a fair bit of numerical instability.

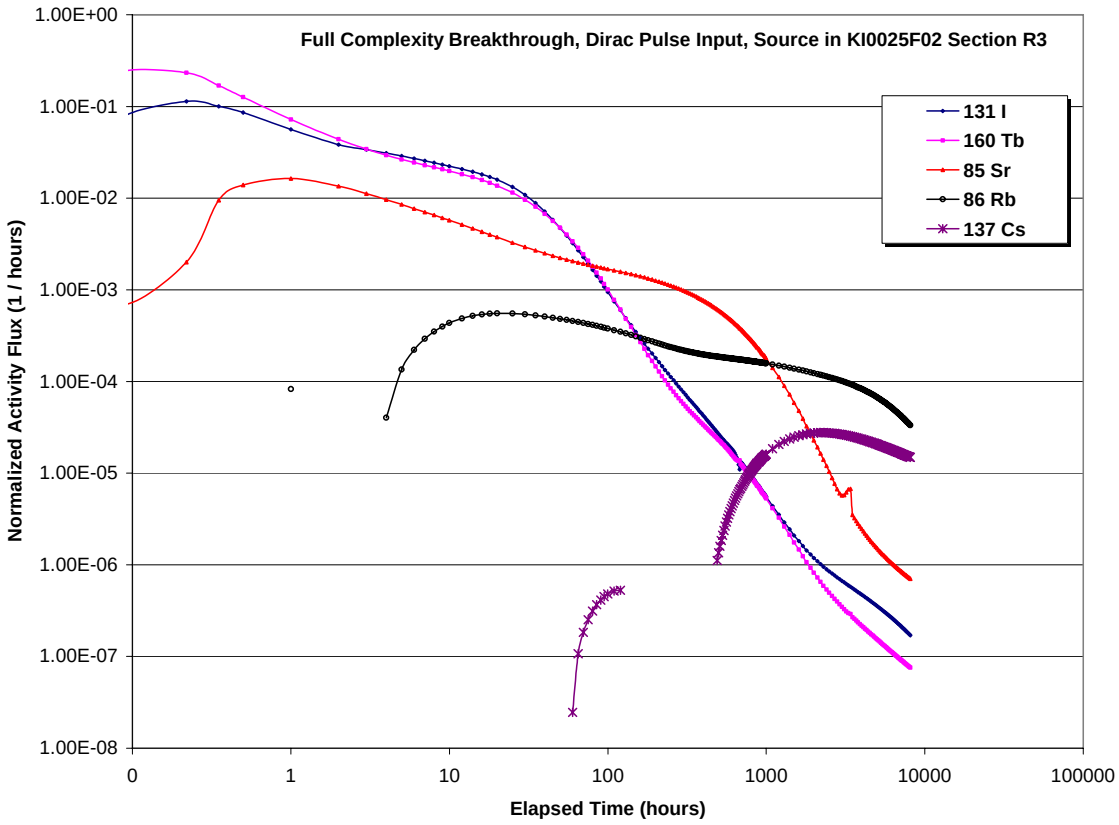

Figure 5-13: *Breakthrough curves for Dirac pulse injection term in borehole KI0025F02 Section 3 (Path I).*

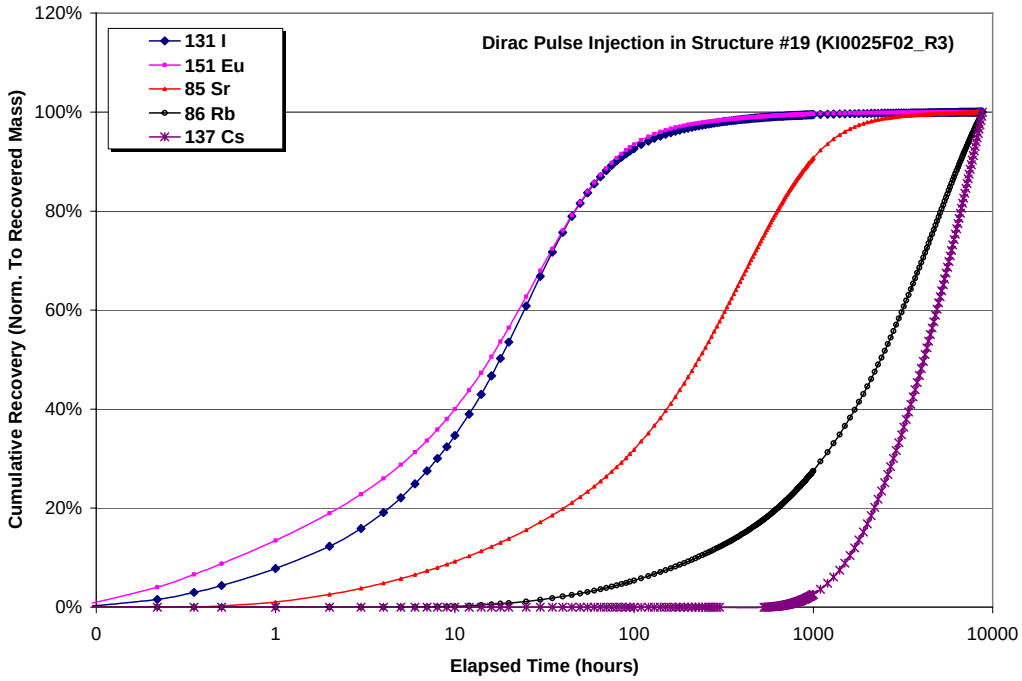

Figure 5-14: *Cumulative recovery curves for Dirac pulse injection term in borehole KI0025F02 Section 3 (Path I).*

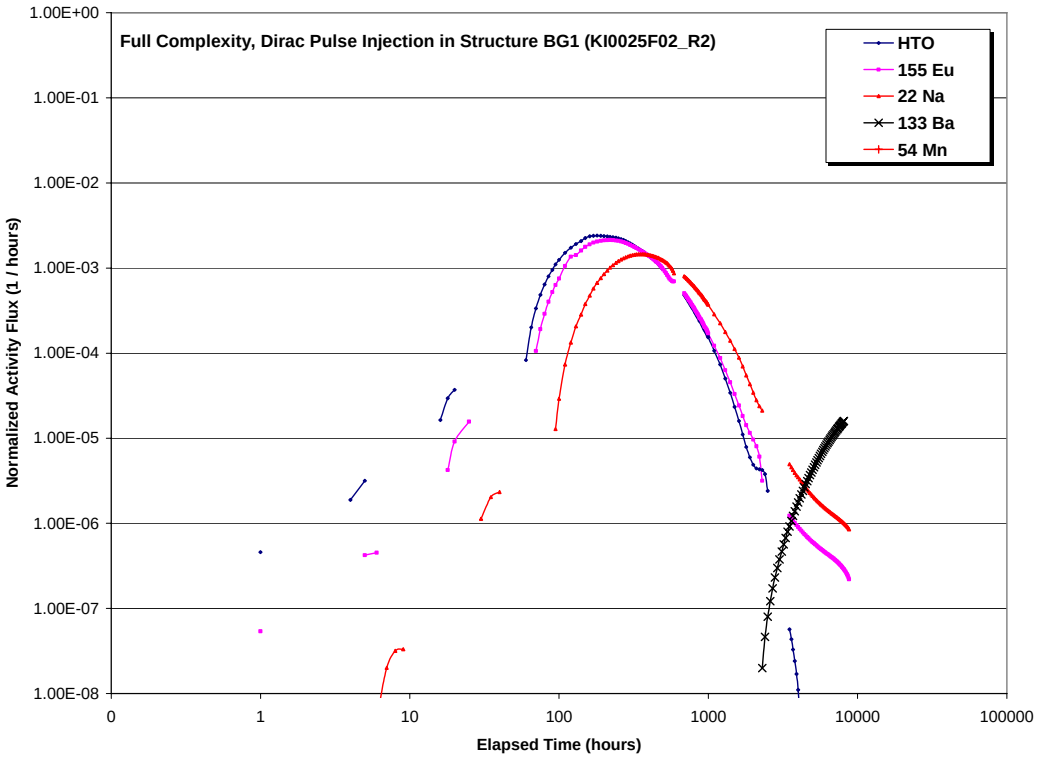

Figure 5-15: *Breakthrough curves for Dirac pulse injection term in borehole KI0025F02 Section 2 (Path II).*

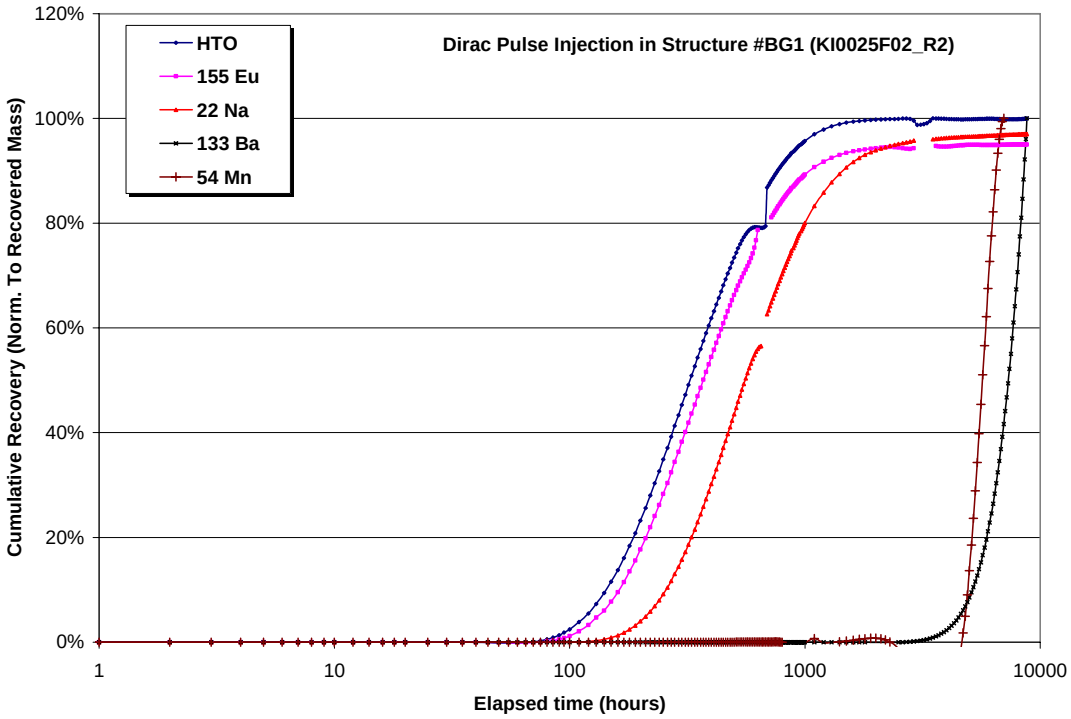

Figure 5-16: *Cumulative recovery curves for Dirac pulse injection term in borehole KI0025F02 Section 2 (Path II).*

Table 5-4: JNC/Golder BS2B model tracer recovery predictions, Model 20, full source term

Tracer	t_5 (hours)	t_{50} (hours)	t_{95} (hours)	Max. Release Rate (1 / hrs)	Predicted Recovery (%)
^{131}I	54.96	549.63	1200.94	2.11×10^{-3}	99.88%
^{160}Tb-DTPA	14.03	54.96	319.96	1.09×10^{-2}	99.96%
^{85}Sr	29.98	269.99	1402.56	2.95×10^{-3}	99.66%
^{86}Rb	249.83	2901.55	N/R	2.48×10^{-4}	71.26%
^{137}Cs	2603.50	N/R	N/R	3.33×10^{-5}	12.31%
HTO	179.70	440.05	999.32	1.91×10^{-3}	99.99%
^{155}Eu-DTPA	210.38	499.66	1200.94	1.75×10^{-3}	99.85%
^{22}Na	290.15	669.72	1797.03	1.33×10^{-3}	99.49%
^{133}Ba	N/R	N/R	N/R	4.93×10^{-6}	0.46%
^{54}Mn	N/R	N/R	N/R	$9.13x\ 10^{-10}$	0.00%

Table 5-5: JNC/Golder BS2B model tracer recovery predictions, Model 20, Dirac pulse source term

Tracer	t_5 (hours)	t_{50} (hours)	t_{95} (hours)	Max. Release Rate (1 / hrs)	Predicted Recovery (%)
^{131}I	0.50	16.04	129.74	1.14×10^{-1}	100%
^{160}Tb-DTPA	0.22	14.03	109.58	2.42×10^{-1}	100%
^{85}Sr	4.00	220.03	1297.37	1.64×10^{-2}	100%
^{86}Rb	90.29	2296.69	5101.81	5.55×10^{-4}	80%
^{137}Cs	1200.94	4102.49	N/R	2.77×10^{-5}	63%
HTO	109.58	319.96	946.73	2.40×10^{-3}	100%
^{155}Eu-DTPA	129.74	360.28	N/R	2.13×10^{-3}	95%
^{22}Na	210.38	549.63	2401.88	1.46×10^{-3}	97%
^{133}Ba	4496.96	N/R	N/R	4.56×10^{-6}	10%
^{54}Mn	4803.77	N/R	N/R	8.26×10^{-10}	19%

5.3 BS2B Forward Modeling: Model Case 9

5.3.1 Water Residence Time

The water residence time distribution was calculated as described in Section 5.2.1; no changes were made. The water residence time distribution for pathways (Path I) within Structure 19 (Figure 5-5) is identical to that of Model 20; the distribution for the modified BG1 pathways (Path II) in Model 9 is presented below in Figure 5-17.

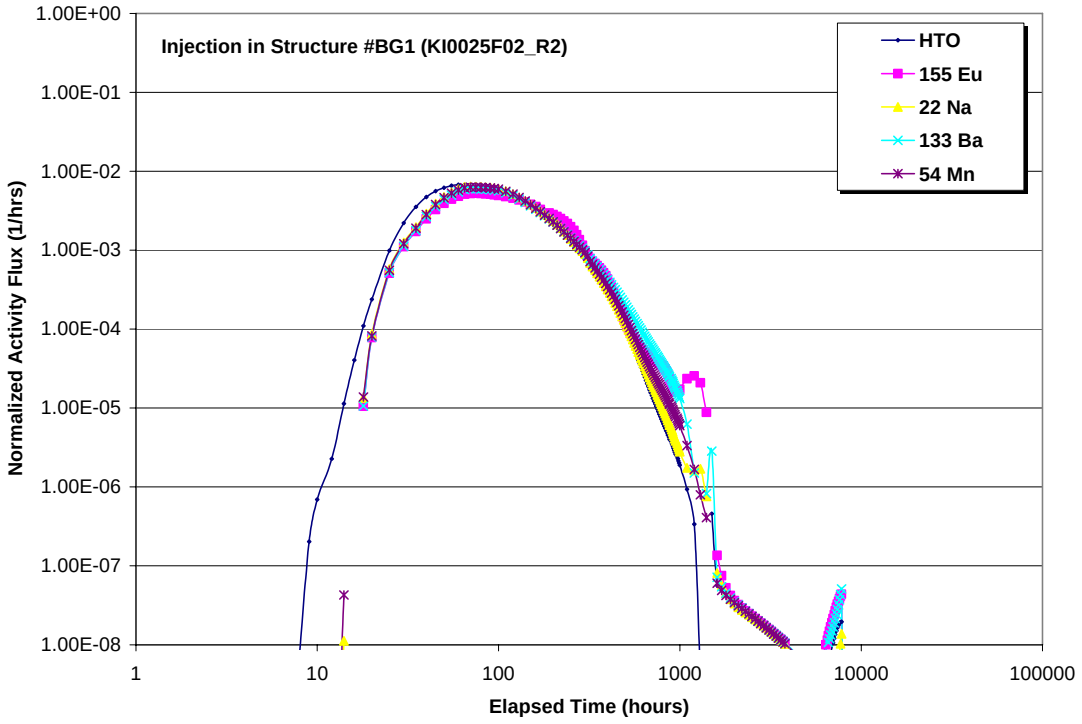

Figure 5-17: *Water residence time distribution (advection-only breakthrough curve) for tracer source in KI0025F02 Section 2 (Path II). Note that, in this simulation, a Dirac pulse input was NOT used (i.e. the input conditions were the specified injection source terms for each tracer).*

5.3.2 Pore Space Implementation

The pore space implementation for Model 9 is the same as for Model 20; no changes to the immobile zones were made. Transport pathways along Structure 19 were unchanged. Figure 5-18 illustrates the changes in the Structure BG1/ Structure 19 pathways in Model 9; note the elimination of the back-connection to KI0025F02 Section 3, cf. Figure 5-7.

5.3.3 Hydrologic Control of Retention

The β-factor was calculated as for Model 20 (see 5.2.3); no changes were made. β-factors for pathways along Structure 19 (Path I) were unchanged. β-factors for pathways involving the background fracture network between Structure BG1 and Structure #9 (Path II) were roughly the same as for Model 20; travel times were decreased by approximately one order of magnitude. Table 5-6 and Figure 5-19 illustrate the τ-β relationship for Model 9.

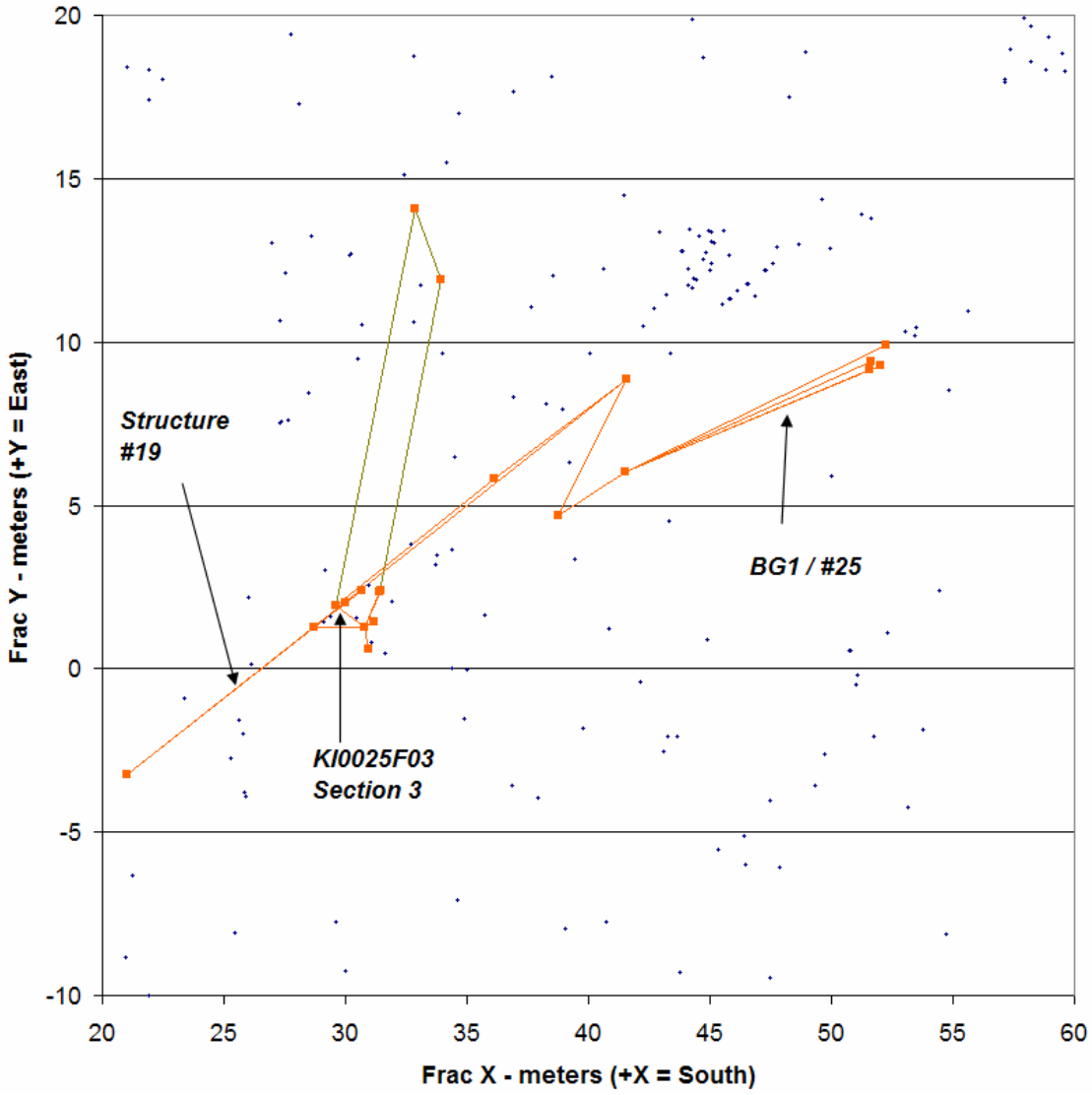

Figure 5-18: *Transport pathways within channel network model between KI0025F02 Section 2 and the sink section (Path II). Principle retardation appears to occur along BG1 and the background fractures that connect it to Structure #19. Note the lack of a 'back-connection' to KI0025F02 Section 3 compared to Model 20; the increase in pipe conductance between BG1 and #19 makes this connection untenable.*

Table 5-6: β distribution for Model 9, BS2B Sorbing Tracer Predictions

	Travel Time τ (hrs)	Beta Factor β (hrs /m)
19 (Path I): KI0025F02R3 to KI0025F03R3		
Mean	5	1.30×10^{5}
Std. Deviation	5	1.72×10^{5}
5%	0.20	1.36×10^{3}
50%	1.48	1.01×10^{4}
90%	10.94	3.90×10^{5}
BG1 (Path II) – KI0025F02R2 to KI0025F03R3		

	Travel Time τ (hrs)	Beta Factor β (hrs /m)
Mean	34	2.82×10^5
Std. Deviation	4	1.77×10^5
5%	29.59	1.44×10^5
50%	32.64	1.59×10^5
90%	39.56	5.25×10^5

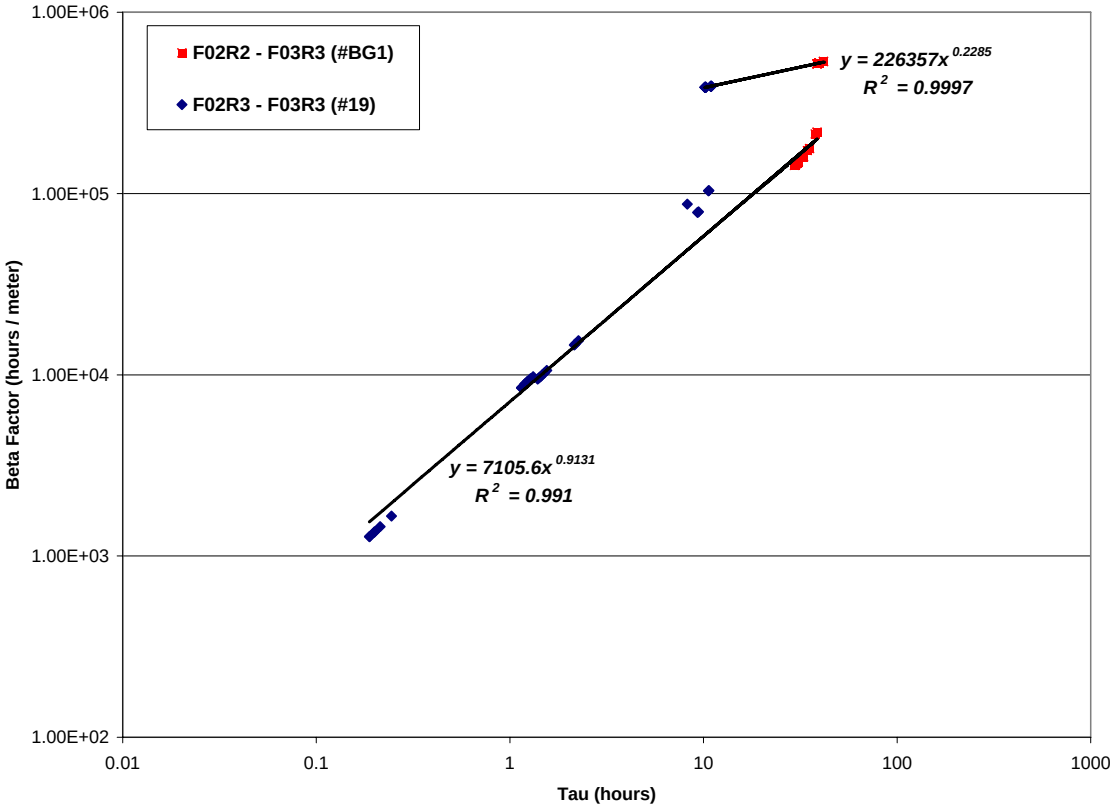

Figure 5-19: *Model 9 τ-β relationship.*

5.3.4 Tracer Breakthrough and Recovery

Figure 5-20 through Figure 5-27 present tracer breakthrough and recovery curves, normalized to injected activities for both the full source term and for a Dirac pulse injection. Table 5-7 and Table 5-8 contain details of activity recovery at critical time thresholds. Breakthrough curves and time statistics for transport within Structure 19 (Path I) are almost identical to those recorded in Model Case 20; only tracers released into Structure BG1 and traveling along background fracture transport pathways between Structures 19 and BG1 (Path II) show differences from Model Case 20.

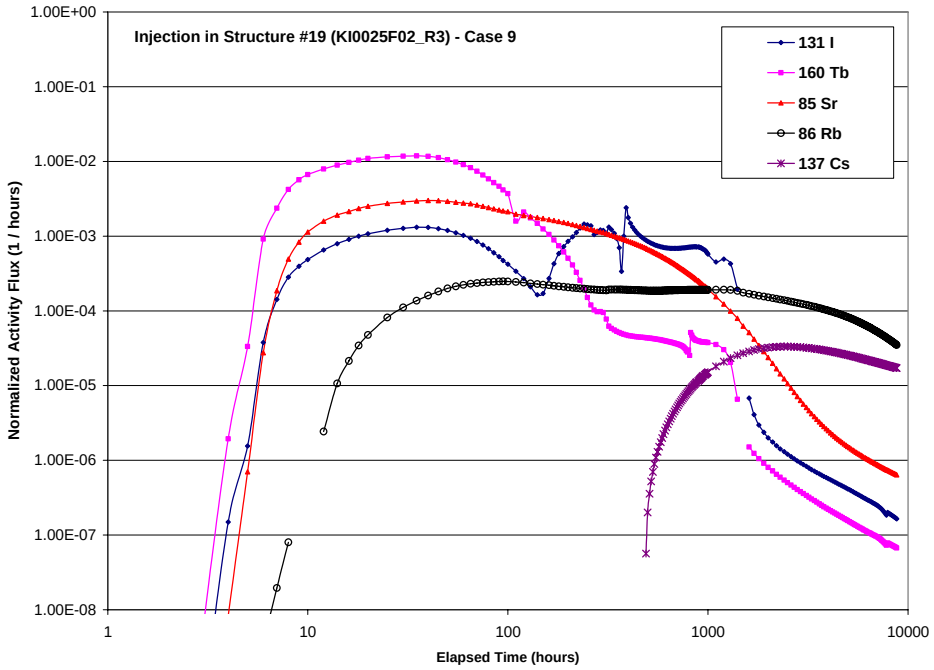

Figure 5-20: *Breakthrough curves for tracers injected for full source term in borehole KI0025F02 Section 3 (Path I), Model 9.*

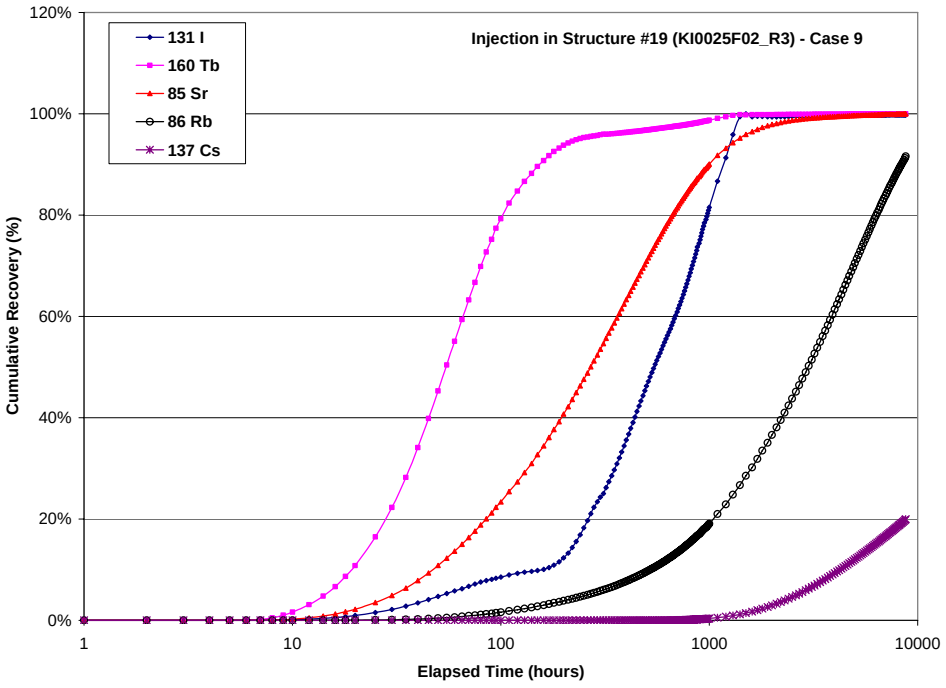

Figure 5-21: *Cumulative recovery curves for tracers injected for full source term in borehole KI0025F02 Section 3 (Path I), Model 9.*

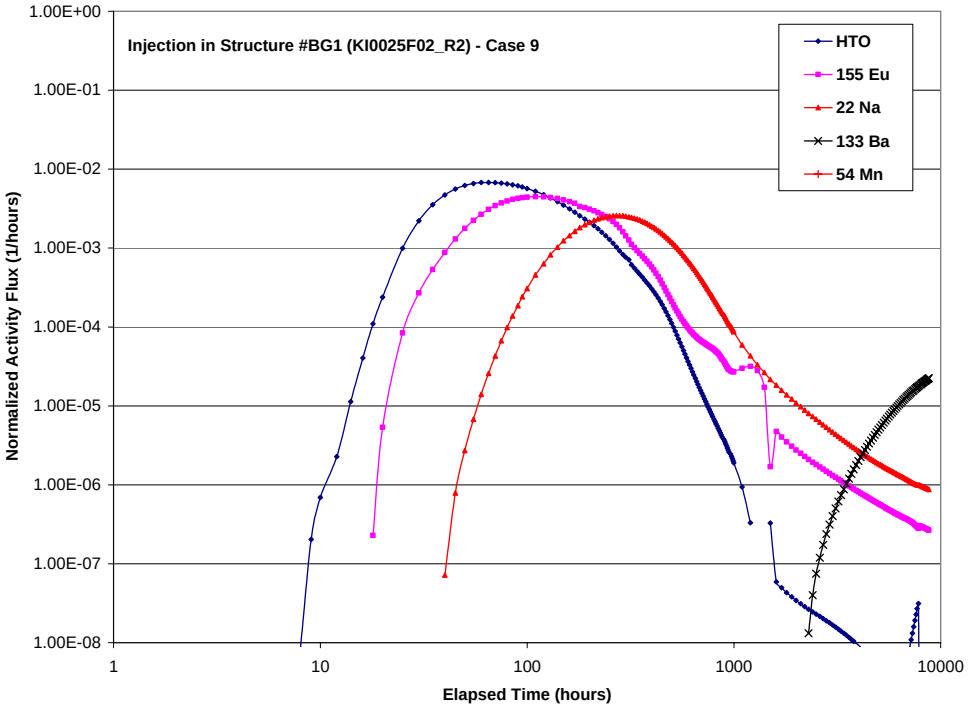

Figure 5-22: *Breakthrough curves for tracers injected for full source term in borehole KI0025F02 Section 2 (Path II), Model 9.*

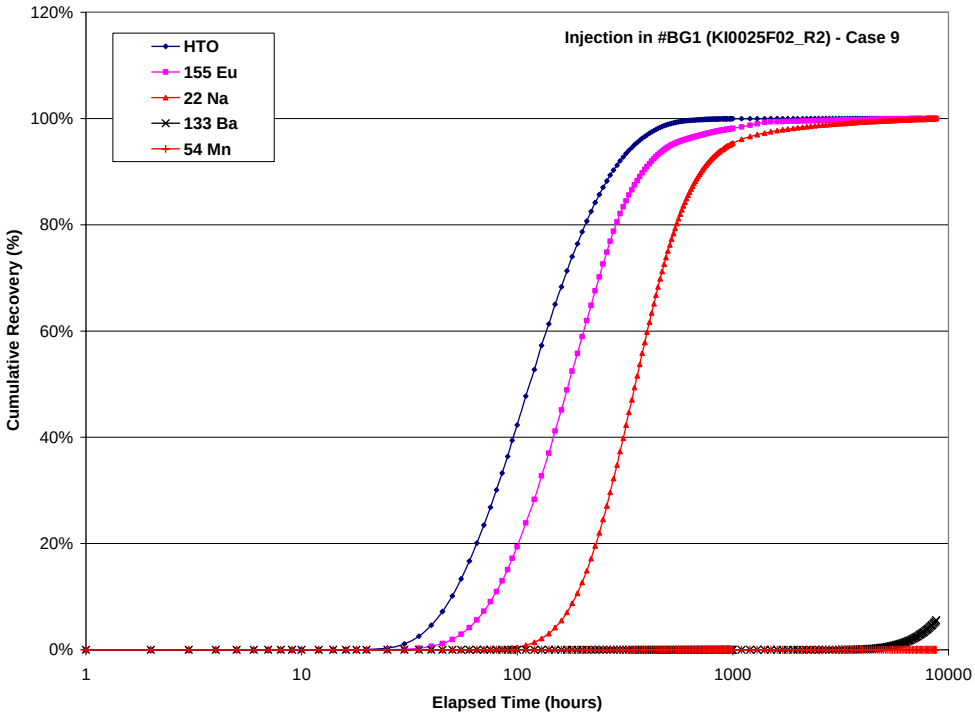

Figure 5-23: *Cumulative recovery curves for tracers injected for full source term in borehole KI0025F02 Section 2 (Path II), Model 9.*

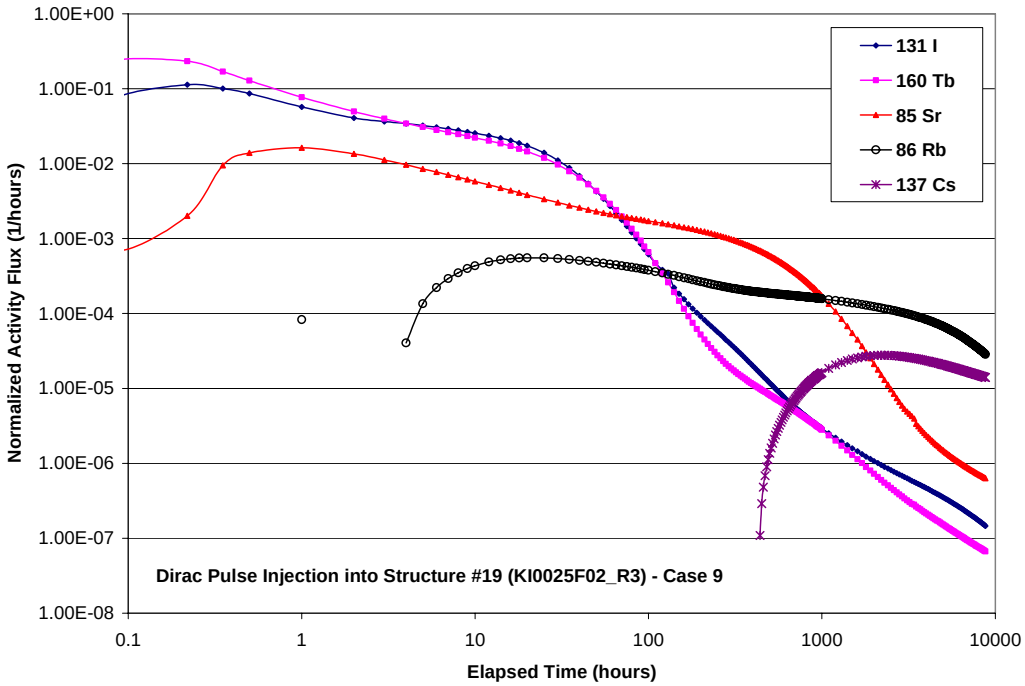

Figure 5-24: *Breakthrough curves for Dirac pulse injection term in borehole KI0025F02 Section 3 (Path I), Model 9.*

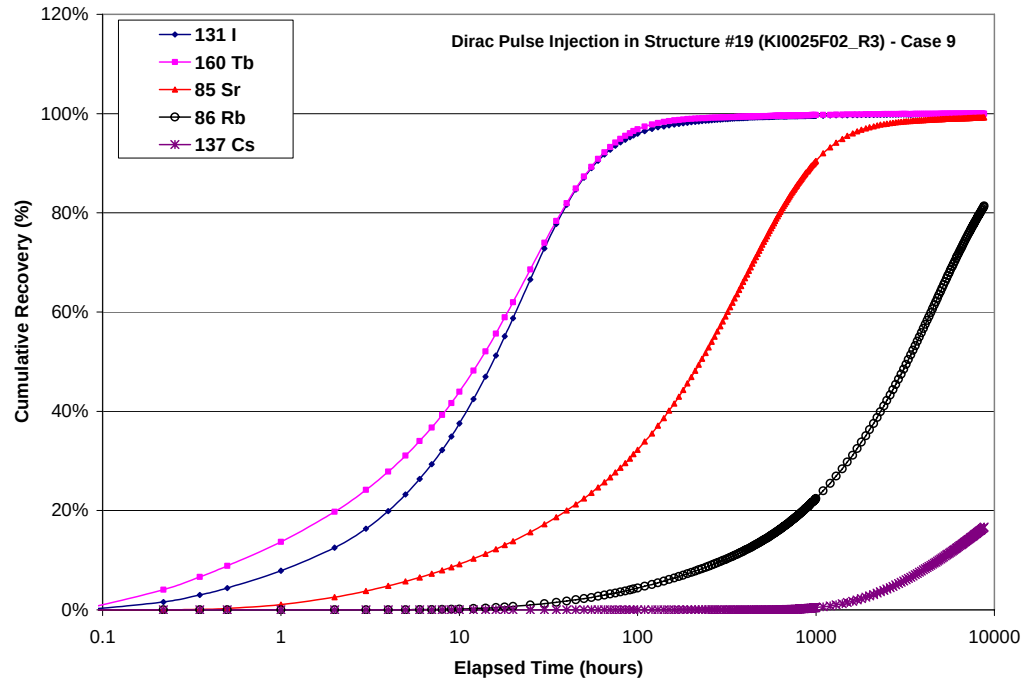

Figure 5-25: *Cumulative recovery curves for Dirac pulse injection term in borehole KI0025F02 Section 3 (Path I), Model 9.*

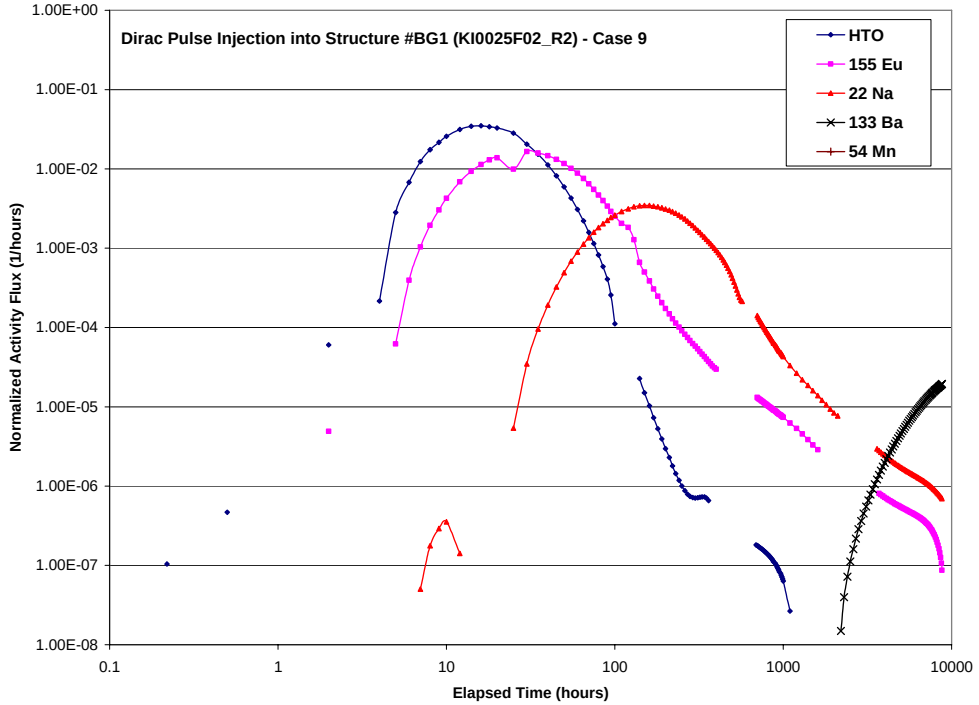

Figure 5-26: *Breakthrough curves for Dirac pulse injection term in borehole KI0025F02 Section 2 (Path II), Model 9.*

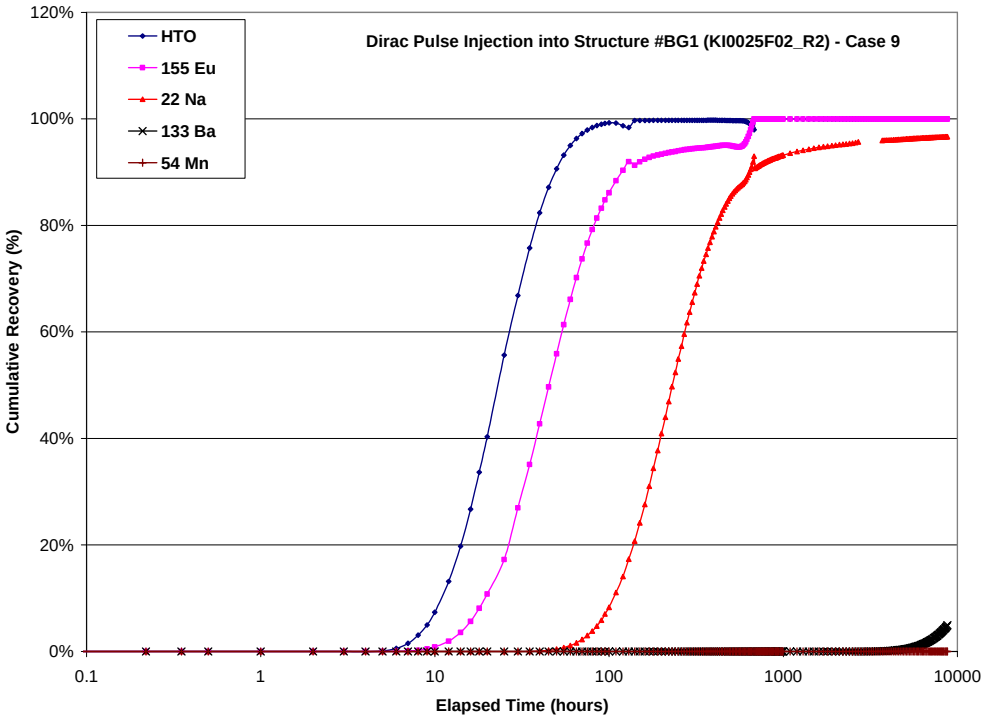

Figure 5-27: *Cumulative recovery curves for Dirac pulse injection term in borehole KI0025F02 Section 2 (Path II), Model 9.*

Table 5-7: BS2B tracer recovery predictions, Model 9, full source term

Tracer	t_5 (hours)	t_{50} (hours)	t_{95} (hours)	Max. Release Rate (1 / hrs)	Predicted Recovery (%)
^{131}I	49.97	539.99	1200.94	2.40×10^{-3}	100.00%
^{160}Tb-DTPA	14.03	49.97	229.67	1.19×10^{-2}	100.00%
^{85}Sr	29.98	260.35	1297.37	2.99×10^{-3}	100.00%
^{86}Rb	249.83	2901.55	5803.09	2.48×10^{-4}	91.61%
^{137}Cs	2603.50	N/R	N/R	3.33×10^{-5}	19.97%
HTO	39.97	109.58	340.12	6.76×10^{-3}	100.00%
^{155}Eu-DTPA	59.96	170.06	510.18	4.46×10^{-3}	100.00%
^{22}Na	149.90	349.76	964.26	2.57×10^{-3}	100.00%
^{133}Ba	8503.02	N/R	N/R	2.25×10^{-5}	5.57%
^{54}Mn	N/R	N/R	N/R	1.13×10^{-9}	0.00%

Table 5-8: BS2B tracer recovery predictions, Model 9, Dirac pulse source term

Tracer	t_5 (hours)	t_{50} (hours)	t_{95} (hours)	Max. Release Rate (1 / hrs)	Predicted Recovery (%)
^{131}I	0.50	14.03	85.03	1.13×10^{-1}	100.00%
^{160}Tb-DTPA	0.22	12.01	80.03	2.42×10^{-1}	100.00%
^{85}Sr	4.00	220.03	1402.56	1.64×10^{-2}	99.24%
^{86}Rb	109.58	3199.59	N/R	5.55×10^{-4}	81.41%
^{137}Cs	2699.93	N/R	N/R	2.77×10^{-5}	16.66%
HTO	9.03	19.99	59.96	3.50×10^{-2}	100.00%
^{155}Eu-DTPA	14.03	44.97	430.41	1.65×10^{-2}	100.00%
^{22}Na	85.03	229.67	1902.22	3.46×10^{-3}	96.68%
^{133}Ba	N/R	N/R	N/R	1.95×10^{-5}	4.95%
^{54}Mn	N/R	N/R	N/R	9.49×10^{-10}	0.00%

5.4 Alternative: Long Isolated Structures

Simulations of both CPT-4c and the BS2B sorbing tracer tests suggested that the geometry of the Structure 19 / Structure BG1 intersection (Path II) was poorly understood. The current conceptual model is that transport first occurs through BG1, and then successively "jumped" through the background fracture network to Structure 19, where it then proceeded downstream to the sink section. However, the results of the pre-test calibration (Figure 5-1 and Figure 5-3) suggested that this is not the case.

The relatively narrow profile and subdued tail of the observed CPT-4c breakthrough for tracers injected in KI0025F02 Section 2 suggests that very little tracer was retarded within immobile zones. However, the relatively late initial breakthrough times (Figure 5-1) indicate that the conservative tracers arrive as a 'package'; they have either traveled a long distance or have taken a relatively slow but geologically simple pathway between KI0025F02 Section 2 and KI0025F03 Section 3.

Therefore, the JNC/Golder team elected to test one of these hypotheses. Structure BG1 was extended more than 50 m to the southwest, and connected directly to Structure 19 through a single background fracture of modest aperture (1×10^{-3} m) and transmissivity (1×10^{-7} m^2/s). Figure 5-28 illustrates the modifications to the base DFN. Transport through the POSIVA flow log fracture or the general background fracture network was suppressed by locally reducing transmissivity on those features between Structures 19 and BG1 to 1×10^{-13} m^2/s. This also offered a chance to test retention processes through a long section of a geologically complex feature (19).

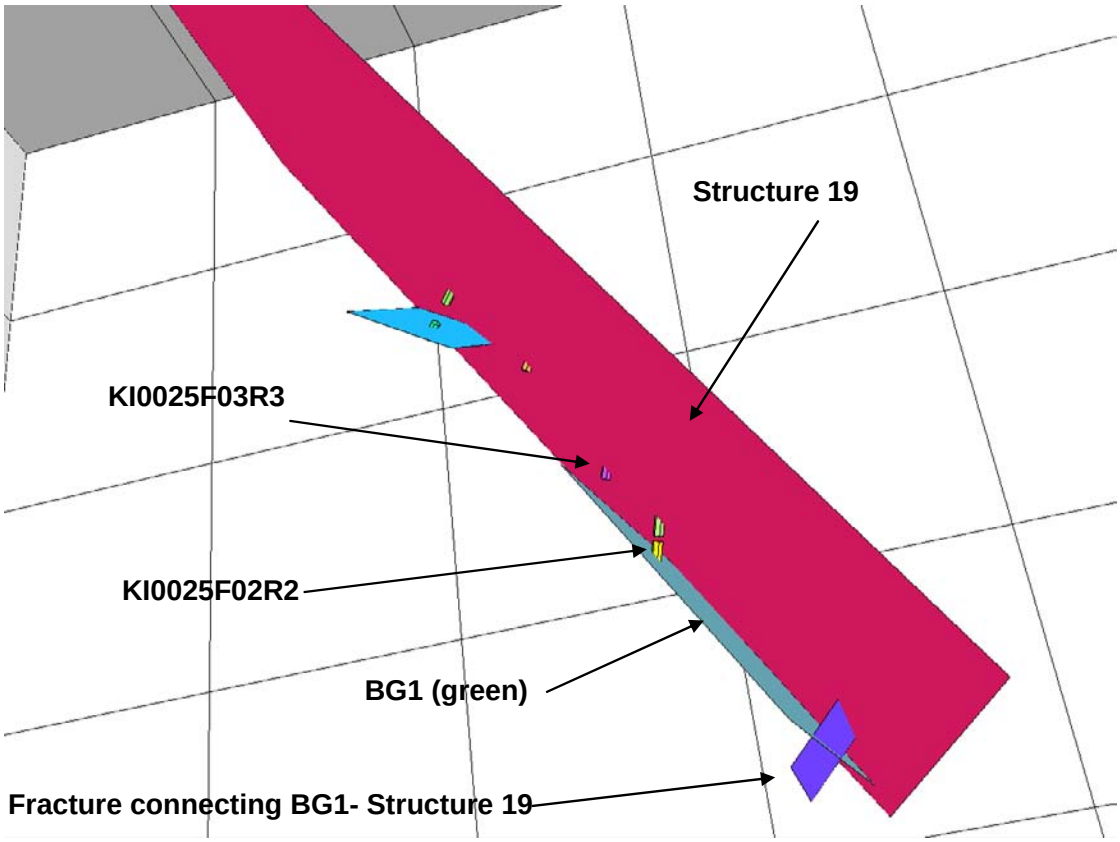

Figure 5-28: *Modifications to BS2B Base DFN to test the effects of long isolated transport pathways through Structure BG1 (Path II). The remainder of the DFN has been removed for clarity.*

A single realization, using the designated CPT-4c full source terms, was completed. All immobile zones and geologic complexity were active. The resulting pathway lengths were on the order of 100 m. The long pathway produced a breakthrough t_5 match that is much closer to the actual tracer breakthrough than either Model 9 or Model 20. However, the simulation results showed a pronounced tail; since CPT-4c used conservative tracers, the tail represented the effects of longitudinal dispersion over a long pathway.

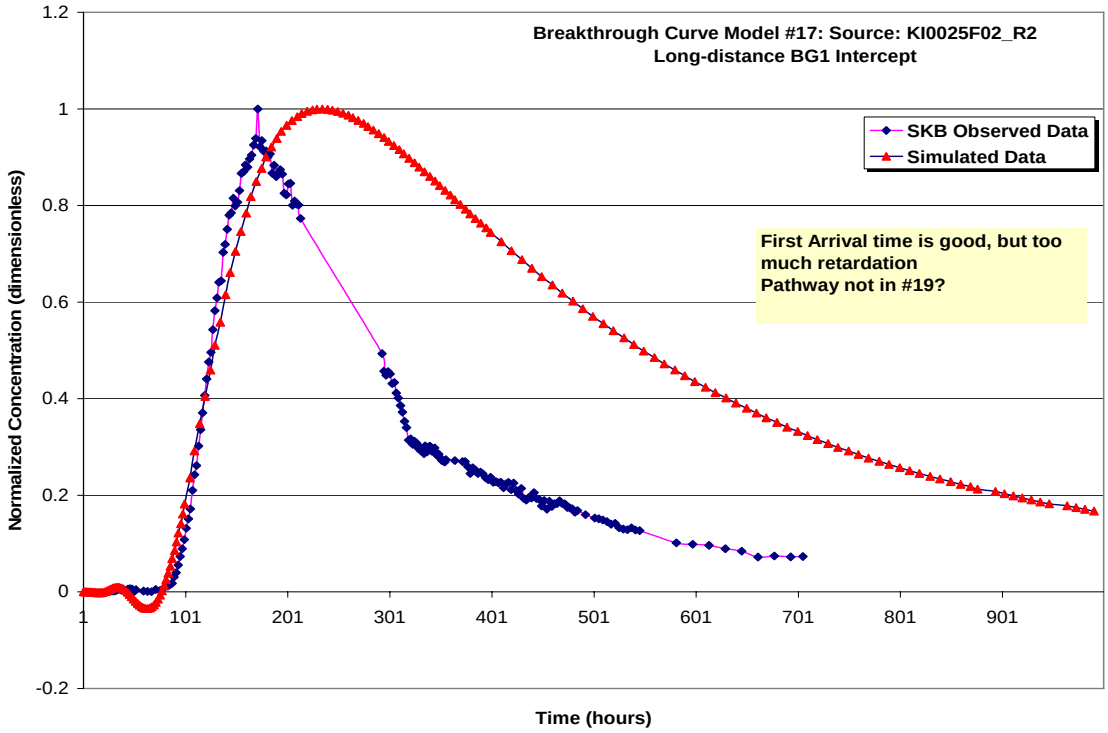

Figure 5-29: *Breakthrough curve for long slow Structure BG1 pathways utilizing Structure 19 (Path II) for full BS2B source terms.*

The results (Figure 5-29) suggest that transport pathways from KI0025F02 Section 2 did not necessarily directly connect to Structure 19. It also suggests that the Structure BG1 connection is not a long-distance one; the pronounced dispersion that comes from a long tortuous pathway is not seen in the breakthrough data recorded during the BS2B tracer pre-tests. Figure 5-18 seems to indicate that the Structure BG1 connection may consist of a moderate-length (35-50 m), geologically simple (Type II fracture) pathway that runs nearly point-to-point from KI0025F02 Section 2 to KI0025F03 Section 3, and may bypass Structure 19 altogether. Further simulations and perhaps additional hydraulic testing could potentially shed more light on this connection.

6 Evaluating the JNC/Golder BS2B Model Performance

Previous chapters describe the JNC/Golder team's efforts towards the prediction of the behavior of reactive tracers in a section of the TRUE Block. Modeling efforts were focused on the blind prediction of sorbing and non-sorbing tracer transport and retention between two boreholes (KI0025F02 and KI0025F03) along two different flow paths (Structure 19 – Path I and Structure BG1 – Path II). All simulations utilized tracer injection data from the actual BS2B experiments.However, these simulations were generally done as 'blind predictions', with little to no knowledge of the actual experimental outcomes. This chapter evaluates the performance of the JNC/Golder BS2B model, relative to the published results of the in-situ experiment.

6.1 Comparison of JNC/Golder Predictions to Experimental Results

JNC/Golder blind predictions are presented in Chapter 5, while the underlying DFN-CN model is described in Chapters 2 and 4. The in-situ results of the BS2B experiment were presented in TRUE BSC Data Delivery #6, and are summarized in Andersson et al. (2005). The following evaluation and reconciliation efforts are focused solely on the JNC / Golder alternative Model 20, which is described in Section 5.1.2. This model alternative was chosen for the following reasons:

- For the fast flow path (Path I) along Structure 19 (KI0025F02_R3 to KI0025F03_R3), Models 20 and 9 produced identical breakthrough curves (Figure 6-1).
- For the slow flow path (Path II) from Structure BG1 to Structure 19 through background fractures (KI0025F02_R2 to KI0025F03_R3), Model 9 results were an order of magnitude too fast (Figure 6-2), suggesting that the modifications to the hydraulic system in Model 9 were too severe.

The experimental tracer breakthrough data provided by SKB was converted from a normalized concentration (Bq/Kg to C/Atot) to a normalized volume flux ($1/m^3$). LTG produces output in terms of an activity flux rate (Bq/year). Both the JNC/Golder model results and the in-situ observational data were converted to volume flux rates by assuming constant pumping rates. This made direct comparisons of the data sets relatively simple. Mass fluxes were converted to volume fluxes by assuming that the solution in the borehole consisted of water at standard temperature and pressure ($1m^3$ water + tracer = 1000 kg).

Figure 6-3 and Figure 6-4 compare the observed BS2B experiment tracer breakthroughs to the JNC/Golder blind predictions (Model 20). Note the abrupt concentration increase for $^{131}I^-$ at approximately 200 hours in the JNC/Golder blind predictions. This concentration increase was due to spikes contained in the on-line injection sampler records used to simulate the tracer injection. These spikes were removed in the reconciliation model by deriving the late-time portions of the $^{131}I^-$ injection mass flux profile solely from the bypass samples (Anderson, 2004c) instead of the on-line sampling records. Table 6-1 presents the results of the JNC/Golder blind prediction for both flow paths in terms of tracer recovery at specified times (t_5, t_{50}, and t_{95}).

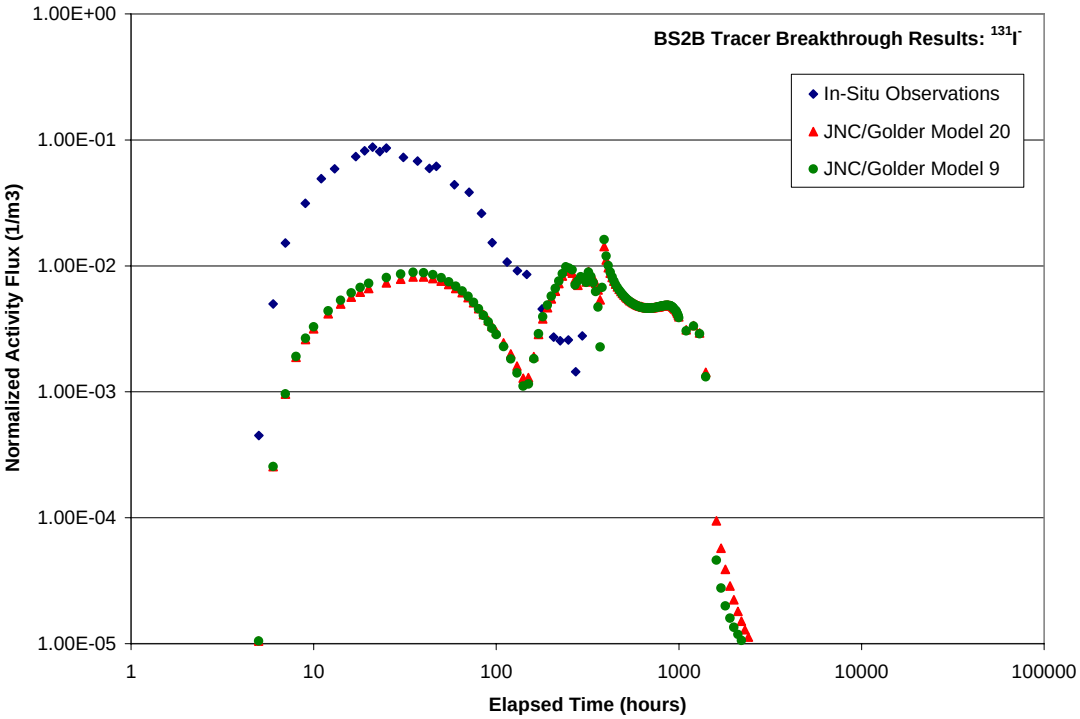

Figure 6-1: *Comparison of tracer breakthrough curves, JNC / Golder Models 9 and 20. Note that both models behave identically for transport within Structure 19 (Path I).*

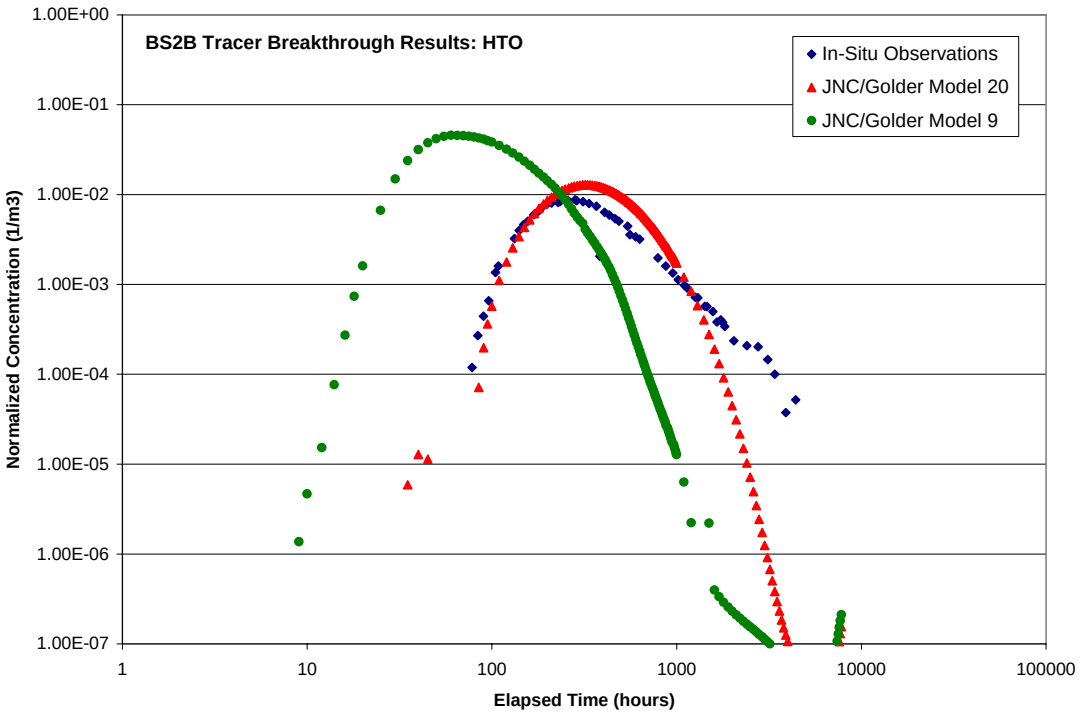

Figure 6-2: *Comparison of tracer breakthrough curves, JNC / Golder Models 9 and 20 (Path II). For a non-reactive tracer (HTO), the Model 9 breakthroughs are an order of magnitude too fast.*

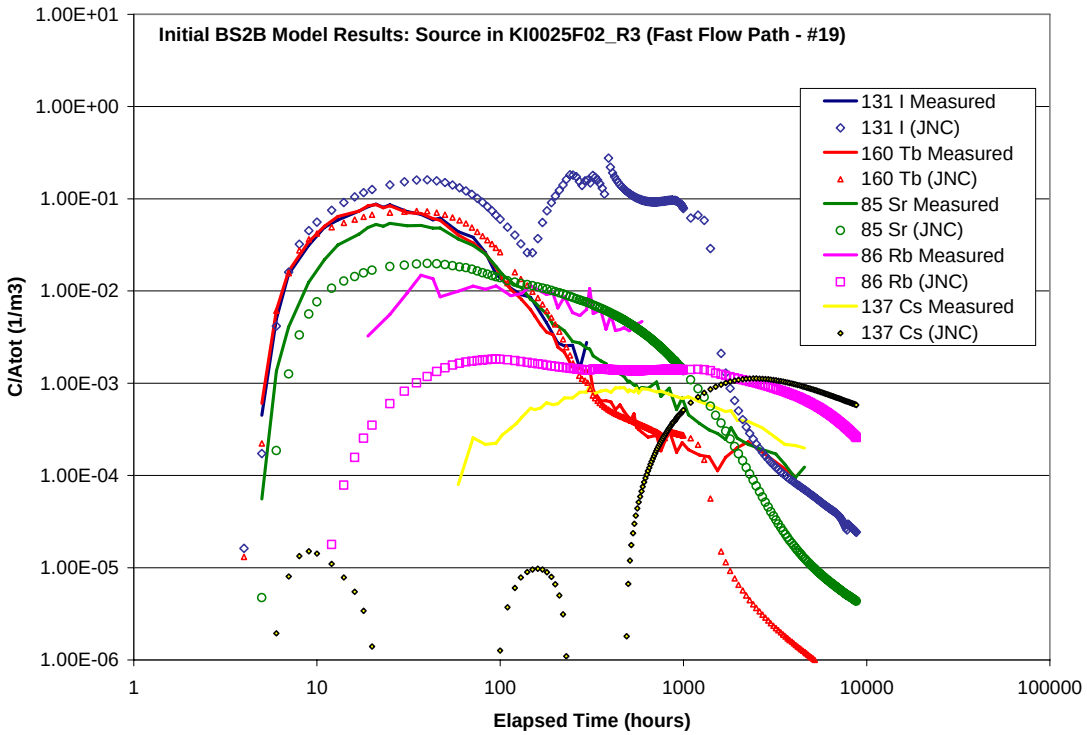

Figure 6-3: *Breakthrough curves for Path I (Structure 19) flow path. In-situ observations are indicated by dashed symbols, while JNC/Golder predictions are indicated by geometric shapes.*

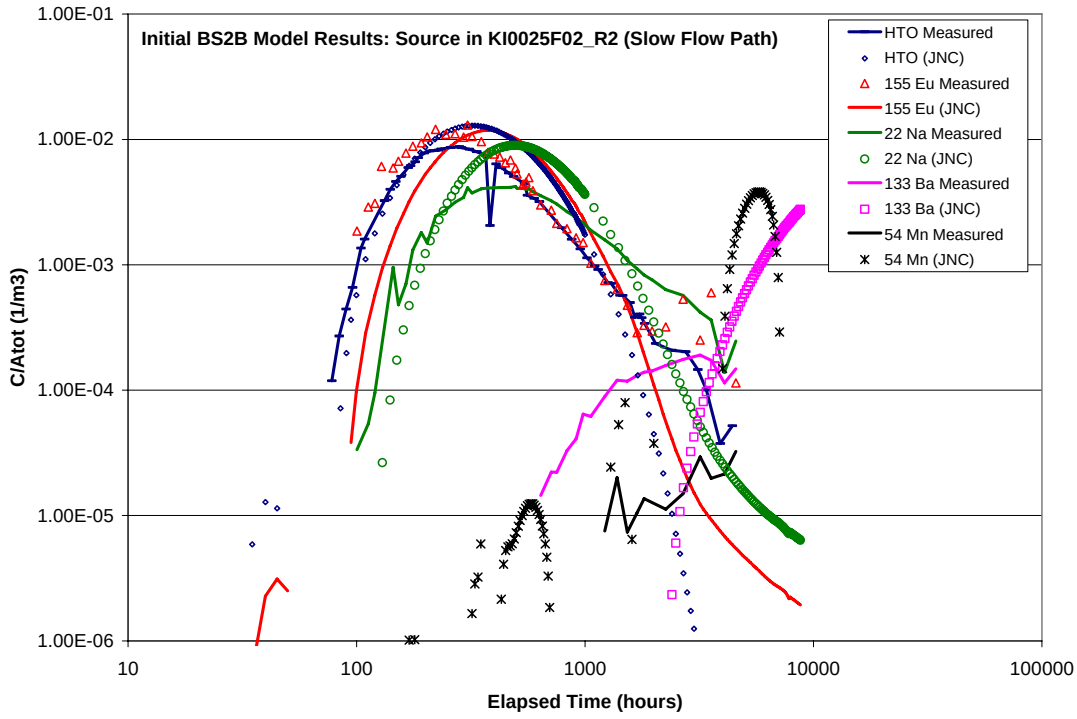

Figure 6-4: *Breakthrough curves for Path II (source in Structure BG1 and sink in Structure #19) flow path. Observations are indicated by 'dashed' symbols, while JNC/Golder predictions are indicated by solid colored lines.*

Initial predicted breakthrough times of the JNC/Golder Model 20 alternative for most conservative tracers compare favorably to BS2B experimental observations. However, the JNC/Golder results predict more longitudinal dispersion and less matrix diffusion than was actually observed in-situ.

There is an additional, somewhat problematic observation. The relatively long tail for HTO in Figure 6-4 suggests that tritiated water (HTO) is behaving as a slightly sorbing tracer with more matrix diffusion than to be expected of a conservative tracer. This is not consistent with the fundamental assumption that HTO is a conservative tracer. Within this assumption, it is not possible to match this long tail observation.

Table 6-2 provides some aggregate statistics of the geometries of the simulated transport pathways used in the JNC/Golder blind prediction. These pathways were derived using a weighted graph theory search within PAWorks, biased towards minimizing the travel time between the injection and sink borehole sections. They represent **potential** flow paths, from which PAWorks derives a downstream network of nodes and pipes for use with LTG. Figure 6-5 illustrates all the PAWorks-identified pathways between KI0025F02_R3 (injection) and KI0025F03_R3 (pumping); these pathways (when combined) represent 'Path I' of the BS2B model specification. As expected, for this test almost all pathways lie entirely within Structure 19; see Figure 5-7 in Chapter 5 for an alternative view of these pathways.

Table 6-1: Comparison of JNC/Golder Blind Prediction Results with BS2B Experimental Tracer test Results.

Tracer Breakthrough Times for Flow Path II (BG1-19)

BS2B Experimental Results					JNC/Golder Model 20 (Blind Prediction)				
	t5 hours	*t50 hours*	*t95 hours*	*% Recovery*		*t5 hours*	*t50 hours*	*t95 hours*	*% Recovery*
HTO	183	790	n/r	68%	HTO	180	440	999	100%
155Eu	155	500	n/r	92%	155Eu	210	500	1201	100%
22Na	300	1490	n/r	72%	22Na	300	675	1797	100%
133Ba	3250	n/r	n/r	8%	133Ba	8695	n/r	n/r	5.25%
54Mn	n/r	n/r	n/r	1%	54Mn	n/r	n/r	n/r	< 1%

Total Time	hrs
HTO	4409
AllOthers	4577

	Good Match to Measured Data
	O.K. Match to Measured Data
	Poor Match to Measured Data

Tracer Breakthrough Times for Flow Path I (19)

BS2B Experimental Results					JNC/Golder Model 20 (Blind Prediction)				
	t5 hours	*t50 hours*	*t95 hours*	*% Rec*		*t5 hours*	*t50 hours*	*t95 hours*	*% Recovery*
131I-	14	62	n/r	80%	131I-	55	550	1300	100%
160Tb	14	63	4075	87%	160Tb	15	60	329	100%
85Sr	19	107	4327	86%	85Sr	30	280	1402	100%
86Rb	51	490	n/r	56%	86Rb	260	2950	n/r	92%
137Cs	555	n/r	n/r	28%	137Cs	n/r	n/r	n/r	<1%

Table 6-2: PAWorks Pathway Statistics for Model 20, JNC /Golder Blind Predictions.

Parameter	Path I F02R3 → F03R3	Path II F02R2 → F03R3
Cartesian Distance	19.5	22
Number of PAWorks Pathways	50	50
Average Pathway Length (m)	43.93	63.63
Maximum Pathway Length (m)	64.22	81.08
Minimum Pathway Length (m)	18.17	57.8
Average % of Path in #19	80.9%	45.23%
Maximum % of Path Length in 19	100%	62.84%
Minimum % of Path Length in 19	14.56%	9.14%

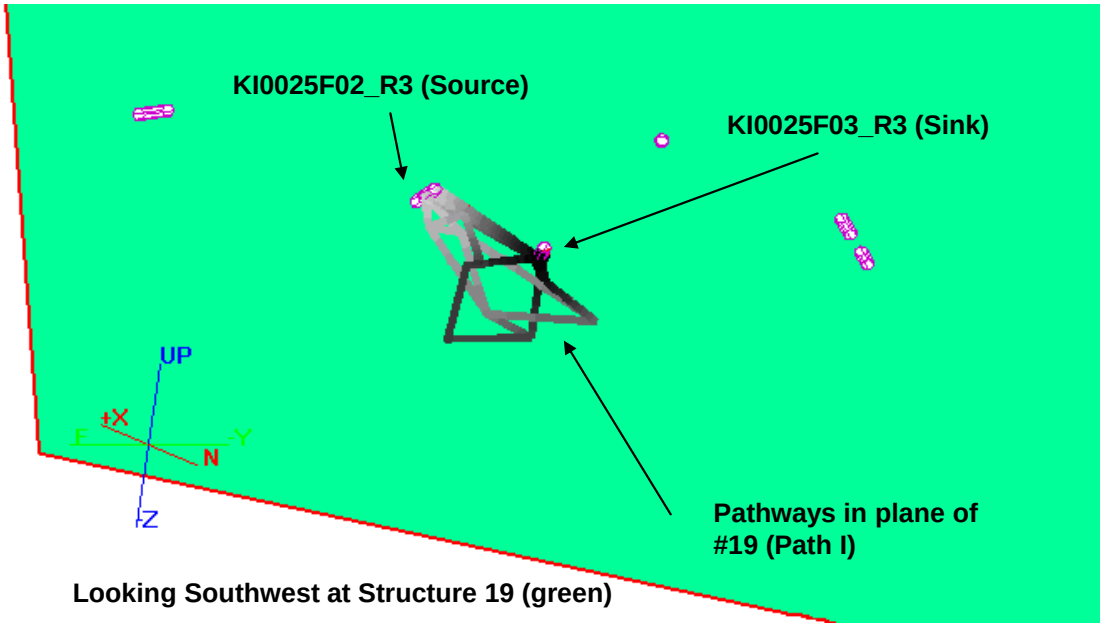

Figure 6-5***:*** *Pathways within Structure 19 (Path I), JNC / Golder channel network model 20 (blind predictions). The black lines represent the combination of 50 potential pathways identified by PAWorks.*

Figure 6-6 illustrates PAWorks-identified potential pathways between KI0025F02_R2 (injection) and KI0025F03_R3 (pumped); this system (Path II) represents transport from Structure BG1 to Structure 19 through the background fracture network. This part of the BS2B experiment was designed to simulate transport predominantly through the background fractures. However, Figure 6-6 suggests that, in this iteration of the JNC/Golder channel network model, a significant number of the potential pathways have a substantial length within the plane of Structure 19.

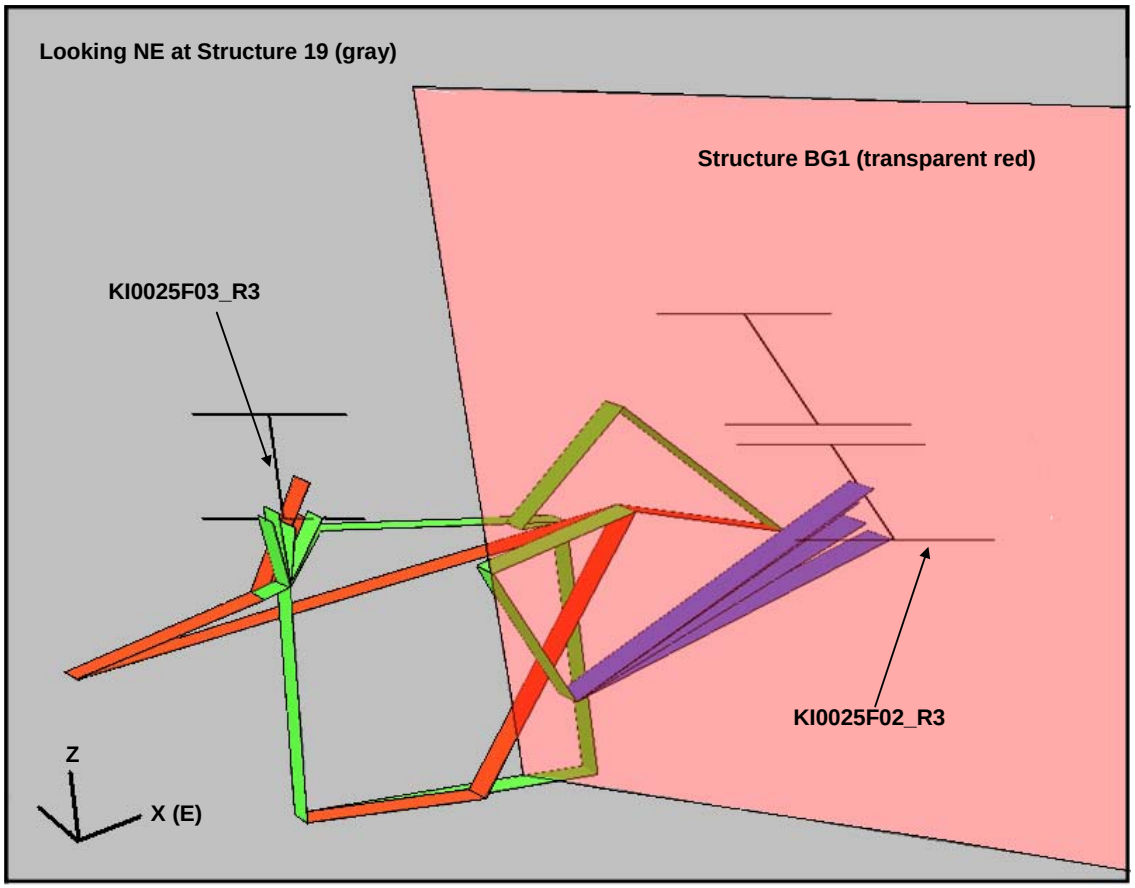

Figure 6-6: *Pathways between Structures 19 and BG1 (Path II), JNC / Golder channel network model 20 (blind predictions). The dark red pipes are potential pathways within the plane of Structure 19, the purple pipes are within the plane of Structure BG1, and the green pipes are on other background fractures. View is looking northeast towards the Aspo HRL.*

In general, the JNC/Golder blind prediction channel-network model over-predicted retention for moderately to strongly-sorbing tracers. This is may be due in part to the simplifying assumptions made for fracture complexity and parallel immobile zone diffusion as described in Chapter 4.

6.2 JNC/Golder Model Issues Discovered During Evaluation

A comparison of the initial JNC/Golder predictions to experimental observations from the BS2B tracer experiment suggests that the DFN/CN model has several issues that need to be further addressed. Specifically:

- The inclusion of sub-horizontal structures not present in the Task 6C semi-synthetic hydrostructural model did not aid in hydraulic calibration; instead, it provided preferential transport pathways, effectively short-circuiting Structure BG1 directly to Structure 19.

- The initial JNC/Golder channel network model predicts overly large (600-700 m) drawdowns in the vicinity of the sink well (KI0025F03_R3). Though significant (>200m) drawdowns are noted in KI0025F03, this overly large drawdown tends to produce hydraulic gradients that are too steep, therefore resulting in faster arrival times only partially compensated for by increased retention and larger fracture hydraulic apertures.

- Assumptions regarding the derivation of 1D channels from a 3D fracture network were over-conservative, resulting in pipe widths (and therefore surface area for retention) that were unrealistically wide. Specifically, the pipe width assignment placed too much emphasis on smaller fracture traces, which resulted in narrow pipes on very large (Structure 19) structures.

- Noisy injection time-series data ($^{131}I^-$) was used, resulting in an over-injection of mass at late time steps.

- The assumption of fracture complexity, when combined with our implementation of retention through multiple immobile zones, provided too much surface area for retention, resulting in far too much retention for strongly sorbing tracers. Specifically, multiplying the fracture perimeter by two to three times in each immobile zone was too extreme. A better method would have been to partition the perimeter increase evenly across all the immobile zones involved with that fracture. For example, for a Complexity 3 structure, ¼ of the perimeter increase would be taken up in the gouge zone, ¼ in the fracture coating immobile zone, ¼ in the alteration zone, and ¼ in the unaltered host rock.

These issues are addressed in the reconciliation studies described in Chapter 7.

7 Reconciliation Modeling of BS2B Experimental Results

This chapter presents an additional step of evaluation of the JNC / Golder DFN/ Channel-Network model, described in Chapters 2 through 5, for evaluaton of the project hypotheses (Ia and Ib) derived in an attempt to explain the observed BS2B experimental results. This analysis was carried out as a series of sensitivity studies, and completed after the conclusion and publication of the BS2B experimental results

Reconciliation modeling was designed to test the BS2B projects two key hypotheses:

- Hypothesis Ia) Microstructural (i.e. detailed geological, mineralogical and geochemical) information can provide significant support for predicting transport of sorbing solutes at experimental time scales,

- Hypothesis Ib) Transport at experimental time scales is significantly different for faults (significant alteration, brecciation and fault gouge) and joints (with or without alteration), due to the indicated differences in microstructure and properties

Hypothesis Ia is addressed primarily by evaluation of how good the TRUE-BSC BS2B predictive modeling carried out based on the microstructural (i.e. immobile zone) properties from site characterization were. The "Step 1" models (Chapter 7.2) of the performed reconciliation addresses Hypothesis Ia. The "Step 1" study below extends this hypothesis to also consider the value of the hydrostructural model (i.e. fracture geometry and geology).

Hypothesis Ib is addressed by comparing the tracer breakthrough for the two pathways (Path I and II) tested in the BS2B experiment. This evaluation can be made based both on a comparison of the experimental results for the two pathways and on the basis of a comparison of the modeling for the two pathways. This evaluation is addressed in "Step 2" of the reconciliation, described in Chapter 7.3).

7.1 Methodology

The purpose of evaluation studies is to learn as much as possible from the comparison between predictive models and experimental sorbing tracer transport results; in the context of the project hypotheses above. To achieve this goal, the evaluation modeling has been divided into two steps:

Step 1 addresses implementation issues that do not affect the underlying microstructural model used for the predictive modeling. Changes within Step 1 show how the JNC/Golder predictive models would have matched the experimental results had these implementation improvements (tracer time series corrections, DFN model additions and subtractions) of the hydrostructural and microstructural models been implemented during the initial JNC/Golder blind prediction modeling. Step 1 thus addresses the Hypothesis Ia. Step 1 will determine whether the hydrostructural model and microstructural model developed from site characterization is sufficient for the purpose of predicting sorbing solute tracer transport

Step 2 addresses the differences between the Structure 19 pathway (Path I) and the Structure BG1 - 19 pathways (Path II). Step 2 seeks to better constrain the possible values of transmissivity and transport aperture for Structure 19 and Structure BG1, so as to remove some of the uncertainty from the transport modeling process. In addition, Phase 2 addresses the possible effect of alternative background fracture realizations on the BG1 pathway.

7.2 Evaluation Step 1: Hydrostructural and Microstructural Model

The comparison of the JNC/Golder BS2B blind prediction model to experimental results provides a mixed picture; the breakthroughs of some tracers were fairly well matched, while others were quite poorly matched. Predictive modeling was carried out under significant time pressure, and therefore did not consider all possible model improvements within the hydrostructural and microstructural models.

The Step 1 evaluation seeks to determine how well the current TRUE-BSC vision of the current hydrostructural/microstructural model can match in-situ observations from the BS2B experiment. The Step 1 modeling effort dealt with issues in the functional JNC/Golder implementation of the Task 6C hydraulic model that were noted during the blind prediction phase, and not with any specific conceptual issues. No significant changes were made to the microstructural model described in Chapters 2 and 4. Step 1 produced a new realization of the JNC/Golder CN-DFN model that addressed most of these issues.

Step 1 modeling addressed the following

- Improvements to DFN Implementation
- Improvements to Pipe Discretization
- Improvements to Hydraulic Model
- Improvements to Tracer Test Boundary Conditions

Step 1 modeling resulted in a new baseline implementation of the JNC/Golder channel-network model. The changes made to the JNC/Golder DFN model (described in Chapter 2) to produce the evaluation baseline DFN are described below in Chapters 7.2.1 and 7.2.2. This “Baseline DFN” was then used for new BS2B transport simulations completed for this evaluation, and compared against in situ measurements to test Hypothesis Ia. This is referred to below as the “Baseline Model.”

7.2.1 Improvements to DFN Implementation

Two improvements were made to the JNC/Golder CN-implementation of the Task 6C DFN used in the blind-prediction modeling effort. The first improvement involves the large sub-horizontal Structures 15, 16, 17, and 18, that were hypothesized in past models to cut across the TRUE Block, and the vertical structures 8 and 11 /Hermanson and Doe, 2002/. The aformentioned structures were not contained in the TRUE Block site model presented in Task 6C /Dershowitz et. al., 2003/. These structures were included in the JNC/Golder BS2B prediction model; the features were assigned a transmissivity of 10^{-10} m^2/s to account for the absence of hydrologic evidence for their existence. While this was considered reasonable at the time, examination of the pathways from the Structure BG1 injection (Path II) in the blind prediction model indicated that the sub-horizontal structures played a significant role in solute transport pathways identified in the simulations. Therefore, these structures were removed from the Baseline DFN.

Figure 7-1 illustrates the new Baseline DFN. This image shows the structures inside the 200 m BS2 experimental volume, and omits the 500-m scale NW fracture set constructed outside the 200m scale test area which provide connectivity to the external boundaries. The 500-m scale structures are included, however, in the Baseline DFN. The main difference between the blind prediction DFN and the new Baseline DFN is that the large subhorizontal structures described above were removed; these features had been tentatively identified during the early stages of the TRUE Block Scale project, but have never been confirmed as being hydraulically important during hydraulic testing.

The second improvement to the JNC/Golder implementation of the Task 6C DFN was a change of the transmissivity and flow aperture of the background fracture Structure BG1. In the JNC/Golder BS2B blind prediction model, it was assumed that there was no knowledge of the transmissivity and aperture of Structure BG1, and therefore the CPT-4C tracer test was used to derive these values. Since the goal of this reconciliation is to honestly implement the hydrostructural and microstructural models, it was decided to instead utilize the Task 6C aperture and transmissivity correlations of Dershowitz et al. /2003/ to assign transmissivity and aperture to the BG1 fracture. Based on the assumed equivalent radius of 15 m (corresponding to a fracture length of 26.6 m), Structure BG1 was assigned a transmissivity of 3.36×10^{-8} m^2/s and a hydraulic aperture of 9.17×10^{-5} m. The size and position of Structure BG1 were constant; we did not test other potential location or size models for this fracture.

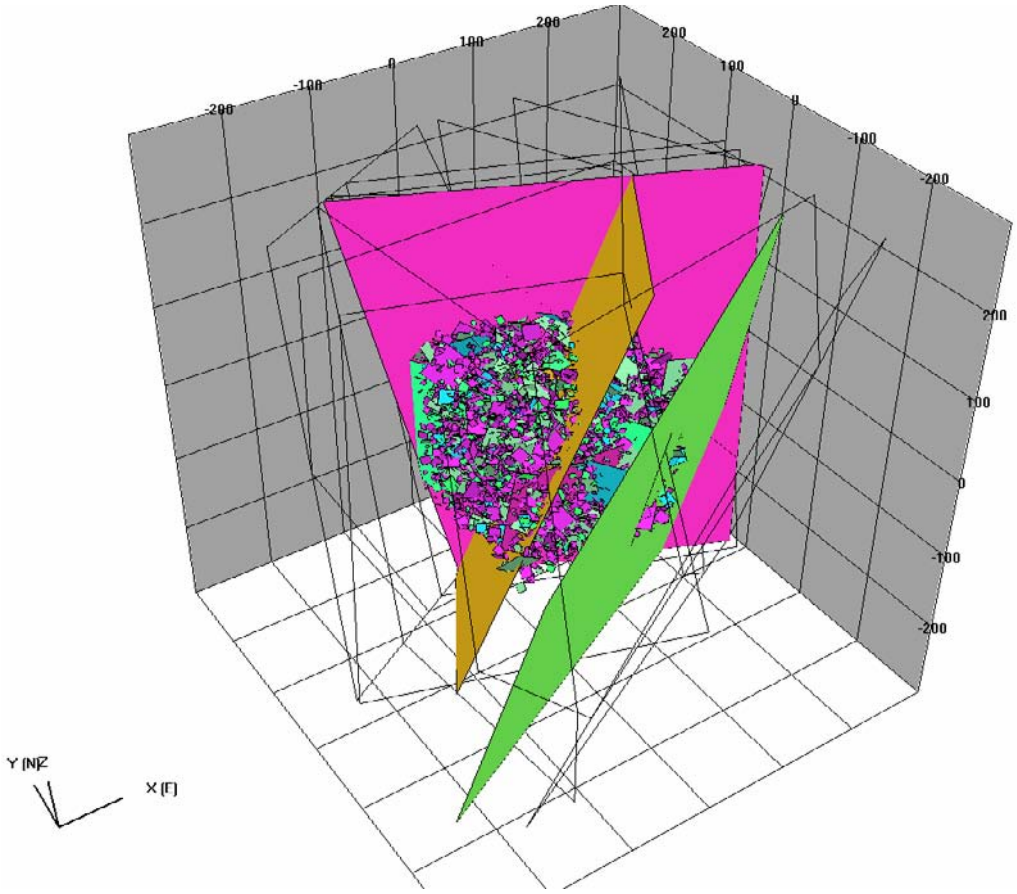

Figure 7-1: *New baseline DFN Model. View is to the northeast, looking towards the Äspö HRL tunnel. The transparent wire frame fractures represent the structures which provide connection to the hydraulic boundaries for the 500 m model. The 500 m scale lognormal fracture set (see Figure 2-5) has been omitted from the visualization, but is still present in the model.*

7.2.2 Improvement to Pipe Network Discretization

As described in Chapter 4, the BS2B blind prediction channel-network model was carried out using a discretization of the DFN into a network of rectangular cross-section pipes using PAWorks/Genpipe. This discretization involves several assumptions which affect the geometry and connectivity of the pipes, and therefore potentially affect solute transport modeling.

Details of the discretization algorithm can be found in Dershowitz et al. /2000/. Discretization of the initial BS2B blind prediction CN model made the following assumptions.

- All pipes are defined between the midpoints of the fracture traces defined by fracture intersections.
- Pipes are defined for every pair of fracture traces, for every fracture in the model, except where such traces would be (a) off the fracture planes, (b) would cross a fracture trace, or (c) would cross another pipe.

- Pipe ‘width’ is calculated based on the weighted average of the two traces at the end of the pipes, with a higher weighting applied to the shorter trace. This generally resulted in narrower pipes, which correspondingly reduces the area available for retention.

Examination of the pipes used in the BS2B prediction indicated the following potential pipe discretization issues:

- The total pipe area was significantly less than the fracture area, due to the use of shorter traces to define pipe width.

- The transport pathways were long and tortuous, due to the lack of direct connection between traces.

Based on this evaluation, three changes were made to the pipe discretization parameters used to create the new Baseline channel-network model:

- Pipe width was calculated from the arithmetic average of the trace length of the two traces at the ends of the pipe, without weighting.

- Additional pipes were added such that the path length between any pair of traces (on a fracture plane) was never greater than twice the Cartesian distance between the traces.

- All pipe widths were then adjusted such that the total area of pipes was equal to 80% of the fracture area for every fracture in the model. This value of 80% was estimated from the percentage of fracture traces which appear “open” on borehole TV images. A smaller number was considered based on preliminary results of the TRUE-1 Continuation epoxy resin injection experiments /Hakami and Wang, in prep/, but it was considered that this would reduce retention significantly below what was observed in the BS2B experiments.

The Baseline pipe network geometry is illustrated in Figure 7-2 and Figure 7-3. In these figures, the width of the channel network ‘pipes’ is set to 0.1 m for visualization purposes; the size on the screen is not the actual width used in transport modeling.

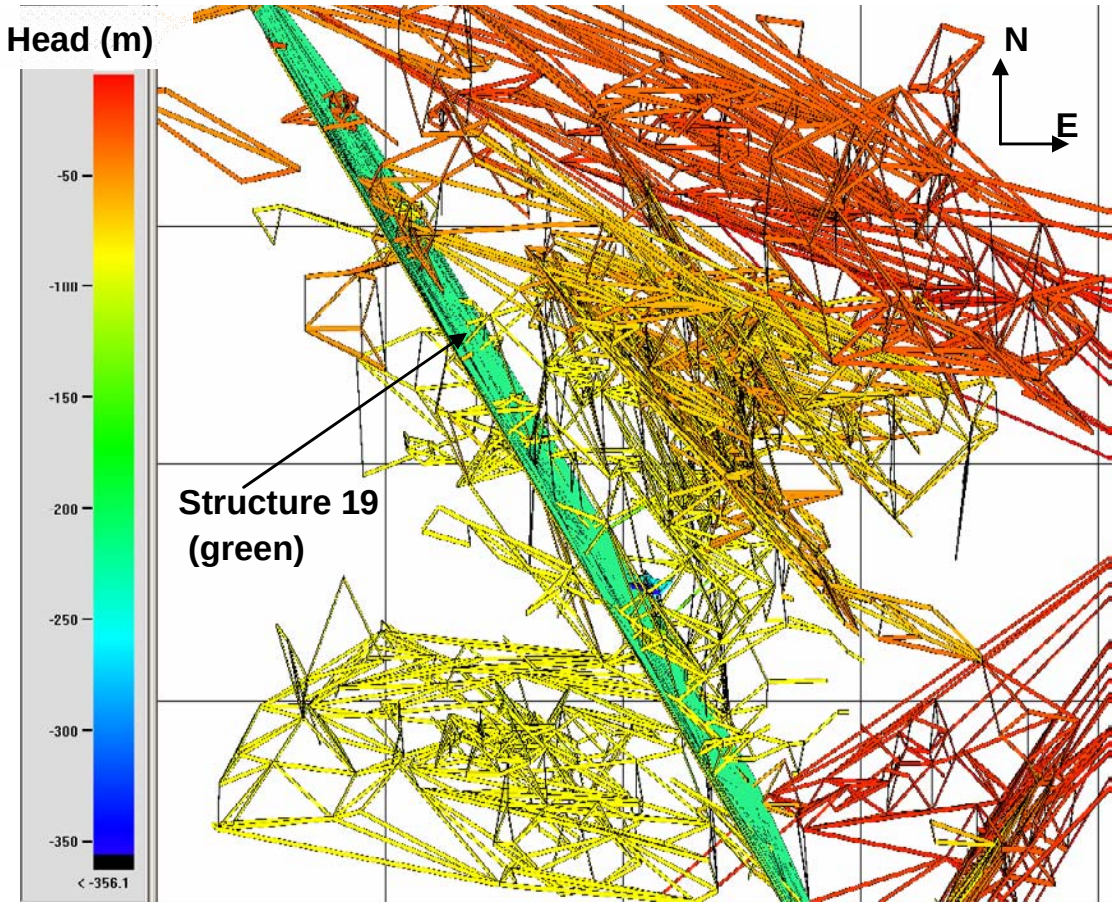

Figure 7-2: *New baseline channel network model. View is looking vertically down the Z-axis. Pipes are colored by the head value (metres above mean sea level (masl)) at the starting node of the pipe.*

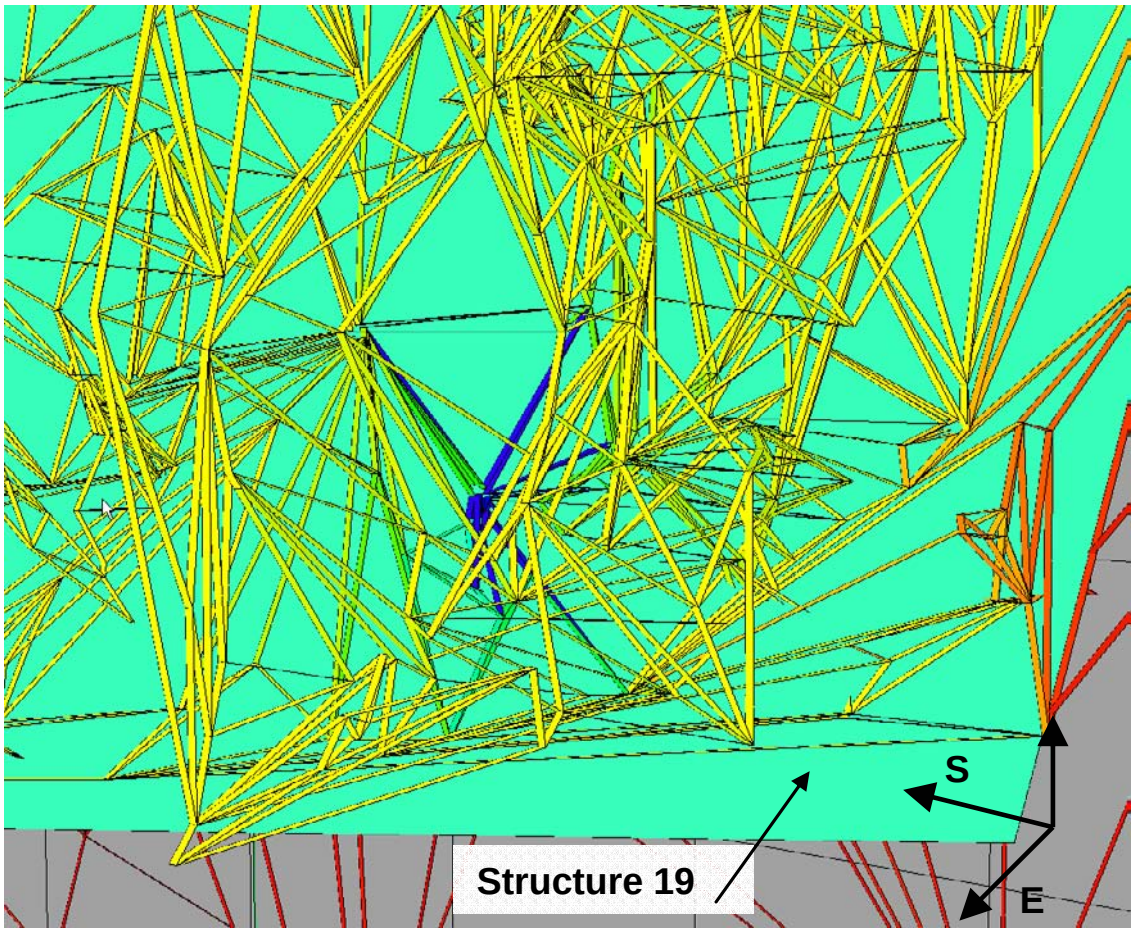

Figure 7-3: *New baseline channel network model. View is looking southwest at Structure #19 (green). The blue pipes represent areas of large drawdowns connected directly to the sink in KI0025F03. The values are colored according to the same head scale as Figure 7-2.*

7.2.3 Improvements to the Hydraulic Model

The JNC/Golder BS2B blind prediction model did not include the effect of the hydraulic skin that is known to occur at borehole-fracture intersections. For the new baseline model (Step 1), hydraulic skin effects were applied to approximate the drawdown observed in the BS2B experiments. The Baseline model included the following two changes from the reference hydrostructural model used for predictive simulations:

1. The average transmissivity of Structure 19 was increased to 6.15 x 10^{-7} m^2/s; a value of 1.02 x 10^{-7} m^2/s was used in the BS2B blind prediction model. This value is still consistent with the semi-stochastic TRUE Block scale hydrostructural model presented in Task 6C, because it is within a standard deviation of the arithmetic mean value presented in Dershowitz et al. (2003).

2. A hydraulic skin of 0.21x was applied to borehole KI0025F03_R3 (the sink section). The transmissivity and flow aperture of the first layer of pipes (those that directly connected to the sink section) were reduced to 1.30 x 10^{-7} m^2/s and 1.47 x 10^{-6} m, respectively. This skin was designed to improve the match between the measured and simulated drawdowns.

Table 7-1 presents the simulated BS2B drawdowns for the new Baseline model. The KI0025F02_R2 drawdown could be matched if a high skin transmissivity of $1x10^{-6}$ m^2/s is applied. However, it was decided that such a skin on a background fracture would be inconsistent with the goals of the original hydrostructural model, and was therefore not applied.

Table 7-1: Observed BS2B drawdowns compared with simulated drawdowns, new Baseline CN model

Borehole	Structure Intersected	Observed Drawdown (m)	New Model Drawdown (m)
KI0025F02_R2	BG1	~246	231.4
KI0025F02_R3	19	~213	213.6
Note: Drawdown is relative to KI0025F03_R3 (pumped well) Observed drawdowns are extrapolated from well pressure observations, assuming steady-state flow conditions			

7.2.4 Improvements to Tracer Test Boundary Conditions

The JNC/Golder BS2B channel network models all use a time-varying activity flux (Bq/yr) boundary condition. This boundary condition is calculated from the time-varying concentration (Bq/kg) boundary conditions as given by an internal project memorandum. The use of time-varying activity flux boundary condition with the LTG transport model makes it easier to keep track of the actual activities released to the model. The conversion is accomplished by assuming a constant injection flow rate at the source borehole, and assuming that the tracer solution can be approximated by normal water at standard temperature and pressure (1 kg of tracer solution occupies approximately 0.001 m^3). For the JNC/Golder blind prediction model, the sampled tracer injection data were used directly to calculate the time-varying activity boundary condition used for LTG simulations.

A re-evaluation of the sampling-derived tracer injection curves used in the JNC/Golder blind prediction of the BS2B experiment was carried out as part of the experiment evaluation. This re-evaluation suggests that the tracer injection history used for the BS2B prediction did not adequately characterize the early-time history of the conservative tracers. In particular, it has been suggested that modeling teams utilize the online measurements in lieu of the sampled results for the fast flow pathways (Structure 19 – Path I) due to tracer dilution issues /Andersson et al., 2005/. In addition, data artifacts in the injection curve for $^{131}I^-$ resulted in corresponding errors in the breakthrough curve for that tracer (see Figure 6-3). Therefore, the BS2B tracer injection profiles used for predictive modeling were updated for the new Baseline transport model. In the updated tracer injection profiles, the early-time boundary conditions were still based on the online data, while at later times a combination of online and sampled concentrations were used.

The result was a series of new tracer injection profiles. These “Composite” injection curves were developed by combining the sampled and the online injection data for the BS2B experiment. The curves are presented in Figure 7-4 and Figure 7-5. The curves were developed as follows.

Borehole KI0025F02_R3 (Structure #19 Pathway):

- $^{131}I^-$: Used online measurements from 0 – 6 hours, sampling results to 103 hours, online measurements to 1000 hours. Note that the artifact in the Iodine injection curve, while reduced, is still visible in the Composite injection curve.
- ^{160}Tb-DTPA: Online measurements to 7.5 hours, sampling results to 1317 hours, extrapolated to 2000 hours.
- $85Sr^{2+}$: Online measurements to 7.5 hours, sampling results to 1317 hours, extrapolated to 2000 hours
- $^{86}Rb^+$: Online measurements to 6 hours, sampling results to 1317 hours, extrapolated to 2000 hours
- $^{137}Cs^+$: Online measurements to 6.5 hours, sampling results to 1224 hours (last sample thrown out as anomalously high), extrapolated to 2000 hours.

Borehole KI0025F02_R2 (BG1 Pathway):

- HTO: Used online measurements from 0 – 6 hours, sampling results to 103 hours, online measurements to 1000 hours.
- ^{155}Eu-DTPA: Online measurements to 7.5 hours, sampling results to 1317 hours, extrapolated to 2000 hours.
- $^{22}Na^+$: Online measurements to 7.5 hours, sampling results to 1317 hours, extrapolated to 2000 hours
- $^{133}Ba^{2+}$: Online measurements to 6 hours, sampling results to 1317 hours, extrapolated to 2000 hours
- $^{54}Mn^{2+}$: Online measurements to 6.5 hours, sampling results to 1224 hours (last sample thrown out as anomalously high), extrapolated to 2000 hours.

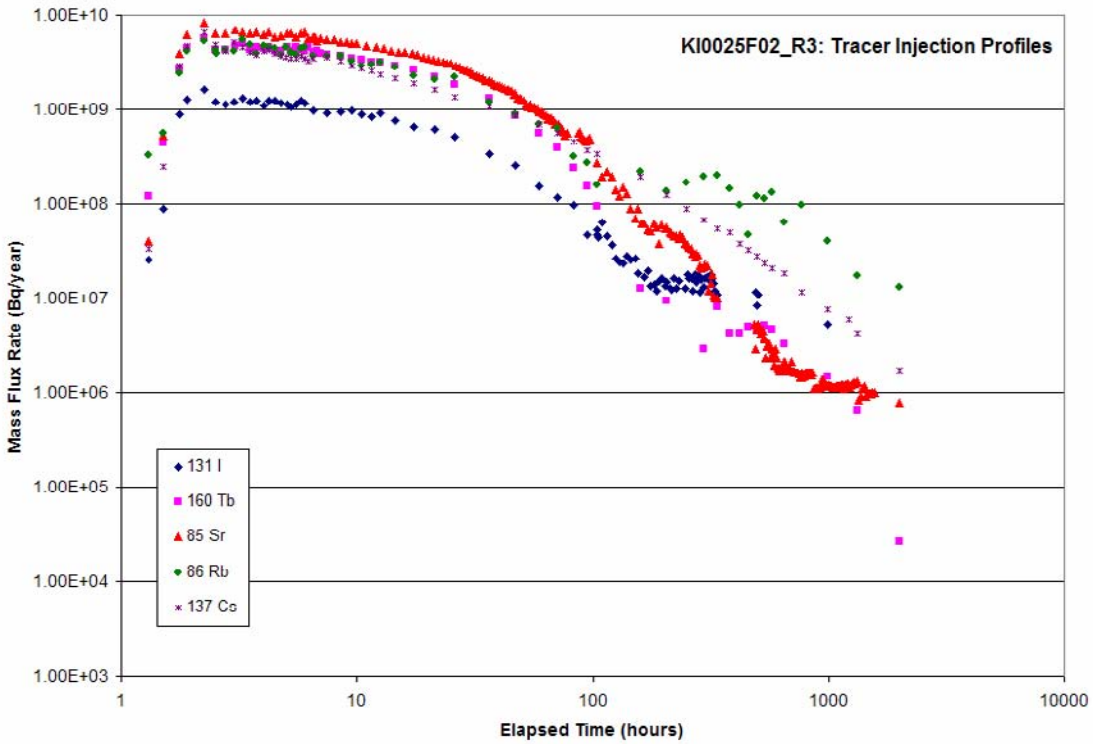

Figure 7-4: *Composite injection profile for new Baseline CN model, KI0025F02_R3 (Structure 19 - Path I)*

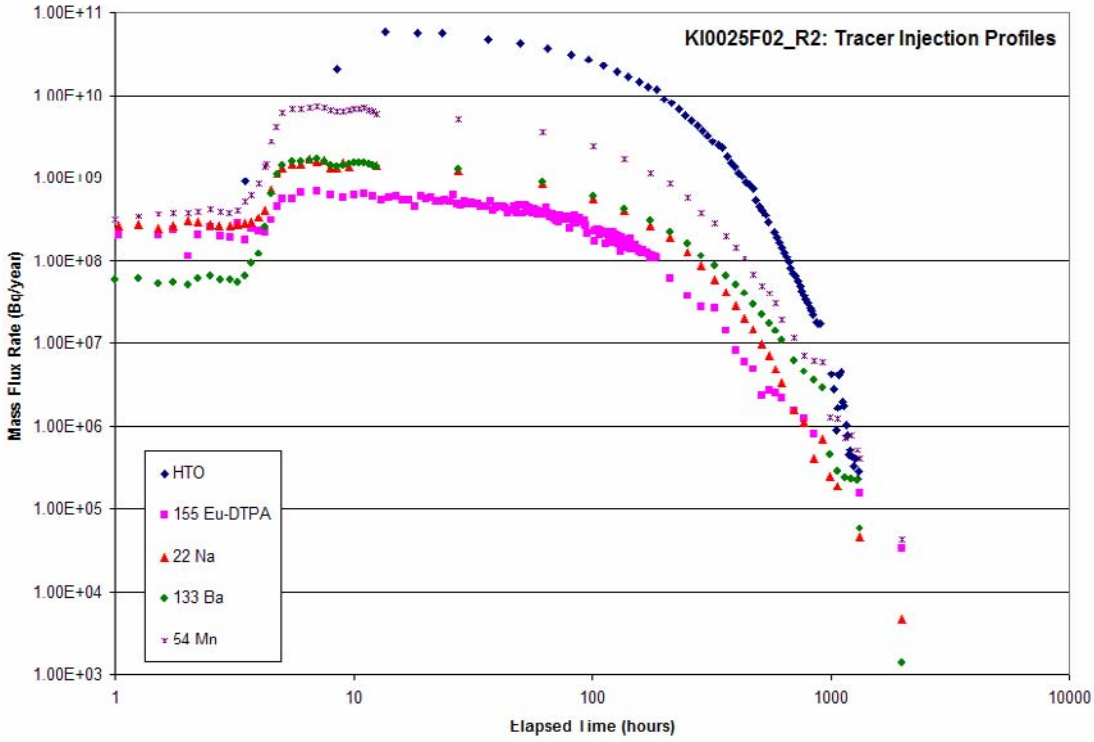

Figure 7-5: *Composite injection profile for new Baseline CN model, KI0025F02_R2 (Structure BG1 > Structure 19 -Path II).*

7.2.5 Evaluation Step 1 Baseline Transport Simulations

The Step 1 Baseline transport simulations were used to establish a new CN model, incorporating the geometric and hydraulic changes described above. The Baseline model assumed the full microstructural model for both Type I and Type II structures, as described in Chapters 2 and 4 and presented in the Task 6C modeling report /Dershowitz et al., 2003/. However, fracture complexity (increase of pipe perimeter available for retention) was **not** implemented in the new Step 1 baseline model. Every fracture in the model was assumed to have a Complexity of 1; no pipe perimeters were adjusted. This change was made because of a lack of evidence that the extra tracer retention was required for the JNC/Golder immobile zone implementation (i.e. the parallel immobile zones were already over-predicting retention).

Breakthrough curves from the Step 1 baseline transport simulations are presented in Figure 7-6 and Figure 7-7. Figure 7-6 provides the normalized breakthrough curves for the injection into Structure 19 (Path I) in KI0025F02_R3. Figure 7-7 provides the normalized breakthrough curves for the injection into Structure BG1 (Path II) in KI0025F02_R2. Table 7-2 presents the breakthrough time statistics from the Step 1 baseline transport simulation.

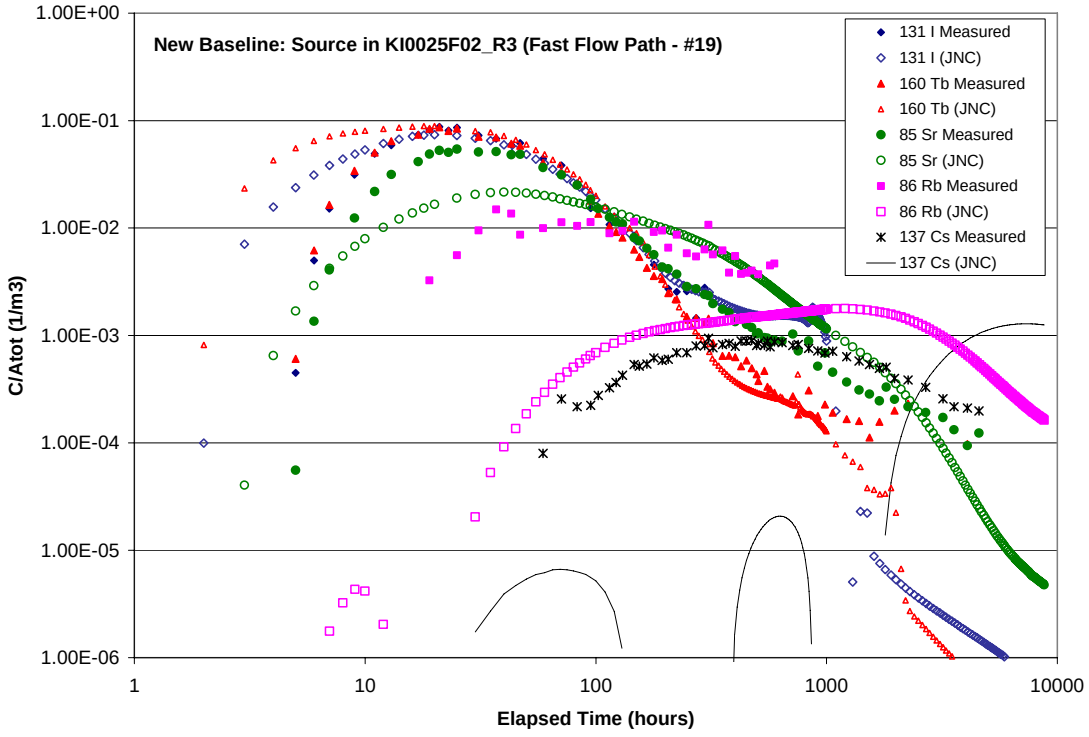

Figure 7-6: *Step 1 baseline CN transport model tracer breakthrough curves for the Structure 19 pathways (Path I).*

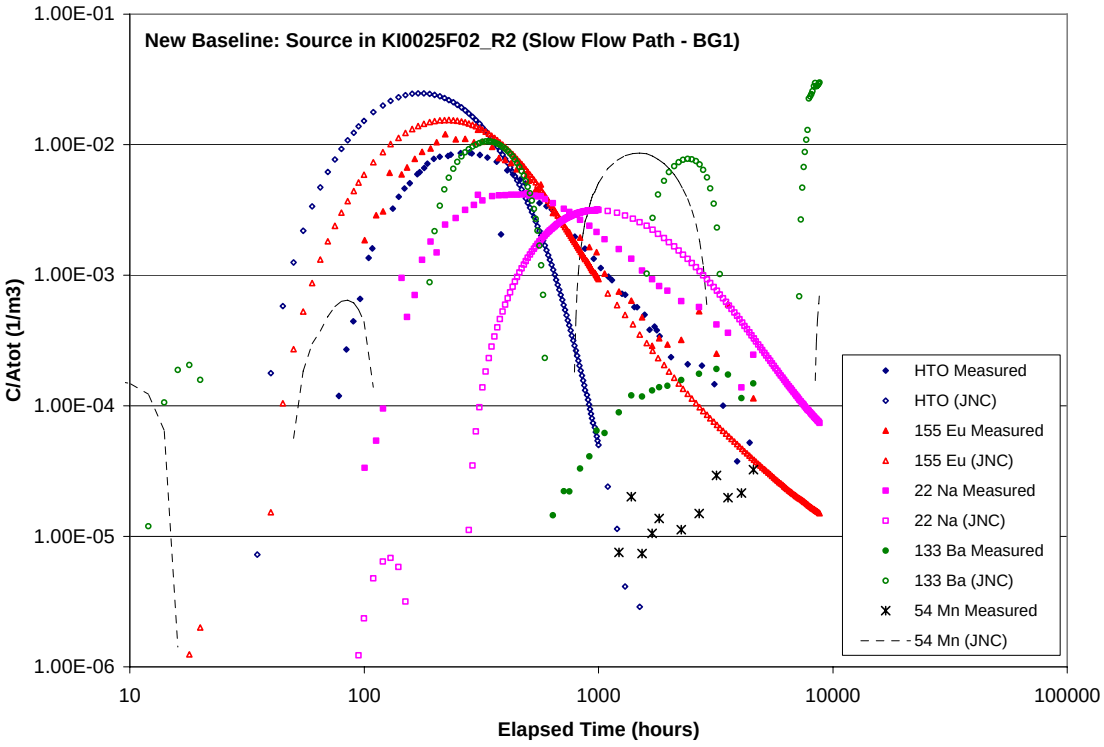

Figure 7-7: *Step 1 baseline CN transport model tracer breakthrough curves for the Structure BG1 > background fractures > Structure 19 pathways (Path II).*

Table 7-2: Breakthrough time statistics for the Step 1 baseline CN transport model

Tracer Breakthrough Times for Flow Path II (BG1 - 19)

BS2B Experimental Results					JNC/Golder New Step 1 Baseline CN Model				
	t5 hours	*t50 hours*	*t95 hours*	*% Recovery*		*t5 hours*	*t50 hours*	*t95 hours*	*% Recovery*
HTO	183	790	n/r	68%	HTO	97	235	520	100%
155Eu	155	500	n/r	92%	155Eu	126	343	1797	100%
22Na	300	1490	n/r	72%	22Na	615	1750	1797	100%
133Ba	3250	n/r	n/r	8%	133Ba	n/r	n/r	n/r	5.25%
54Mn	n/r	n/r	n/r	1%	54Mn	n/r	n/r	n/r	< 1%

Total Time	hrs
HTO	4409
AllOthers	4577

	Good Match to Measured Data
	O.K. Match to Measured Data
	Poor Match to Measured Data

Tracer Breakthrough Times for Flow Path I (19)

BS2B Experimental Results					JNC/Golder New Step 1 Baseline CN Model				
	t5 hours	*t50 hours*	*t95 hours*	*% Recovery*		*t5 hours*	*t50 hours*	*t95 hours*	*% Recovery*
131I-	14	62	n/r	80%	131I-	12	64	855	100%
160Tb	14	63	4075	87%	160Tb	8.5	48	329	100%
85Sr	19	107	4327	86%	85Sr	29	255	1402	100%
86Rb	51	490	n/r	56%	86Rb	369	2250	n/r	92%
137Cs	555	n/r	n/r	28%	137Cs	n/r			<1%

A comparison of the breakthrough time statistics for the Step 1 baseline CN transport model against the observed experiment measurements does not show a noticeable improvement in the match. However, late-time tracer recovery for the Baseline reconciliation model is drastically improved when compared to the original JNC/Golder blind prediction model. It is expected that this is probably due to the use of a complexity factor of 1 for the Baseline transport simulations, which reduced overall retention.

7.3 Step 2: Evaluation of the Hydrostructural and Transport Models

One of the key goals of the Step 2 evaluation simulations was to evaluate the usefulness of the new Baseline hydrostructural model, as implemented in Step 1 (Chapter 7.2). Consequently, changes made to better match the BS2B tracer experiments were only made within the context of this hydrostructural model. No changes were made to the microstructural model or immobile zone parameters.

Five evaluation modeling studies were completed as components of Step 2:

- Evaluation of pathways within Structure 19 (Path I);
- Evaluation of pathways between Structure BG1, Structure 19, and the background fracture network (Path II);
- Monte Carlo simulation of variation within the semi-stochastic background fracture network (Structure BG1 is not changed);
- Evaluation of the effects of the reduction of the flow-wetted surface area inside the channel network to 5-10% of the calculated fracture surface area;
- Evaluation of the difference between Structure 19 (Path I) and Structure BG1 (Path II) pathways using the results of the BS2B experiment.

7.3.1 Step 2: Evaluation of Structure 19 Pathways (Path I)

An examination of the breakthrough curves in Figure 7-6 indicates that the Baseline CN model has too high an advective velocity and too much longitudinal dispersion. Additional simulations using the Baseline CN model were therefore carried out, using a range of larger transport aperture values and lower longitudinal dispersion values. The following CN model changes were found to produce a better match to experimental breakthrough curves for $^{131}I^-$, ^{155}Eu-DTPA, and $^{85}Sr^{2+}$ for flow paths within Structure 19 (Path I); $^{86}Rb^+$ and $^{137}Cs^+$ were relatively unaffected and still exhibit poor matches:

- Hydraulic aperture of Structure 19 increased by a factor of two (3.61×10^{-4} m);
- Longitudinal dispersion length reduced from 10 m to 2 m;
- No changes to the microstructural model and the immobile zones described in Chapter 4. However, fracture complexity was not enabled in Step 2 simulations; all fractures were assigned a Complexity of 1.

The change in hydraulic aperture (3.61×10^{-4} m) is still consistent with values presented in the Task 6C semi-stochastic hydrostructural model being within the standard deviation range for the Task 6C correlation of transmissivity with aperture. The decrease in longitudinal transmissivity is closer to the generally accepted longitudinal dispersion value of 10% of the average Cartesian pathway length (2 m = 10% of 20 m).

Breakthrough curves for the Step 2 simulations that tested the above-mentioned transport model changes are presented as Figure 7-8 through Figure 7-12. Breakthrough curves for $^{131}I^-$, ^{155}Eu-DTPA, $^{85}Sr^{2+}$, and $^{86}Rb^+$ show significant improvement, indicating that the hydrostructural and microstructural models are consistent with the observed breakthrough, and supporting Hypothesis Ia. The simulated breakthrough curve for $^{137}Cs^-$ still shows too much retention. An improved match for $^{137}Cs^-$ would require changes to the sorption coefficient K_d, or a decrease in the volume of available immobile zones. Since the other tracers are providing a good match, it is somewhat more likely that the problem for $^{137}Cs^-$ is related to either non-equilibrium sorption behavior, or incorrect sorption coefficients for $^{137}Cs^-$. Breakthrough time statistics for all tracers in the Step 2 Path I evaluation simulations are presented in Table 7-3.

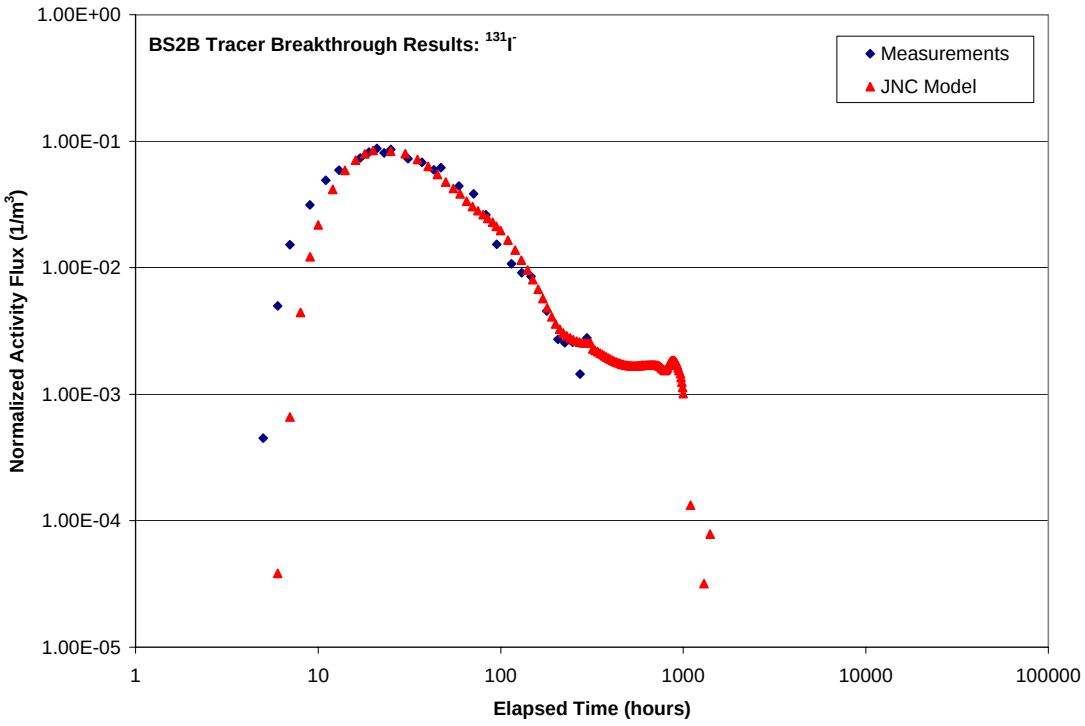

Figure 7-8: *Step 2 CN Model, Structure 19 Pathways (Path I), $^{131}I^-$, tracer injection in KI0025F02_R3.*

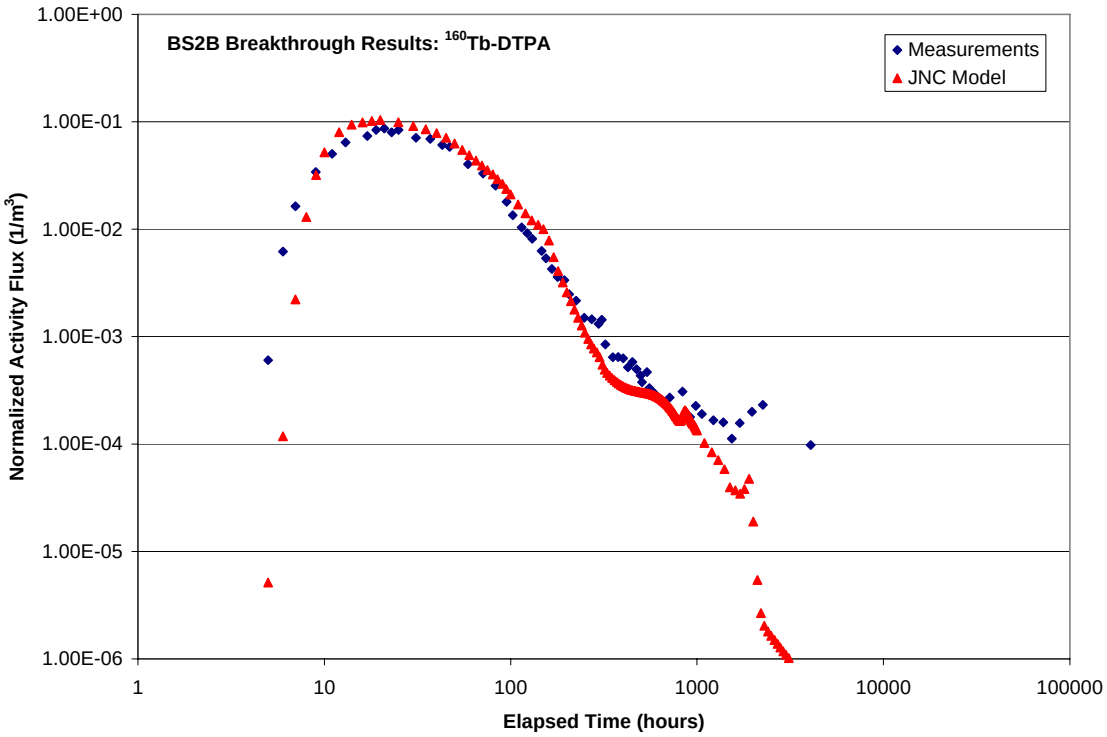

Figure 7-9: *Step 2 CN Model, Structure 19 Pathways (Path I), ^{155}Eu-DTPA, tracer injection in KI0025F02_R3.*

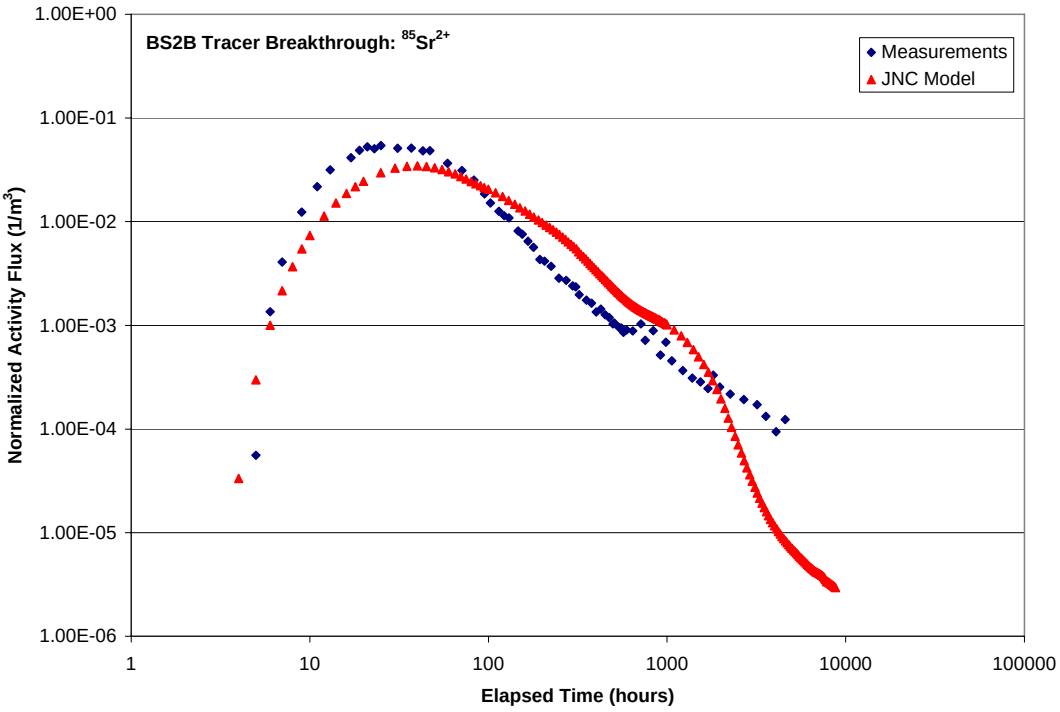

Figure 7-10: *Step 2 CN Model, Structure 19 Pathways (Path I), $^{85}Sr^{2+}$, tracer injection in KI0025F02_R3.*

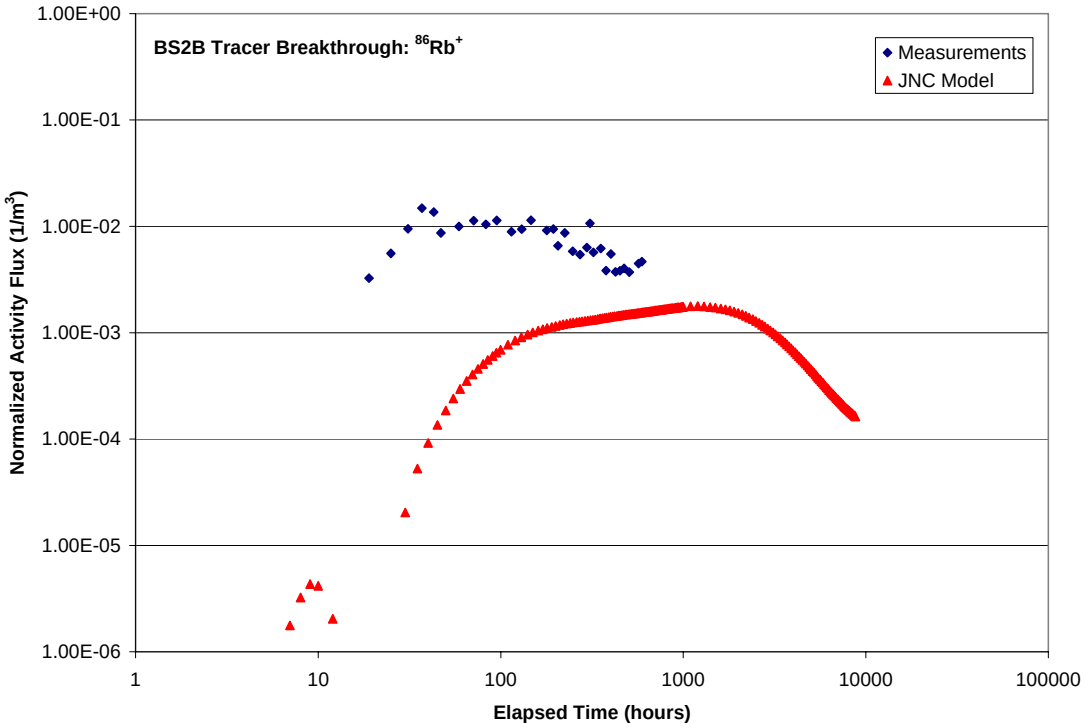

Figure 7-11: *Step 2 CN Model, Structure 19 Pathways (Path I), $^{86}Rb^{+}$, tracer injection in KI0025F02_R3.*

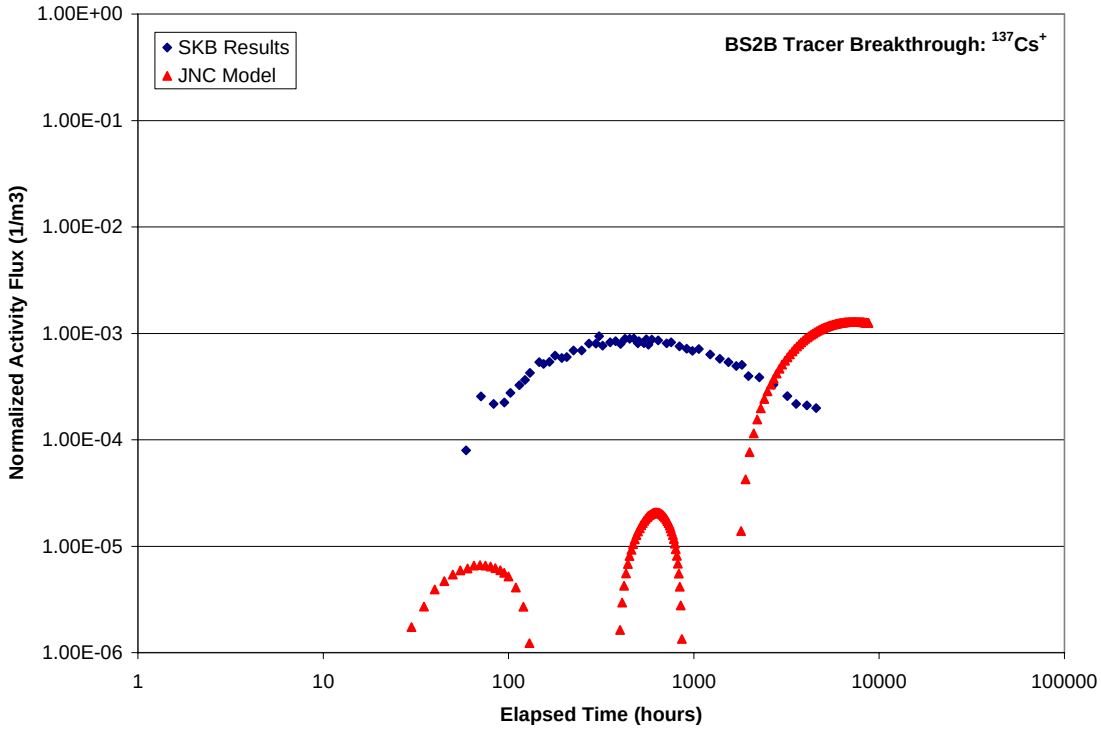

Figure 7-12: *Step 2 CN Model, Structure 19 Pathways (Path I) for $^{137}Cs^{-}$. Tracer injection in KI0025F02_R3.*

Table 7-3: Breakthrough time statistics for the Step 2 CN transport model, Paths I and II (focused on Structure 19).

Tracer Breakthrough Times for Flow Path II (BG1 - 19)

BS2B Experimental Results					Step 2 Structure 19 Modeling				
	t5 hours	*t50 hours*	*t95 hours*	*% Recovery*		*t5 hours*	*t50 hours*	*t95 hours*	*% Recovery*
HTO	183	790	n/r	68%	HTO	96	233	526	100%
155Eu	155	500	n/r	92%	155Eu	127	347	1850	100%
22Na	300	1490	n/r	72%	22Na	619	1760	5850	100%
133Ba	3250	n/r	n/r	8%	133Ba	n/r	n/r	n/r	5.25%
54Mn		n/r	n/r	1%	54Mn	n/r	n/r	n/r	< 1%

Total Time	hrs	
HTO	4409	
AllOthers	4577	

	Good Match to Measured Data
	O.K. Match to Measured Data
	Poor Match to Measured Data

Tracer Breakthrough Times for Flow Path I (19)

BS2B Experimental Results					Step 2 Structure 19 Modeling				
	t5 hours	*t50 hours*	*t95 hours*	*% Recovery*		*t5 hours*	*t50 hours*	*t95 hours*	*% Recovery*
131I-	14	62	n/r	80%	131I-	16.5	66	850	100%
160Tb	14	63	4075	87%	160Tb	13.7	52.5	n/r	93%
85Sr	19	107	4327	86%	85Sr	26	155	1450	100%
86Rb	51	490	n/r	56%	86Rb	305	1560	5970	100%
137Cs	555	n/r	n/r	28%	137Cs	n/r	n/r	n/r	<1%

7.3.2 Step 2: Evaluation of Structure BG1 Pathways (Path II)

Step 2 evaluation breakthrough curves for the Structure BG1 pathway are provided in Figure 7-13 through Figure 7-17. These simulations are based on the same changes to the Baseline model given in Section 7.3.1. Breakthrough curves for the strongly sorbing tracers are not continuous due to several issues revolving around the LTG solver and the JNC/Golder implementation of the microstructural model. Specifically, the microstructural model predicts too much diffusion and sorption, which results in a great deal of numerical instability in the early- to mid-time histories simulated by LTG. Breakthrough statistics are presented in Table 7-3. For strongly sorbing tracers, the breakthrough statistics for the BG1 pathways were approximated from the discontinuous breakthrough curves obtained by PAWorks/LTG.

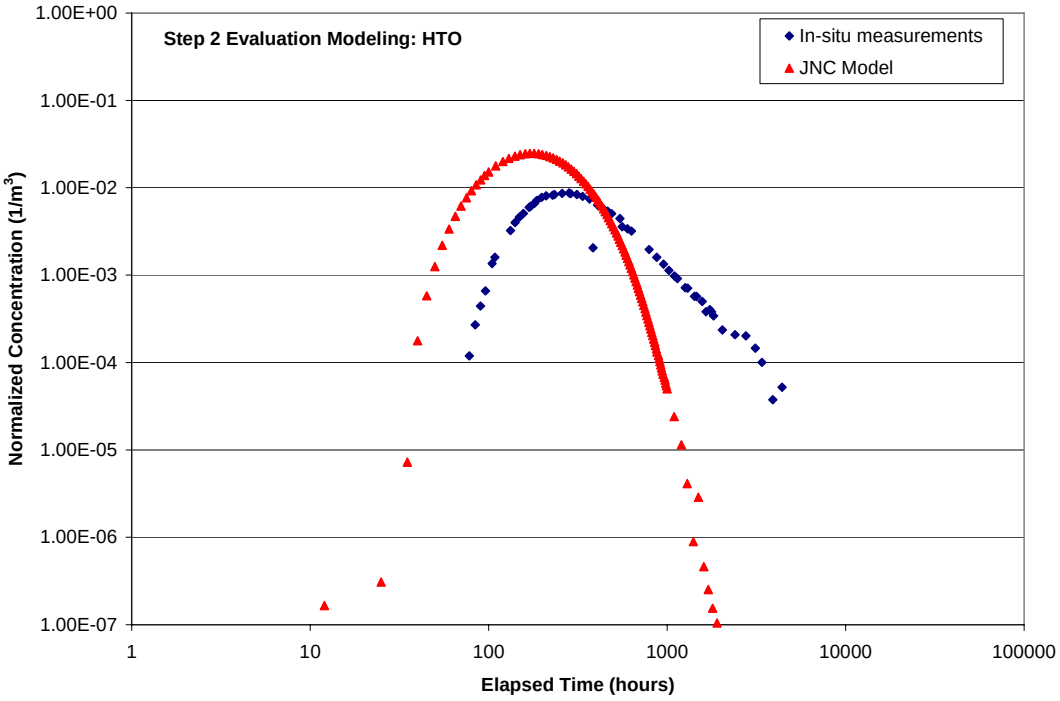

Figure 7-13: *Step 2 evaluation breakthrough curves for Structure BG1 injection (Path II), HTO, injection in KI0025F02_R2.*

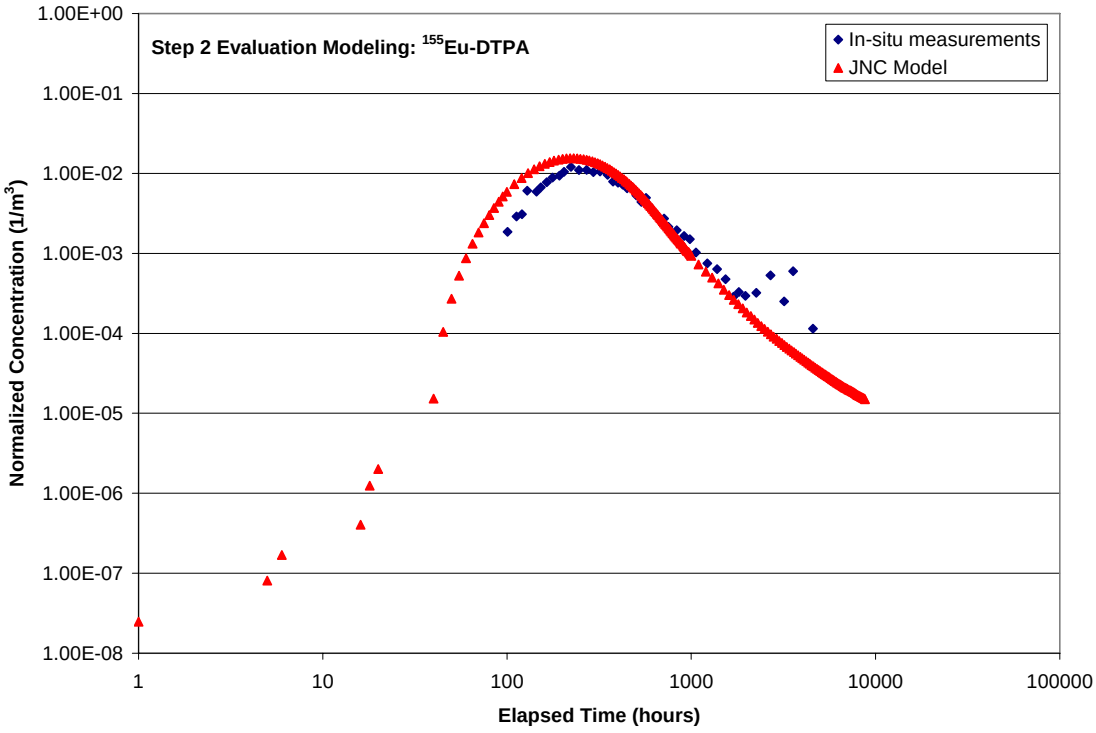

Figure 7-14: *Step 2 evaluation breakthrough curves for Structure BG1 injection (Path II), ^{155}Eu-DTPA, injection in KI0025F02_R2.*

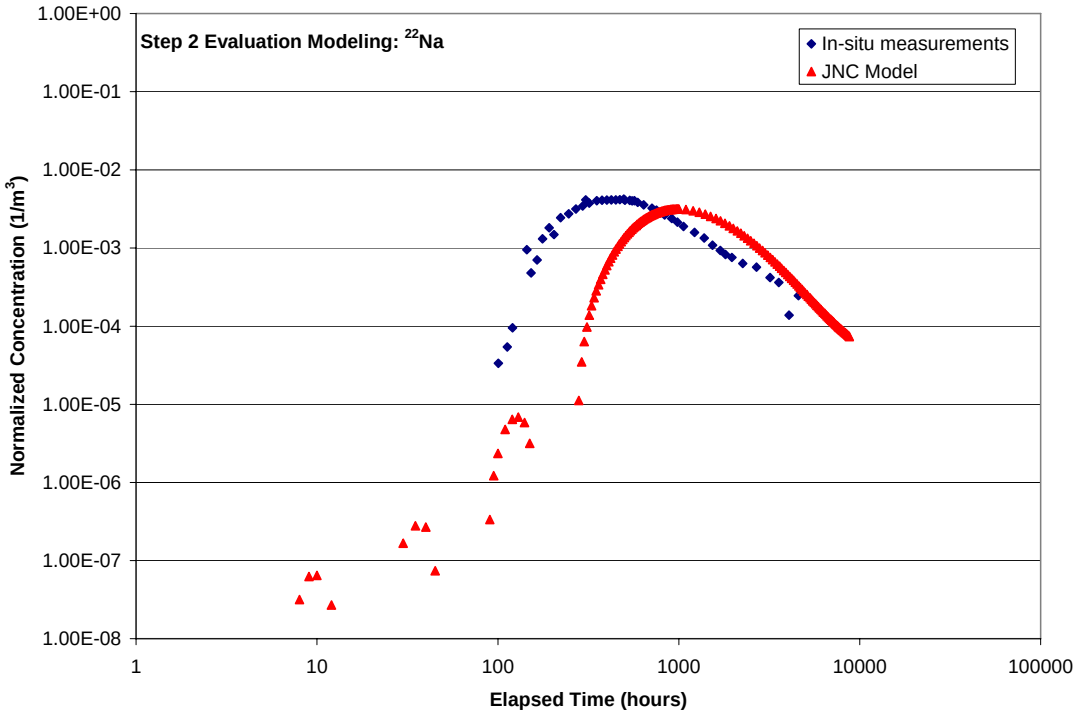

Figure 7-15: *Step 2 evaluation breakthrough curves for Structure BG1 injection (Path II), $^{22}Na^{+}$, injection in KI0025F02_R2.*

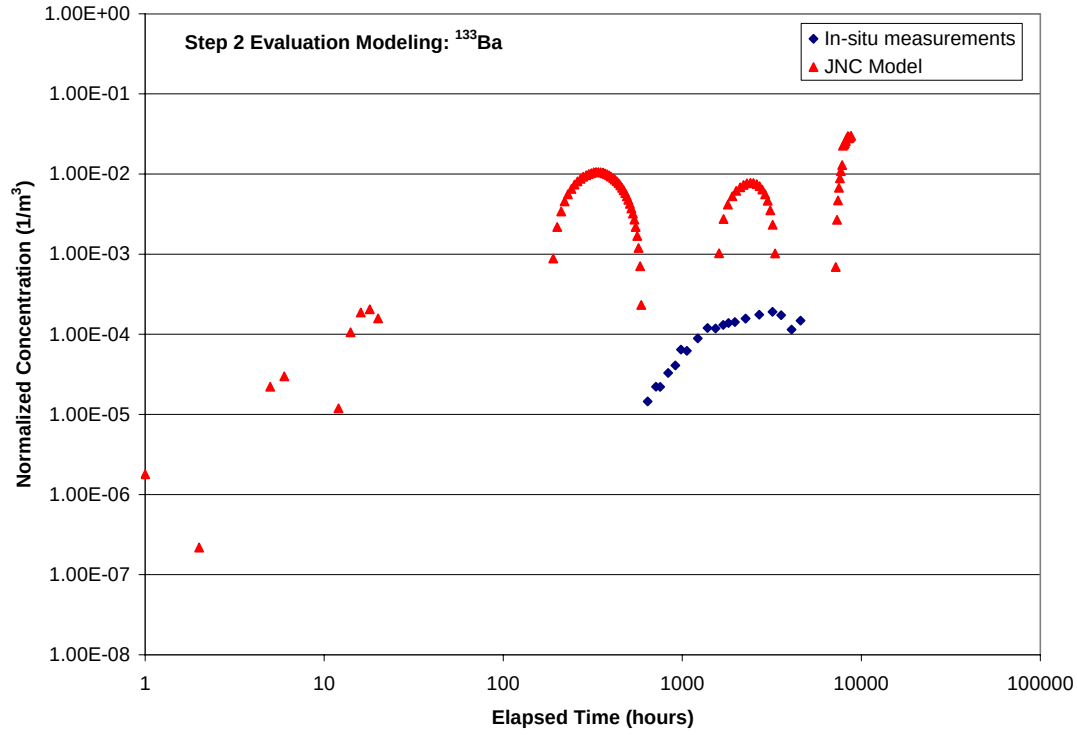

Figure 7-16: *Step 2 evaluation breakthrough curves for Structure BG1 injection (Path II), 133Ba2+, injection in KI0025F02_R2. Note that, for this breakthrough curve, the JNC model data was normalized to released mass (recorded by LTG), and not to actual injected mass. The 'released' mass was less than 1000 Bq.*

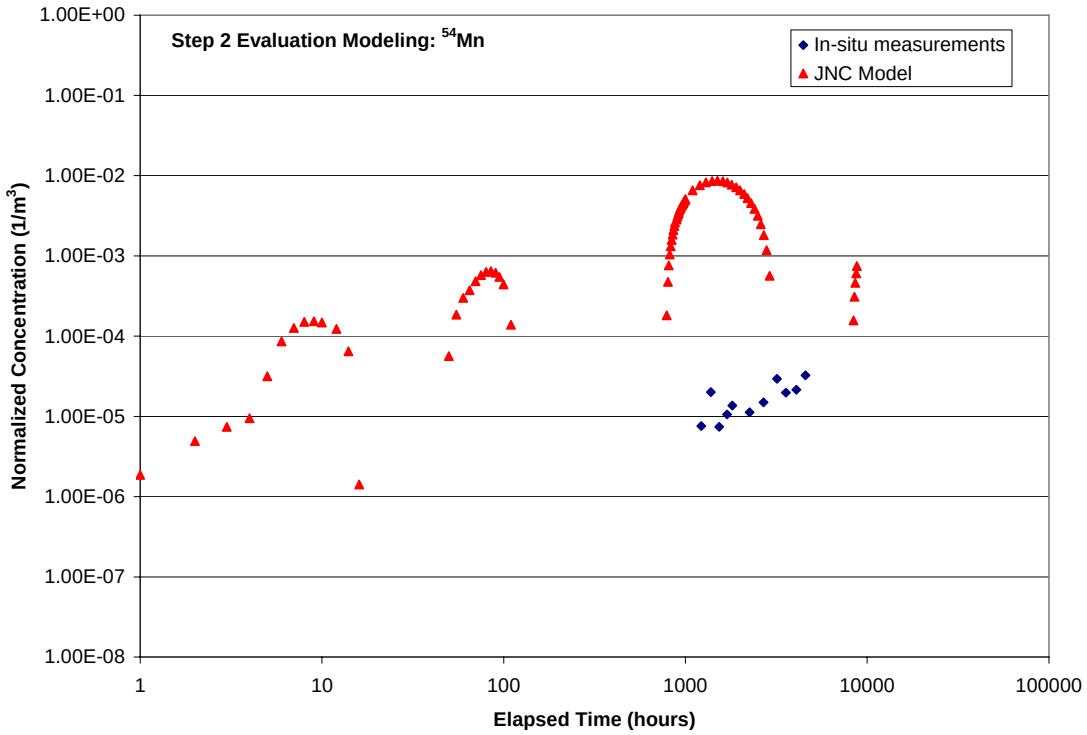

Figure 7-17: *Step 2 evaluation breakthrough curves for Structure BG1 injection (Path II), $^{54}Mn^{2+}$, injection in KI0025F02_R2. Note that, for this breakthrough curve, the JNC model data was normalized to released mass (recorded by LTG), and not to actual injected mass. The 'released' mass was less than 1000 Bq.*

The key observations from these reconciliation simulations are as follows:

1. The Step 2 evaluation simulation breakthrough curves for non-sorbing tracers HTO and ^{155}Eu-DTPA show a good match. However, the in-situ BS2B measurements suggest significantly more retention of HTO than the JNC/Golder model predicts. HTO may be acting as a weakly sorbing tracer within the tested path, rather than as a truly conservative tracer. The root cause of this behavior is unknown.

2. The breakthrough curve for HTO derived from in-situ BS2B experimental observations (Figure 7-13) shows an unusually long tail, which cannot be matched without assuming sorption or a higher diffusion rate (which is inconsistent with known HTO properties)

3. The Step 2 evaluation simulation breakthrough curves for sorbing and strongly sorbing tracers ^{22}Na, ^{133}Ba, and ^{54}Mn show significantly greater sorption than was observed in the experiments. This is seen in the inconsistent nature of the breakthrough curves above (the concentration values are normalized to what LTG actually released into the system, and NOT what was actually injected). This is most likely due to the JNC/Golder implementation of parallel immobile zones; this implementation results in too much available reactive surface area.

The results of the Step 1 and Step 2 evaluations suggest that additional work was necessary to explain the behavior of strongly sorbing tracers in the Structure BG1 > Background Fracture Network > Structure 19 system. Two studies were carried out to further investigate the discrepancy between the reconciliation simulations and the sorbing tracer breakthrough.

The first study addressed the effect that stochastic realizations of background fractures might have on the difference between measured and simulated tracer breakthrough. The second study considered the possibility that a smaller flow-wetted surface area (i.e., scaling the perimeter available for sorption) could resolve the discrepancy between measured and simulated tracer breakthrough. These studies are described in Sections 7.4 and 7.5, respectively.

7.4 Additional Background Fracture Realizations in Support of Hypothesis Ib

The fractures that connect Structure BG1 to Structure 19 were generated stochastically from the statistics of Dershowitz et al. (2003); all JNC/Golder simulations to this point utilized the same sample background fractures that were included as examples in the Task 6C report. Hydraulic interference data suggest a weak connection between the features; this is supported by the drawdown responses observed during the BS2B experiment (Andersson et al., 2005). Therefore, we addressed the issue of the influence of background fracture patterns on the transport pathways through the Monte-Carlo simulation of alternative background fracture realizations.

Statistics for the pathway geometry for Structure 19 and Structure BG1 reconciliation simulations are provided in Table 7-4. Figure 7-18 and Figure 7-19 illustrate the geometric patterns of these pathways. Key observations from Table 7-4 include the following:

1. In the background fracture realization used in both the blind prediction and the Step 1 / Step 2 evaluation simulations, the Structure BG1 transport pathways between KI0025F02_R2 and KI0025F03_R3 were all through the background fracture network; the pathways did not immediately 'jump' to Structure 19.

2. The Cartesian distances for both the Structure 19 pathways (Path I) and the pathways through Structure BG1 and the background fracture network (Path II) were approximately 20 m. However, the simulated Structure 19 pathway lengths were generally on the order of 20 m to 35 m.

3. The PAWorks-identified CN pathways for Path II (BG1) were much longer than those identified for Path I (Structure 19), with lengths on the order of 55 m. The background fracture pathways can therefore be assumed to truly reflect the influence of multiple background fractures. This would include fracture intersection effects not present on the Structure 19 pathway (Path I).

4. Based on experimental results, the advective velocity from the BS2B conservative tracer experiments was approximately ten times as long in the BG1 pathway (Path II) as in the Structure 19 pathway (Path I). For example, the time to 5% breakthrough (t_5) for $^{131}I^-$ in Structure 19 (Path I) was only 14 hours, while t_5 for ^{155}Eu-DTPA through Structure BG1 and the background fracture network (Path II) was 155 hours (see Table 7-3).

5. Based on the simulations described in Sections 7.1 through 7.3, the retention properties of the Structure BG1 pathways would need to be decreased to obtain a better match to observed sorbing tracer breakthrough, while the retention properties of the Structure 19 pathways as modeled produce results that are more consistent with in situ measurements.

These key observations indicate that the behaviors seen in the Structure BG1 pathways (a) may be representative of the behavior of networks of background fractures, and (b) background fracture network pathways are different from transport in single, larger structures such as Structure 19. This is potentially significant result for the Hypothesis Ib, since it indicates that there is a difference in transport between the smaller scale (Structure BG1 and the background fracture network) type structures and the larger scale (Structure 19) features. The significantly longer advective travel time for the BG1 pathway may be due to the difference between transport in larger faults and smaller background fractures.

This conclusion is potentially significant for safety assessment, since it is generally assumed that although background fractures have smaller flow, they may have comparable groundwater velocities due to the correlation between aperture and transmissivity. However, the results provided in Table 3-4 were based on a single realization. Ten Monte Carlo realizations of the background fracture network were therefore generated to determine the likelihood that this conclusion is justified.

The Monte Carlo background fracture simulation was carried out as follows. In this study, the Structure BG1 was treated as a deterministic structure, with a transmissivity of 1.42×10^{-8} m^2/s and a hydraulic aperture of 5.97×10^{-5} m. Background fracture network characteristics (Table 7-5) were taken from the Task 6C report (Dershowitz et al., 2003).

Table 7-4: Pathway geometries from Step 2 evaluation modeling (Chapter 7.3)

Step 2 Evaluation Modeling Parameter	**Structure 19 Path I** F02_R3 - F03_R3	**Structure BG1 Path II** F02_R2 > F03_R3
Cartesian Distance (m)	19.5	22
Number of PAWorks Pathways	78	20
Average Pathway Length (m)	35.05	50.82
Maximum Pathway Length (m)	54.88	55.52
Minimum Pathway Length (m)	18.17	47.92
Average % of Path in #19	10.31%	0%
Max. Path Length in #19	21.12	0
Min. Path Length in #19	0	0

For the Structure 19 pathways (F02R03 to F03R03) described in Table 7-4, there were a large number of pathways for which a significant portion of the length was not within the plane of Structure 19. However, due to the much larger aperture of Structure 19 with respect to the background fracture network, the bulk of tracer mass is transported on those pathways that are primarily within the plane of Structure 19. The PAWorks graph theory search identified all potential pathways (up to a user-specified maximum of 100 paths); however, the first ten or so pathways tended to be the most conductive.

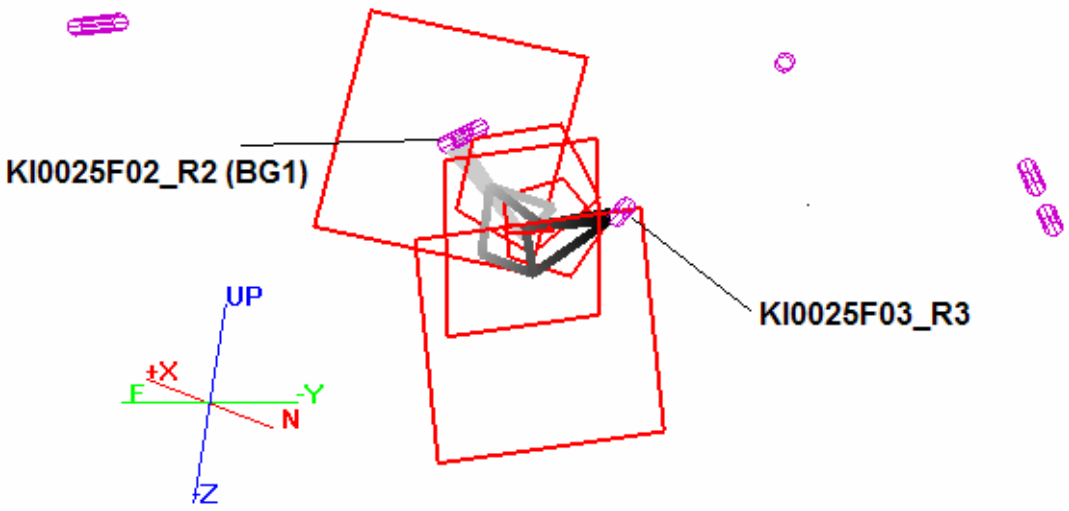

Figure 7-18: *PAWorks-identified channel pathways between KI0025F02_R2 and KI0025F03_R3 (Path II), Step 2 evaluation modeling.*

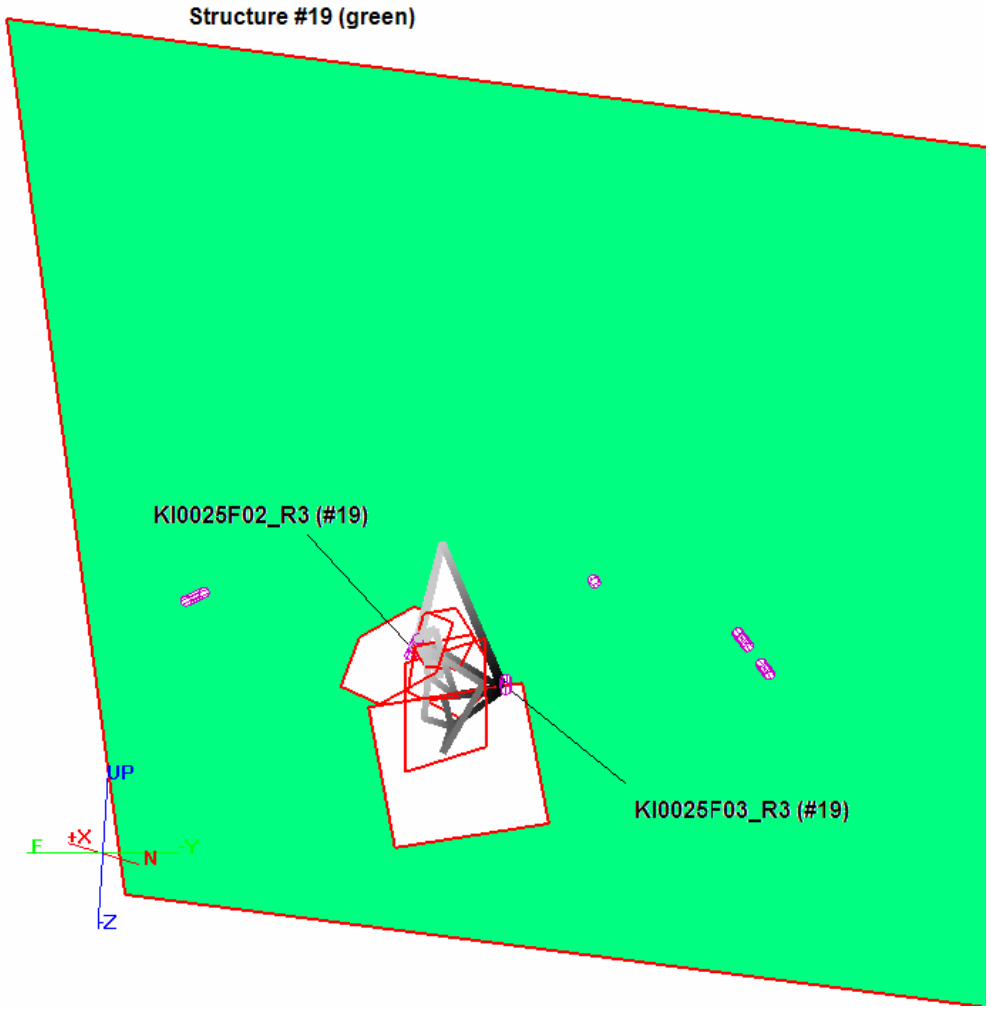

Figure 7-19: *PAWorks-identified channel pathways between KI0025F02_R3 and KI0025F03_R3 (Path I, Structure 19), Step 2 evaluation modeling.*

Figure 7-19 illustrates a number of background fractures involved in the pathways between source and sink within Structure 19 (Path I). The graph-theory search results suggest that, in the situation where sources and sinks are relatively close together, significant pathways through the background fracture network do exist. Note that neither this figure nor the statistics presented in Table 7-4 say anything about the hydraulic significance of the pathways. Evaluation modeling suggests that, in general, most of the reactive transport along Path I is occurring only on a few pathways within Structure 19. Changes to the hydraulic (transmissivity, aperture) and transport (perimeter, immobile zone thicknesses) along Structure 19 caused significant changes to the modeled breakthrough curves, However, changes to the hydraulic or transport parameters of the background fracture network used for the blind predictions and for the Step 1 / Step 2 evaluation modeling had little overall affect on the shape of the breakthrough curve (arrival times do change, however).

Table 7-5: Background fracture model for Monte Carlo simulations (from Task 6C report, Dershowitz et al., 2003)

	BGF Set A	BGF Set B
Untruncated P_{32}		
Truncated P_{32}	0.047	0.038
Orientation Model	Fisher	Fisher
Mean Pole (trend, plunge)	211, 0.6	250, 54
Dispersion	9.4	3.8
Size Model	LogNormal	LogNormal
Radius Mean, Std. Dev.	2, 2	2, 2
Upper Size Truncation (m)	500	100
Lower Size Truncation (m)	2	2
Transmissivity Model	LogNormal	LogNormal
Mean Transmissivity (m^2/s)	1.00×10^{-8}	1.00 x 10-8
Std. Dev. Transmissivity (m^2/s)	9.5×10^{-8}	9.5 x 10-8
Upper T Truncation (m^2/s)	1	1
Lower T Truncation (m^2/s)	1.0×10^{-10}	1.0 x 10-10

Pathway geometry statistics for these stochastic simulations are summarized below in Table 7-6. Geometric pathway statistics were computed for each background fracture realization. Table 7-6 shows that, given the background fracture statistics of Table 7-5, there is a wide range of possible pathway geometries. The mean path length of these ten realizations varies from 44 m to 197 m, indicating a tortuosity (path length / Cartesian distance) that ranged from 2 times to 9 times. The mean path length of 50 meters, as derived in the Step 2 evaluation modeling, is near the center of this range. It is also fairly representative in terms of the potion of the path length that is on Structure 19. This supports the use of the Structure BG1 tracer breakthrough results within the context of Hypothesis Ib.

Figure 7-20 shows the relationship between the tortuous path length and the percentage of the path length in Structure 19, for pathways utilizing Structure BG1 (Path II). As would be expected, the longer path lengths have proportionally smaller lengths in Structure 19. Therefore, the longer length pathway simulations are more representative of the behavior of "background fractures".

Table 7-6: Statistics for Path II pathways from stochastic background fracture network modeling

Monte Carlo	*Mesh Details*		*# of*	*Mean Path*	*Max Path*	*Min Path*	*# of Paths*	*Average % of*
Run #	*# Nodes*	*# Pipes*	*Pathways*	*Length (m)*	*Length (m)*	*Length (m)*	*In #19*	*Path Length in #19*
Default	2021	5537	20	43.95	49.17	36.65	8	33.70%
MC1	2723	6969	12	47.16	58.02	37.72	12	36.10%
MC2	2584	6640	55	56.15	102.80	26.86	55	38.80%
MC3	2607	6687	35	81.51	96.87	66.33	35	65.90%
MC4	2520	6499	75	89.29	113.00	56.63	75	54.01%
MC5	2575	6798	100*	196.66	343.16	63.84	100	62.58%
MC6	2795	7285	20	135.82	148.98	120.73	20	92.30%
MC7	2570	6610	60	46.61	62.68	34.07	60	27.59%
MC8	2536	6642	80	53.22	64.60	46.43	80	60.46%
MC9	2617	6733	35	53.97	71.78	37.37	35	47.61%
MC10	2743	7015	95	50.80	85.03	39.06	95	39.93%

** 100 iterations set as a search maximum*

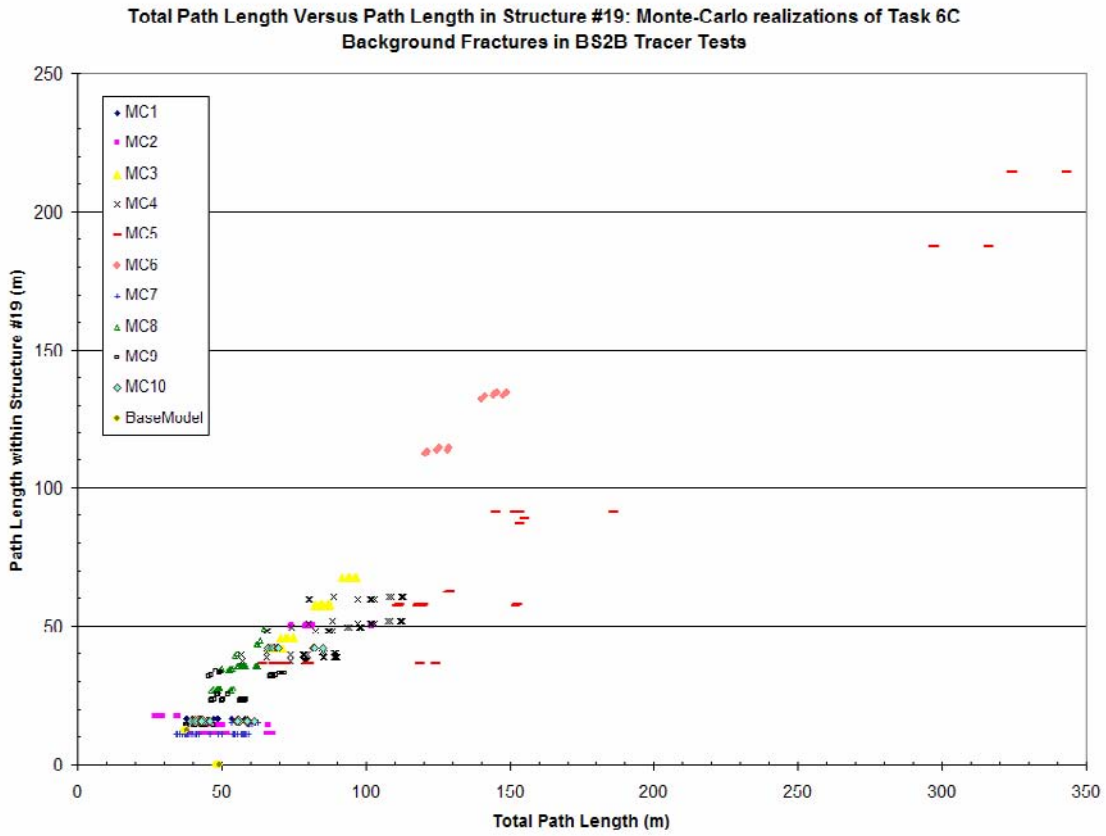

Figure 7-20: *Total length versus length within Structure 19 for Path II pathways, stochastic background fracture network simulations.*

The effect of variability in background fracture realizations on tracer transport was further studied through transport simulations on the Monte Carlo background fracture network realizations. Two specific realizations (MC5 and MC6) were selected for further study. Both of these background fracture models contained geometric pathways that were significantly longer on average (> 100m), indicating very tortuous transport pathways.

As was performed in previous simulations (Step 1 and Step 2), for realizations MC5 and MC6, borehole skin factors were adjusted to match in-situ drawdowns measurements observed in borehole sections connected to Structure 19. Specifically, transmissivity adjustments were made to Structure 19 pipes directly connected to KI0025F02_R3 and KI0025F03_R3. Tracer transport was then simulated using the same transport parameters and assumptions of the Step 2 evaluation simulations (described in Section 7.3.1). Breakthrough curves for Path II pathways (Structure BG1 > background fracture network > Structure 19) are provided in Figure 7-21 through Figure 7-30. Breakthrough time statistics are provided in Table 7-9 and Table 7-10, while stochastic background fracture model pathway geometries are presented in Table 7-7 and Table 7-8 for the simulated model cases. Sample channel network pathways identified through PAWorks graph-theory searches for realizations MC5 and MC6 are presented in Figure 7-31 through Figure 7-34.

The results of these two Monte Carlo simulations are somewhat surprising. These two background fracture network iterations were selected because both MC5 and MC6 feature relatively long and tortuous Path II pathways. It was expected that MC6 would have a longer advective travel time and greater retention due to the wider spread in potential path lengths (Table 7-6). However, the breakthrough statistics show that the longer advective travel time actually corresponds to the Monte Carlo simulation MC5. This indicates that within background fracture networks, the existence of longer pathways does not necessarily result in longer travel times. The average pathway length, rather than the spread of potential pathways, appears to be of greatest importance.

The breakthrough time statistics (and breakthrough curves) for realizations MC5 and MC6 illustrate the degree of variability in solute transport that can be expected with uncertainty in the background fracture network. This variability is quite large, and as a consequence, and conclusions reached for the background fracture pathway must be tempered by the understanding that these conclusions may only apply for a specific background fracture realization.

Table 7-7: Realization MC5 Pathway Geometry Statistics

MC5 Pathway Statistics Parameter	***Structure #19 Path I F02_R3 → F03_R3***	***Structure #BG1 Path II F02_R2 → F03_R3***
Cartesian Distance (m)	19.5	22
Number of PAWorks Pathways	50	49
Average Pathway Length (m)	43.93	63.63
Maximum Pathway Length (m)	64.22	81.08
Minimum Pathway Length (m)	18.17	57.80
Average % of Path in #19	80.90%	45.23%
Max. Path Length in #19	100.00%	62.84%
Min. Path Length in #19	14.56%	9.14%

Table 7-8: Realization MC6 Pathway Geometry Statistics

MC6 Pathway Statistics Parameter	***Structure #19 Path I F02_R3 → F03_R3***	***Structure #BG1 Path II F02_R2 → F03_R3***
Cartesian Distance (m)	19.5	22
Number of PAWorks Pathways	53	20
Average Pathway Length (m)	78.51	135.82
Maximum Pathway Length (m)	122.79	148.98
Minimum Pathway Length (m)	29.49	120.73
Average % of Path in #19	100%	92.3%
Max. Path Length in #19	100%	94.2%
Min. Path Length in #19	100%	88.7%

Table 7-9: Breakthrough time statistics for stochastic background fracture simulation case MC5 transport model

Tracer Breakthrough Times for Flow Path II (BG1-19)

BS2B Experimental Results					MC5				
	t5 hours	*t50 hours*	*t95 hours*	*% Recovery*		*t5 hours*	*t50 hours*	*t95 hours*	*% Recovery*
HTO	183	790	n/r	68%	HTO	134	722	4860	100%
155Eu	155	500	n/r	92%	155Eu	310	4050	n/r	66%
22Na	300	1490	n/r	72%	22Na	1240	4390	n/r	100%
133Ba	3250	n/r	n/r	8%	133Ba	n/r	n/r	n/r	0.00%
54Mn	n/r	n/r	n/r	1%	54Mn	n/r	n/r	n/r	0%

Total Time	hrs
HTO	4409
AllOthers	4577

Good Match To Measured Data
O.K. Match to Measured Data
Poor Match to Measured Data

Tracer Breakthrough times for Flow Path I (19)

BS2B Experimental Results					MC5				
	t5 hours	*t50 hours*	*t95 hours*	*% Recovery*		*t5 hours*	*t50 hours*	*t95 hours*	*% Recovery*
131I-	14	62	n/r	80%	131I-	6	43	811	100%
160Tb	14	63	4075	87%	160Tb	5	33	146	100%
85Sr	19	107	4327	86%	85Sr	8.2	64	780	100%
86Rb	51	490	n/r	56%	86Rb	42	718	n/r	92%
137Cs	555	n/r	n/r	28%	137Cs	n/r	n/r	n/r	<1%

Table 7-10: Breakthrough time statistics for stochastic background fracture simulation case MC5 transport model

Tracer Breakthrough Times for Flow Path II (BG1-19)

BS2B Experimental Results					MC6				
	t5 hours	*t50 hours*	*t95 hours*	*% Recovery*		*t5 hours*	*t50 hours*	*t95 hours*	*% Recovery*
HTO	183	790	n/r	68%	HTO	51	135	377	100%
155Eu	155	500	n/r	92%	155Eu	99	268	1690	100%
22Na	300	1490	n/r	72%	22Na	449	1350	5660	100%
133Ba	3250	n/r	n/r	8%	133Ba	n/r	n/r	n/r	< 1%
54Mn	n/r	n/r	n/r	1%	54Mn	n/r	n/r	n/r	< 1%

Total Time	hrs
HTO	4409
AllOthers	4577

	Good Match to Measured Data
	O.K. Match to Measured Data
	Poor Match to Measured Data

Tracer Breakthrough Times for Flow Path I (19)

BS2B Experimental Results					MC6				
	t5 hours	*t50 hours*	*t95* hours*	*% Recovery*		*t5 hours*	*t50 hours*	*t95 hours*	*% Recovery*
131I-	14	62	n/r	80%	131I-	8.5	47	815	100%
160Tb	14	63	4075	87%	160Tb	6.5	36	155	100%
85Sr	19	107	4327	86%	85Sr	18	122	730	100%
86Rb	51	490	n/r	56%	86Rb	201	1450	n/r	92%
137Cs	555	n/r	n/r	28%	137Cs	n/r	n/r	n/r	<1%

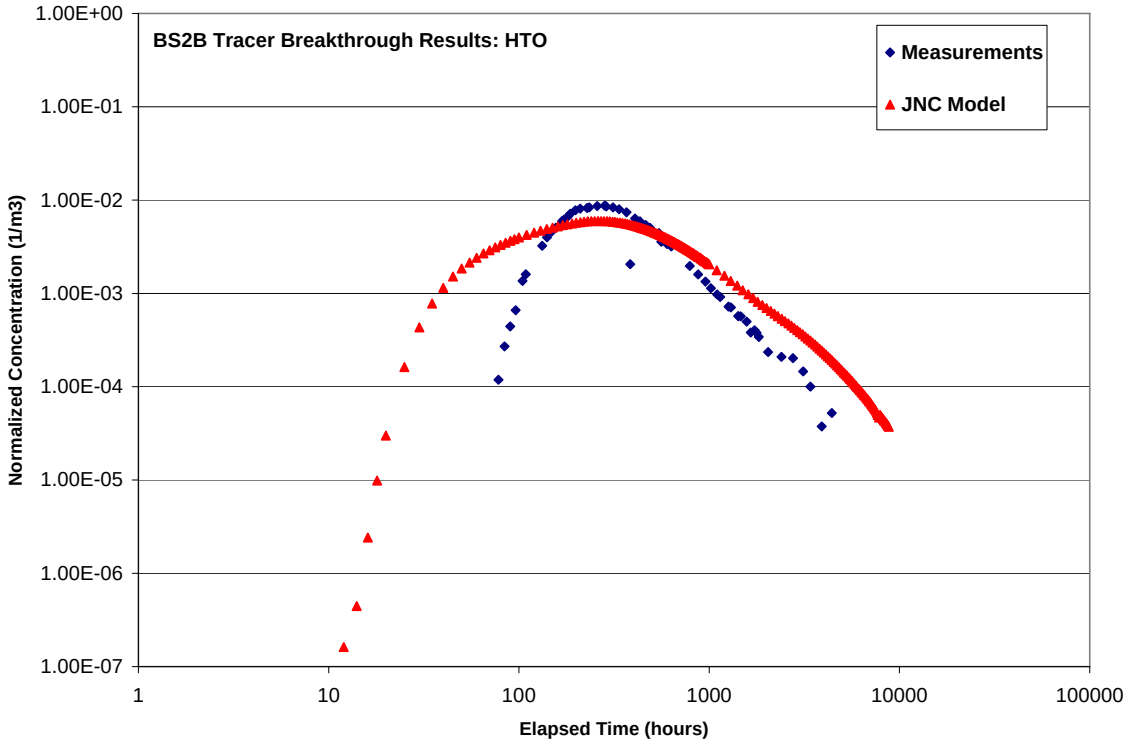

Figure 7-21: *Breakthrough curve for HTO, Path II (BG1), stochastic background fracture model MC5.*

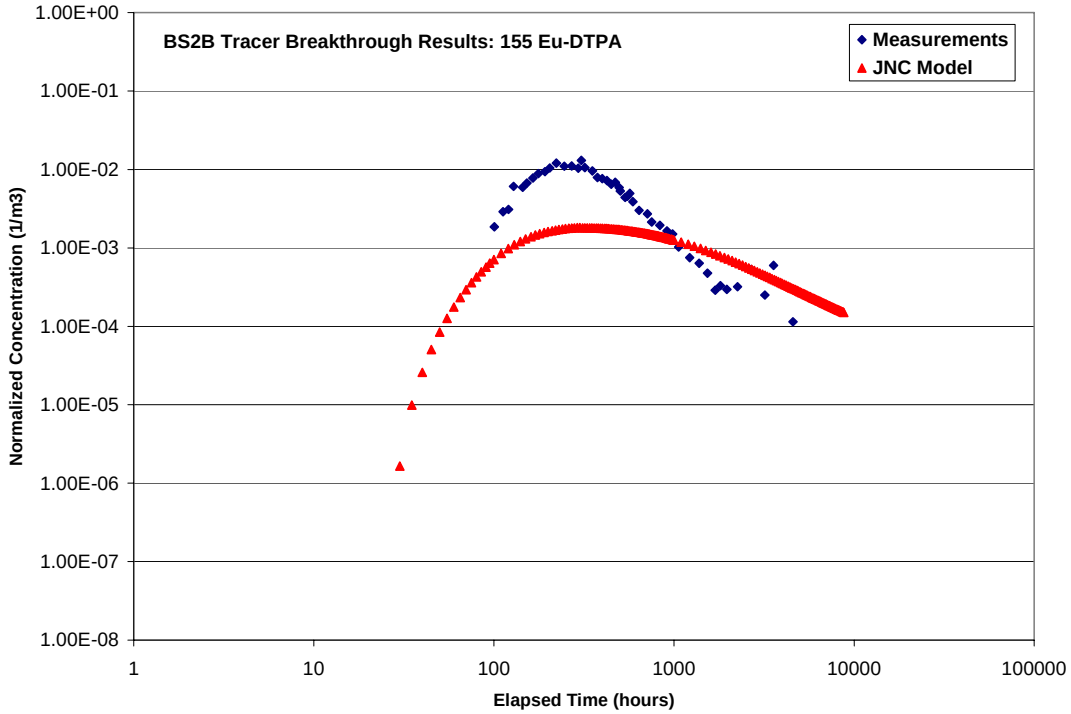

Figure 7-22: *Breakthrough curve for ^{155}Eu-DTPA, Path II (BG1), stochastic background fracture model MC5.*

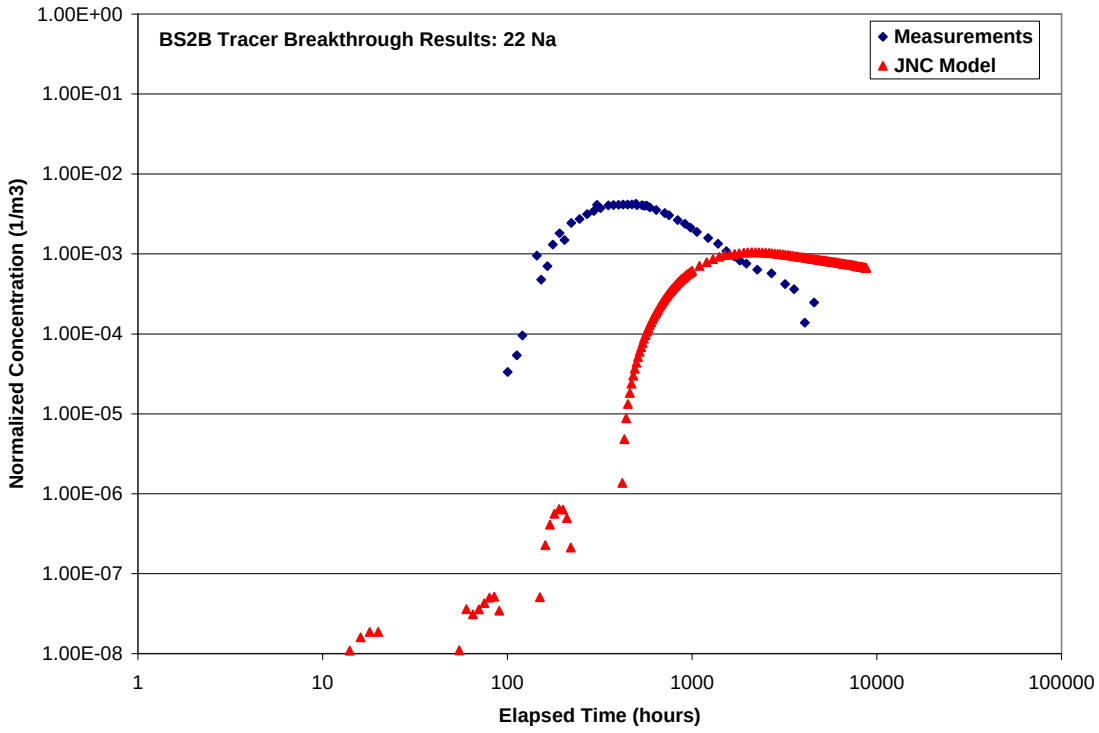

Figure 7-23: *Breakthrough curve for $^{22}Na^{+}$, Path II (BG1), stochastic background fracture model MC5.*

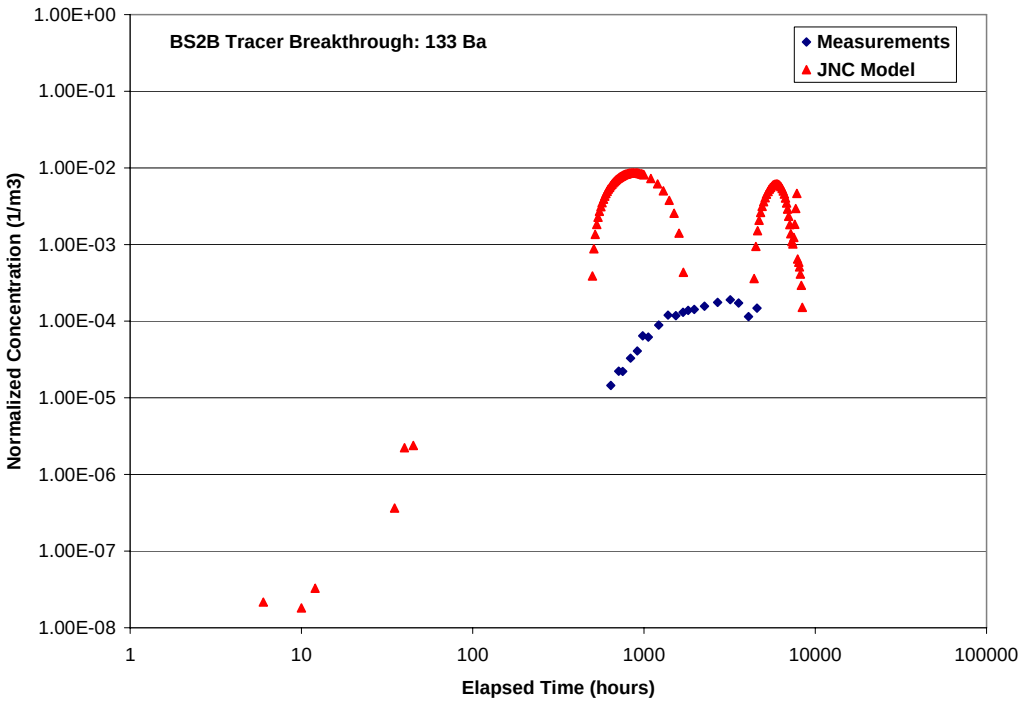

Figure 7-24: *Breakthrough curve for $^{133}Ba^{2+}$, Path II (BG1), stochastic background fracture model MC5.*

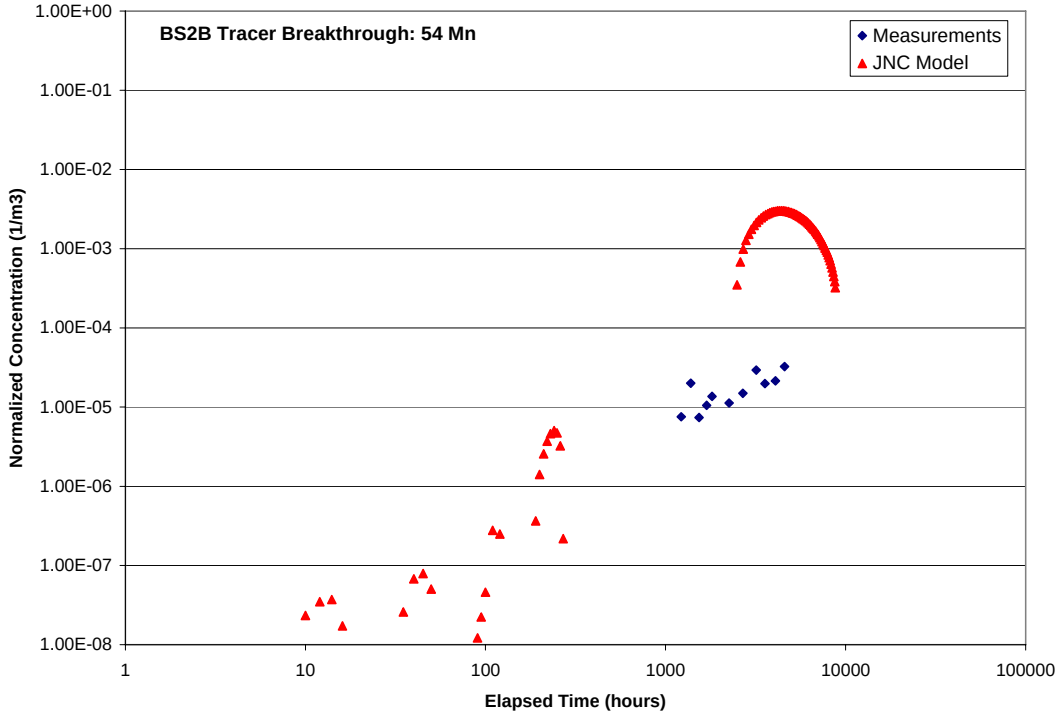

Figure 7-25: *Breakthrough curve for $^{54}Mn^{2+}$, Path II (BG1), stochastic background fracture model MC5.*

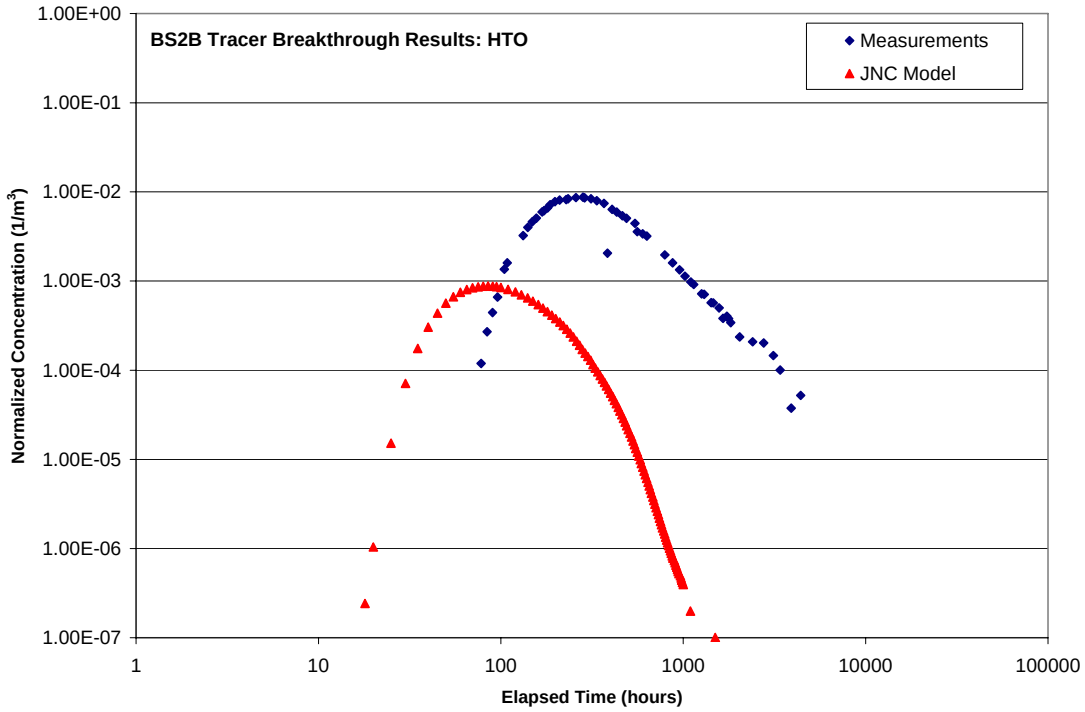

Figure 7-26: *Breakthrough curve for HTO, Path II (BG1), stochastic background fracture model MC6.*

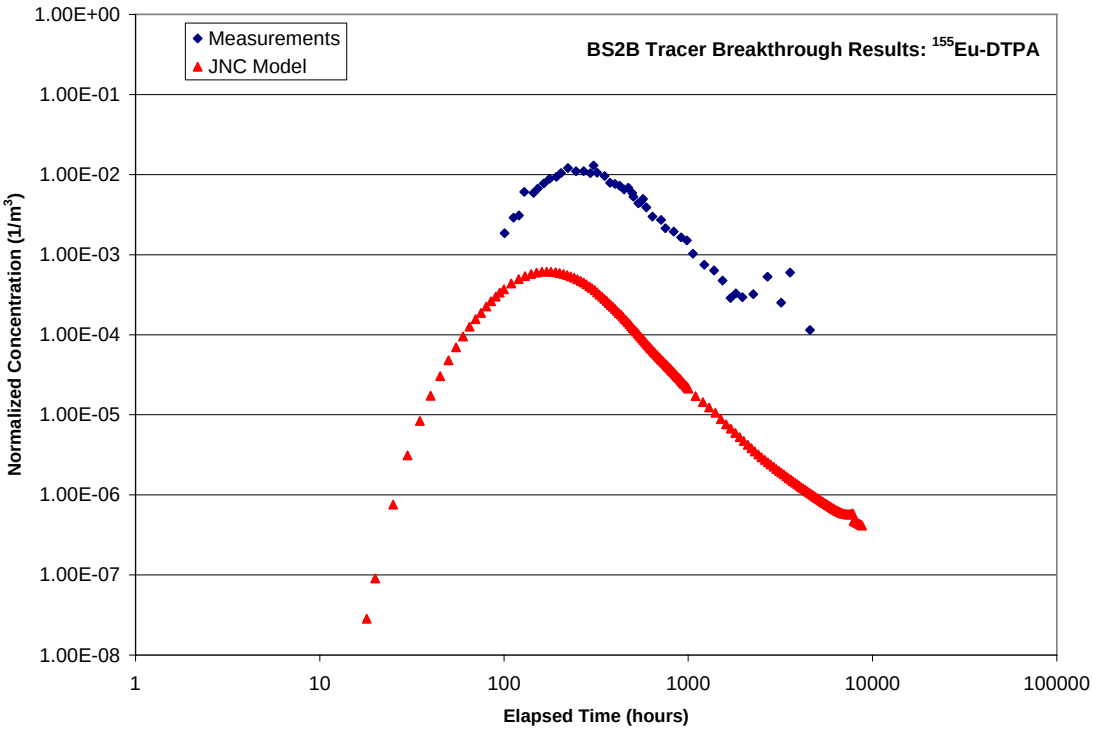

Figure 7-27: *Breakthrough curve for ^{155}Eu-DTPA, Path II (BG1), stochastic background fracture model MC6.*

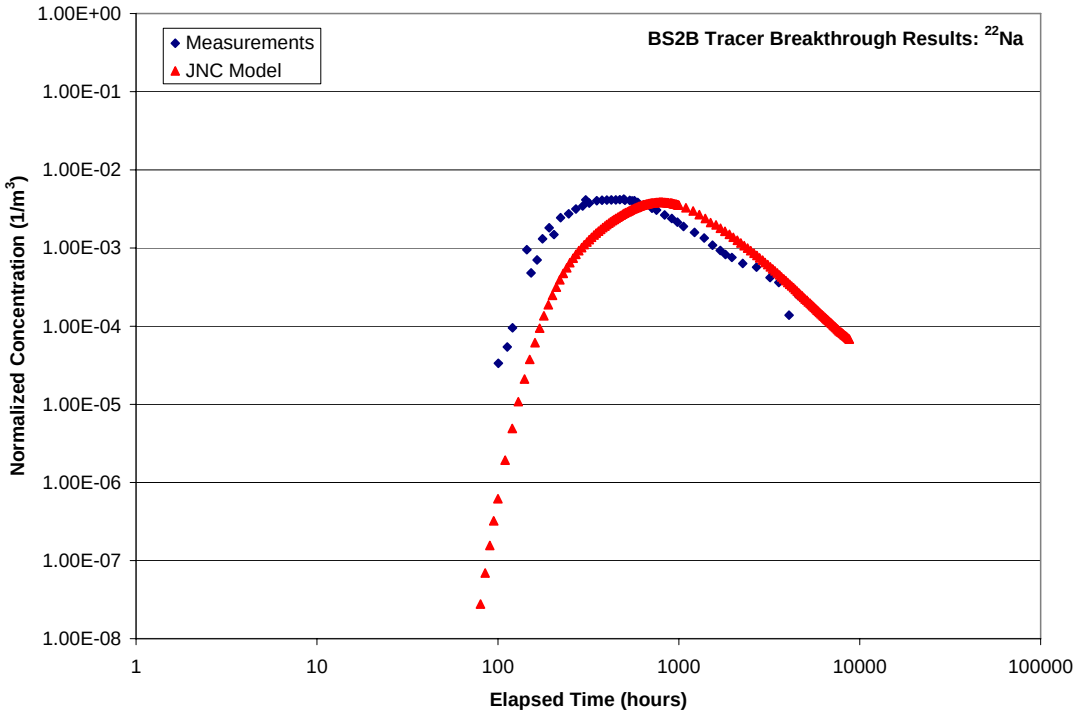

Figure 7-28: *Breakthrough curve for $^{22}Na^{+}$, Path II (BG1), stochastic background fracture model MC6.*

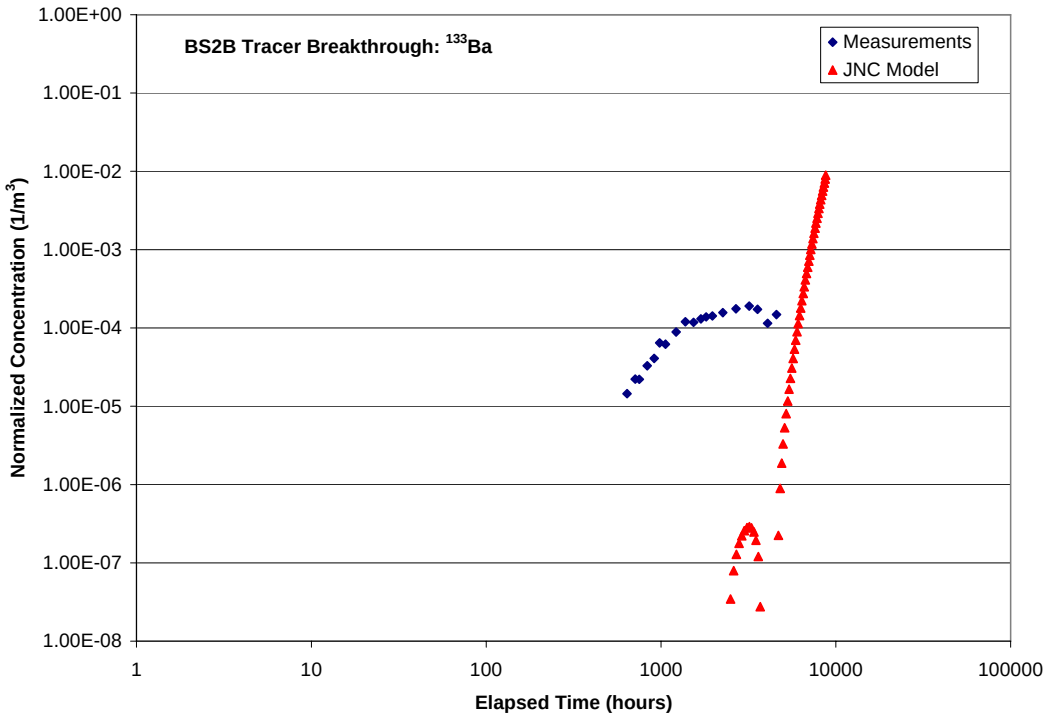

Figure 7-29: *Breakthrough curve for $^{133}Ba^{2+}$, Path II (BG1), stochastic background fracture model MC6.*

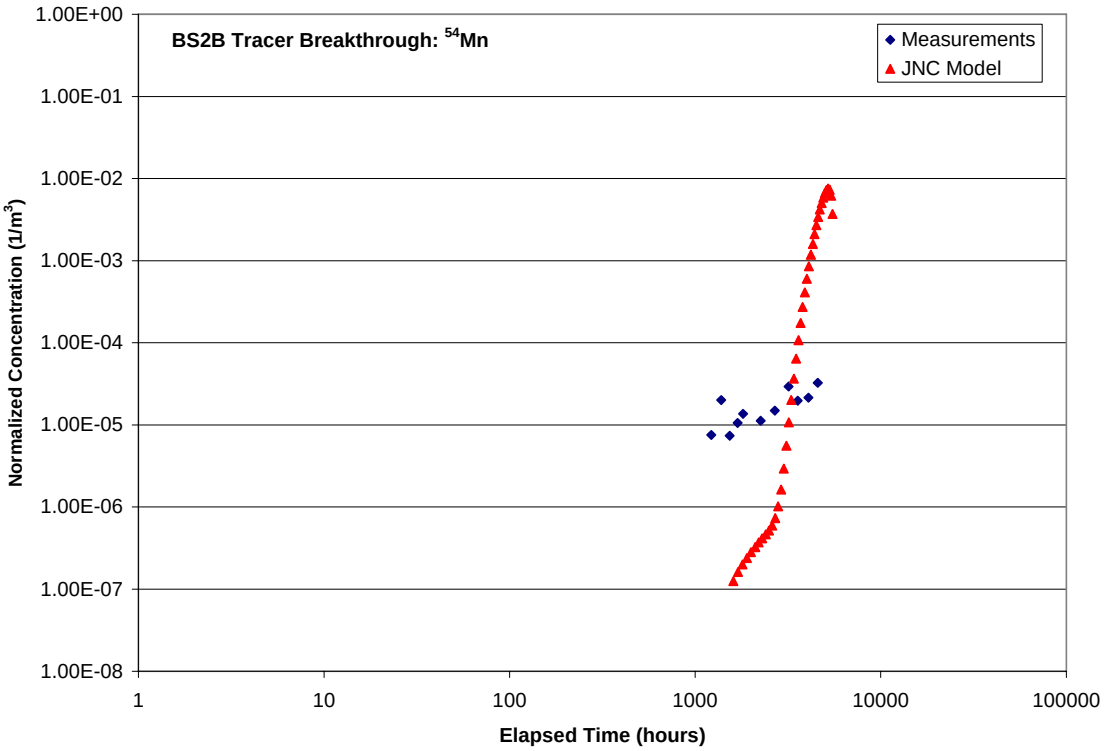

Figure 7-30: *Breakthrough curve for $^{54}Mn^{2+}$, Path II (BG1), stochastic background fracture model MC6.*

Figure 7-31 through Figure 7-34 illustrate several of the potential channel-network pathways identified by PAWorks through a graph-theory traversal search. Note the significant variation that occurs between the two different stochastic background fracture models. Again, this indicates that, even for a well-characterized geologic domain such as the TRUE Block Scale rock volume, significant uncertainty in transport pathways is still possible when utilizing stochastic background fracture models.

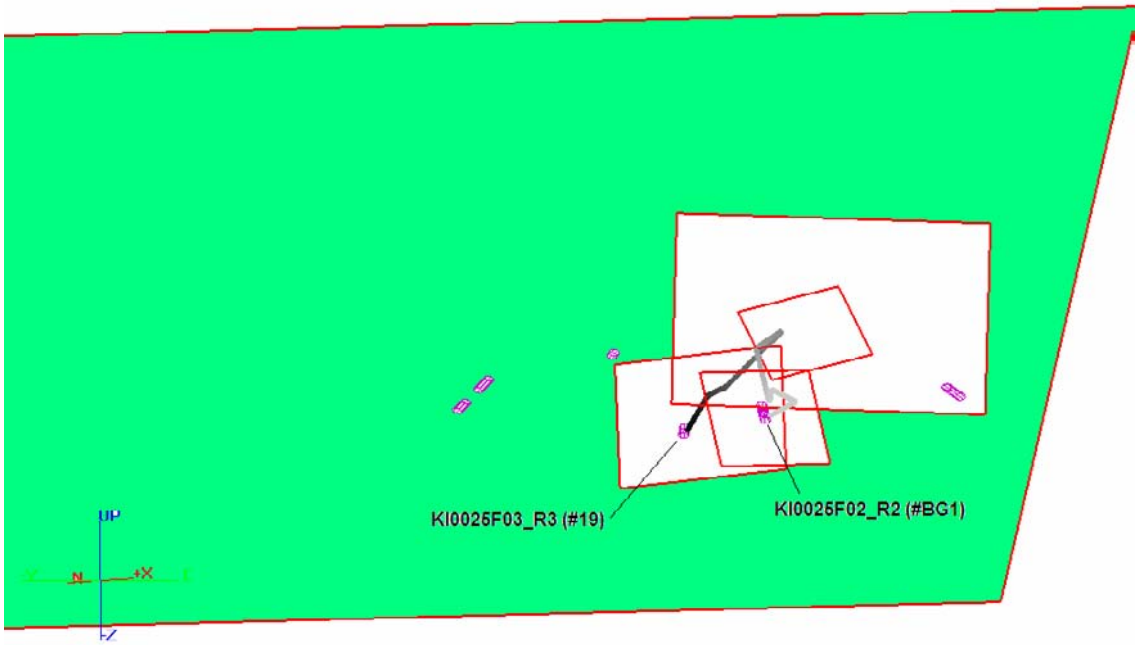

Figure 7-31: *PAWorks-identified channel network pathway (Path II) between KI0025F02_R2 (Structure BG1 and KI0025F03_R3 (Structure 19); stochastic background fracture model MC5.*

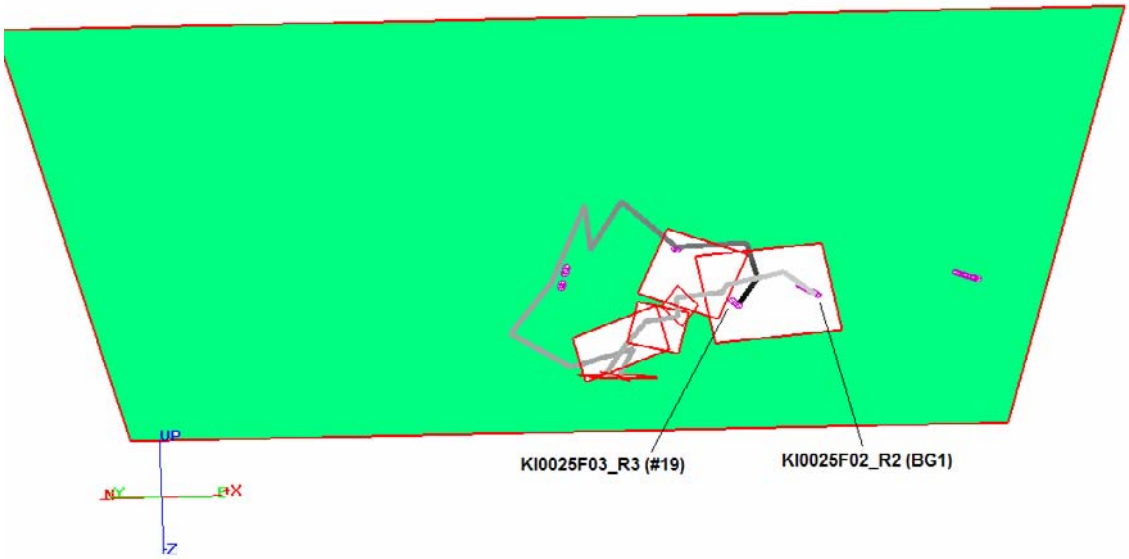

Figure 7-32: *PAWorks-identified channel network pathway (Path II) between KI0025F02_R2 (Structure BG1) and KI0025F03_R3 (Structure 19), stochastic background fracture model MC5. Note the significant path length within Structure 19 (gray line to the left of the background fracture cluster).*

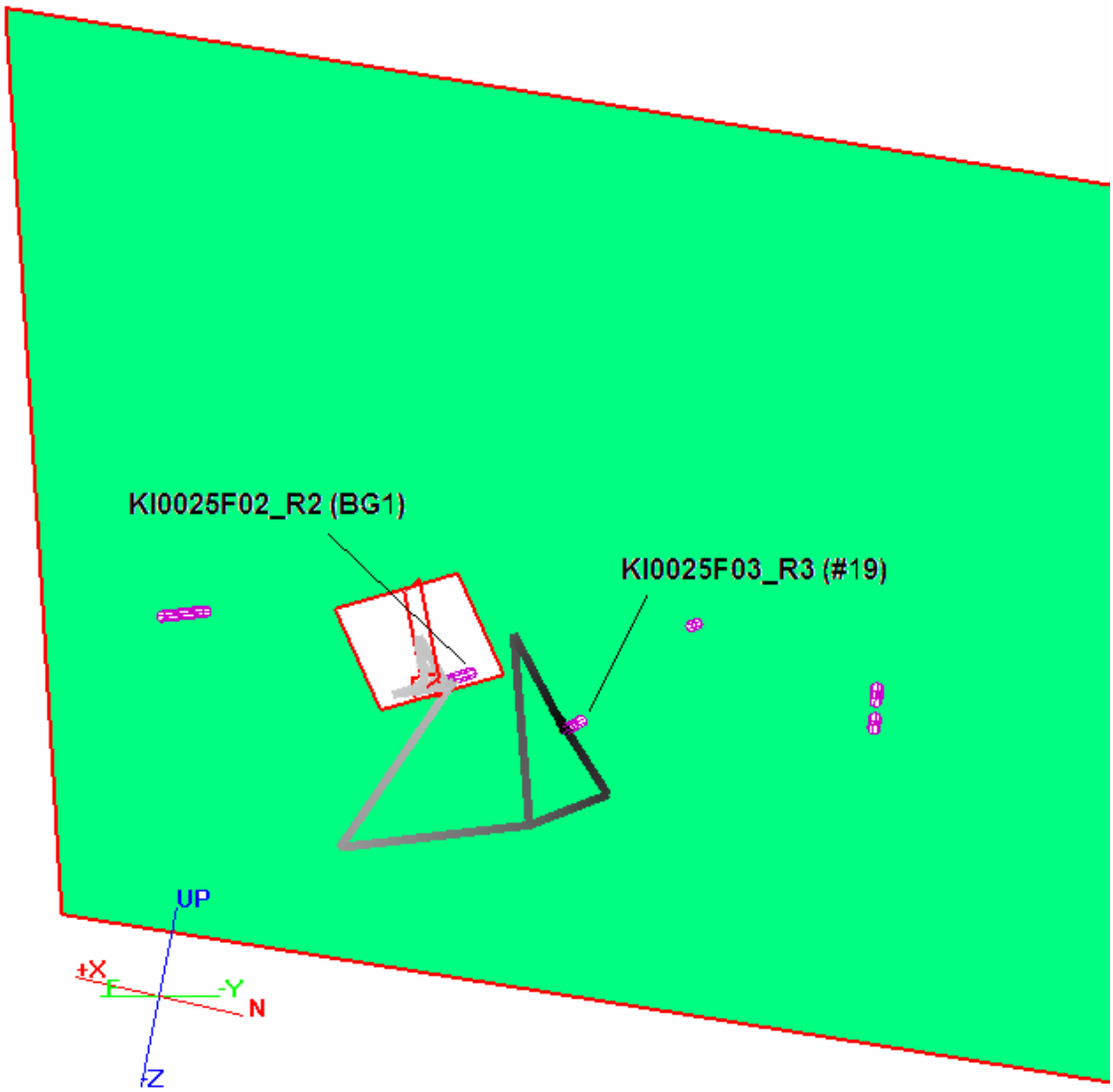

Figure 7-33: *PAWorks-identified channel network pathway (Path II) between KI0025F02_R2 (Structure BG1) and KI0025F03_R3 (Structure 19), stochastic background fracture model MC6. Again, note the significant pathway lengths within the plane of Structure 19.*

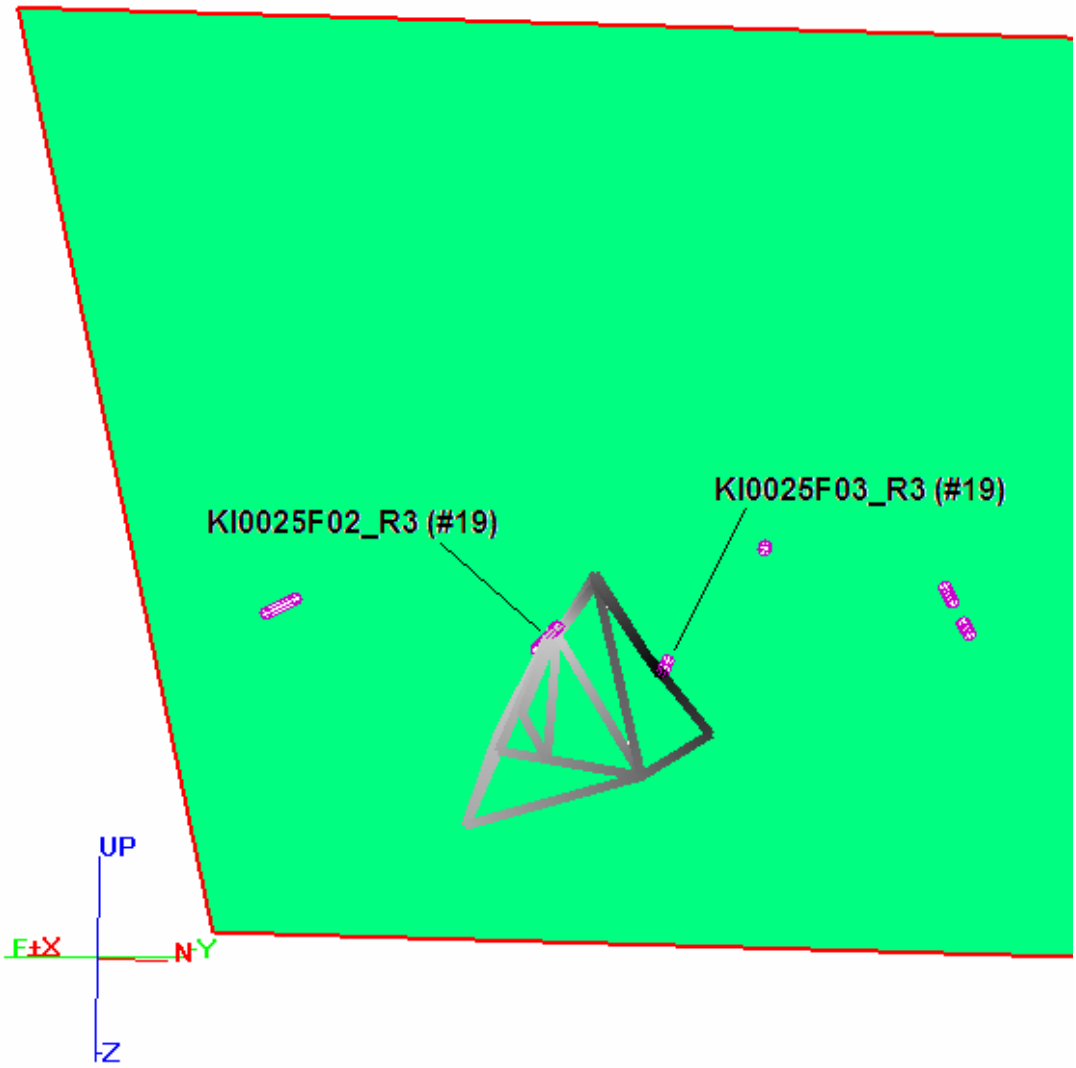

Figure 7-34: *PAWorks-identified channel network pathway (Path II) between KI0025F02_R3 (Structure 19) and KI0025F03_R3 (Structure 19), stochastic background fracture model MC6. Note that though this pathway is entirely within Structure 19, it is a very long and tortuous path.*

7.5 Simulating the effects of reduced diffusion perimeter in support of Hypothesis Ib

The TRUE-BSC microstructural conceptual model (Sections 2.3 and 4.4) includes a combination of parallel and series immobile zones. The diffusion from the advective flow channel to the fault gouge and fracture coating is assumed to occur in parallel, while the diffusion from the fracture coating to the altered wall rock and intact rock is assumed to occur in series.

In both the JNC/Golder BS2B blind prediction simulations and in the Step 1 / Step 2 evaluation simulations, diffusion and sorption were implemented as parallel processes within parallel immobile zones. Each process had access to the entire fracture flow wetted perimeter. It was recognized that this implementation would produce an over-estimate of diffusion. However, for the time scales involved, it was anticipated that this would not significantly over-estimate the amount of matrix diffusion and sorption within the rock mass, because the high porosity immobile zones (fault gouge, coating) would dominate during the short timeframe of the BS2B experiment.

The area available for diffusion in the JNC/Golder blind prediction simulations and in the BS2B evaluation modeling was assumed to be the full pipe perimeter used in the flow solution. This area was made available for all of the immobile zones, such that the total area available for diffusion was equal to the pipe perimeter multiplied by the number of immobile zones. This dramatic reduction in the area available for diffusion is more consistent with the pattern of flow suggested by imagery of results from the TRUE-1 Continuation epoxy resin injection tests /Hakami and Wang, in prep./.

This section describes a sensitivity study carried out to assess the effect of this assumption. For the sensitivity study, the area available for diffusion for each immobile zone was reduced by assuming that a total of 10% of the fracture surface area was available for diffusion, and this area itself was divided among the various immobile zones (i.e., of the 10% perimeter of each pipe, the perimeter available to each immobile zone is an additional fraction, $1/5^{th}$ for each immobile zone in a Type I structure and $1/3^{rd}$ for each Type II structure).

Simulations results for this assumption are presented in Figure 7-35 through Figure 7-46 and Table 7-11. The match to observed breakthrough is dramatically improved in these simulations, particularly for the more strongly sorbing tracers. This improvement is evident for both the Structure 19 (Path I) and Structure BG1 (Path II) pathways. These results indicates that the use of channelized pathways at 10% of the fracture surface (or less) is more consistent with tracer transport observations from the BS2B experiment then an assumption of complete channelization (i.e. access to the full fracture volume).

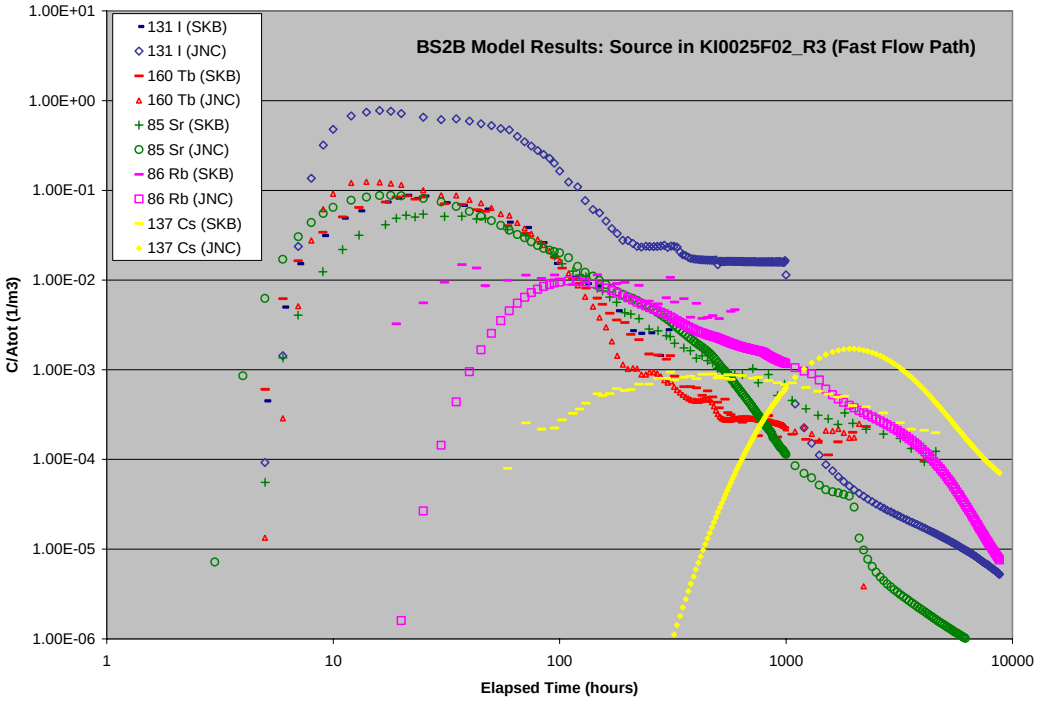

Figure 7-35: *Breakthrough curves for Path I simulations utilizing the Step 2 evaluation CN model, assuming 10% flow wetted surface area available for transport processes.*

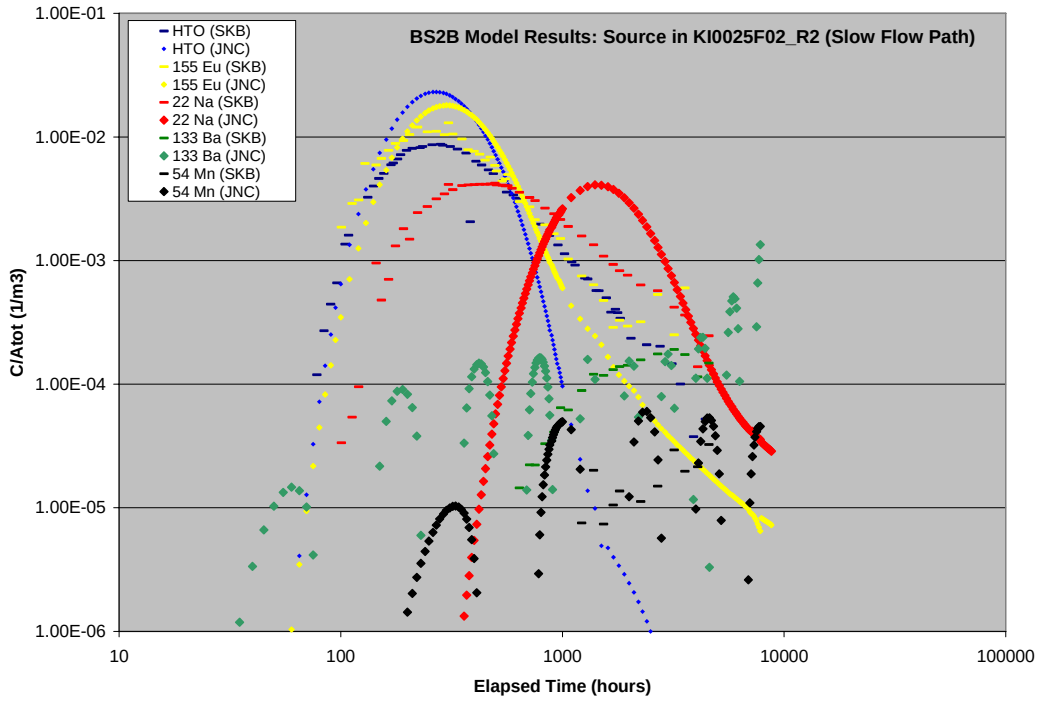

Figure 7-36: *Breakthrough curves for Path II simulations utilizing the Step 2 evaluation CN model and assuming 10% of actual flow wetted surface area is available for transport processes. The source term masses for Mn and Ba are scaled by 1.0 x 10^{-14} to reflect the actual injection into the model.*

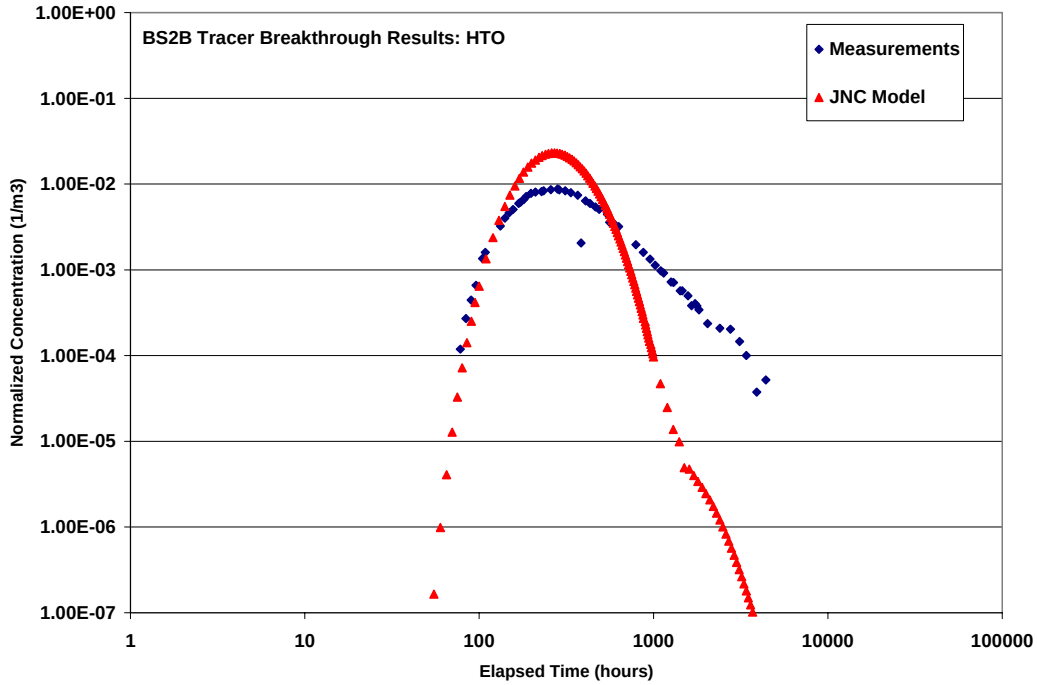

Figure 7-37: *Breakthrough curve for HTO, Path II (BG1), Injection in KI0025F02_R2, 10% FWS.*

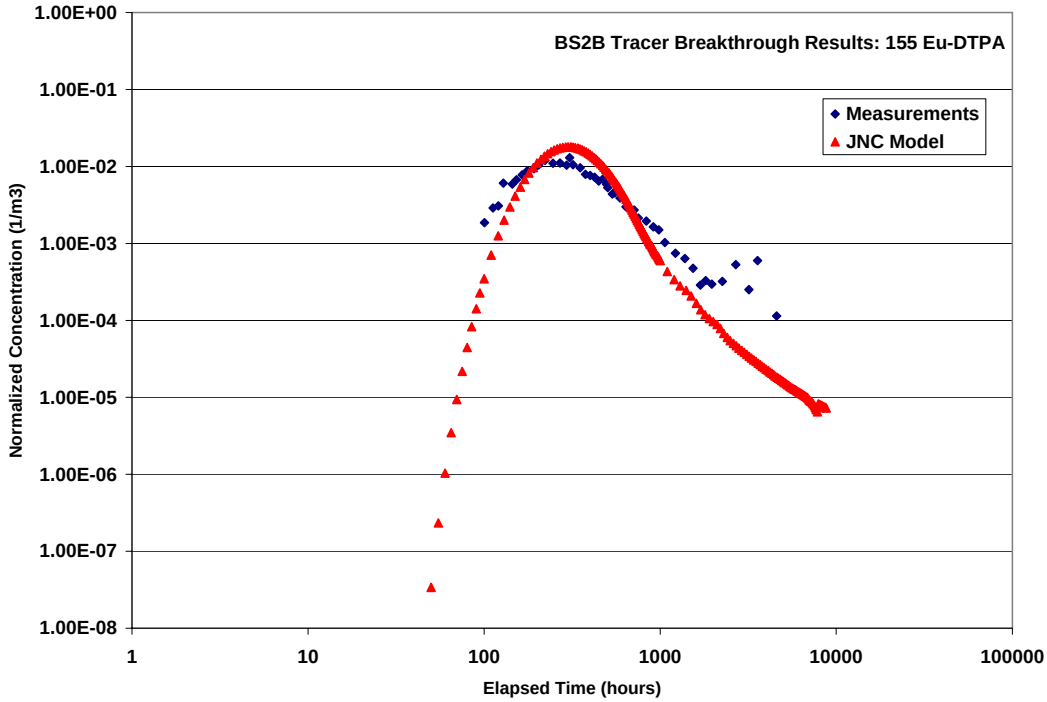

Figure 7-38: *Breakthrough curve for ^{155}Eu-DTPA, Path II (BG1), Injection in KI0025F02_R2, 10% FWS.*

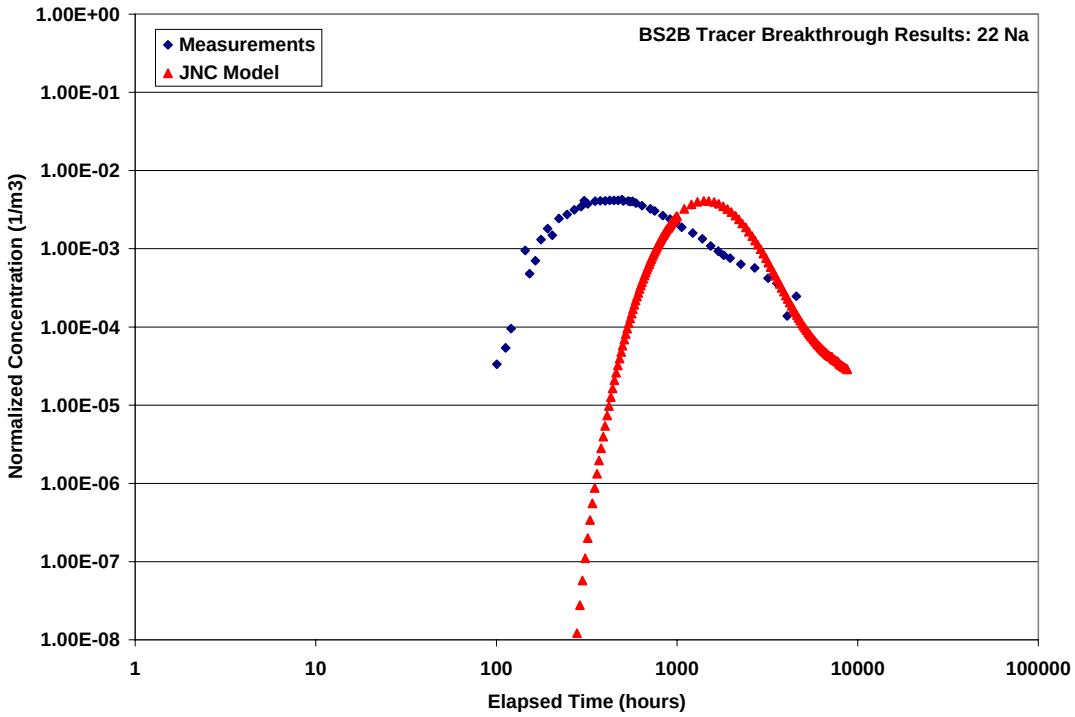

Figure 7-39: *Breakthrough curve for $^{22}Na^{+}$, Path II (BG1), Injection in KI0025F02_R2, 10% FWS.*

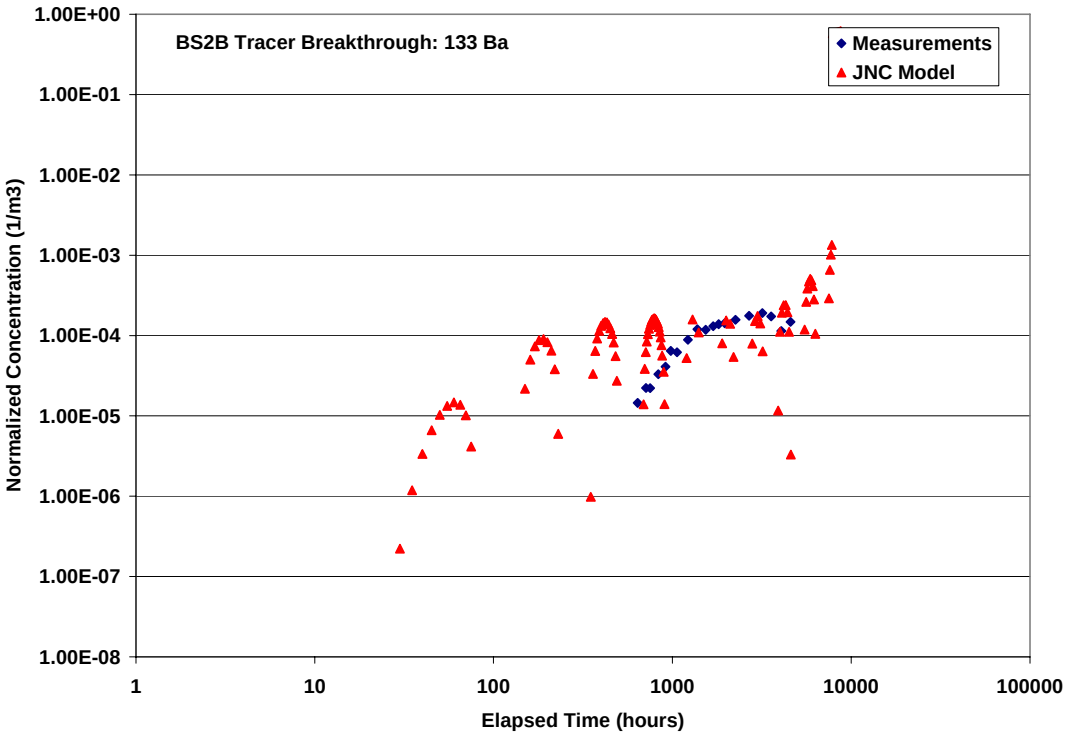

Figure 7-40: *Breakthrough curve for $^{133}Ba^{+}$, Path II (BG1), Injection in KI0025F02_R2, 10% FWS.*

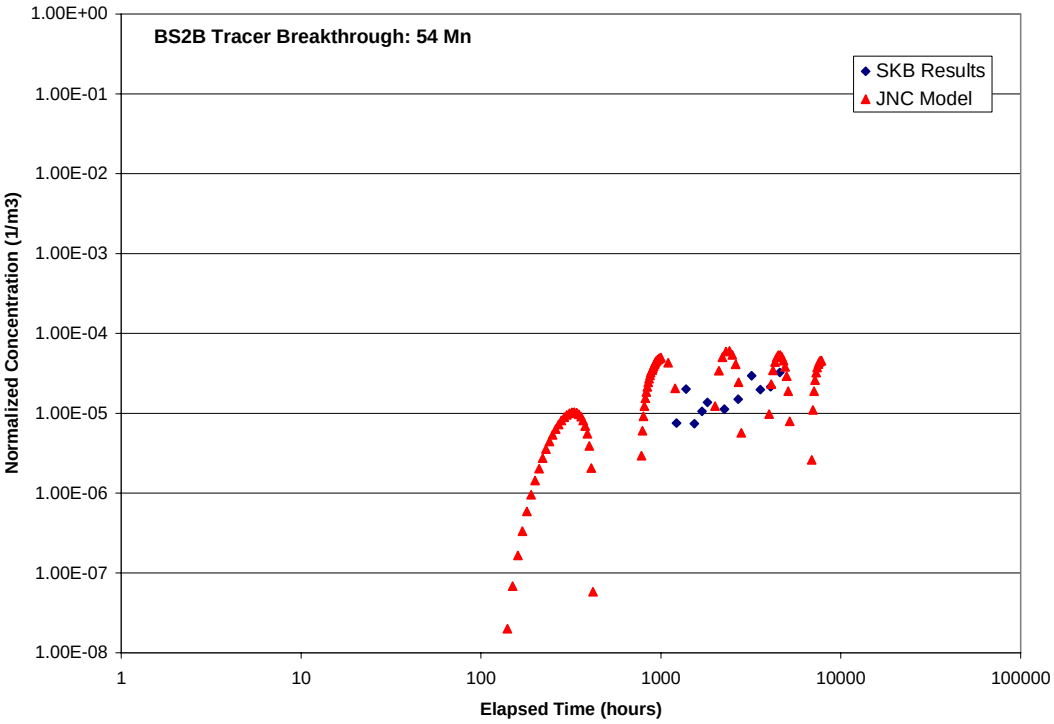

Figure 7-41: *Breakthrough curve for $^{54}Mn^{2+}$, Path II (BG1), Injection in KI0025F02_R2, 10% FWS.*

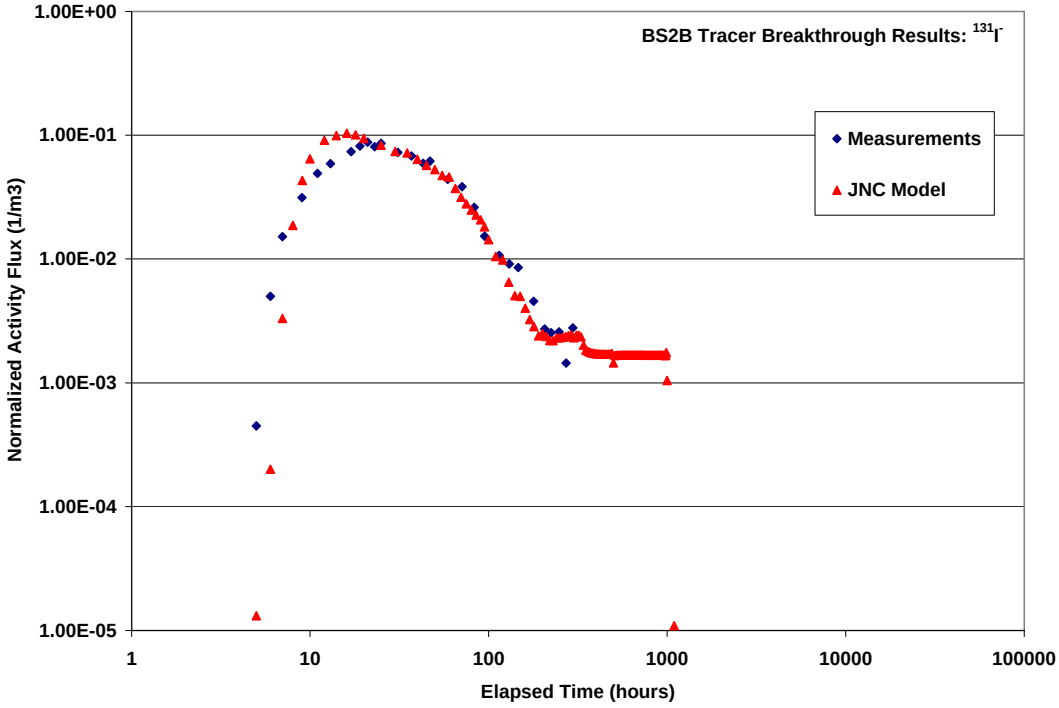

Figure 7-42: *Breakthrough curve for ^{131}I, Path I (Structure 19), Injection in KI0025F02_R3, 10% FWS.*

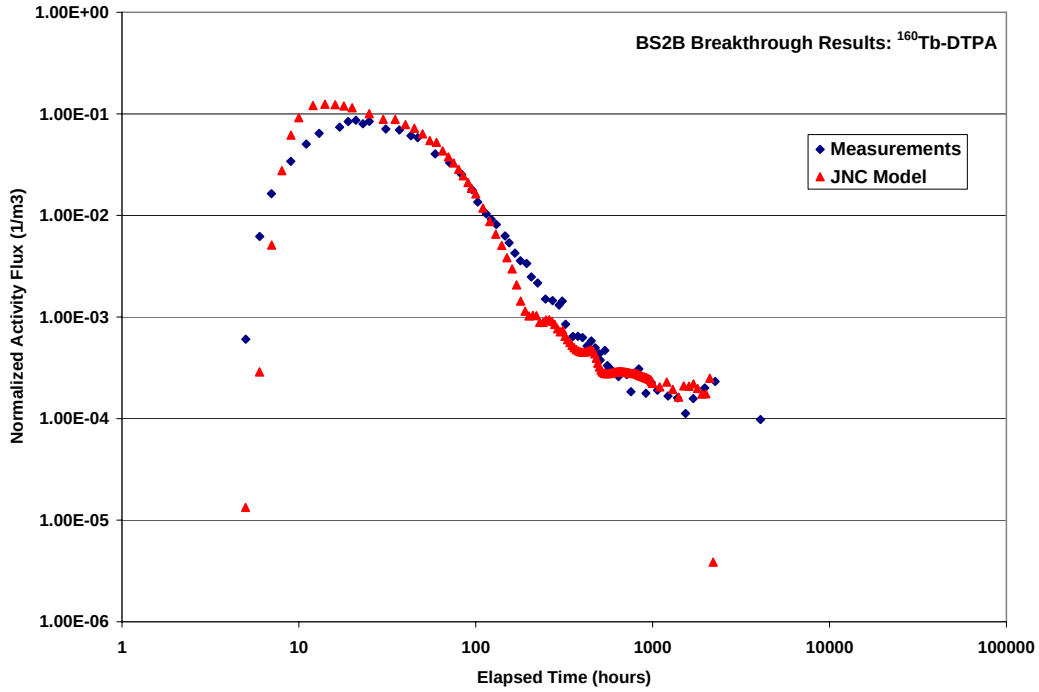

Figure 7-43: *Breakthrough curve for ^{160}Tb-DTPA, Path I (Structure 19), Injection in KI0025F02_R3, 10% FWS.*

Figure 7-44: *Breakthrough curve for ^{85}Sr, Path I (Structure 19), Injection in KI0025F02_R3, 10% FWS.*

Figure 7-45: *Breakthrough curve for ^{86}Rb, Path I (Structure 19), Injection in KI0025F02_R3, 10% FWS.*

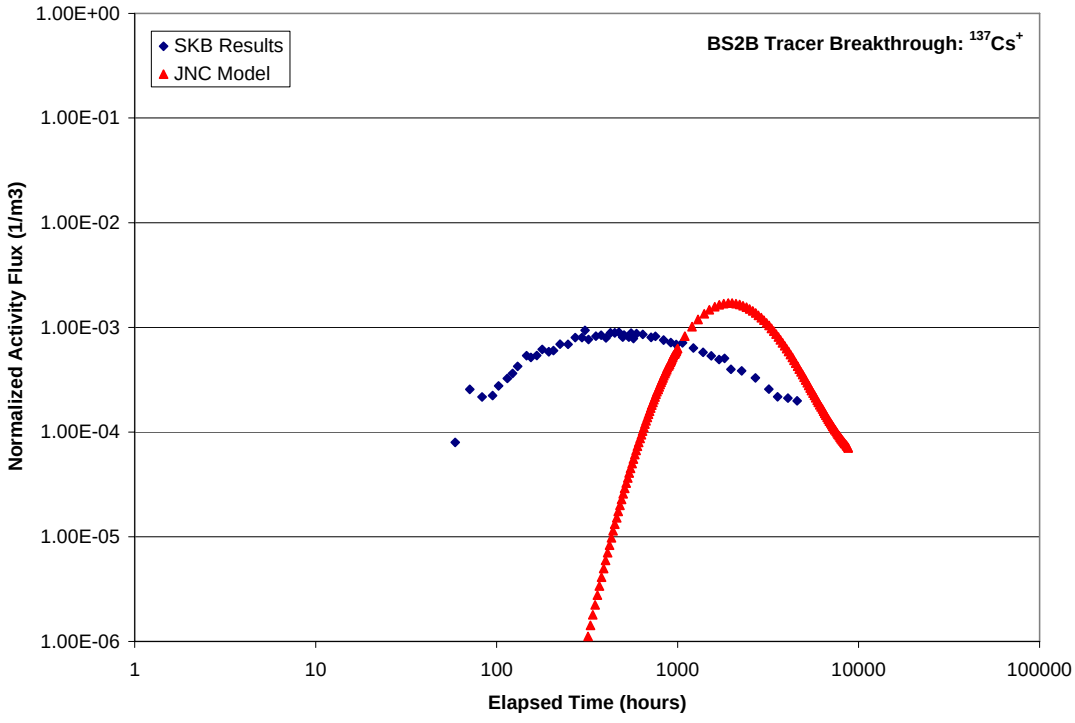

Figure 7-46: *Breakthrough curve for ^{137}Cs, Path I (Structure 19), Injection in KI0025F02_R3, 10% FWS.*

Table 7-11: Breakthrough time statistics for 10% FWS area transport simulations

Tracer Breakthrough Times for Flow Path II (BG1-19)

BS2B Experimental Results					10% of Immobile Zone FWS Area				
	t5 hours	*t50 hours*	*t95 hours*	*% Recovery*		*t5 hours*	*t50 hours*	*t95 hours*	*% Recovery*
HTO	183	790	n/r	68%	HTO	165	313	613	100%
155Eu	155	500	n/r	92%	155Eu	162	315	659	100%
22Na	300	1490	n/r	72%	22Na	697	1275	2455	100%
133Ba	3250	n/r	n/r	8%	133Ba	n/r	n/r	n/r	< 1%
54Mn	n/r	n/r	n/r	1%	54Mn	n/r	n/r	n/r	< 1%

Total Time	hrs	
HTO	4409	
AllOthers	4577	

	Good Match to Measured Data
	O.K. Match to Measured Data
	Poor Match to Measured Data

Tracer Breakthrough Times for Flow Path I (19)

BS2B Experimental Results					10% of Immobile Zone FWS Area				
	t5 hours	*t50 hours*	*t95 hours*	*% Recovery*		*t5 hours*	*t50 hours*	*t95 hours*	*% Recovery*
131I-	14	62	n/r	80%	131I-	12.25	51	806	100%
160Tb	14	63	4075	87%	160Tb	11	40	585	100%
85Sr	19	107	4327	86%	85Sr	9.7	42	231	100%
86Rb	51	490	n/r	56%	86Rb	66.5	645	n/r	67%
137Cs	555	n/r	n/r	28%	137Cs	457	1090	n/r	81%

7.6 A Comparison of Experimental Data from Structure 19 and Structure BG1 Pathways

In addition to the evaluation modeling described in Sections 7.1 through 7.5, an attempt was made to evaluate the differences between the Structure 19 (fault) and Structure BG1 (fracture network) pathways directly through the comparison of the BS2B tracer experimental results.

Table 7-12 compares the strength of experimental immobile zone retention observed in the tracer experiments for the two different pathways (Path I and II) against the effective retardation of the fracture coating. The fracture coating was chosen as the reference standard for comparison because it is active for both the fault-type ("Type 1") and non-fault-type ("Type 2") fractures represented by Structure 19 and Structure BG1.

The relative strength of immobile zone retention for each pathway is obtained by comparing the breakthrough statistics for 5%, 50%, and 95% normalized cumulative mass breakthrough for the sorbing tracer against the corresponding non-sorbing tracer. For the Structure 19 pathways (Path I), this is $^{131}I^-$. For the Structure BG1 pathways (Path II), this is ^{155}Eu, as the HTO breakthrough curve has an anomalously long tail that suggests non-conservative behavior. In addition, the relative strength of retention is calculated as the ratio of the times for 95% tracer recovery to time for 50% recovery for the sorbing tracer itself.

Table 7-12: Comparison of Experimental Solute Retention to Effective Retention of Coating

Pathway	Tracer	Effective Retardation due to Matrix Sorption	t_{95} (hours) Estimated from breakthrough curves	Comparaison against Conservative Tracer			Comparison for Same Tracer
				t_5/t_{5c}	t_{50}/t_{50c}	$*t_{95}/t_{95c}$	$*t_{95}/t_{50}$
Path I	^{131}I-	1	1725.4	1	1	1	1
Path I	^{160}Tb-DTPA	1	5963.3	1	1.02	3.46	3.39
Path I	$^{85}Sr^{2+}$	14.1	12360.0	1.36	1.73	7.16	4.14
Path I	$^{86}Rb^{+}$	298	N/R	3.64	N/R	N/R	N/R
Path I	$^{137}Cs^{+}$	2969	N/R	39.64	N/R	N/R	N/R
Path II	HTO	1	1496895.6	1.18	0.63	408.7	648.7
Path II	^{155}Eu-DTPA	1	3662.7	1	1	1	1
Path II	$^{22}Na^{+}$	12.4	14838.6	1.94	2.98	4.1	1.38
Path II	$^{133}Ba^{2+}$	1542	N/R	20.97	N/R	N/R	N/R
Path II	$^{54}Mn^{2+}$	9704	N/R	N/R	N/R	N/R	N/R

Matrix Retardation Factor $R_m = 1 + (\rho_s * Kd / n)$, where n is porosity, ρ_s is the immobile zone density (for fracture coating), and Kd is the distribution coefficient. Breakthrough times are in hours.

95% recovery not reached during experiment duration (4577 hours); t_{95} estimated from breakthrough curves where possible

8 Conclusions and Recommendations

The blind prediction and evaluation modeling studies reported in this document seek to improve the knowledge of transport in fracture networks based on the comparison of DFN simulations with the results of the BS2B tracer experiments carried out in Structure 19 and Structure BG1, and the surrounding fracture network. This section provides conclusions regarding the TRUE-BSC hypotheses, and recommendation regarding the application of this and future work.

8.1 Hypotheses

Hypothesis Ia) Microstructural (i.e. detailed geological, mineralogical and geochemical) information can provide significant support for predicting transport of sorbing solutes at experimental time scales,

1. The somewhat successful prediction of solute transport for the BS2B experiment utilizing the Task 6C microstructural model demonstrates that it is valuable to have available the detailed microstructural model information for predicting solute transport.

2. Even with detailed microstructural information, it was not possible to carry out a pure forward-model prediction of solute transport due to the lack of definitive information concerning the geometry of the background fracture pathway.

3. The implementation of the microstructural model is also significant with respect to the quality of predictions. In the present modeling, the microstructural model was significantly simplified to parallel rather than series diffusion, which resulted in an over-prediction of retention.

4. The hydrostructural model (i.e. identification of fracture geologic type, complexity, and geometry) is also important for defining the transport. In particular, the TRUE-BSC hydrostructural model provide the geometry framework for the tracer pathways, and the assignment of microstructural models to different fractures.

5. In the JNC/Golder BS2B blind prediction model, the implementation of identified complexity by proportionally increasing the area available for diffusion over-predicted retention and was therefore removed from the reconciliation modeling.

6. Step 1 and Step 2 evaluation modeling over-predicted retention of strongly sorbing tracers. This was potentially due to the use of the full transport channel width for each of the immobile zones in parallel.

Hypothesis Ib) Transport at experimental time scales is significantly different for faults (significant alteration, brecciation and fault gouge) and joints (with or without alteration), due to the indicated differences in microstructure and properties,

1. The solute transport in the Structure 19 pathway experienced a shorter advective travel time (as indicated by initial breakthrough time t_5) than the pathway involving the Structure BG1. This can be presumed to be a consequence of the differences between faults such as Structure 19 and no-fault fractures such as Structure BG1. This supports Hypothesis Ib.

2. The implementation of different microstructural models for the Structure 19 fault pathways (Path I) and the Structure BG1 pathways (Path II) provided for greater retention on the Structure 19 pathway. When comparing the tracer breakthrough experimental results to the simulations, the Path II predictions still made a greater over-prediction of solute retention. This indicates that solute retention along Structure BG1 pathways, and even along the related background fractures, may be even less than was provided by the modeled implementation of the microstructural model.

Hypothesis Ic) Longer distance pathways are dominated by fault rock zone behaviour, while shorter pathways (representative for fractures in the vicinity of a deposition hole) may be more likely to be dominated by joint fracture characteristics.

1. Both of the pathways tested in the BS2B sorbing tracer experiment had approximately the same Cartesian length (20 m), which made it difficult to reach conclusions regarding this hypothesis.

2. However, the Structure 19 retention behavior within the experiment was dominated by the immobile zone retention (fault gouge and fracture coating, principally). Since Structure 19 extends for over 100 m, it is reasonable to conclude that this same fault rock zone behavior would dominate at the larger scale.

3. Nevertheless, the Structure BG1 pathway, which was not dominated by fault rock behavior, showed that it is possible to develop pathways of significant length (tortuous distances in excess of 50 m, for example), made up of non-fault fractures. These non-fault fractures appear to have different advective transport behavior, with lower advective velocities and lower retention. This evidence indicates that such networks of “background fractures” might also occur at larger scales.

Hypothesis II c) Fracture retention properties tend to be scale-dependent primarily due to differences in microstructure.

1. The dramatically shorter advective travel time for the Structure 19 pathways (Path I) is not solely a microstructure issue arising from the difference between fault and non-fault fractures, but related instead to the longer, tortuous flow path Path II It may also be related to areas of low gradient along Path II, which is not as well characterized.

2. The difference in retention for the Structure BG1 and Structure 19 pathways could potentially be extrapolated as a “scale dependent” difference, because the Structure 19 has a much larger scale than Structure BG1. However, this extrapolation is not firmly based in the available data.

8.2 Recommendations

The following recommendations can be made based on reconciliation modeling and comparison of predictive simulations to BS2B experimental results r

1. The stochastic background fracture modeling for the Structure BG1 pathways (Path II) illustrates the large range of path lengths and fracture properties that can be encountered on transport pathways that have not been geometrically constrained by extensive site characterization. In general, however, the background fracture pathways appear to be longer and more tortuous than previously assumed

2. The variability of Structure BG1 pathway transport simulation results from the Monte Carlo simulation probably correspond to the range of results that could have been found in the tracer experiments on that same pathway. Any conclusions based on these experimental results need to be tempered by the probability that different results (within the range defined by the Monte Carlo simulations) are equally likely to the result observed.

3. Model implementation issues can have a dramatic influence on tracer transport modeling, even within the same assumed hydrostructural and microstructural model. In the predictive and reconciliation modeling, the assumption of parallel diffusion to all immobile zones was particularly important.

4. Further experiments on background fracture pathways are necessary to provide a statistical basis for conclusions.

9 References

Andersson P, Byegård J, Holmqvist M, Skålberg M, Wass E, Widestrand H, (2001): TRUE Block Scale Tracer Test Stage, Tracer Test Phase C, International Progress Report IPR-01-33, Svensk Kärnbränslehantering AB (SKB), Äspö Hard Rock Laboratory.

Andersson, P., Byegård, J., Doe, T., Hermanson, J., Meier, P., Tullborg, E-L., and Winberg, A., (2002a): TRUE Block Scale Project Final Report – 1, Characterisation and model development, Technical Report TR-02-13, Svensk Kärnbränslehantering AB (SKB).

Andersson, P., Byegård, J., and Winberg, A., (2002b): TRUE Block Scale Project Final Report – 2. Tracer tests in the block scale, Technical Report TR-02-14, Svensk Kärnbränslehantering AB (SKB).

Andersson, P., Gröhn, S., Nordqvist, R., and Wass, E. (2004a): Complementary Investigations at the TRUE Block Scale Site, Crosshole interference, dilution, and tracer tests, CPT-1 – CPT-4, Geosigma AB,. Äspö HRL International Progress Report, IPR-04-25, Svensk Kärnbränslehantering AB (SKB).

Andersson, P. (2004b): TRUE Block Scale Continuation- Data Delivery #4, ZIP file with associated Microsoft Word document ”Datadelivery#4_BS2B.doc” (20040625). Unpublished internal project memorandum.

Andersson, P., Byegård, J., Nordqvist, R., and Wass, E. (2005): TRUE Block Scale Continuation – BS2B Tracer Tests with Sorbing Tracers. TRUE Block Scale Continuation Project, Äspö HRL International Progress Report, IPR-05-01. Svensk Kärnbränslehantering AB.

Bear, J. (1972): Dynamics of Fluids in Porous Media, American Elsevier Publishing Co., New York, New York.

Byegård, J. et al. (1992): Field and laboratory studies of the reduction and sorption of technetium (VII), Radiochimica Acta, Vol. 58/59, pp. 239-244.

Byegård, J., and Tullborg, E-L (2004): Proposed sorption, porosity, and diffusivity data for the modeling of the TRUE Block Scale Continuation sorbing tracer experiment, Version 1.1 (10/14/2004). Unpublished internal project memorandum.

Cvetkovic, V., Selroos, J-O., and H. Cheng (1999): Transport of reactive solute in single fractures, Journal of Fluid Mechanics, Volume 318, pp. 335-356.

Deer, W., Howie, R., Zussman, J., (1974): An introduction to the rock-forming minerals, Halsted Press, John Wiley and Sons, New York.

Dershowitz, W.; Foxford, T.; Sudicky, E.; Shuttle, D.; Eiben, Th.; Alhstrom, E. (2000): PAWorks: Pathways Analysis for Discrete Fracture Networks Version 1.62, Golder Associates, Inc., Redmond, WA

Dershowitz, W., Winberg, A., Hermansson, J., Byegård, J., Tullborg, E-L., Andersson P., and Mazurek, M., (2002): Task 6C: Construction of block scale semi-synthetic hydrostructural models and attribution of hydraulic and transport properties, Svensk Kärnbränslehantering AB (SKB), Stockholm, Sweden.

Dershowitz, W.; Winberg, A.; Hermanson, J.; Byegård, J.; Tullbord, E-L; Andersson, P.; and Mazurek, M. (2003): A Semi-Synthetic Model of Block Scale Conductive Structures at the Äspö Hard Rock Laboratory, IPR-03-13, Svensk Kärnbränslehantering AB (SKB), Stockholm, Sweden.

Elert, M, and J-O Selroos, (2002): SKB TASK 6D Modeling task specification, Version 1.0. SKB, Stockholm, November 2002.

Golder Associates, Inc. (2004): FracWorks XP Discrete Feature Simulator, User Documentation Version 4.0, Redmond, WA.

Hakami, E. and W. Wang (in prep). TRUE-1 Continuation Project. Fault Rock Zones Characterisation. Characterisation and quantification of resin-impregnated samples of rock using image analysis. Äspö Hard Rock Laboratory, International Progress Report IPR-06-XX. Svensk Kärnbränskehantering AB.

Hermanson, J. and Doe, T. (2000): TRUE Block Scale Project Tracer Test Stage; March 2000 Structural and Hydraulic Model Based on Borehole Datat from KI0025F03, IPR-00-34, Svensk Kärnbränslehantering AB (SKB).

Holmqvist M, Andersson P, Trick T, Fierz T, Eichinger L, Scholtis A (2000): Test of new possible non-reactive tracers - experimental description and evaluation, Äspö Hard Rock Laboratory, ITD-00-07

Jansson, M., and Eriksen, T., (2001): CHEMLAB; A probe for in-situ radionuclide experiments, Technical Report TR-01-14, Svensk Kärnbränslehantering AB (SKB), Stockholm, Sweden.

Klein, C., and Hurlbut Jr., C. (1993): Manual of Mineralogy, John Wiley and Sons, New York.

Miller, I., Lee, G., and Dershowitz, W. (2001): MAFIC – Matrix/Fracture Interaction Code With Heat and Solute Transport User Documentation, Version 2.0, Golder Associates, Inc., Redmond, Washington

Poteri, A. (2004): Performance measures and presentation formats for BS2B, Technical Memorandum, 26 June, 2004.

Poteri A, Billaux D, Cvetkovic V, Dershowitz B, Gómez-Hernández J-J, Hautojärvi A, Holton D, Medina A and Winberg A, 2002: TRUE Block Scale Project. Final Report – 3. Modelling of flow and transport. Swedish Nuclear Fuel and Waste Management Company. Technical Report TR-02-15.

SKB (2004): TRUE Block Scale Continuation Project – Phase BS2B, Project Plan draft version 0.3 (10/24/2004), Document # F56P1-03-XX.

Shuttle, D., and Dershowitz, W. (2001): User Documentation for LTG V 3.0, Golder Associates Inc., Redmond, WA.

Sudicky, E., (1989): "The Laplace Transform Galerkin technique: A time-continuous finite element theory and application to mass transport in groundwater", Water Resources Research, v. 18 no. 3, p. 1833-1846.

Sudicky, E., (1990): "The Laplace Transform Galerkin technique for efficient time-continuous solution of solute transport in double-porosity media", Geoderma, v. 46, p. 209-232

Sudicky, E., and McLaren, R., (1992): "The Laplace Transform Galerkin technique for large-scale simulation of mass transport in discretely fractured porous formations", Water Resources Research, v. 28. no 2, p. 499-514.

Tullborg, E-L., and Hermanson, J. (2004): Assignment of distribution of geological structure type, complexity, and parameters of the micro-structural model applicable to the predictive modelling of the BS2B sorbing experiment, Technical Memorandum, TRUE Block Scale Continuation project, 15 June, 2004.

Winberg, A., Selroos, J., and Svemar, C., (2003): TRUE Block Scale Continuation Project – Phase BS2B Project Plan, Svensk Kärnbränslehantering AB (SKB), Stockholm, Sweden.